

Walter Bartelmus

**CONDITION MONITORING OF
OPEN CAST MINING MACHINERY**



Oficyna Wydawnicza Politechniki Wrocławskiej
Wrocław 2006

Recenzenci
Jan Adamczyk
Aleksander Lutyński

Skład i łamanie
Danuta Szyszka

Projekt okładki
Danuta Szyszka

Wydrukowano na podstawie dostarczonych materiałów

© Copyright by Walter Bartelmus, Wrocław 2006

OFICYNA WYDAWNICZA POLITECHNIKI WROCŁAWSKIEJ
Wybrzeże Wyspiańskiego 27, 50-370 Wrocław

ISBN 83-7085-961-5

Drukarnia Oficyny Wydawniczej Politechniki Wrocławskiej. Zam. nr 00/2006.

Contents

| | |
|--|----|
| 1. Role of engineering diagnostics and testing in maintenance of surface mining machines | 14 |
| 1.1. Introduction | 14 |
| 1.2. Engineering diagnostics and related disciplines | 19 |
| 1.2.1. Monitoring of machine condition | 21 |
| 1.2.2. Destructive and nondestructive testing | 23 |
| 1.2.3. Nondestructive testing (NDT) | 31 |
| 1.2.4. Recapitulation | 34 |
| 1.3. References | 34 |
| 2. Some basic terms | 36 |
| 2.1. Basic terms in machine diagnostics | 36 |
| 2.2. Basic terms in machine reliability | 37 |
| 2.3. Basic terms in machine maintenance | 38 |
| 2.4. Other basic terms | 38 |
| 2.5. References | 39 |
| 3. Machine maintenance procedures | 40 |
| 3.1. References | 41 |
| 4. Introduction to mechanical vibration | 42 |
| 4.1. Basic notions relating to vibration | 42 |
| 4.2. Basic physical quantities in equations of machine motion | 45 |
| 4.2.1. Stiffness of machine elements | 46 |
| 4.2.2. Coefficient of longitudinal stiffness | 47 |
| 4.3. Damping of vibration | 48 |
| 4.3.1. Logarithmic decrement | 51 |
| 4.3.2. Investigation of damping coefficient | 52 |
| 4.3.3. Free vibration of suspended mass | 55 |
| 4.4. Introduction to equations of machine motion | 56 |
| 4.5. Analysis of dynamics of simple machine system | 60 |
| 4.5.1. Effect of changes in external load | 63 |
| 4.6. Unbalance forces, principles of balancing | 66 |
| 4.7. Forced vibration | 71 |
| 4.8. References | 77 |
| 5. Modelling of power transmission system dynamics | 78 |
| 5.1. References | 85 |
| 6. Modelling of gear meshing dynamic behaviour | 86 |

| | | |
|---------|--|-----|
| 6.1. | Introduction | 86 |
| 6.2. | Distribution of velocities at point of instantaneous contact between two meshing teeth | 87 |
| 6.3. | Friction forces and moment of friction in meshing | 90 |
| 6.3.1. | Friction power | 91 |
| 6.4. | Analytical description of changes in meshing stiffness, moments of friction, tooth errors, intertooth backlash, gear intertooth forces | 92 |
| 6.4.1. | Analytical description of changes in moments of friction | 93 |
| 6.4.2. | Analytical description of intertooth force with intertooth backlash taken into account | 95 |
| 6.4.3. | Interpretation of intertooth force function notation | 96 |
| 6.4.4. | Analytical notation of error function | 96 |
| 6.5. | Dynamical model of toothed gear | 98 |
| 6.6. | Inter-tooth forces and dynamical overload factor | 99 |
| 6.7. | Normalization of dynamic meshing forces | 105 |
| 6.8. | Effect of changes in meshing stiffness and that of friction coefficient on meshing dynamics | 107 |
| 6.9. | Relationship between intertooth forces and relative acceleration of gear wheels | 112 |
| 6.10. | References | 118 |
| 7. | Modelling of kinematics and dynamics of rolling bearings | 119 |
| 7.1. | References | 126 |
| 8. | Modelling of belt conveyors | 127 |
| 8.1. | Modelling of forces in belt | 127 |
| 8.2. | Dynamical model of belt conveyor route section | 131 |
| 8.3. | References | 137 |
| 9. | Forms of wear of mining machine elements | 138 |
| 9.1. | References | 141 |
| 10. | Description of secondary processes accompanying operation of machine as carrier of information about its condition | 142 |
| 10.1. | Basic description of vibroacoustic signal | 142 |
| 10.1.1. | Process estimators and their application to vibroacoustic diagnostics | 153 |
| 10.2. | Wear products as signal of machine's condition | 162 |
| 10.3. | Thermal effects as signals of machine's condition | 171 |
| 10.4. | Ultrasounds and acoustic emission as machine condition signal | 172 |
| 10.4.1. | Ultrasounds | 172 |
| 10.4.2. | Acoustic emission | 174 |
| 10.5. | Corrosion monitoring | 177 |
| 10.6. | References | 177 |
| 11. | Diagnostic inference from vibroacoustic signal | 179 |
| 11.1. | References | 190 |
| 12. | Integrated diagnostic inference from vibration signal and wear products | 191 |

| | |
|---|-----|
| 12.1. References | 192 |
| 13. Standardization and classification of machine states | 193 |
| 13.1. Introduction | 193 |
| 13.2. Standardization in vibration diagnostics | 193 |
| 13.3. Diagnostics standardization based on analysis of wear products | 195 |
| 13.4. References | 197 |
| 14. Fundamentals of gear transmission diagnostics | 198 |
| 14.1. Gear transmission loading and gearing condition, life of gearing | 198 |
| 14.2. Description of change in gear transmission condition and effect of design, technological and operational factors on form of signal | 200 |
| 14.3. Vibroacoustic diagnostics, properties of vibroacoustic signal generated by gear transmission; sources of gear transmission vibroacoustic processes .. | 201 |
| 14.4. Unit damage to gearing | 207 |
| 14.5. Influence of gearing error randomness and external load randomness on diagnostic signal | 211 |
| 14.6. References | 215 |
| 15. Diagnostics of rolling bearings | 217 |
| 15.1. References | 223 |
| 16. Diagnostics of belt conveyors | 224 |
| 16.1. Introduction | 224 |
| 16.2. Diagnostics of belt conveyor gear transmissions | 226 |
| 16.3. Diagnostics of runners | 237 |
| 16.3.1. Application of thermovision to runner diagnostics | 237 |
| 16.3.2. Use of vibration and noise for assessment of runner condition | 237 |
| 16.4. Diagnostics of condition of conveyor belts with steel cables | 239 |
| 16.5. Benefits stemming from use of technological diagnostics | 242 |
| 16.6. Statistical analysis of diagnostic database | 245 |
| 16.7. References | 248 |
| 17. Diagnostics of bucket wheel excavators and stackers | 251 |
| 17.1. Introduction | 251 |
| 17.2. Diagnostics of gear transmissions | 256 |
| 17.3. Diagnostics of hoisting ropes | 259 |
| 17.3.1. Equipment for magnetic inspection of ropes – assessment of rope condition | 262 |
| 17.4. Diagnostics of hydraulic systems | 263 |
| 17.5. Diagnostics of slewing unit's principal bearing | 266 |
| 17.6. References | 268 |
| 18. Expert systems in technological diagnostics | 269 |
| 18.1. Expert system | 269 |
| 18.2. Expert systems based on neural networks | 270 |
| 18.3. Reference | 270 |
| 19. System of technological diagnostics for strip mine | 271 |

| | |
|--|-----|
| 19.1. Introduction | 271 |
| 19.2. Gear transmission diagnostics subsystem | 273 |
| 19.3. Steps to be taken into account when introducing technological diagnostics method | 284 |
| 19.4. Example of machines operation subsystem | 286 |
| 19.5. References | 289 |

List of more important symbols

| | |
|----------------------|--|
| a_{ux} | – auxiliary value (0 - 1) |
| A | – vibration amplitude, m |
| $A(t)$ | – signal envelope |
| C | – viscous damping coefficient for compression, N·s/m; for torsion, N·m·s/rad |
| C_k | – critical damping coefficient, N·s/m or N·m·s/rad |
| $C(\tau)$ | – stochastic process cepstrum |
| d | – diameter, m; or gear contact path length, m |
| e | – eccentricity, m or gearing involute error, m |
| E_k | – system kinetic energy, joule |
| E | – Young's modulus, MPa |
| $E(a, e, r, r_a)$ | – gearing error function with parameters |
| f | – vibration frequency |
| f_{pw} | – frequency of ball passage over damaged place on inner bearing race, Hz |
| f_{pz} | – frequency of ball passage over damaged place on outer bearing race, Hz |
| f_p | – frequency of contact of damaged place on ball with race, |
| f_{ko} | – bearing cage revolutions frequency, Hz |
| $\text{frac}(z/z_o)$ | – fraction part of two numbers ratio |
| F | – force, N |
| F | – cross-sectional area, m ² ; or intertooth elasticity force, N |
| F_d | – damping force, N |
| $F(t)$ | – exciting force function, N |
| F_o | – force amplitude, N |
| G | – modulus of transverse rigidity, MPa |
| $H(f)$ | – diagnostic signal flow transmittance, |
| I | – mass moment of inertia, kg·m ² |
| I_o | – geometrical moment of inertia, m ⁴ |
| I_s | – motor rotor mass moment of inertia, kg·m ² |
| k | – stiffness for compression, N/m; for torsion, N·m/rad |
| k_z | – gearing stiffness, N/m |
| k_r | – period multiplication factor, |
| K_d | – dynamical coefficient of teeth overload |
| ECD | – excavator-belt conveyor-dumping machine |
| l | – cylinder or element length, m |
| l_i | – random variable, |
| l_o | – number of tool cutting edges |

| | |
|---------------------|--|
| l_u | – intertooth clearance, m |
| L_1, L_2 | – machine element life, h |
| L_{10} | – 90% life of bearing, h; or in load change cycles |
| m | – mass, kg |
| M | – moment of force, moment of stiffness, N·m |
| M_h | – moment of viscous damping, N·m |
| M_s | – electric motor torque, N·m |
| $M(t)$ | – external load moment time function, N·m |
| $M_s(\dot{\phi}_1)$ | – motor torque characteristic function, N·m |
| M_n | – rated motor torque, N·m. |
| M_r | – external load torque, N·m |
| M_t | – moment of friction in gearing, N·m |
| M_c | – instantaneous power of friction in gearing, W |
| $M_s(var)$ | – characteristic of motor with changing driving torque at starting |
| $M_s(const)$ | – characteristic of motor with constant starting torque |
| $M_r(w,r,pw,rp,kr)$ | – external load torque with parameters |
| n | – exponent; rotational speed, rev./min |
| N | – motor power, W |
| N_{str} | – friction loss power, W |
| NDT | – Non-Destructive Testing |
| p_w | – coefficient defining instant of maximum load entry (0-1) |
| $p(s)$ | – stochastic process probability density function |
| P | – stiffness force, N |
| P_n | – normal force in gearing, N |
| $P(t)$ | – external load force time function, N |
| r | – coefficient of random external load change range (0-1), or radius of cylinder or circle, m |
| r_a | – coefficient representing random changes in position of gearing error maximum values |
| $s(t)$ | – any time function of diagnostic signal |
| S | – elasticity force, N |
| S_t | – damping force, N |
| $S(\dot{x})$ | – function defining friction force direction, assuming values (1, 0, -1) |
| t | – time, s |
| T | – vibration period, s; friction force, N; duration of diagnostic signal realization, s |
| T_r | – period of external load variation, s |
| T_d | – period of damped vibration, s |
| u | – gear ratio |
| w | – external load variation coefficient ≥ 0 |
| W_1, W_2 | – machine element load, N |

| | |
|--------------------|---|
| $W(f)$ | – function of stochastic process spectral concentration, |
| $W(a,b)$ | – local wave transform |
| x | – displacement, m |
| \dot{x} | – velocity, m/s |
| \ddot{x} | – acceleration, m/s ² |
| X | – vibration amplitude, |
| y | – vertical displacement, m |
| \dot{y} | – vertical velocity of belt vibration |
| \ddot{y} | – vertical acceleration of belt vibration |
| z | – number of teeth of gear wheel |
| $z(t)$ | – analytical time signal |
| (Z_u, K) | – wear and corrosion products |
| (Z_u, K, Z_a) | – wear and corrosion products and impurities |
| v | – linear velocity, m/s |
| v_p | – slipping velocity, m/s |
| α | – gearing pressure angle, degree, belt rotation angle due to sag or total angle of belt wrap around belt conveyor drum, rad |
| $\gamma(f)$ | – function of stochastic process coherence |
| $\gamma(f_1, f_2)$ | – function of stochastic process bicoherence |
| $\Delta \omega$ | – range of angular frequency, rad/s |
| ε | – angular acceleration, rad/s |
| η | – efficiency coefficient |
| $\kappa[s(t)]$ | – Hilbert transform |
| μ | – coefficient of friction |
| μ_s | – average value of stochastic process run |
| τ | – time, s |
| φ | – angle of rotation, rad |
| $\dot{\varphi}$ | – angular velocity, rad/s |
| $\ddot{\varphi}$ | – angular acceleration, rad/s ² |
| ϕ | – phase angle, rad |
| σ_s^2 | – stochastic process variance |
| Ψ^2 | – signal rms value |
| $\psi(\tau)$ | – autocorrelation function of stochastic signal |
| ω | – angular velocity, rad/s |
| ω_n | – eigenfrequency, rad/s |
| ω_d | – damped vibration frequency, rad/s |

Book's aim and scope

This book is intended primarily for mining faculty students attending lectures on technological diagnostics within the Operation of Mining Machinery speciality but also as an auxiliary textbook supplementing lectures on: Mining Machinery for Earth Resources Management speciality students and Mechanical Engineering Fundamentals for students of all engineering specialities. It can be helpful for PhD students doing research in technological diagnostics and serve as a basis for further study for the engineering personnel of strip mines.

The book is devoted mainly to the assessment of condition of machinery and equipment used in surface mining for which the Mining Faculty of Wrocław University of Technology educates engineering personnel. But it can be used in other industries and by students studying machine operation management. Providing an introduction to the relatively new field of computer simulation, which enhances the diagnostician's knowledge about the dynamical properties of the investigated object and the properties of the diagnostic signal, the book can be useful for both beginners and accomplished diagnosticians, using technological diagnostics to a different degree in their engineering practice. It also treats extensively problems relating to the analysis of the products of wear of machine kinematic pairs.

In **chapter 1** the role of diagnostics in the rational maintenance of machines, based on the knowledge acquired through monitoring their condition and diagnostic inference, is discussed. The links between diagnostics and related fields such as non-destructive testing and condition monitoring are highlighted. The subject of technological diagnostics and the extent to which it is covered in this book are described. Examples of applications of machine condition monitoring are given. Different tests performed on machine elements and subassemblies are described.

In **chapter 2** some basic terminology used in machine diagnostics and other essential terms are explained.

In **chapter 3** principal methods of machine maintenance are presented and the advantages of machine maintenance based on monitoring and technological diagnostics are highlighted.

In **chapter 4** the principles of modelling the dynamics of mechanical objects are described. The basics of the dynamics and mechanical vibration of objects, needed to better understand the phenomena accompanying changes in the condition of machines and making for better diagnostic inference, are presented. The relationship between the condition of machines and their dynamical state (vibration measurements serve as the basis for the diagnosis of the condition) is described. The principles of constructing models for computer simulation enabling the acquisition of experience needed for

diagnostic inference are explained in detail. The physical quantities in machine motion equations are described and the principles of writing such equations are given. As an example, the dynamics of a simple machine system are analyzed. The causes of the excitation of vibration by machines, such as unbalance and changes in the external load of the machine are discussed. In other words, this chapter introduces the student to computer simulation, which makes it possible to study the influence of design, technological and operational (motion) factors and changes in the condition of machines. The results of simulations are presented in the form of time plots and frequency plots (derived from time plots). In this way the dynamic characteristic of the investigated object are obtained. Together with the experience gained from industrial practice they represent substantial knowledge about the properties of a machine and provide the basis for a correct diagnosis of its condition (mechanical vibration parameters are symptoms of the condition).

In **chapter 5** a simplified model of power transmission system dynamics, in the form of equations of motion, is described and computer simulation results showing the basic dynamical properties of the power transmission system are presented as time plots of different physical quantities such as angular velocity, power, torque and efficiency.

Chapter 6 deals with the modelling of the gearing properties of gears. Details of the modelling of different factors contributing to the generation of vibration by the gear are given in analytical notation. A model of a gear operating in a power transmission system is presented. Friction in the gear and causes of changes in the gear's stiffness are analyzed. The model also includes intertooth clearance and gearing involute faults caused by improper manufacturing and changes in the condition of the gearing and the bearings. Results of computer simulations of the intertooth forces (for under-resonance, resonance and over-resonance operation of the gear), referred to the actual intertooth force measurements are presented. Good agreement between them becomes apparent. The causes of the unstable operation of the gear at resonance and the instability arising when intermeshing errors exceed the boundary value are discussed. The computer simulation results made it possible to describe the influence of design, technological, operational and change-of-condition factors on the pattern of the intertooth forces. Also computer simulation results showing the relationship between the intertooth forces and the vibration accelerations (constituting the gearing condition signal) are discussed.

In **chapter 7** the kinematics, velocity distributions and angular relationships between the elements of the rolling bearing are presented. Formulas for the frequency of vibration excitation by a damaged rolling bearing are derived. A simple model of the dynamics of the rolling bearing is described.

In **chapter 8** a conventional model of the belt conveyor is described. The model makes it possible to determine the axial forces in the belt and the velocity in the direction in which winning is conveyed. A new model of a belt conveyor route section,

which enables the analysis of the vertical vibrations of the belt and the runners, is presented. Illustrative computer simulation results in the form of time vibration velocity plots for the frame and the middle of the belt between runners in the belt conveyor's driving and driven strands are given.

In **chapter 9** the main forms of wear of the surface of machine elements constituting kinematic pairs are presented. Among others, running-in and seizing of the elements are described.

In **chapter 10** processes (not purposeful) which accompany machine operation and make up the machine condition signal are described. The fundamentals of vibroacoustic signal description are explained. A classification of vibroacoustic signals, their representations and correlations between the representations (signal estimators) are presented. Some vibroacoustic signal estimators used in technological diagnosis are described. The wear products formed as a result of kinematic pair interaction, their classification and their identification by means of analytical ferrography are presented. The equipment used for analytical ferrography is described and ferrograms of different wear products are shown. Different methods of continuous monitoring the particles generated by a machine are presented. The thermal phenomena, which accompany machine operation, ultrasounds, acoustic emission and corrosion monitoring are described.

Chapter 11 is devoted to diagnostic inferring on the basis of the vibroacoustic signal, with the focus on the signal spectrum. The relationship between spectral components and machine condition is described. Gear signal spectra obtained by computer simulation are shown. The identification of spectral components and their linkage to the condition of kinematic pairs belongs to the key problems of technological diagnostics.

Chapter 12 deals with integrated diagnostic inference based on different diagnostic symptoms which describe the condition of a particular kinematic pair. A complex of such symptoms constitutes a syndrome of the kinematic pair's condition.

In **chapter 13** the problem of normalization and classification of machine condition is discussed. Different classifications used in vibroacoustic diagnostics are presented. The relationship between life and the contamination class (the size and number of particles of impurities in oil) is described.

Chapter 14 deals with the diagnostics of gears. The relationship between the condition of a gearing, its state of load and its life is described. It is shown that a change in the condition of a gearing causes a change in its state of load and as a result reduces its life, which leads to a failure of the gear. Different ways of identifying the condition of gearing by means of appropriate diagnostic signal estimators are presented. The vibration signal generated by a gear in relation to the latter's condition is described. Vibration signal plots for different types of gear condition (a partially broken or fatigue cracked tooth and a completely broken tooth) are shown. Forms of the vibration signal

for different random intermeshing errors are distinguished. The effect of random changes in the load on the form of the vibration signal is described.

In **chapter 15** methods of diagnosing rolling bearings are presented. Illustrative applications of spectral analysis to the identification of rolling bearing condition are given. The Shock Pulse Method (SPM) for determining the thickness of the rolling bearing lubricant film is described.

Chapter 16 deals with the diagnostics of belt conveyors – one of the links in the technological system of the strip mine. The main components of the belt conveyor are described. A vibrational method of diagnosing gears, the interpretation of gear condition classes and classifications of: gearing condition, high-speed shaft operation condition and rolling bearing condition are presented. In addition, classifications of: gearing condition and rolling bearing condition for the ferrographic method are given. The possibilities of applying the thermovision method and the vibrational method to the assessment of the condition of runners are discussed. The latest method of assessing the condition of conveyor belt with steel cables is presented. Using as an example the vibrational method of diagnosis, the benefits stemming from gear diagnostics are demonstrated.

Chapter 17 deals with the diagnostics of bucket wheel excavators and stackers. The basic structural components of the BWE are shown. The diagnosis of the bucket wheel drive's gear by means of the vibrational method and the ferrographic method is described. A computer system for the assessment of the condition of the bucket wheel drive gear is presented. The gear condition signals are the vibration signal envelope signals. The structure of the power transmission systems of the bucket wheel boom's hoisting gears is described. A diagnostic method for assessing the condition of gearing in the boom's hoisting gears is proposed. The diagnostics of steel ropes in the BWE's hoisting systems is discussed. Examples of hydraulic systems used in bucket wheel excavators are given and methods consisting in the analysis of wear products and impurities are proposed for the assessment of their condition. Trial applications of ferrographic diagnostics to the assessment of the condition of the loader-stacker's bucket wheel drive hydraulic system are presented. Ferrographic diagnostics is proposed for the assessment of the purity of the medium lubricating the principal bearings of the turn-table of the BWE or the stacker.

In **chapter 18** selected problems related to the use of expert systems and artificial neural networks in the diagnostics of machinery are discussed.

Chapter 19 deals with diagnostic systems and subsystems for the strip mine. A diagnostic subsystem for gears used in the drives of belt conveyors is presented. The elements of a system for introducing the technological diagnostics method into the strip mine are described. A belt conveyor maintenance subsystem is presented.

1. Role of engineering diagnostics and testing in maintenance of surface mining machines

1.1. Introduction

The use of engineering diagnostics in the operation of mining machines is an essential element of their rational maintenance. And yet in the case of surface mining machinery engineering diagnostics is applied only to a small extent. The reason is lack of proper knowledge of diagnostic methods on the part of both engineering and maintenance personnel responsible for the operation of such machines. This makes the spread of diagnostic methods impossible. Also mining faculty graduates need some basic knowledge of diagnostics. The rational management of a mine requires data on the current condition of its machinery. This condition is a dynamic factor which changes in time. Modern information transfer means enable the monitoring of this condition. The obtained data should be exploited to increase the mine's productivity, reduce production costs and prevent failures which may result in situations as the ones shown in figs 1.1 and 1.2. (Courtesy of [1.1]). Fig. 1.1 shows a "wrenched off" drive shaft of an SchRs1200 excavator's bucket wheel and the consequences of it. Another failure of an SchRs1200 bucket wheel excavator is shown in fig. 1.2.

The subject of engineering diagnostics in this book are surface mining machines. A general view of a surface mine with machinery is shown in fig. 1.3. A machine is defined as a technical device containing a mechanism or an assembly of mechanisms in a common housing, used to convert energy or perform specified mechanical work – a working machine. From the energy point of view machines may generate mechanical energy (at the expense of another energy) – these are motors or they may consume energy – working machines. A machine as a structure may consist of several machines – energy converters.

A mechanism is a system of interconnected machine elements able to perform specified motions as a result of the consumption of mechanical energy.

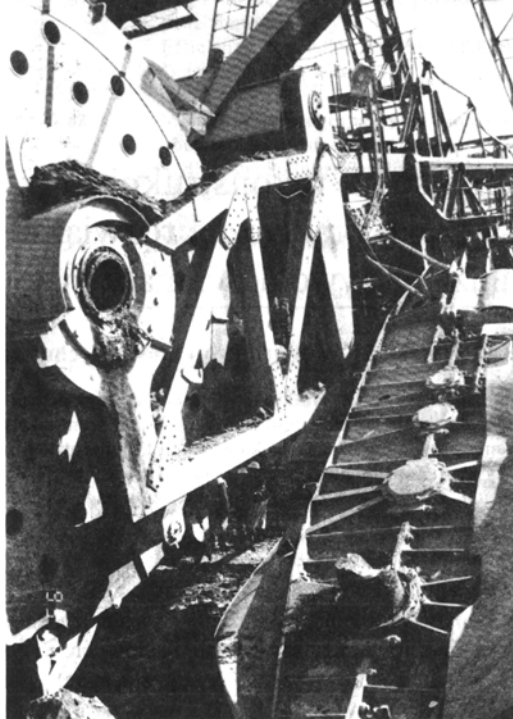


Fig. 1.1. Damaged drive shaft of SchRs1200 excavator's bucket wheel [1.1].



Fig. 1.2. Failure of SchRs1200 bucket wheel excavator [1.1].



Fig. 1.3. General view of surface mine.

A machine element is an integral component of a machine, e.g. a shaft, a bolt, a ball, an inner ring, an outer ring, a cage; the last four elements make up a rolling bearing. We sometimes say that a rolling bearing as a whole constitutes a machine element. From the engineering diagnostics point of view it is essential that the bearing is regarded as an assembly of machine elements forming kinematic pairs, e.g. the bearing race and the ball make up a kinematic pair. To understand engineering diagnostic methods, one must consider them in the context of kinematic pairs. It is precisely this approach to engineering diagnostics that the present book represents. A diametrically opposite approach would be to consider a machine as a “black box” about which we do not know what there is inside it but we receive certain signals from it, which we analyze and on this basis we identify the machine’s condition.

The subject of the diagnostics of surface mining machines are machines which in the structure sense constitute wholes, e.g.

- a bucket wheel **excavator**,
- a belt **conveyor**,
- a **dumping** machine.

The three machines make up, in the technological sense, the so-called ECD system shown in fig. 1.3.

The subject of the diagnostics of surface mining machines are machines in the structure or design sense, whose reliability depends on the reliability of the constituent kinematic pairs.

The reliability of machines is their ability to perform tasks in a given environment. The environment here is the surface mine's environment. A notion connected with reliability is the durability of a machine. The durability of an object or a machine is its ability to operate, expressed by a number of work cycles, mileage and time. When we say reliability, we mean reliability for an assumed durability. The durability of machine elements depends on the state of load and for a toothed gear meshing or a rolling bearing the relationship between durability and load can be written as

$$L_1/L_2=(W_2/W_1)^n \quad (1.1)$$

where: L_1 – durability for load W_1 ,
 L_2 – durability for load W_2 ,
 n – an exponent which is
 $n = 6$ for a toothed gear meshing,
 $n = 3$ for ball bearings,
 $n = 10/3$ for roller bearings.

The reliability of a machine is assured mainly through a proper choice of design features at the design stage. Operating practice shows that the maintenance of the assumed reliability depends on the upkeep of machines. It is the duty of the mine's machine maintenance service to prevent breakdowns leading to production losses. If engineering diagnostic methods are used, mine machinery maintenance services have an influence on both the failure rate and the costs of repairs and a machine is diagnosed as in need of repair on the basis of specific criteria expressed by measurable parameters (symptoms). In other words, a decision is made to have a machine repaired when its condition warrants it. As a result the costs of repair and thus the total machinery operating costs are kept to a minimum. A breakdown is defined as serious damage to a machine which makes its further operation impossible. Three basic machinery maintenance strategies are distinguished:

- operation until a failure,
- planned-preventive maintenance,
- maintenance dependent on a machine's condition, condition based maintenance.

Engineering diagnostics is associated mainly with the condition based maintenance strategy. Thus engineering diagnostics is understood as the identification of a machine's condition from the symptoms which accompany its operation. A machine's condition is the totality of factors characteristic of the machine and influencing the interaction of its kinematic pairs. Examples of such symptoms are physical quantities which describe mechanical vibration, quantities which describe wear products (wear debris particles), a temperature distribution on a machine's surface, etc. An increase

in vibration intensity in one or several components of a vibration spectrum is a symptom of a change in the condition of a particular kinematic pair. In an extreme case this may be a symptom of the loss of load-carrying ability by a particular kinematic pair, which is tantamount to the failure of the machine. In the traditional mode of maintaining machinery (the planned-preventive maintenance strategy) we learn about the condition of many kinematic pairs only after the machines designated for repair are disassembled.

A repair means actions aimed at recovering a machine's operability through the detection and removal of any malfunctions or damage incurred in service. The planned-preventive maintenance strategy inevitably leads to an expected number of breakdowns. Moreover, machines which do not need repair are repaired. This happens because of the criterion used for designating machinery for repair such as being in service for a certain number of hours, a certain output in tons or cubic meters, etc. Thus losses are incurred due to money spent on repairs of machines which are in satisfactory condition. A simple example of a rolling bearing provides a good illustration of the problem. Fig. 1.4 shows a relationship between reliability, expressed by the probability of fulfilling a given life requirement, and durability expressed in millions of revolutions of the rolling bearing. Such a bearing was chosen that durability L_{10} is 500000 rev. 10 means that at a durability of 500000 rev. 10% of the bearings have lower reliability, i.e. the probability of meeting the specified life L_{10} requirement is 90%, which means that the reliability is 90%. It follows from fig. 1.4 that about 10% of the rolling bearings have durability $20L_{10}$. If a planned-preventive maintenance strategy is used, machines whose condition is so bad that high expenditures would be incurred in order to bring them back to their original condition [1, 2] (sometimes this is even impossible).

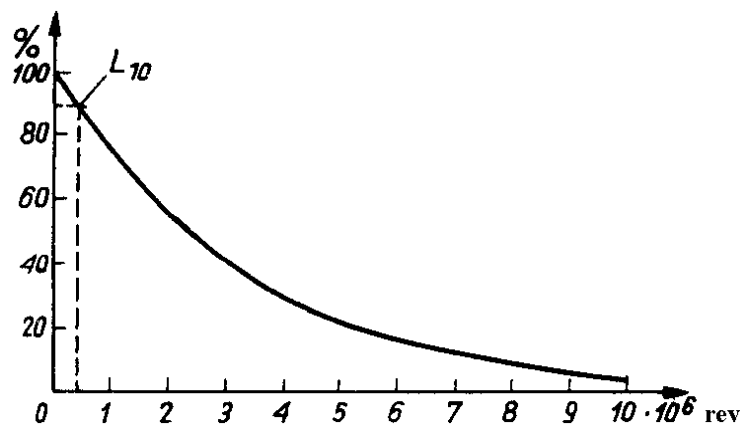


Fig. 1.4. Bearing's reliability

The surface mine environment is a peculiar one (differing much from a typical industrial environment) and it affects considerably the durability and reliability of machines which operate in it. This effect is a random one and so it is impossible to take it fully into account in the design of a machine. Also the machine's state of load has random character. Therefore it is necessary to monitor (track) the machine's condition and its state of load. In mines condition monitoring is usually done not by means of any technical devices but through subjective assessment based on sensory impressions. In addition, all kinds of surveys are conducted. These are periodical, subjective and limited in their extent due to lack of access to some kinematic pairs. Engineering diagnostics recommends monitoring using technical means which measure physical quantities, i.e. symptoms of the machine's condition. Practical experience shows that despite the fact that the condition is identified indirectly, the accuracy of the diagnosis may be as high as 100%.

1.2. Engineering diagnostics and related disciplines

Engineering diagnostics is understood as the identification of a machine's malfunctions on the basis of symptoms. A complex of symptoms constitutes a syndrome which is characteristic of the machine's condition. Diagnosis requires a skill in identifying a machine's malfunctions from symptoms. In other words, the term diagnosis is understood here similarly as in medicine where diseases are identified from symptoms or a complex of symptoms constituting a syndrome characteristic of a disease.

Nondestructive testing, and monitoring are disciplines related to engineering diagnostics. Monitoring is closely connected with diagnostics. The condition of a machine can be diagnosed only on the basis of monitored signals (symptoms).

Monitoring (supervision, tracking) can be the tracking of a machine's condition or a machine's work process, using technical means or without them by means of senses.

Symptom is a carrier of information about a machine's condition, perceived or observed by instruments by a person who makes a diagnosis and indicates a malfunction of the machine.

Besides physical quantities needed to assess a machine's condition, physical quantities which specify the relative positions of machine assemblies are monitored to avoid collisions of the latter. Power consumption is monitored in order not to exceed loads permissible for mining machines. One can distinguish monitoring:

- for diagnostic purposes,
- for machine operation safety purposes,
- for machine's process parameters and its operation.

The terms *monitoring* and *diagnostics* are often used interchangeably, e.g. as implied by the name of the **Condition Monitoring** Conference organized by the University College of Swansea, the Department of Mechanical Engineering. This conference

deals with engineering diagnostics problems, i.e. with monitoring and inferring from symptoms, i.e. diagnosing.

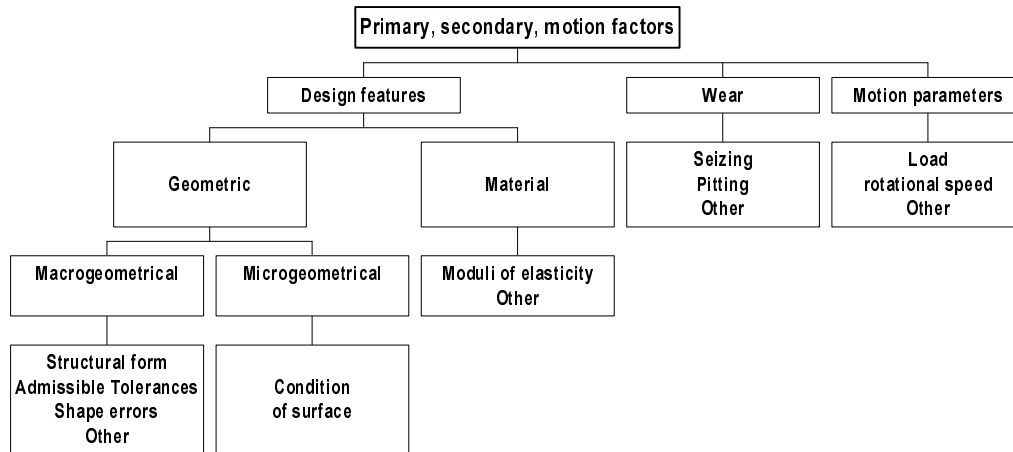


Fig. 1.1. Factors affecting diagnostic signal [1.4].

Certain separateness of the two terms is implied by the name of the Condition Monitoring and Diagnostic Engineering Management (COMADEM) Conference initiated by the COMADEM. This conference has been held in different centres in the UK and abroad (India 1994, Canada 1995, Sheffield 1996, Finland 1997, Australia 1998, UK 1999, USA 2000, UK 2001).

The conference's aims are defined as the use of condition monitoring, diagnostics and management to obtain the most effective solutions for the multifaceted problem of maintenance, reliability, quality, safety and energy saving, associated with the upkeep of an enterprise's fixed assets to satisfy the needs of its customers and employees.

In the present book the relationship between monitoring and diagnostics is seen as follows: to make a diagnosis one needs monitored physical quantities corresponding to machine condition symptoms. By engineering diagnostics we understand a field of knowledge which combines machine condition monitoring with diagnosing from symptoms. To diagnose a machine's condition one needs to monitor symptoms and have knowledge about the relation between symptoms and condition, expressed by design factors, a change in the condition (wear) and motion parameters (operational factors), which during the operation of the machine are converted into machine condition symptoms. It leads to "Design, Production Technology, Operation, Condition Change, factors based diagnostics" (DPTOCC factors based diagnostics). In [1.3] these factors are called primary, secondary and motion factors. The parameters which make them up are presented schematically, according to [1.4], in fig. 1.5.

1.2.1. Monitoring of machine condition

As mentioned earlier, the monitoring of a machine's condition includes measurements of physical quantities used for "tracking" the course of the work process. This ensures the proper operation of the machine, its safety and the safety of the machine's users. Points at which sensors are attached to ensure the proper and safe operation of a wheel excavator are shown in fig. 1.6, after [1.5]. One cannot see there any sensors that would enable the tracking of changes in the machine's condition. No physical quantities on the basis of which the condition could be diagnosed are measured. All the functions performed by the particular sensors attached to the wheel excavator are described in detail in [1.5]. In this chapter only some elements of monitoring are presented.

Hydrodynamic couplings are used to protect the toothed gear of the bucket wheel's drive against overloading. As the load exceeds a prescribed load that the coupling can carry, slip occurs on it. Excessive slip results in excessive heat release. The aim of monitoring is to track the rotational speeds of the coupling's two parts (active and passive). If the speed difference exceeds a prescribed value, the bucket wheel's drive is switched off. If the monitoring system were damaged, the oil would heat up too much, the protective stopper would melt and the oil would escape from the hydrodynamic coupling. Two non-contact rotational speed transducers are used for the monitoring. Rotational speeds can be watched on the meters installed in the wheel excavator operator's cabin. As the speed difference limit is exceeded, the alarm is activated, and then the machine is switched off. The place where sensors "tracking" the angular velocities of the coupling's elements are attached are denoted by numeral 1 in fig. 1.6.

Also the temperature of the oil in the hydrodynamic coupling is monitored (3). If the temperature exceeds 140°C , the drive is switched off. The bucket wheel overload is monitored via the intensity of the current drawn by the electric motor. The current intensity is a measure of the power consumption by the electric motor that drives the bucket wheel. When current intensity goes beyond a value corresponding to the exceeding of power consumption by 50%, the drive is switched off. (The hydrodynamic coupling is switched off when the gearing load torque exceeds the nominal torque by 60%). Also the excavator's sluing drives are protected, e.g. by a magnetic particle coupling (fig. 1.6, item 27). When 3% slip is exceeded, the drives are switched off. Numeral 9 indicates the place where the magnitude of belt slip relative to a belt conveyor's driving drum is monitored. When slip exceeds 30%, the machine is switched off. The rotational speed of the excavator's sluing mechanism is monitored by speedometer (26). In fig. 1.6 also the limit switches are marked (with numbers). For some motions two sensors for one constraint are used. To protect the excavator against excessive external forces, the tension in the winches' carrying ropes (30) is monitored. The other protection functions are described in [1.5].

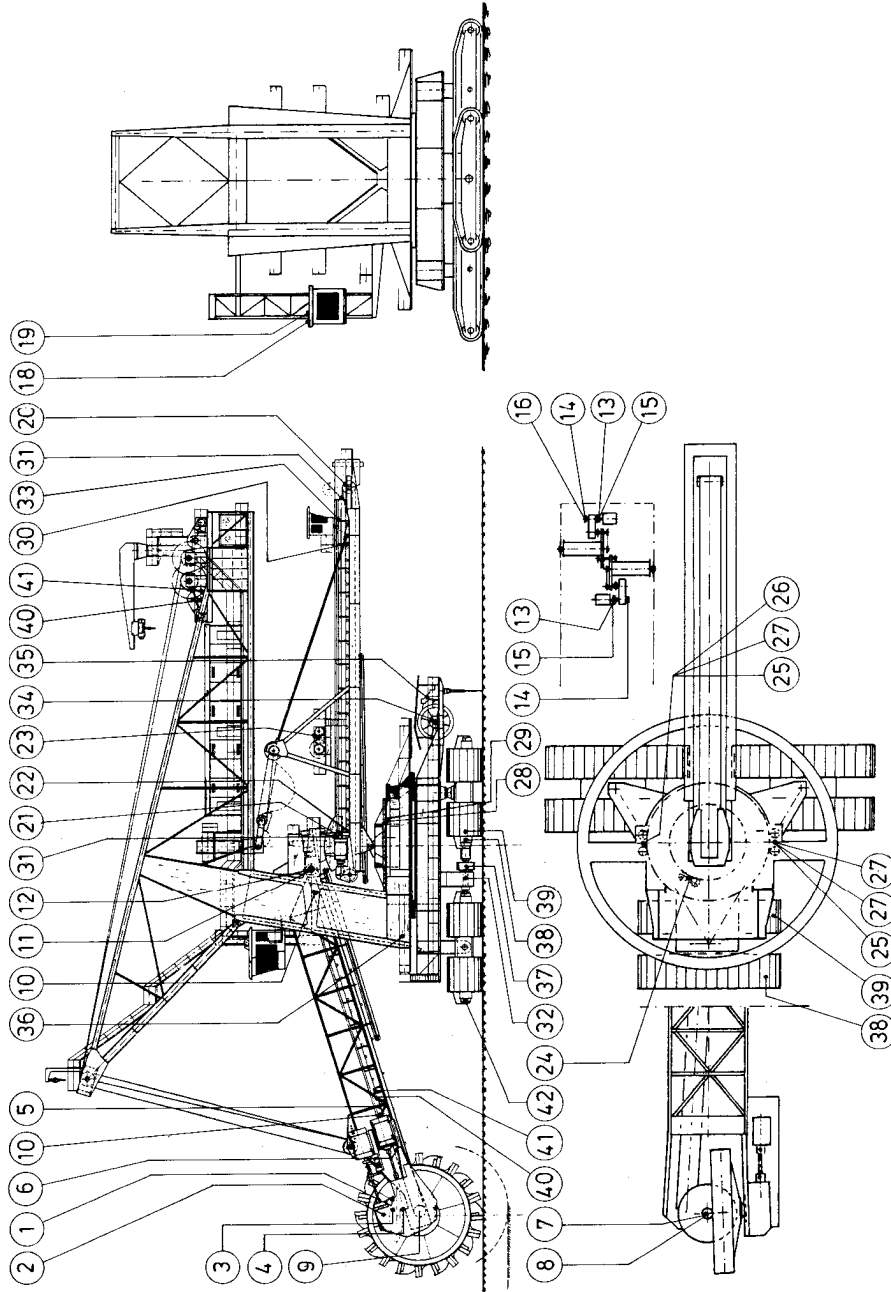


Fig. 1.1. Arrangement of safety sensors (1-42) for monitoring wheel excavator's operating parameters and condition [1.5].

Devices used to monitor the condition of a belt conveyor are shown schematically in fig. 1.7. The rate of belt travel, belt run-off, belt wear and the drum's rotational speed are monitored. Metal elements in the transported winning are detected. Drum slip, which above a certain value may be dangerous for the belt, can be determined on the basis of the drum's rotational speed and the velocity of a belt.

The above examples shed some light on the concept of monitoring the operating condition of mining machinery. Such monitoring, however, is not the subject of this work. The principles of monitoring described in this chapter had to be understood by the designer when making a choice of machine design features.

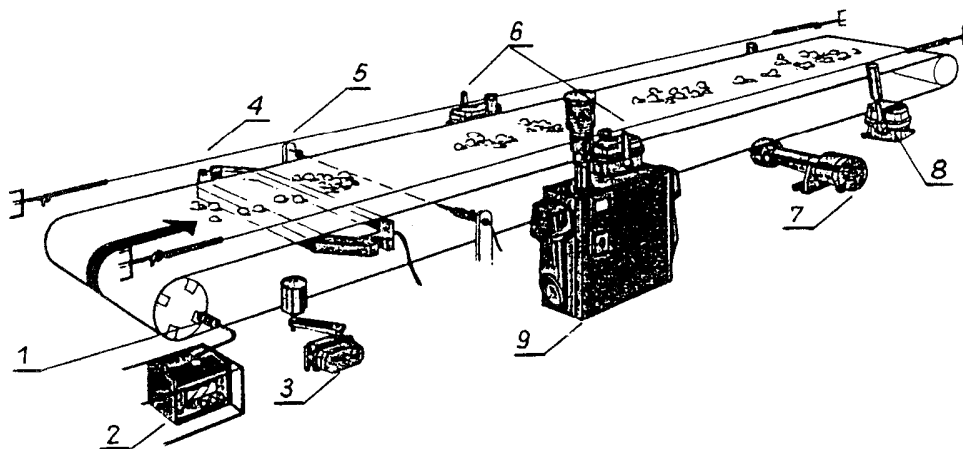


Fig. 1.2. Arrangement of devices for monitoring operating parameters and condition of belt conveyor:

- 1 – impulse sensor, 2 – drum rotational speed monitor, 3 – belt run-off monitor, 4 – metal detector,
- 5 – belt wear monitor, 6 – rope tension monitor, 7 – belt speed monitor, 8 – belt run-off monitor,
- 9 – signalling device

One should add that a designer of a mining machine should make such a selection of machine design features which takes into account machine condition assessment through engineering diagnostics means.

1.2.2. Destructive and nondestructive testing

To ensure reliable operation of machines, more precisely operation with specified reliability, destructive and nondestructive tests are conducted.

Destructive tests of materials are conducted on specimens. As an example of such testing, tests on materials for wheel excavator turntable rolling bearing races (figs 17.1 and 17.19) are described, after [1.5]. The tests were carried out on a test stand shown in fig. 1.8. The stand consists of the following main components: bottom beam (1)

with bottom race, top beam (2) with top race, middle beam (3) – movable. Beam (3) is put in (to-and-fro motion) plane-reverse motion by arm (5) with a connecting-rod mechanism driven by a motor via a toothed gear. There are tested balls between the races.

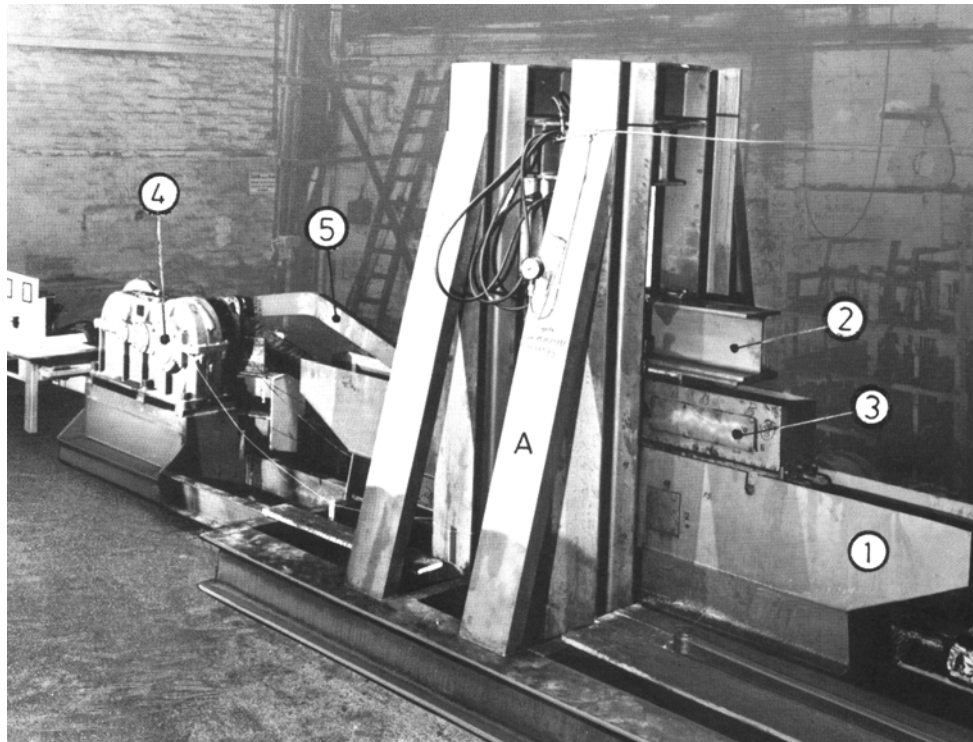


Fig. 1.1. Stand for testing materials for wheel excavator turntable rolling bearing races [1.5]:
 1 – bottom beam with bottom race, 2 – top beam with top race, 3 – middle beam (movable),
 4 – driving gearbox, connecting-rod arm

Steel Ck45N (as denoted in [1.5]), for which the races did not show significant damage, proved to be the most suitable material.

Typical destructive tests are tests carried out on materials to determine their static or fatigue strength. For a static load a stress-strain diagram is obtained from the test. To determine the fatigue strength, stress cycles relationship (a Wöhler diagram) is determined.

To establish guidelines for the selection of design features for surface mining machines, ensuring the latter's reliable operation, special test stands (figs 1.9 and 1.10, after [1.6]) are built. The stands are designated: STS – static test stand and DTS – dynamic test stand.

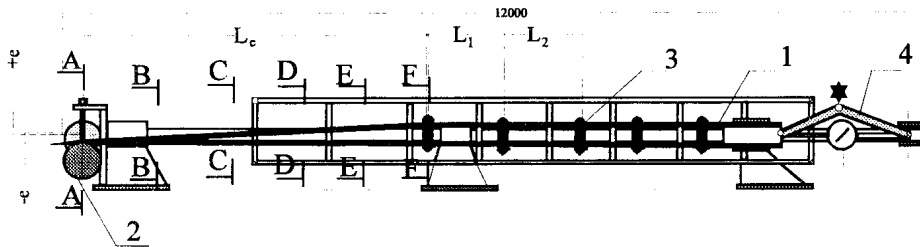


Fig. 1.2. Static test stand (STS) for testing pipe conveyor belt [1.6]:
 1 – tested belt, 2 – drum, 3 – set of rollers, 4 – belt-tightening mechanism, A-A to F-F – places of belt cross-sections shown in figs 1.11 and 1.12

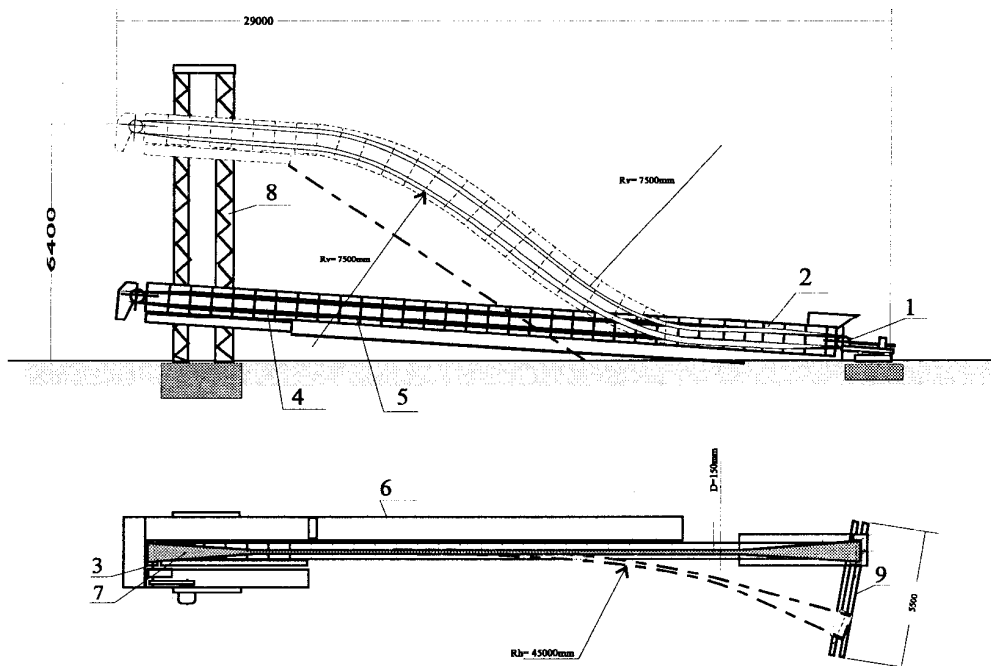


Fig. 1.3. Dynamic test stand (DTS) for testing pipe conveyor [1.6]:
 1 – reverse drum, 2 – pipe conveyor's top strand, 3 – driving drum, 4 – pipe conveyor's bottom strand,
 5 – conveyor support system frame, 6 – platform, 7 – belt's transitional section (output unloading),
 8 – support tower

The shape obtained by conveyor belts (with a core of different design), in the pipe conveyor's belt cross-section in transitional section, was studied on the stand shown in fig. 1.9. The different cross-sectional forms are shown in fig. 1.11.

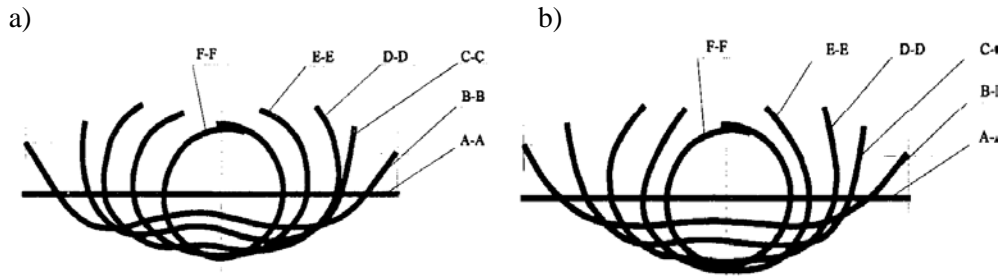


Fig. 1.4. Belt cross-sections in transitional section ($D = 300$ mm, $L_c = 5.5$ m, $F = 30$ kN, $e = 0$):
a – belt no. 1, b – belt no. 2 [1.6]

To study the deformations of the transitional section a nondestructive test – a photoelastic analysis – was applied. The obtained belt stress patterns are shown in fig. 1.12.

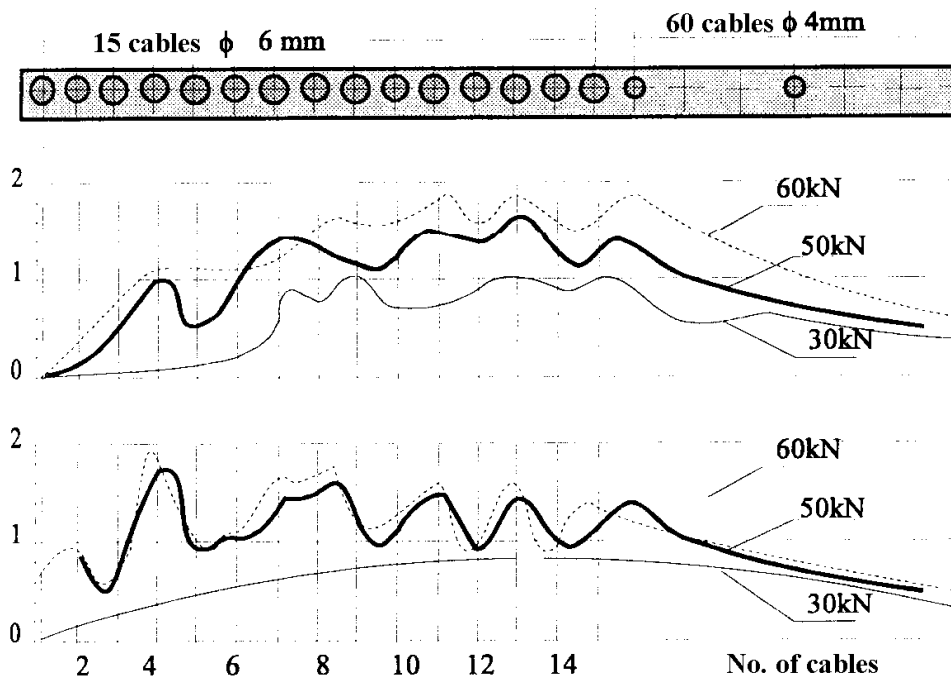


Fig. 1.5. Belt stress patterns in transitional section near conveyor's drum:
a – belt's cross-section, b – transitional section of length $L = 7.5$ m, c – transitional section of length $L = 5.5$ m.

Through destructive and nondestructive tests one can determine the ability of machine assemblies or subassemblies to perform specific operating functions. Destructive

tests are conducted on material specimens (in accordance with appropriate standards), machine subassemblies (mechanisms) or whole machines – testing of prototypes. If destructive tests are to fulfil their purpose – the provision of material data – different load change patterns, corresponding to the actual changes in the service load, should be applied. This condition is largely satisfied in many practical cases since the use of appropriate material data and calculation procedures ensures the required reliability for assumed low factors of safety. But in the case of mining machines the results are not fully satisfactory since it is difficult to determine their state of load and the effect of the mine environment. This load should correspond to the service load.

Another problem in prototype testing is shortening of time, i.e. the use of relation (1.1). It is impossible for the prototype testing time to be as long as the machine's service time, i.e. its life $L [h]$. Therefore increased loads are substituted for the actual loads.

The main disadvantage of machine prototype testing is that the tested machines are often destroyed in the process. And its limitation is the fact that only a small number of machines can be tested.

Nondestructive tests have no such limitations. They can be conducted even on new machines and after testing sold.

To ensure high reliability of machines and to reduce losses due to lost operating ability appropriate maintenance measures are used. To support the maintenance of machines, nondestructive testing and diagnostic examination are applied. The subject of this book is diagnostic examinations. One should also mention here a rig/stand testing on which diagnostic methods are based. For example, the meshing condition tests presented in [1.3] constitute a basis for a search for a suitable method of diagnosing the condition of a gearbox meshing. An example of a test stand used for such tests is shown in fig. 1.13.

Results obtained from mathematical modelling and computer simulation, forming a basis for explaining the dynamic processes which occur when the condition of the kinematic pairs of a machine changes and for selecting diagnostic signal processing techniques, are presented in chap. 14.

A test-rig for investigating the relationship between diagnostic signals received directly from a gear and signals received from different points on the gearing wall is shown in fig. 1.13. The relationship was studied by means of an analogue testing equipment setup (fig. 1.14) for measuring a coherence function (formula 10.49).

Using the measurements, a diagnostic method of assessing the condition of a gear's meshing was developed. The basics of this method are presented in chap. 10.1. Gear wheels of different quality, modified gear wheels and gear wheels damaged by pitting were investigated. The condition of meshing of gear wheels severely damaged by pitting is shown in fig. 1.15. Meshing condition vectors for gear wheels in different quality and condition are shown in fig. 1.16. A more accurate description of a quality and condition vector is given in chap. 10.1.

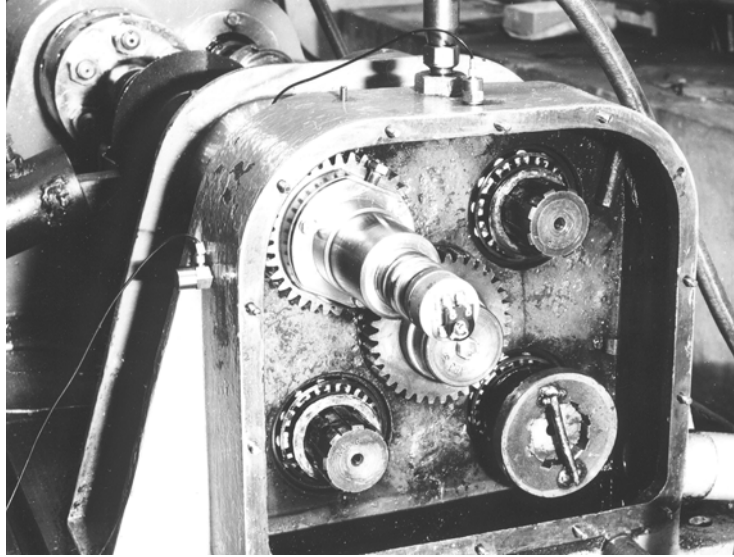


Fig. 1.6. Test stand for testing condition of gear wheels [1.3].

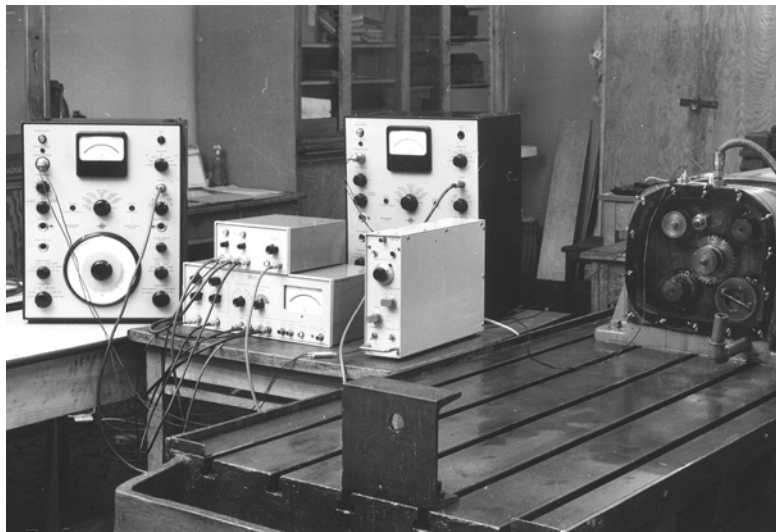


Fig. 1.7. Equipment setup for diagnostic meshing condition measurements [1.3].

Tests on which another diagnostic method is based are described in [1.7]. Fig. 1.17 shows a railway wheel set which was made to vibrate and the resulting sonic effect was used to assess the negative allowance joint between the wheel centre and the rim. An objective method of assessing the condition of such joints on the basis of a sound fading curve has been used to assess the negative allowance joint between the wheel centre and the rim.

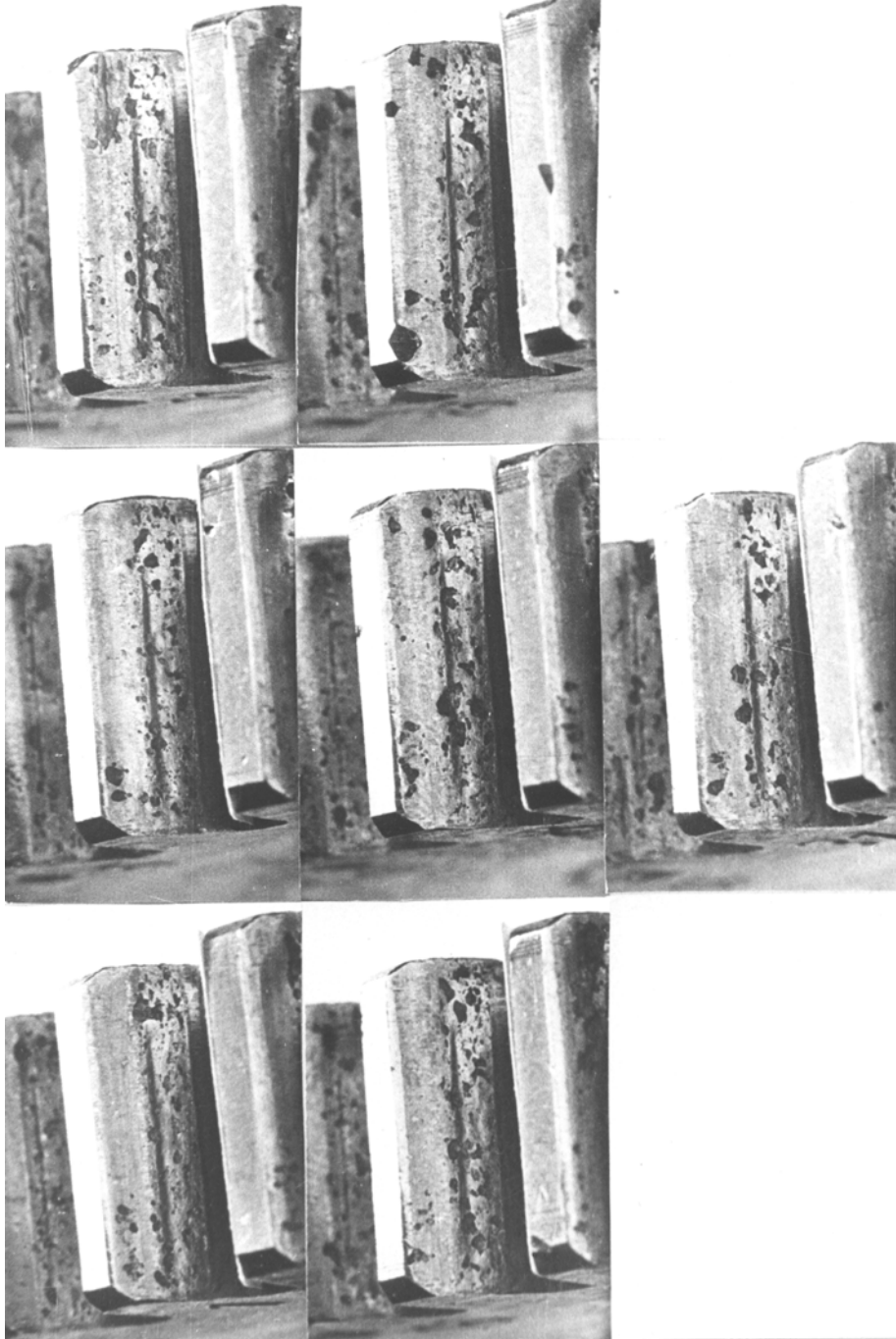


Fig. 1.8. Condition of meshing of gear damaged by pitting.

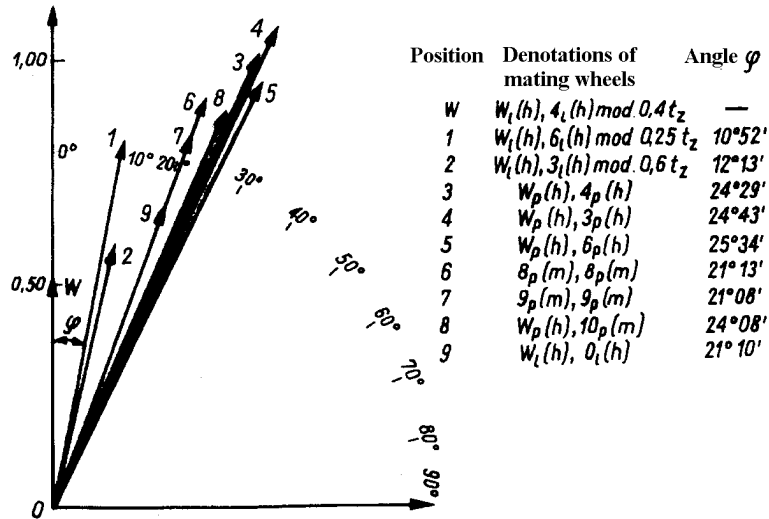


Fig. 1.9. Output (diagnostic) signal vectors for wheels with simple modified and unmodified teeth: W, 1, 2 – modified wheels, 3, 4, 5 – unmodified wheels (class 8, PS), 6, 7, 8 – unmodified wheels (class 7, PS), 9 – unmodified wheels (class 6, PS) [1.3], PS - Polish Standard similar to ISO

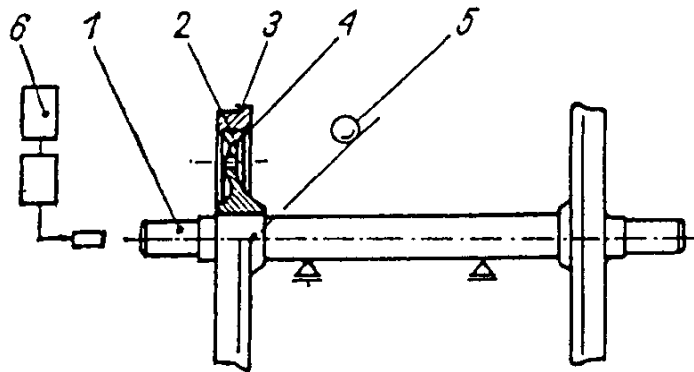


Fig. 1.10. Wheel set during testing [1.7]: 1 – axle, 2 – wheel centre, 3 – rim, 4 – clamping ring, 5 – steel ball, 6 – measuring set with microphone

Sound fading curves for joints in proper condition – curve *a* and in improper condition – curve *b* are shown in fig. 1.18. It has been established that the sound emitted by the excited wheel set characterizes the degree of “adhesion” between the elements (the wheel centre, the rim and the clamping ring). And the sound fading curves (sonic characteristics) are related to the height of irregularities on the joined surfaces and to the wheel centre and rim shape errors, which result in uneven pressures between the joined surfaces. The characteristics do not specify the magnitude of negative allowance – a difference between the elements’ diameters before they are joined.

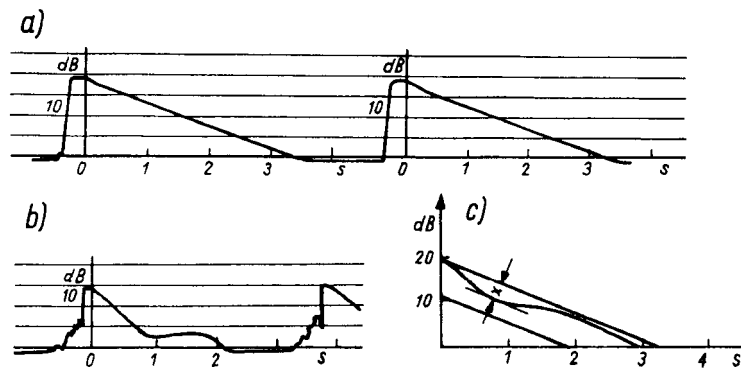


Fig. 1.11. Sound fading characteristic curves: a – exemplary sound fading characteristic for standard wheel, b – sound fading for wheel with improper quality of joint, c – limits of variation of sound fading curve deviation (x) for confidence level of 0.98 [1.7].

The provided examples of tests used for developing diagnostic methods indicate what engineering diagnostics as a field of knowledge deals with. Diagnostic tests belong to nondestructive tests and their principle feature is the testing of the condition of a machine during its operation. It is only when the machine is running that signals for diagnostic analysis are generated.

1.2.3. Nondestructive testing (NDT)

Nondestructive testing is defined as a field of knowledge which includes methods of identifying or measuring properties, abilities to function (operate) and characteristics of materials of which machine elements, assemblies or loadbearing structures are made, which do not entail any loss of the assemblies' (mechanisms') or subassemblies' ability to function. According to this definition, nondestructive tests, as opposed to destructive tests, do not lead to the destruction of the tested elements, assemblies or loadbearing systems. NDT and the associated field of knowledge appeared at the same time as engineering diagnostics developed and so the latter and NDT have much in common. Hence some authors classify a certain method as diagnostic while others include it among nondestructive tests. A common feature of the two classes is non-destructiveness. The difference is that signals in diagnostic testing are symptoms that appear during normal operation (within certain limitations) whereas NDT is usually conducted when a machine is idle and it focuses on material properties. The identification of kinds of damage and material condition by nondestructive tests is limited. In most cases, the material properties of tested objects are determined by nondestructive tests indirectly. Generally, NDT gives a qualitative assessment of condition, whereas

destructive testing supplies quantitative valuations. Examples of nondestructive tests are ultrasonic tests, magnetic particle inspections, etc.

NDT plays (should play) a major role in identifying the condition of surface mining machines. In [1.8] it is proposed to apply nondestructive, magnetic and ultrasonic testing methods to the testing of the nodes in the KWK 1400 excavator's carrying structure (fig. 1.19). The tested nodes are denoted by numbers in the figure and the proposed tests are compiled in table 1.1. Different types of nodes are shown in fig. 20a-f.

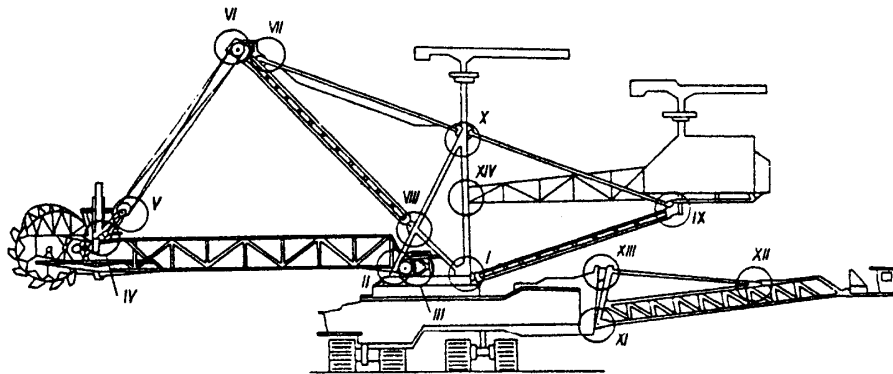


Fig. 1.1. Diagram of KWK 1400 excavator with marked elements of nodes: (I-XIV) (methods of testing nodes are compiled in table 1.1) [1.8]

Tabela 1.1. Nondestructive methods of testing node elements of KWK 1400 excavator (nodes shown in fig. 1.19) [1.8]

| Node number | Tested elements of node | Test method |
|---------------------|-------------------------|-------------|
| I, II, IV, VIII, XI | a) welded node | MM and MU |
| VII, IX, X | b) bolt | MU |
| III, VIII | a) welded node | MM and MU |
| | b) screws | MM and MU |
| V, VI | a) welded node | MM and MU |
| | b) axle | MU |
| XII | a) riveted node | MM and MU |
| XIII | a) welded node | MM and MU |
| | b) riveted joints | MM and MU |
| XIV | a) welded node | MM and MU |

MM – magnetic method, UM – ultrasonic method

Magnetic methods are based on the phenomenon of magnetic field dissipation or a change in magnetic permeability at places where defects occur. There are different ways of detecting dissipated magnetic fields. In on-site conditions a magnetic-particle method is widely used. It is suitable for detecting all kinds of cracks and other surface and subsurface crack-like defects, but only in ferromagnetic substances. In nonde-

structive testing also penetration methods, consisting in the penetration of a liquid (penetrant) into a defect, are used. Excess liquid is removed so that liquid remains only in the cracks. Penetration methods are used to detect material surface discontinuities in the form of open surface defects (all kinds of cracks, porosities, pitting, delamination, lapping).

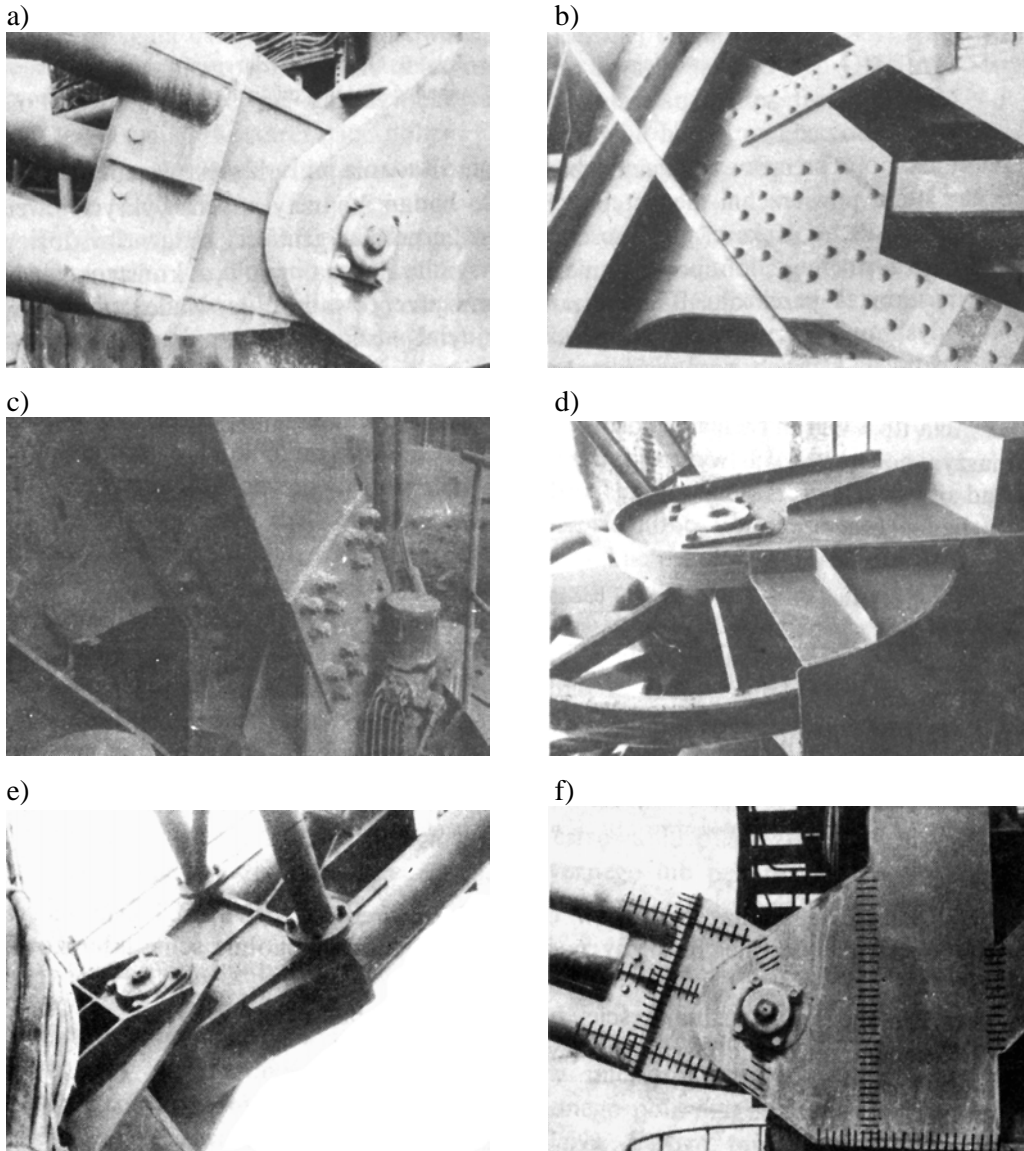


Fig. 1.2. Examples of node designs: a – welded node with bolt, b – node with riveted joints, c – node with screw joints, d – access to cable wheels, e – access to bolt, f – fragment of welded node with marked spots where nondestructive magnetic and ultrasonic tests are carried out.

1.2.4. Recapitulation

It follows from the above considerations that tests performed on machines can be divided into destructive and nondestructive tests. Destructive testing is applied to:

- materials,
- subassemblies and
- machines.
- Nondestructive testing includes:
- nondestructive tests and
- diagnostic tests.
- Depending on its aim diagnostic testing can be divided into:
- identification of the class of a condition,
- identification of the condition.
- The following conditions are identified:
- the current condition,
- the quality/workmanship,
- how the technological process proceeds,
- if the choice of design features is proper.

In this book the basics of diagnostics as applied to the identification of the class of a machine's condition and to the current assessment of changes in a machine's condition caused by operation are presented.

Monitoring as regards its purpose can be classified as monitoring of:

- symptoms,
- process parameters,
- safety parameters,
- operation parameters.

1.3. References

- [1.1] Kanczewski P.: Complex Reconstruction and Retrofitting as Practical Measure to Prolong Life of Basic Machinery (in Polish), *Górnictwo Odkrywkowe*, No. 3, pp. 1-17, 1994.
- [1.2] Bartelmus W.: Vibration Condition Monitoring of Gearboxes, *Machine Vibration*, No. 1, pp. 178-189, 1992.
- [1.3] Bartelmus W.: Application of Some Vibration Signal Statistical Estimators as Meshing Condition Assessment Criteria (in Polish), *Scientific Papers of Silesian Polytechnic, Mining*, No. 616, 1979.
- [1.4] Bartelmus W., Nosowicz B.: Relationship Between Vibroacoustic Diagnostics and Machines Design Basics (in Polish), *26th Open Seminar on Acoustics*, Wrocław-Oleśnica, 1979, Wrocław University of Technology, 1979.

- [1.5] Durst W., Vogel W.: Bucket Wheel Excavator, *Trans Tech Publications, Series on Mining Engineering*, Vol. 7, 1988.
- [1.6] Bartelmus W., Gładysiewicz L., Jonkisz J.: Pipe Conveyor Belts (in Polish), *Górnictwo Odkrywkowe*, No. 5, 1995.
- [1.7] Bartelmus W.: Acoustic Diagnostics of Negative Allowance Joints (in Polish), *Archiwum Akustyki*, No. 4, pp. 357-372, 1975.
- [1.8] Sozański L., Pelc W.: Nondestructive Testing in Monitoring of Basic Surface Mining Machinery (in Polish), *Górnictwo Odkrywkowe*, No. 3, pp. 25-30, 1987.

2. Some basic terms

The definitions provided are in many cases in a restricted form in view of the considered subject: the machine.

2.1. Basic terms in machine diagnostics

Attribute – a significant and essential feature of an object, here of a machine.

Engineering diagnostics – the identification of a machine's malfunctions on the basis of symptoms. The art of diagnosis is a skill of identifying a machine's malfunctions on the basis of symptoms. The term diagnostics is understood here as in medicine, i.e. the identification of a disease from symptoms.

Diagnosing – inferring from symptoms.

Information – each factor owing to which a receiving object (a human, a living organism, an organization, an automatic system) can improve its knowledge of the environment and perform its purposeful actions more efficiently.

Classification – a disjoint and exhaustive division of a set into subsets according to a fixed criterion.

Monitoring (**supervision, tracking**) – **the tracking of a machine's condition or a working process by means of technical devices or without them – by means of senses.**

Parameter – a physical quantity playing a significant role in a given process, a quantity characteristic of a machine.

Process – changes occurring in subsequent stages of development; a series of changes occurring in matter leading to its transformation.

Condition – the totality of factors affecting the mating of a machine's kinematic pairs (machine elements).

Symptom – a carrier of information about a machine's condition, perceived by a person making a diagnosis and indicating a malfunction in the machine; one can distinguish subjective symptoms perceived by the diagnostician and objective symptoms determined by measuring physical quantities.

Syndrome – a complex of symptoms describing the state of meshing of kinematic pairs (machine elements).

System – an internally ordered assemblage of elements, having specific structure.

Subsystem – an assemblage of functionally interdependent elements but not forming a separate whole when a product is assembled (e.g. a machine tool's hydraulic system, a car's braking system).

Information system – an organised set of means (e.g. computers, memory devices, software, transmission devices) for the acquisition, processing and transferring of information.

The definitions of the terms: **attribute**, **parameter** and **symptom** indicate that these notions have a common feature – they are expressed by physical quantities, sometimes by using our senses. The three terms are used interchangeably in this book and in the author's opinion they may facilitate understanding this text.

2.2. Basic terms in machine reliability

Breakdown (failure) – serious damage to a machine restricting its operation or making its further operation impossible.

A machine's reliability is variously understood.

A **machine's reliability** [2.1] is the probability of fulfilling by the machine the requirements imposed on it.

A **Machine's reliability** is understood as a characteristic of its ability to fulfil functions in a specific environment.

According to [2.2], a **machine's reliability** is understood as the probability⁽⁴⁾ that the object will fulfil⁽²⁾ its function⁽¹⁾ in assumed conditions⁽³⁾ for a specified time⁽⁵⁾. According to this definition, the following five notions are associated with reliability:

1. function,
2. fulfilment,
3. condition,
4. probability,
5. time.

In order to determine the reliability of an object, it is necessary to consider these five characteristics of its reliability.

Durability (life) – an object's ability to function if properly serviced; the service includes all kinds of repairs, surveys, adjustments and the replacement of elements. An object's durability can be measured by the amount of performed work which can be expressed in physical work units, work cycles, mileage or time.

2.3. Basic terms in machine maintenance

Exploitation – the winning and utilisation of natural resources.

Operation – the management and use of machines and equipment in working places.

Repair – actions taken to restore machines and equipment to operational readiness by detecting and removing any malfunctions or failures which occurred in service.

Machine maintenance strategies – three basic strategies are distinguished:

- operation until a failure,
- planned-preventive maintenance,
- maintenance dependent on a machine's condition, condition based maintenance.

2.4. Other basic terms

Design features [2.3]

Geometric design features determine the boundaries of the area occupied by the material and thus they determine the geometric structure.

Material design features determine the internal properties of structure.

Dynamic design features make it possible to determine initial loads as a material state.

Mechanical vibration – changing in time quantities, characteristic of the motion, of a mechanical system during which they become alternately larger and smaller than a certain average or reference value.

Element of a machine – an inseparable part of the latter, e.g. a shaft, a bolt, a ball, an internal ring, an external ring and a cage; the last four elements make up a rolling bearing.

Machine – an apparatus containing a mechanism or an assembly of mechanisms in a common casing, designed for converting energy or performing specific mechanical work – a working machine. From the energy point of view, machines can generate mechanical energy (at the expense of another kind of energy) – such machines are motors. Working machines consume energy. A machine in a structural sense can consist of several energy converting machines.

Mechanism – a system of interconnected machine elements which can execute specific motions as a result of the consumption of mechanical energy.

Kinematic pair – machine elements connected together in respect of motion. Rolling motion or sliding motion or the two motions simultaneously may occur between machine elements. The latter may be in point, linear or surface contact.

Physical quantity – a phenomenon's feature occurring in a machine, which is measurable, has a numerical value and a unit of measure, e.g. 10 m/s.

2.5. References

- [2.1] Reliability Handbook (in Polish), Collective Work Edited by J. Migdalski, WPM, WEMA, Warsaw, 1982.
- [2.2] BSI British Standard Institute.
- [2.3] Dietrych J. et al.: Fundamentals of Machine Design (in Polish), Part 1, 3rd Edit., WNT, Warsaw, 1969.
- [2.4] Encyclopaedia of Technology, Machine Building (in Polish), WNT, Warsaw, 1969.
- [2.5] WEBSTER'S II New Riverside University Dictionary, 1988.
- [2.6] Lexicon (in Polish), PWN, Warsaw, 1972.

3. Machine maintenance procedures

Three basic machine maintenance procedures, which follow from operation modes, are distinguished:

- operation until a failure,
- planned-preventive maintenance,
- maintenance dependent on a machine's condition, condition based maintenance.

An analysis of the three basic machine maintenance procedures can be found in [3.1]. Two of them are referred to as traditional maintenance procedures. Maintenance dependent on a machine's condition makes it possible to apply techniques of engineering diagnostics and condition monitoring.

The first (from failure to failure) machine maintenance procedure is applied to machines which are of secondary importance in a manufacturing process or when there is a failure, a reserve (duplicate) machine is used. This procedure can be used only when a failure of a machine does not cause any hazard. Under this procedure it is possible to apply diagnostic techniques to assess the condition of machines. On this basis the cause of a failure can be determined and appropriate elements necessary for the repair of a machine can be ordered in advance. Under the considered procedure one should also take into account the degradation of a machine during its service, which may lead to a failure. In some cases, a machine may be worn-out so much that the costs of repair will be very high or it will not be possible to renovate the machine fully. This problem is discussed in [3.2]. In the light of it, one cannot agree with the arguments put forward in [3.1] that during operation until a failure the full service potential of a machine's elements is used. The potential of the elements can be used fully only when a change in the condition of one of the machine's elements does not affect the operating conditions of its other elements.

If no reserve in the form of a duplicate is available and an unexpected failure may cause considerable production losses, so-called planned-preventive maintenance is usually used. This means that after a specific time, in which a machine executed its task, it is sent for repair regardless of its condition. It is known from operating practice that a machine's time of operation until a failure is a random variable characterised by a specific statistical distribution which, if known, can be used to determine the time after which the machine should be sent for repair. This time is calculated under an assumption that a certain percentage of machines may break down in a shorter time than the assumed one. But a considerable number of the machines could be in service for a longer time than the one determined from the maintenance policy referred to as

planned-preventive maintenance. This policy is not very economical and may result in losses due to the fact that some of the machines sent for repair are in good condition and could still be in service. This problem is illustrated for the roller bearing in fig. 1.4. The example shows that some of the bearings will be damaged in a shorter time than the assumed life and some of them will have a longer life than the assumed one. If a “good” machine is repaired, its serviceability may worsen as a result. Any intrusion into a machine in good condition lowers its serviceability. The question arises: “Can a machine’s condition be identified without intruding into the machine?”. According to the present knowledge, the answer to this question is yes: a machine’s condition can be identified from symptoms by means of diagnostic methods supplemented with non-destructive tests. Diagnostic and non-destructive testing enables condition based maintenance, maintenance dependent on a machine’s condition. A machine is designated for repair if its condition identified from symptoms is improper. By systematically monitoring a machine’s condition one can estimate changes in this condition and determine the right moment for sending the machine for repair and thus keep the operating costs and the machine standstill losses to a minimum (see fig. 16.23 and chap. 16).

3.1. References

- [3.1] El-haram M., Knezevic J.: Coefficient of Utilisation as Indicator of Maintenance Strategy Effectiveness, *Proceedings of 9th International Congress COMADEM’96*, Sheffield Academic Press Ltd, Sheffield, 1996.
- [3.2] Bartelmus W.: Vibration Condition Monitoring of Gearboxes, *Machine Vibration*, No. 1, pp. 178-189, 1992.

4. Introduction to mechanical vibration

4.1. Basic notions relating to vibration

Any system which has mass and elasticity is capable of vibration. Mechanical vibrations are changing in time quantities characteristic of a mechanical system's motion during which they become alternately larger or smaller than a certain average or reference value. Such characteristic quantities are, for example, displacements, velocities and accelerations of a mass as well as changing internal forces in a system, e.g. stiffness force. A case of a mechanical vibrating system in the form of a mass suspended from a spring (fig. 4.1) is considered.

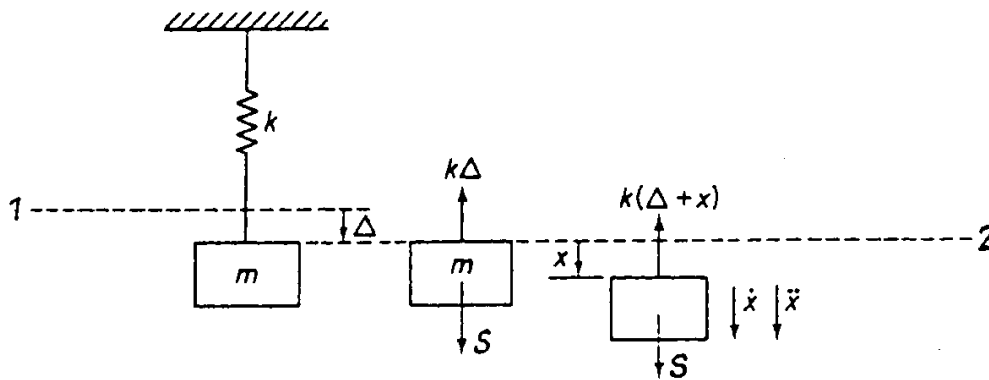


Fig. 4.1. Mass-elasticity system: 1 – length of mass-less spring, 2 – length of spring in state of static equilibrium.

Stiffness is understood as a ratio of forces S [N] to deformation x [m], i.e. $k = S/x$, [N/m]. The motion of a freely suspended mass (fig. 4.1) can be described by an equation of motion based on Newton's second law according to which inertial force $m\ddot{x}$ is equal to the sum of all forces F , both internal and external, acting on the mass:

$$m\ddot{x} = F \quad (4.1)$$

where: \ddot{x} – mass acceleration, m/s^2 ;

m – mass, kg ;

F – sum of forces, N .

For a system as in fig. 4.1.

$$m \ddot{x} = S - k(\Delta + x) = S - k\Delta - kx \quad (4.2)$$

where: S – gravity force, N ;

Δ – static deformation under gravity force S , m .

Since $S = k\Delta$, the equation of motion becomes

$$m \ddot{x} = -kx \quad (4.3)$$

Expression

$$\omega = (k/m)^{1/2} \text{ rad/s} \quad (4.4)$$

specifies the eigenfrequency/natural frequency, i.e. equation of motion (4.3) assumes this form

$$\ddot{x} = -\omega^2 x \quad (4.5)$$

The solution of the equation of motion is the following function

$$x = A \sin(\omega t), \text{ m} \quad (4.6)$$

$$dx/dt = \dot{x} = \omega A \cos(\omega t) = \omega A \sin(\omega t + \pi/2), \text{ m/s} \quad (4.7)$$

$$dx^2/dt^2 = \ddot{x} = -\omega^2 A \sin(\omega t) = \omega^2 A \sin(\omega t + \pi), \text{ m/s}^2 \quad (4.8)$$

where A is the amplitude of mass deflection, m .

The motion described above is called harmonic motion. Quantities: x, \dot{x}, \ddot{x} are shown in fig. 4.2. The plots shown in the figure are periodic functions with period T and the following relation holds for them

$$x(t) = x(t + T) \quad (4.9)$$

Fig. 4.2.

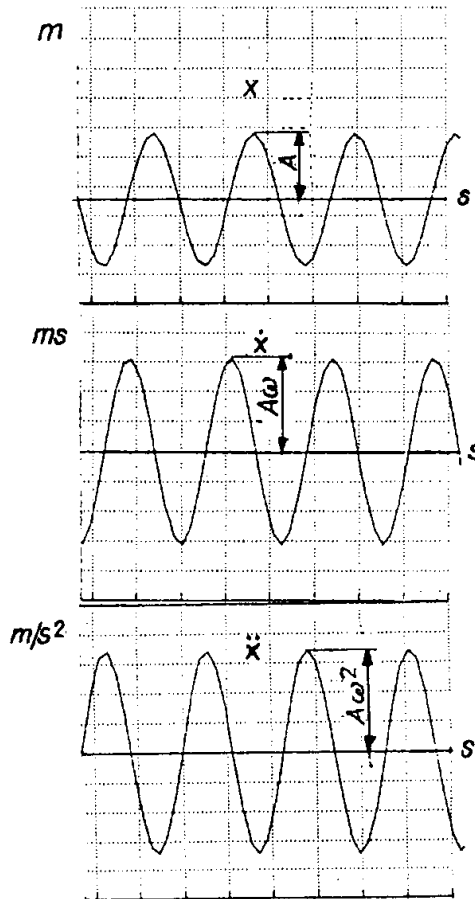


Fig. 4.2. Basic physical quantities describing harmonic vibration of a mass suspended from spring.

Period T can be determined from relationship $\omega T = 2\pi$, i.e.

$$T = 2\pi / \omega \quad (4.10)$$

The inverse of the period is called frequency

$$f = 1/T, \quad 1/s \quad (4.11)$$

If period $T = 1$ s, the object vibrates at a frequency of 1 Hz. The relationship between angular frequency and frequency is expressed by relationship $\omega = 2\pi f$, rad/s. Then for the system in fig. 4.1 we get

$$f = \omega / 2\pi = (k/m)^{1/2} / (2\pi), \quad 1/s \quad (4.12)$$

4.2. Basic physical quantities in equations of machine motion

In most cases, models of the motion of a machine are based on considerations of its rotary motion. The simplest case of rotary motion is a system consisting of one mass with inertia I [kgm^2].

The moment of inertia for a homogenous cylinder is

$$I = mr^2/2 \quad (4.13)$$

where: m – the cylinder's mass;

r – the cylinder's outside radius, m.

If torque M [Nm] acts on the cylinder and the vector of the torque is directed along the cylinder's axis, the equation of motion assumes this form

$$\ddot{\varphi} I = M, Nm \quad (4.14)$$

where: $\ddot{\varphi}$ – acceleration, rad/s^2 ;

M – torque, Nm.

Torque M can be a function of time or angular velocity $\dot{\varphi}$ [rad/s]. The mass moment of inertia for the cylinder relative to axis z (fig. 4.3) can be calculated as follows: the inertia of an elementary cylinder is

$$m_e r_i^2 \quad (4.15)$$

where: m_e – the elementary cylinder's mass, kg;

r_i – the elementary cylinder's radius, m.

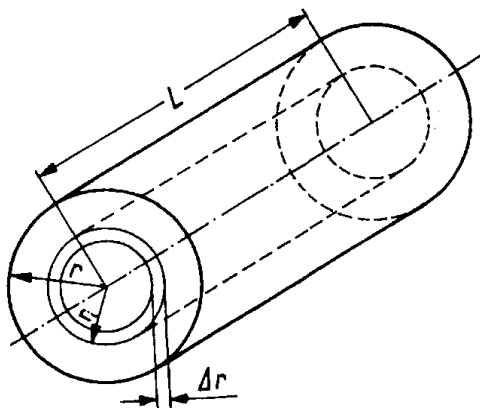


Fig. 4.1 Quantities for calculation of solid cylinder's mass moment of inertia.

The elementary cylinder's mass can be expressed as follows

$$M_e = 2\pi r_i \Delta_r l \rho \quad (4.16)$$

where: Δ_r – an elementary increment in the radius, m;
 ρ – the cylinder's density, kg/m³;
 l – the cylinder's length, m.

The total moment of inertia is equal to the sum of elementary moments of inertia. If the moment of inertia is expressed in the form of infinitely small increments dr , the value of the total moment of inertia can be expressed by this integral:

$$I = \int_0^r 2\pi l \rho r^3 dr \quad (4.17)$$

$$I = 2\pi l \rho r^4/4 \quad (4.18)$$

Since the cylinder's total mass is:

$$m_c = \pi r^2 l \rho \quad (4.19)$$

then:

$$I = m_c r^2/2 \quad (4.20)$$

This formula is often used since many machine elements subject to rotary motion are in the shape of a solid cylinder or a sleeve (a hollow cylinder) for which it is easy to calculate the mass moment of inertia as a difference between the moments of inertia.

4.2.1. Stiffness of machine elements

Machine elements are subject to deformation, e.g. under a torsional moment they undergo torsion. If a cylinder of length l [m] and diameter d [m] is twisted by torsional moment M [Nm], then the value of the torsional deflection angle by [4.1] is

$$\varphi = Ml/(GI_o), \text{ rad} \quad (4.21)$$

where: G – a shear modulus; for steel it is $8.05 \cdot 10^4$ MPa;

I_o – the geometrical moment of inertia of the cylinder's cross-section, m⁴.

The moment of inertia of the circular cross-section is determined from the following formula [4.1]

$$I_o = \pi d^4/32, m^4 \quad (4.22)$$

The expression for the torsional angle can be transformed to this form

$$\varphi = M/(GI_o/l) = M/k, \text{ rad}; k = GI_o/l, \text{ Nm/rad} \quad (4.23)$$

where k is torsional stiffness in Nm/rad.

The value of torsional moment M can be expressed as

$$M = k\varphi, Nm \quad (4.24)$$

For the assumed shape of the element (fig. 4.4), consisting of several joined cylinders twisted by torsional moment M , the torsional angles of the element's segments can be determined:

$$\varphi_1 = M/k_1, \quad \varphi_2 = M/k_2 \quad (4.25)$$

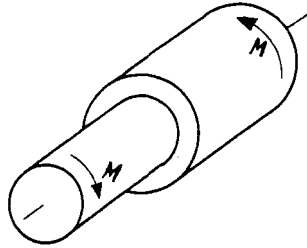


Fig. 4.1. Element with two diameters.

The total torsional angle is

$$\varphi = \varphi_1 + \varphi_2 \quad (4.26)$$

If a notion of resultant torsional stiffness k_w is introduced, the total torsional angle is

$$\varphi = M/k_w \quad (4.27)$$

then:

$$\varphi = M/k_w = M/k_1 + M/k_2 \quad (4.28)$$

From the above equation one can calculate the value of resultant coefficient k_w

$$k_w = 1/(1/k_1 + 1/k_2) \quad (4.29)$$

For any number of cylinder segments the resultant rigidity

$$k_w = 1/(1/k_1 + 1/k_2 + \dots + 1/k_n) \quad (4.30)$$

where n is a number of diameters.

4.2.2. Coefficient of longitudinal stiffness

The value of the deformation of a machine element under tension is calculated from this formula [4.1]

$$x = Pl/(EF), m. \quad (4.31)$$

where: P – the force tensioning the element/bar, N ;

l – the considered element's length, m ;

F – the element's cross-section, m^2 ;

E – a longitudinal modulus of elasticity; for steel it is $2.06 \cdot 10^5$ MPa.

The expression for elongation can have this form

$$x = P/(EF/l) = P/k, m.; \text{ where } k = EF/l, N/m. \quad (4.32)$$

where k [N/m] is a coefficient of longitudinal stiffness.

The magnitude of the force can be represented as follows:

$$P = kx, N \quad (4.33)$$

4.3. Damping of vibration

Mechanical systems which vibrate as a result of excitation are characterised by stiffness, but also by internal damping. The latter is described by a damping-coefficient-dependent damping force. The equation of motion for the system shown in fig. 4.5, when the motion is excited by force $F(t)$ and force F is a function of time t , is:

$$m \ddot{x} + F_d + kx = F(t) \quad (4.34)$$

$$F_d = C \dot{x}$$

where: F_d – a damping force, N ;

C – a damping coefficient, Ns/m .

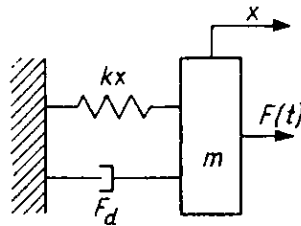


Fig. 4.1. Diagram of system with viscous damping and elasticity.

It follows from the theory of differential equations [4.2] that the general solution of the above equation is a sum of its particular solution and the general solution of the homogenous equation. If $F(t) = 0$, the following homogenous differential equation is obtained

$$m \ddot{x} + C \dot{x} + kx = 0 \quad (4.35)$$

Assuming the solution of the equation [4.2] as

$$x = e^{st} \quad (4.36)$$

where s is a constant, we get

$$(ms^2 + Cs + k)e^{st} = 0 \quad (4.37)$$

The above expression is equal to zero for all values t when

$$s^2 + Cs/m + k/m = 0$$

The above equality is called a characteristic equation. The characteristic equation has the following solutions

$$s_{1,2} = -C/2m \pm \sqrt{(C/(2m))^2 - k/m} \quad (4.38)$$

The general solution of the homogenous differential equation has this form

$$x = Aexp(s_1t) + Bexp(s_2t) \quad (4.39)$$

where A and B are constants dependent on initial conditions $x(0)$, $\dot{x}(0)$.

After substitution into the expression for x we get

$$x = e^{-(C/(2m))t} (Ae^{bt} + Be^{-bt}) \quad (4.40)$$

where

$$b = \sqrt{(C/(2m))^2 - k/m} \quad (4.41)$$

The expression

$$e^{-(C/(2m))t} \quad (4.42)$$

decreases exponentially.

The term in brackets depends on the root value, and it may be positive, equal to zero or negative. If the expression with damping $(C/(2m))^2$ is greater than k/m , the index exponent is a real number and no vibration occurs and the damping is referred to as over-damped $(C/(2m))^2 > k/m$. If $(C/(2m))^2 < k/m$, index exponents b are imaginary numbers

$$\pm i\sqrt{k/m - (C/(2m))^2} t \quad (4.43)$$

Henceforward the root expression will be denoted by a . Since

$$exp(\pm at) = \cos(at) \pm i\sin(at) \quad (4.44)$$

the expression in the bracket (4.40) is a periodic function in time and vibration occurs. Then the damping is referred to as under-damped.

Critical damping demarcates the boundary between the under-damped and over-damped damping. It occurs when the root expression is equal to zero, i.e.

$$(C/(2m))^2 = k/m = \omega_n^2 \quad (4.45)$$

When the above equality holds, damping C corresponding to critical damping is denoted by C_k . If the above relation is used, we get

$$C_k^2/(4m^2) = k/m = \omega_n^2 \quad (4.46)$$

hence

$$C_k = 2\sqrt{km} \quad (4.47)$$

$$C_k^2/(4m^2) = \omega_n^2 \quad (4.48)$$

hence

$$C = 2m\omega_n \quad (4.49)$$

It is convenient to represent the damping value in relation to critical damping, i.e.

$$\xi = C/C_k \quad (4.50)$$

The expression when divided by $2m$ assumes this form

$$C/(2m) = \xi C_k/(2m) = \xi \omega_n \quad (4.51)$$

If the above relations are substituted in the roots of the characteristic equation, we get

$$s_{1,2} = (-\xi \pm \sqrt{\xi^2 - 1})\omega_n = (-\xi \pm i\sqrt{1 - \xi^2})\omega_n \quad (4.52)$$

The solution of the equation of vibration for $\xi < 1$ (under-damped damping) assumes the following form

$$x = \exp(-\xi \omega_n t)(A \exp(i d \omega_n t) + B \exp(-i d \omega_n t)) \quad (4.53)$$

where

$$d = \sqrt{1 - \xi^2} \quad (4.54)$$

and so the frequency of damped vibration is

$$\omega_d = \omega_n \sqrt{1 - \xi^2} \quad (4.55)$$

The expression for x can be also presented in the following form

$$x = X \exp(-\xi \omega_n t) \sin(d \omega_n t + \Phi) \quad (4.56)$$

hence the frequency of damped vibration is

$$\omega_d = \omega_n d \quad (4.57)$$

The plot of value x is shown in fig. 4.6.

So far the solution of equation of motion (4.34) for $F(t) = 0$ has been presented. Considerations relating to the solution of the analytical non-homogenous equation $F(t) > 0$ are continued in chap. 4.7.

4.3.1. Logarithmic decrement

The plot of x in fig. 4.7 shows that the notion of a logarithmic decrement should be introduced. The plot in fig. 4.7 has the following analytical form

$$x = X \exp(-\xi \omega_n t) \sin(\omega_d t + \Phi) \tag{4.58}$$

for $\Phi = 0$

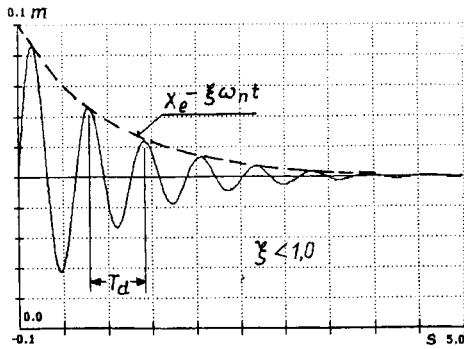


Fig. 4.1. Plot of vibration for system shown in Fig. 4.5.

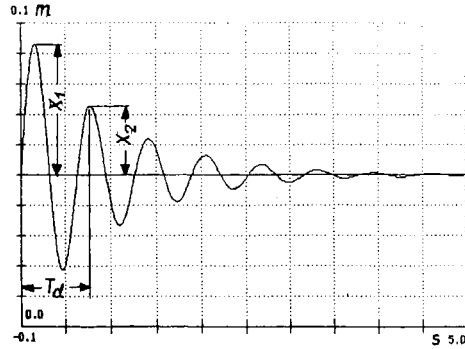


Fig. 4.2. Plot of vibration with amplitudes x_1 and x_2 .

A logarithmic decrement is defined as

$$\delta = \ln(x_1/x_2) \tag{4.59}$$

Putting values x_1 and x_2 into expressions for δ we get

$$\delta = \xi \omega_n T_d \tag{4.60}$$

$$T_d = 2\pi / \omega_d \tag{4.61}$$

hence

$$\delta = 2\pi \xi / d \tag{4.62}$$

If values x_1 , x_2 and T_d are known from the plot, then damping coefficient C can be determined on their basis; from (4.60) we calculate ξ and substitute expression (4.59) for δ

$$\xi = \delta / (\omega_n T_d) = \ln(x_1/x_2) / (\omega_n T_d) \quad (4.63)$$

knowing ξ we calculate C

$$C = \xi C_k \quad (4.64)$$

C_k is calculated from formulas (4.47) or (4.49).

The appropriate values for formula (4.63) are obtained from the graph in fig. 4.7. It is also necessary to calculate eigenfrequency ω_n . The damping coefficient is calculated also from the relations given below by introducing the notion of a time constant whereby it is not necessary to know the eigenfrequency:

$$T_x = 2m/C \quad (4.65)$$

Since

$$\ln(x_1/x_2) = \xi \omega_n T_d = C/C_k \omega_n T_d \quad (4.66)$$

After putting in $C_b = 2m\omega_n$ and transformations we get:

$$\begin{aligned} \ln(x_1/x_2) &= C/(2m)T_x \\ T_x &= T_d / \ln(x_1/x_2) \end{aligned} \quad (4.67)$$

hence

$$C = 2m/T_x \quad (4.68)$$

The appropriate values to be put in (4.67) are obtained from fig. 4.7. Belt damping coefficient C can be determined without knowing stiffness coefficient k .

4.3.2. Investigation of damping coefficient

A system such as the one shown in fig. 4.8 can be used to investigate the damping coefficient. There are two masses m_d and m_o for which the gravity forces are:

$$S_o = (m_d + m_o)g \quad (4.69)$$

$$P_o = m_o g \quad (4.70)$$

where $g = 9.81 \text{ m/s}^2$ is gravitational acceleration.

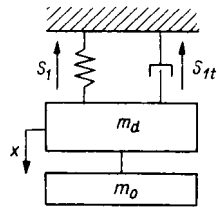


Fig. 4.1. Diagram of system for testing belt properties (damping).

The system is initially loaded with gravity force S_o , then mass m_o detaches itself and the system is excited to vibration accompanying the transition from the state of initial equilibrium to a state in which the system is loaded with gravity force $S_o - P_o$.

If it we assume that the initial state lasts for $t \leq 1$ s, due to the system's elasticity the specimen will deform by $x = S_o/k$. The equation of motion for the system for $t \leq 1$ s is as follows

$$(m_d + m_o) \ddot{x} = S_o - (S_I + S_{It}) \quad (4.71)$$

$$S_I = kx \quad (4.72)$$

$$S_{It} = C \dot{x} \quad (4.73)$$

The system will be in a state of equilibrium, no motion will occur since $S_o = S_I$ and if there is no motion, $S_{It} = 0$. For $t > 1$ the equation of motion has this form

$$m_d \ddot{x} = S_o - P_o - (S_I + S_{It}) \quad (4.74)$$

Since the gravity forces and force S_I which was originally generated (for $t \leq 1$ s) do not balance, the system will be excited to vibration if damping is below critical. For specific data: $k = 1.767 \cdot 10^6$, $m_d = 581$ kg, the value of critical damping is

$$C_k = 2(km_d)^{1/2} = 2(1.767 \cdot 10^6 \cdot 581)^{1/2} = 6.4082 \cdot 10^4, \text{ Ns/m.} \quad (4.75)$$

For the assumed parameters the critical damping is $C_k = 6.4082 \cdot 10^4$.

Computer simulations of the system's behaviour were run for different damping values: $C = 6.4082E4$, 5000, 200000 Ns/m. The results of the simulations are presented in figures:

Fig. 4.9 shows plots of the system gravity force; the cause of vibration: a jump in the force (a change in force S_o by P_o) is visible. The change in the gravity force results from the cut off of mass m_o .

Fig. 4.10. shows the deflection (vibration) of the mass at damping coefficient $C = 5000$ Ns/m, i.e. for under-damped damping.

Figs 4.11 a and b show the deflection of the mass for critical damping $C = 6.4082E4$ Ns/m.

Fig. 4.11 b shows the plot for an extended time scale.

Fig. 4.12. shows the plot of damped vibration when damping C exceeds considerably the value of critical damping, $C = 200000$ Ns/m.

Fig. 4.13 shows no damped vibration, $C = 0$.

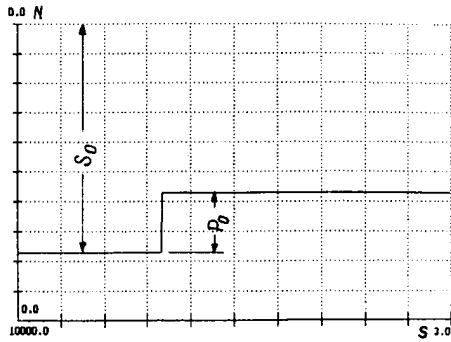


Fig. 4.2. Plot of gravity forces.

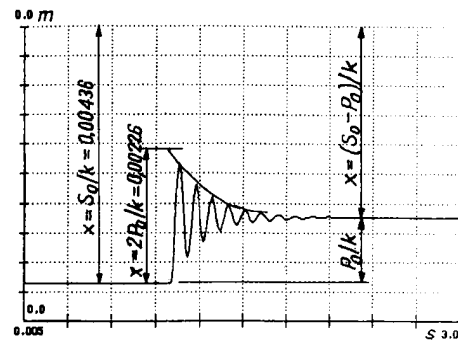


Fig. 4.3. System response to abrupt excitation.

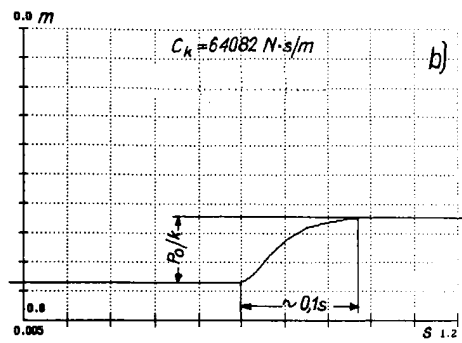
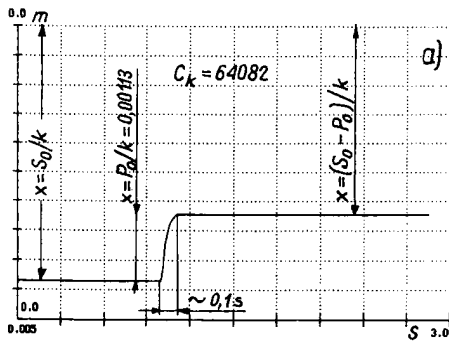


Fig. 4.4. System response to abrupt excitation at critical damping: time scale in fig. (b) extended relative to that in fig. (a).

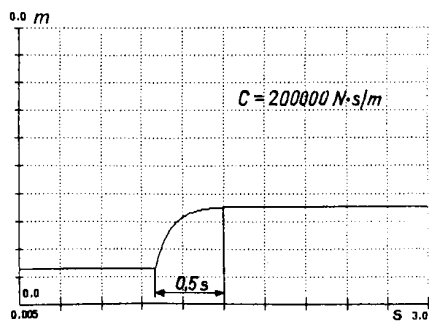


Fig. 4.5. System response at over-damped damping.

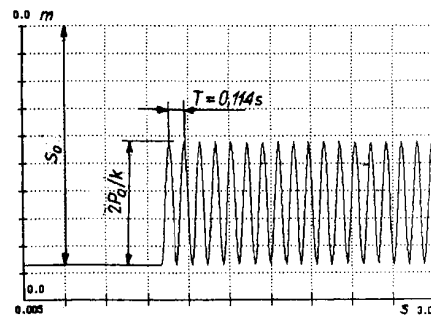


Fig. 4.6. System response at no damping (free vibration).

4.3.3. Free vibration of suspended mass

The deflections of the mass at free vibration $C = 0$ are shown in fig. 4.13. Fig. 4.14 shows a plot for 1 s in a range of 1-2 s and figs 14a, b and c show respectively plots of deflection, velocity and mass acceleration. The acceleration which the mass undergoes for $t = 1$ s is

$$-P_o = m_d a \quad (4.76)$$

hence

$$a = -P_o/m_d = -2000/580 = -3.45 \text{ m/s}^2 \quad (4.77)$$

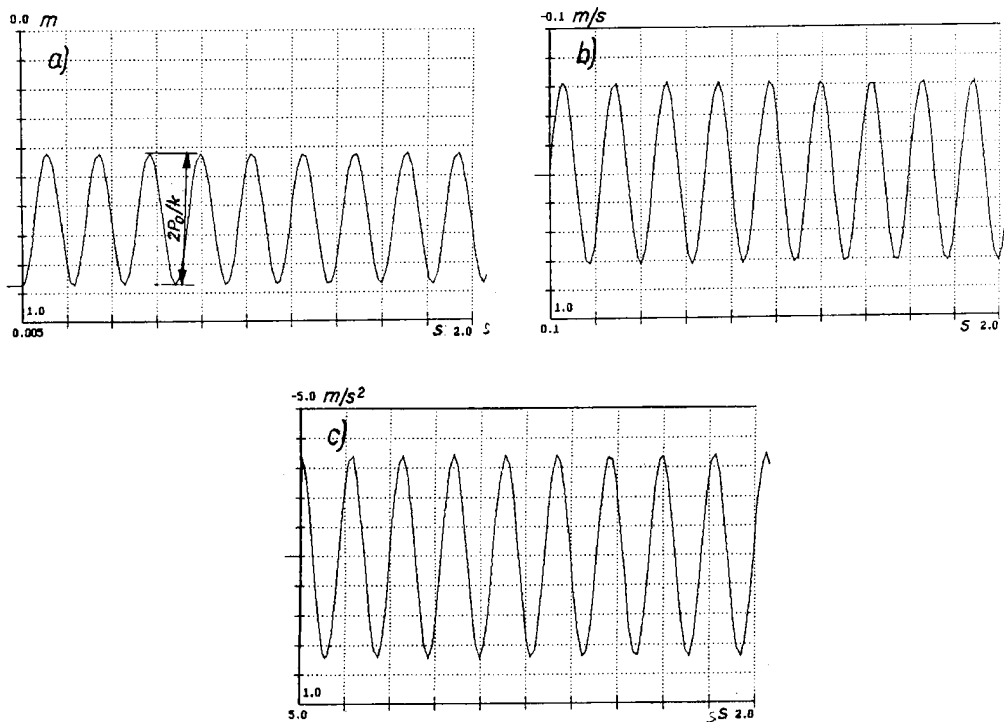


Fig. 4.1. Comparison of plots of basic physical quantities for free vibration: a – mass displacement, b – mass velocity, c – mass acceleration.

The calculated acceleration is the initial acceleration and since the vibration is free, the absolute value of this acceleration is an amplitude of changes in acceleration as shown in fig. 4.14c. Fig. 4.14 shows also phase shifts between the particular plots of the physical quantities, which is expressed by formulas (4.6), (4.7) and (4.8).

4.4. Introduction to equations of machine motion

The system which a machine constitutes is characterised by elasticity and mass so it vibrates. Thus the system shown in fig. 4.15 loaded with variable moment $M(t)$ executes rotational motion with vibration. Equations of motion for such a system are as follows

$$I_1 \ddot{\varphi}_1 = M(t) - M_1 \quad (4.78)$$

$$I_2 \ddot{\varphi}_2 = M_1 \quad (4.79)$$

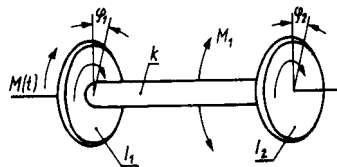


Fig. 4.1. System in rotational motion for two inertias joined by stiffness.

The shaft inner torsional moment is

$$M_1 = k(\varphi_1 - \varphi_2) \quad (4.80)$$

where: k – a coefficient of torsional stiffness, Nm/rad, calculated from relation (4.23);

$\ddot{\varphi}_1, \ddot{\varphi}_2$ – angular acceleration of mass 1 and 2, rad/s²;

φ_1, φ_2 – torsional angle of the masses, rad.

The above applies also to the system shown in fig. 4.16 (the system executes translational motion). The equations of motion for a system executing translational motion and vibrating are as follows:

$$m_1 \ddot{x} = P(t) - S \quad (4.81)$$

$$m_2 \ddot{x} = S \quad (4.82)$$

where: $P(t)$ – an external force moving the system, N;

m_1, m_2 – the moved masses, kg.

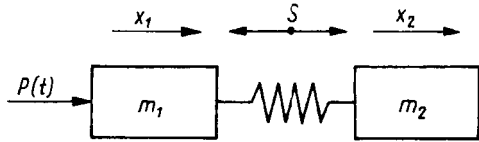


Fig. 4.2. Two-mass vibratory translational motion system with its masses joined by elasticity.

Force S can be determined from the following relation

$$S = k(x_1 - x_2) \tag{4.83}$$

where: k – longitudinal coefficient of stiffness, N/m, calculated from relation (4.32).

Mechanical systems have a vibration damping ability (this was discussed in chap. 4.3). Viscous damping is proportional to vibration velocity. A coefficient of viscous damping is defined as a ratio of a force necessary for a displacement to the velocity produced by this force.

$$C = S_v / \dot{x} \tag{4.84}$$

The damping force in a system as in fig. 4.17 is determined from this relation

$$S_t = C(\dot{x}_1 - \dot{x}_2) \tag{4.85}$$

where C is a viscous damping coefficient, N · s/m.

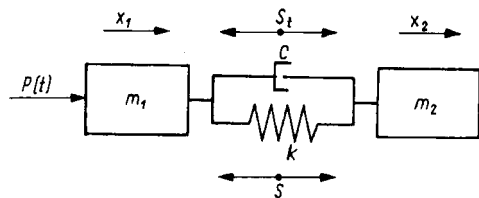


Fig. 4.3. Two-mass vibratory system joined by damping and elastic element.

Equations of motion for a more complex system are shown in fig. 4.18. They are as follow

$$m_1 \ddot{x}_1 = P(t) - (S + S_t) \tag{4.86}$$

$$m_2 \ddot{x}_2 = S + S_t \tag{4.87}$$

where S and S_t are as given above.

The equations of motion for a more complex system are shown in fig. 4.18. They are as follows:

$$m_1 \ddot{x}_1 = P(t) - (S_1 + S_{1t}) \tag{4.88}$$

$$m_2 \ddot{x}_2 = (S_1 + S_{1t}) - (S_2 + S_{2t}) \tag{4.89}$$

$$m_3 \ddot{x}_3 = S_2 + S_{2t} \tag{4.90}$$

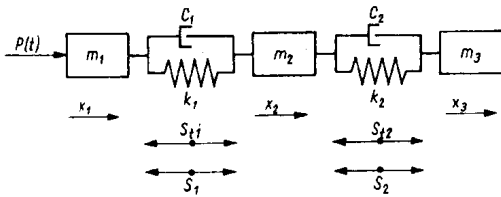


Fig. 4.4. Three-mass vibratory system joined by elastic and damping elements.

The elastic forces and the damping forces are as follows:

$$S_1 = k_1(x_1 - x_2) \tag{4.91}$$

$$S_2 = k_2(x_2 - x_3) \tag{4.92}$$

$$S_{1t} = C_1(\dot{x}_1 - \dot{x}_2) \tag{4.93}$$

$$S_{2t} = C_2(\dot{x}_2 - \dot{x}_3) \tag{4.93a}$$

Besides viscous damping, dry friction forces may occur in a mechanical system, damping its vibration. A system in which a friction force occurs besides an stiffness force and viscous damping is shown in fig. 4.19. The equation of vibration for the system can be given the following form

$$m \ddot{x} = F(t) - S - S_f - TS(\dot{x}) \tag{4.94}$$

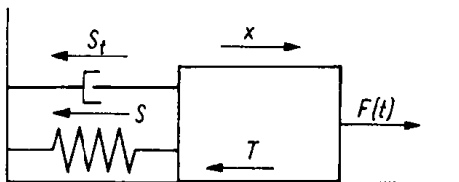


Fig. 4.5. One-mass vibratory system with viscoelastic properties and dry-friction damping.

The elastic force is

$$S = kx \tag{4.95}$$

The viscous damping force is

$$S_t = C \dot{x} \tag{4.96}$$

The dry friction force is

$$T = \mu P_n = \mu mg \tag{4.97}$$

where: μ – a coefficient of friction,

P_n – a normal to motion direction force originating from the body's weight, N,
 g – gravitational acceleration, m/s².

The friction force is oppositely directed to the motion. To take this phenomenon into account, function $S(\dot{x})$ having these properties:

if $\dot{x} > 0$, then $S(\dot{x}) = 1$

$$\text{if } \dot{x} = 0, \text{ then } S(\dot{x}) = 0 \tag{4.98}$$

if $\dot{x} < 0$, then $S(\dot{x}) = -1$

was introduced.

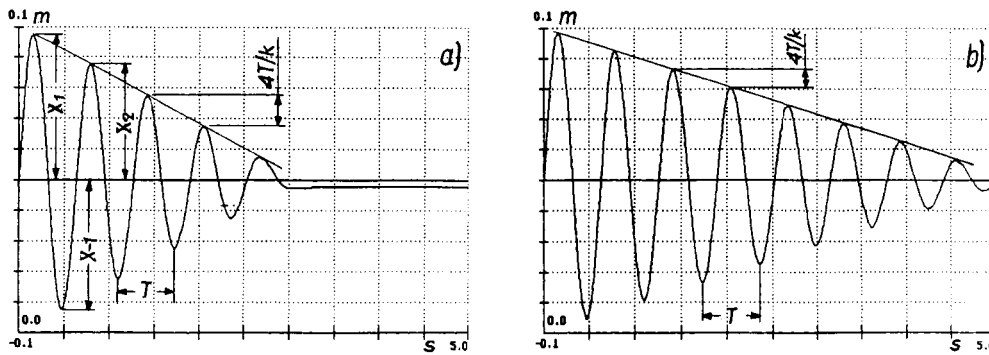


Fig. 4.6. Traces of displacement amplitude reduction for dry friction damping: a) friction force $T = 5\text{N}$,
 b) friction force $T = 3\text{N}$

If the system shown in fig. 4.19 is excited to vibration and friction damping of the vibration occurs, then the physical quantities describing the vibration will decay as shown in fig. 4.20 where plots of mass deflection for different friction force values are presented. The decrease in amplitude in time for dry friction damping of vibration is

linear. The magnitude of a change in vibration amplitude per one period can be determined from the energy conservation law. The energy contained in the spring at its maximum deflection is $E_p = kX^2/2$, the velocity of the mass at the maximum deflection is equal to zero (fig. 4.2) and the system's kinetic energy is equal to zero. During the damping of vibration the amplitude changes in the middle of the period from X_1 to X_{-1} , as shown in fig. 4.20. A change in the system's energy after half of period T [s] is $k(X_1^2 - X_{-1}^2)/2$. The energy change is used up for friction work that amounts to $T(X_1 + X_{-1})$ where T [N] is the friction force. A comparison of the change in potential energy in the spring with the friction work shows that the change in amplitude in the middle of the vibration period is $X_1 - X_{-1} = 2T/k$, i.e. the change in vibration amplitude in the whole period is twice larger and it amounts to $X_1 - X_2 = 4T/k$ (fig. 4.20a and b).

When vibration is damped by viscous friction, the vibration amplitude decay is non-linear (fig. 4.21a and b). A plot of mass deflection and a plot of forces $S + S_t$ are shown respectively in fig. 4.21a and fig. 4.21b. Impulse force $F(t) = 1000$ N was applied to excite the vibration, the force action time was 0.01 s, coefficient of stiffness $k = 1000$ N/m, mass $m = 10$ kg, friction force $T = 5$ N or 3 N, damping coefficient $C = 0$ (fig. 4.20a and b) or $T = 0$ and $C = 15$ N · s/m (fig. 4.21).

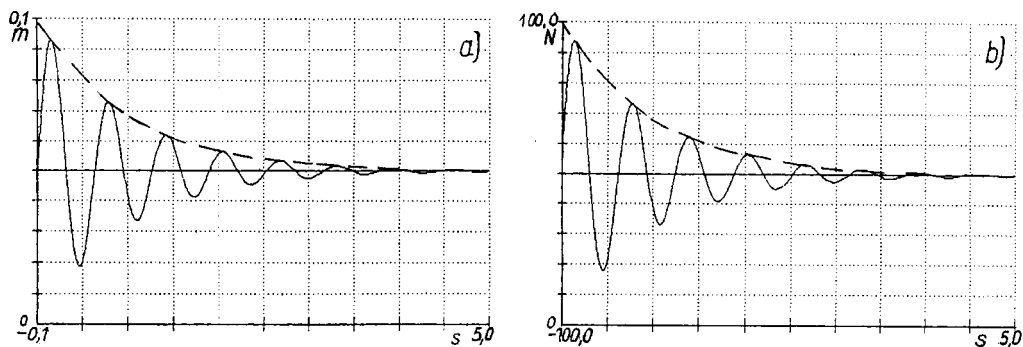


Fig. 4.7. Viscous-friction damping of vibration: a – displacement, b – sum of stiffness forces and damping.

4.5. Analysis of dynamics of simple machine system

Correct diagnostic inference from a vibration signal requires knowledge of the dynamic properties of the diagnosed objects. The basic properties of a mechanical system excited to vibration and damped were presented in chap. 4.1–4.4. According to

[4.3], [4.4], [4.5], the dynamic properties of machines are determined by four groups of factors:

- design factors,
- production technological factors,
- operating (motion) factors,
- condition change factors.

The factors are presented in detail in fig. 1.5. and they are discussed in the different chapters.

The dynamic range of the properties describing an object depends on the mathematical model used. In this chapter a simple physical model of the machine and a mathematical model (based on the physical model) for computer simulation are used. The physical model is shown in fig. 4.22. It consists of two inertias joined by torsional elasticity k [Nm/rad] and viscous damping C [Nms/rad]; one can say that it is a two-parameter (k, C) model.

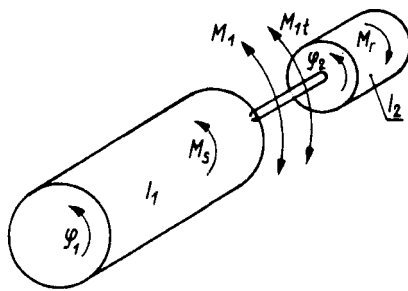


Fig. 4.1. Elementary physical model of machine.

The inertia of the motor's rotor is represented by I_1 . The inertia of the other machine elements executing rotational motion is reduced to inertia I_2 . Depending on the dynamic model's configuration, it becomes necessary to reduce the masses from rotational motion to translational motion and vice versa and to reduce the inertias rotating at different angular velocities ω . When modelling belt conveyors, the inertias of the {idlers}runners (in rotational motion) are reduced to translational motion and to the runners' reduced mass and then added to the mass of the belt and the winning. The new dynamical system resulting from the mass reduction must be equivalent to the original system. Two mechanical systems are equivalent when their energy does not change as a result of the conversion from one system to the other. If the runner rotates at angular velocity ω , its kinetic energy is

$$E_k = I_k \omega^2 / 2 \quad (4.100)$$

where: I_k – the mass moment of runner inertia, $\text{kg} \cdot \text{m}^2$,

ω – a runner angular velocity, rad/s;

E_k – a runner kinetic energy, J.

If the belt moves at velocity v [m/s], the sought runner reduced mass has the following kinetic energy

$$E_k = m_{sz}v^2/2 \quad (4.101)$$

By comparing the kinetic energy of rotational motion and that of translational motion one can determine the sought reduced mass. After putting in relation $v = \omega r$ we get

$$m_{sz} = I_k/r^2 \quad (4.102)$$

After units are put in the expression we get:

$$m_{sz}[\text{kgm}^2/\text{m}^2] = m_{sz}[\text{kg}]$$

which means that, as expected, the sought quantity has a mass dimension.

Another example of the reduction of masses is the system shown in fig. 4.23. The denotations of the mass moments of inertia of the elements are given in fig. 4.23. The equality of the kinetic energy of the reduced system and that of the system before reduction is expressed by this formula

$$I_{sz}\omega_1^2/2 = (I_1\omega_1^2 + I_2\omega_2^2 + I_3\omega_2^2 + I_4\omega_3^2)/2 \quad (4.103)$$

hence

$$I_{sz} = (I_1\omega_1^2 + I_2\omega_2^2 + I_3\omega_2^2 + I_4\omega_3^2)/\omega_1^2 \quad (4.104)$$

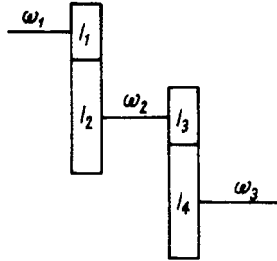


Fig. 4.2. Schematic of two-stage gear.

A simplified characterisation of the motor was adopted for simulation tests. M_s stands for the electric motor's driving torque which is a function of rotational speed $\dot{\varphi}_1$, i.e. the torque supplied by the electric motor can be written as $M_s(\dot{\varphi}_1)$; this quantity describes a motor characteristic whose simplified model is shown in fig. 5.3c. The simplified characteristic can be expressed analytically as follows: if $n_1 = 980$ rev./min. and the synchronous rotational speed is $n_s = 1000$ rev./min., then the corresponding angular velocities are

$$\dot{\varphi}_1 = \pi 98/3; \dot{\varphi}_1 = \pi 100/3 \quad (4.105)$$

If it is further assumed that the motor's maximum torque is twice as high as the rated torque, then $M_s(\dot{\varphi}_1)$ in interval $[0, \dot{\varphi}_1]$ is

$$M_s(\dot{\varphi}_1) = 2M_n \quad (4.106)$$

and for $\dot{\varphi} > \dot{\varphi}_1$

$$M_s(\dot{\varphi}_1) = 2M_n(\pi 100/3 - \dot{\varphi}_1)3/(2\pi) \quad (4.107)$$

As mentioned before, the system which a machine constitutes can be reduced to a system shown in fig. 4.22. According to the principles given in chap. 4.4, the equations of motion for the system are as follows (the same notation as in fig. 4.22):

$$I_1 \ddot{\varphi}_1 = M_s(\dot{\varphi}_1) - M_1 - M_{1r} \quad (4.108)$$

$$I_2 \ddot{\varphi}_2 = M_1 + M_{1r} - M_r \quad (4.109)$$

$$M_1 = k(\varphi_1 - \varphi_2) \quad (4.110)$$

$$M_{1r} = C(\dot{\varphi}_1 - \dot{\varphi}_2) \quad (4.111)$$

M_r is the machine's external load torque.

4.5.1. Effect of changes in external load

The operating (motion) factors include the effect of an external load, particularly that of changes in external load M_r . The function of changes in the external load is shown in fig. 4.24. The function is periodic. A relative value of the period was assumed in an interval of $[0, 1]$. Function M_r (fig. 4.24) can be written in the form of linear functions in two intervals. According to fig. 4.24, in interval $[0, p_w]$

$$M_r = M_n w/p_w \text{ aux}_1 + M_n = M_n(w/p_w \text{ aux}_1 + 1) \quad (4.112)$$

where: w – an overload factor for the external load, $(0 - 1)$;

p_w – a maximum load entrance coefficient,

aux_1 – an auxiliary value.

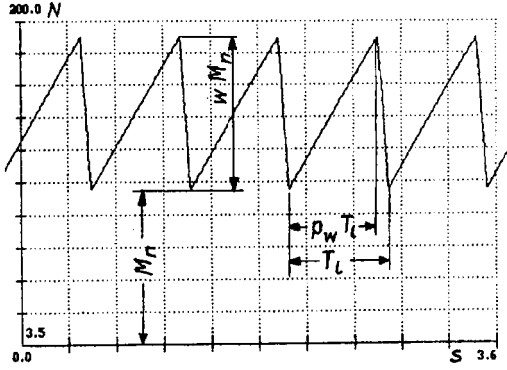


Fig. 4.1. Machine's external load originating from its cutting tool.

The auxiliary value can be determined in the following way:

$$aux_1 = \text{frac}(\varphi / okr) \quad (4.113)$$

$$okr = 2\pi / l_o \quad (4.114)$$

where: l_o – a number of, e.g., cutting edges in a tool;

φ – an angle of rotation of the tool, rad.

In interval $(p_w, 1]$

$$M_r = M_n w (aux_1 - 1) / (1 - p_w) + M_n = M_n (1 - w (aux_1 - 1) / (1 - p_w)) \quad (4.115)$$

Coefficients: w , p , p_w describing the variation of the load can be given a random character. The variation of coefficient w can be defined as follows

$$w(\text{variable}) = [1 - r(1 - l_i)]w \quad (4.116)$$

where: w – a maximum variation value, range $w(0 - 1)$;

r – a variation range coefficient, range $r(0 - 1)$;

l_i – a random value, range $(0 - 1)$.

For example, if $l_i = 1$ and $r = 1$, then $w(\text{variable}) = [1 - 1(1 - 1)]w$; when $l_i = 0$ and $r = 1$, then $w(\text{variable}) = [1 - 1(1 - 0)]w = 0$. This means that $w(\text{variable})$ varies from 0 to 1 for $r = 1$; in the case when $r = 0.5$, $w(\text{variable})$ assumes values from $w(\text{variable}) = 0.5$ to 1, when $w = 1$. Value l_i is selected once per a load variation period. Coefficient p_w can be given a similar random character

$$p_w(\text{variable}) = [1 - r_p(1 - l_i)]p_w \quad (4.117)$$

An exemplary plot of the variable load is shown in figs 4.24, 4.25 and 4.26a. The plot was obtained for $w = 1$, $r = 0.5$, $p_w = 0.9$ (fig. 4.26a). To describe the variation of the external load, the following symbolic notation: $M_r(w; r, p_w; r_p; k_r)$ was used [4.6]. The particular coefficients were defined above, except for coefficient k_r . Coefficient $k_r = T_r / T$ where T_r is a load variation period and T is an error repetition period for a diag-

nosed element. For the plots presented in figs 4.24 and 4.26a the symbolic notation for changes in the external load is as follows: $M_r(1; 0; 0.9; 0; 0)$; $M_r(1; 0.5; 0.9; 0; 0)$. Value k amounts to zero when this coefficient is not taken into account.

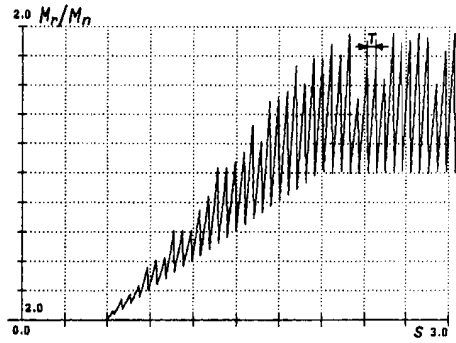


Fig. 4.2. Plot of relative external load torque.

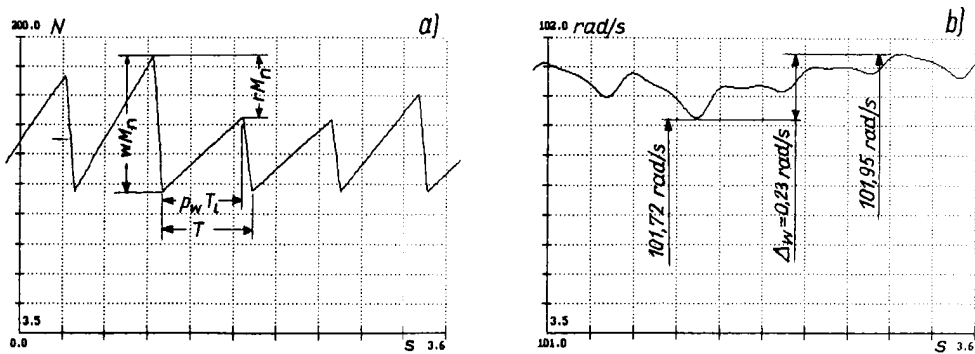


Fig. 4.3. a – fragment of load plot, b – fragment of angular velocity plot.

The properties of the dynamical system were investigated by means of computer simulation. The synchronous angular velocity for a system with ratings such as those of the motor was $\omega_s = \dot{\phi}_s = 104.7 \text{ rad/s}$. The plot of motor angular velocity $\dot{\phi}_1$ variation in a range of 0-110 rad/s is shown in fig. 4.27. The motor operates loaded with only inertial forces for 0-1.8 s, it runs idle in time range $t = 1.8 - 2.2 \text{ s}$, then the rotational speed decreases in range $t = 2.2 - 2.8 \text{ s}$ and for $t > 2.8 \text{ s}$ the motor runs loaded with torque $M_r(1; 0; 0.9; 0; 0)$ – in brackets the load described by parameters $(w; p_w)$, $w = 1; p_w = 0.9$ is given. The fluctuation of the electric motor's rotational speed (inertia I_J) is shown in fig. 4.28.

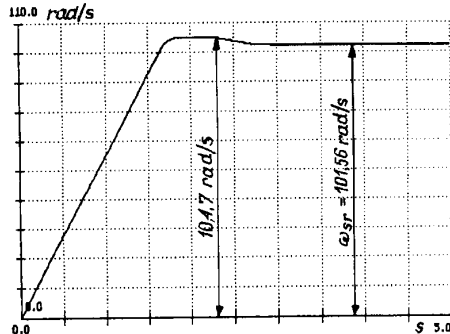


Fig. 4.4. Plot of driving motor rotor angular velocity.

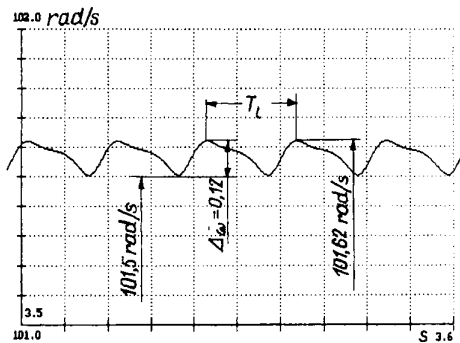


Fig. 4.5. Rotor angular velocity fluctuation due to regular variation in load.

The simulation covers 0.1 s and an angular velocity fluctuation range of about 0.12 rad/s. Fig. 4.25 shows a plot of load increment with fluctuations (a fragment of the external load plot for the fixed parameters). Fig. 4.24 is for $t > 2.8$ s. Variation in load M_r when $r = 0.5$ is shown in fig. 4.26a and the rotor angular velocity fluctuation (the fluctuation range is 0.23 rad/s) under these load conditions is shown in fig. 4.26b.

4.6. Unbalance forces, principles of balancing

Unbalance in rotating machines is frequently a source of vibration. The dynamics of motion of a system in which an unbalance occurs will be considered for the system shown in fig. 4.29. Vibration limited to the vertical direction is assumed. An unbalance is caused by unbalance mass m [kg] shifted by value e [m] relative to the centre of rotation. Mass m on arm e rotates at constant angular velocity ω [rad/s]. If x is a displacement of a no rotating part of mass M from the position of static equilibrium, then the displacement of mass m is

$$x + e \sin(\omega t) \quad (4.118)$$

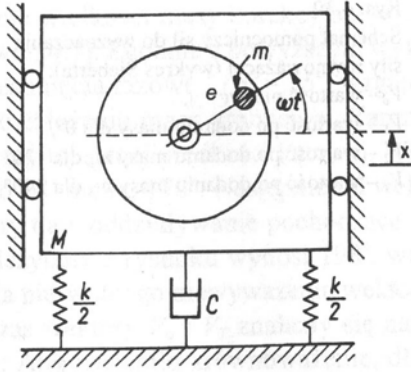


Fig. 4.1. Diagram of mechanical system excited to vibration by unbalance mass.

The equation of motion assumes this form

$$(M - m)\ddot{x} + m\frac{d^2}{dt^2}(x + e\sin(\omega t)) = -kx - C\dot{x} \quad (4.119)$$

where: kx – a stiffness force, N;

$C\dot{x}$ – a viscous damping force, N · s/m.

After transformations we get

$$M\ddot{x} = me\omega^2 \sin(\omega t) - kx - C\dot{x} \quad (4.120)$$

The amplitude of the unbalance force is $F_w = me\omega^2$. The force changes periodically with frequency ω .

To eliminate the unbalance, mass m_1 equal to the unbalance mass should be fixed on the opposite side on arm e_1 equal to arm e . Then unbalance forces originating from mass m and m_1 shall balance each other. In practice the magnitude of the unbalance mass, its action arm and its position are unknown. Only the effects (vibration) produced by the force resulting from the unbalance can be determined. Since the force is periodic with frequency ω , it produces vibration which can be measured via displacement vibration amplitude, velocity and acceleration. A phase shift occurs between these physical quantities (fig. 4.2) and their amplitudes are proportional to one another – expressions (4.6) to (4.8). They are also proportional to the unbalance force. By measuring one of the physical quantities which describe the vibration one can determine the quantity proportional to the unbalance force value.

The balancing procedures described below are applied only when there is no other possibility of balancing, e.g. by means of a balancing machine. Balancing will take place in the disk's or the rotor's bearings. To determine the value of the mass counterbalancing, the unbalance force and its location, one can use the Siebert diagram (fig. 4.30), courtesy of [4.7]. To draw the diagram, a measurement of, e.g. vibration dis-

placement amplitude V_o , is made. An instrument with a turn-able filter, set to vibration frequency $f = \omega/(2\pi)$, can be used for this purpose.

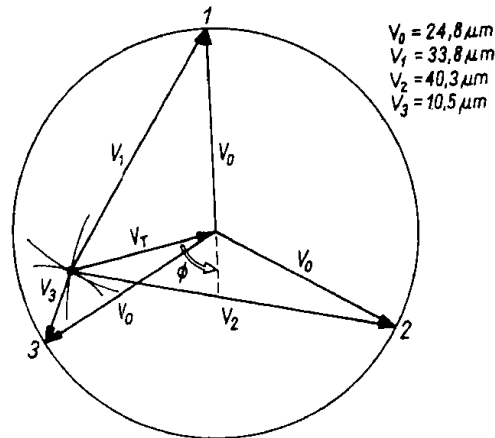


Fig. 4.2. Diagram for determining equilibrant of forces (Siebert diagram):

V_o – primary value,
 V_1 – value after addition of mass for 0° ,
 V_2 – value after addition of mass m_p for 120° ,
 V_3 – value after addition of mass m_p for 240° .

Three positions spaced at every 120° are marked on a prescribed radius on the unbalanced disk. The positions are denoted as 1, 2, 3 in fig. 4.30. They are located on a circle proportional to vibration displacement value V_o . Three measurements of the amplitude of the vibration caused by the primary unbalance and test mass m_p , located in three consecutive places spaced at every 120° at a constant distance from the axis of rotation are needed to determine the value of the corrective mass. Vibration displacement amplitudes, denoted respectively as V_1 , V_2 , V_3 , can be determined for three consecutive mass positions and three consecutive runs. On the chart in fig. 4.30 arcs proportional to the given values are drawn and a common point of their intersection is found. The point specifies the length of the unbalance vector resulting from the action of test mass m_p . Vectors V_1 , V_2 , V_3 are sums of the vectors originating from the primary imbalance V_o and unbalance vector V_T resulting from the action of the test mass, as shown in fig. 4.30. If the values of the test mass and vectors V_o and V_T are known, the corrective mass value can be calculated from

$$m_k = m_p V_o / V_T \quad (4.121)$$

The place where the corrective mass should be attached is specified by angle ϕ (fig. 4.30). The corrective mass will produce an unbalance force oppositely directed (and equal) to the primary unbalance force, as shown in fig. 4.30. Four amplitude value measurements for four runs were needed to determine the test mass and its position.

In practice another method of measurement is used. To balance a disk *in situ*, a stroboscopic tube, a turn-able band-pass filter set to the disk's revolution frequency and a meter for measuring vibration (the amplitude of displacement, velocity or accel-

eration) and the phase angle are employed. The phase angle can be measured by affixing an angular scale to the balanced element. The scale is lighted by the stroboscope actuated by a filtered vibration signal. If the meter can measure the phase, a non-contact tachometer sensor, which can be actuated by any point marked on the balanced disk, is used. The procedure of searching for the corrective mass value and the point of application of the mass consists of the following operations. Vibration amplitude V_o and phase angle α_o (relative to any fixed point on the object) are measured. The principle of determining the value of corrective mass m_k illustrates fig.4.31 made in scale, based on [4.7]. In this way vibration amplitude $V_o = 15 \text{ mm/s}$ and phase shift $\alpha_o = 55^\circ$ were measured relative to the reference point. The second measurement was made for test mass m_p . Again the disk was set into rotational motion at the same angular velocity. Amplitude V_i and angle α_i amounted to respectively 18 mm/s and 170° . Then vector V_o was subtracted from vector V_i and vector V_T was obtained. The latter represents the reaction from test mass m_p . The angle (read out from the figure) at which this vector is situated relative to the reference point is 198° . To balance the initial unbalance, vector V_T was additionally rotated by an angle of 37° (fig. 4.31). Then vectors V_o and V_T aligned but were oppositely directed. In order to achieve balance, the vectors' lengths must be so matched that the vectors are equal. The compensating vector will be produced by a compensating mass whose value can be calculated from formula (4.19).

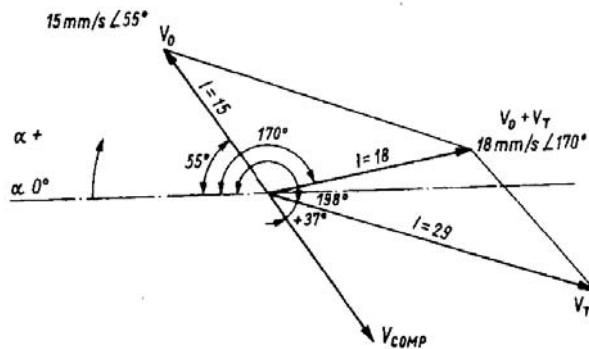


Fig. 4.3. Auxiliary diagram for determining balancing force.

This procedure can be applied to the dynamic balancing of disks. Rotors must be balanced dynamically in two planes. An amplitude and phase measuring system is used for this purpose. The amplitude is measured at two points on the rolling bearings' supports. The vibration velocity amplitudes representing the original state of unbalance, vectors $V_{1,0}$ and $V_{2,0}$ and the corresponding angles of phase shift relative to the reference points are measured. The vectors are shown in fig. 4.32. Then test mass m_{p1}

is attached at any place in plane 1 and influence vectors of the combined action of unbalance and test mass m_{p1} : $\mathbf{V}_{1,0}$ in plane 1 and $\mathbf{V}_{2,0}$ are obtained. The vectors, including the direction of their influence, are marked in fig. 4.32. After second test mass m_{p2} is attached, the combined action of the unbalance mass and test mass m_{p2} in plane 1 – vector $\mathbf{V}_{1,2}$ and in plane 2 – vector $\mathbf{V}_{2,2}$ is measured. The vectors of these influences are shown in fig. 4.32 where vectors of the following vector differences can be read out:

- $\mathbf{V}_{1,1} - \mathbf{V}_{1,0}$ – the vector of influence of mass m_{p1} at measuring point 1;
- $\mathbf{V}_{1,2} - \mathbf{V}_{1,0}$ – the vector of influence of mass m_{p2} at measuring point 1;
- $\mathbf{V}_{2,1} - \mathbf{V}_{2,0}$ – the vector of influence of mass m_{p1} at measuring point 2;
- $\mathbf{V}_{2,2} - \mathbf{V}_{2,0}$ – the vector of influence of mass m_{p2} at measuring point 2.

The original unbalance mass influence vectors and the influence vectors for the test masses are shown separately in fig. 4.32. To achieve balance, the corrective mass values must be matched and located in such places that the test mass unbalance vectors coincide with the direction of the original unbalance vector.

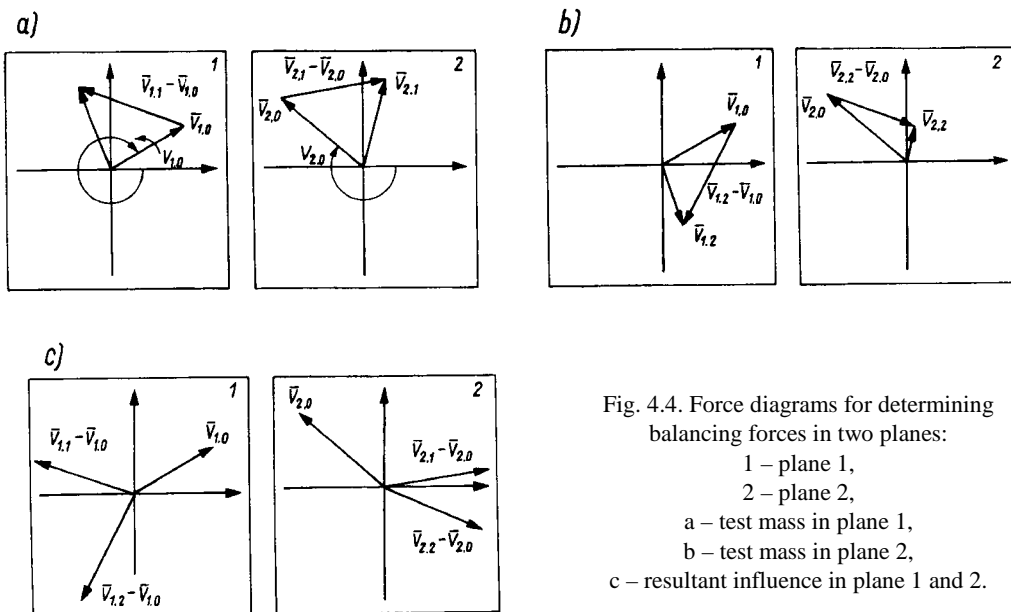


Fig. 4.4. Force diagrams for determining balancing forces in two planes:
 1 – plane 1,
 2 – plane 2,
 a – test mass in plane 1,
 b – test mass in plane 2,
 c – resultant influence in plane 1 and 2.

The corrective mass values for plane 1 and 2 are calculated from the following formulas:

$$m_{kl} = V_{1,0}/V_{1,1} - V_{1,0} + V_{1,0} m_{p2}/V_{1,2} - V_{1,0} \quad (4.122)$$

$$m_{k2} = V_{2.0}/V_{2.1} - V_{2.0} + V_{2.0} m_{p2}/V_{2.2} - V_{2.0}$$

To recapitulate, the balancing of rigid elements includes: the balancing of disks (fig. 4.33a) and the balancing of rotors where the unbalance forces form a couple of forces (fig. 4.33b). The unbalance forces reduce themselves to two oppositely directed forces acting in two planes perpendicular to the axis of rotation and the axis of inertia passes through the system's centre of gravity. In general (fig. 4.33c), the influences of the two forces are arbitrarily directed in the two planes and the axis of inertia does not pass through the system's centre of gravity.

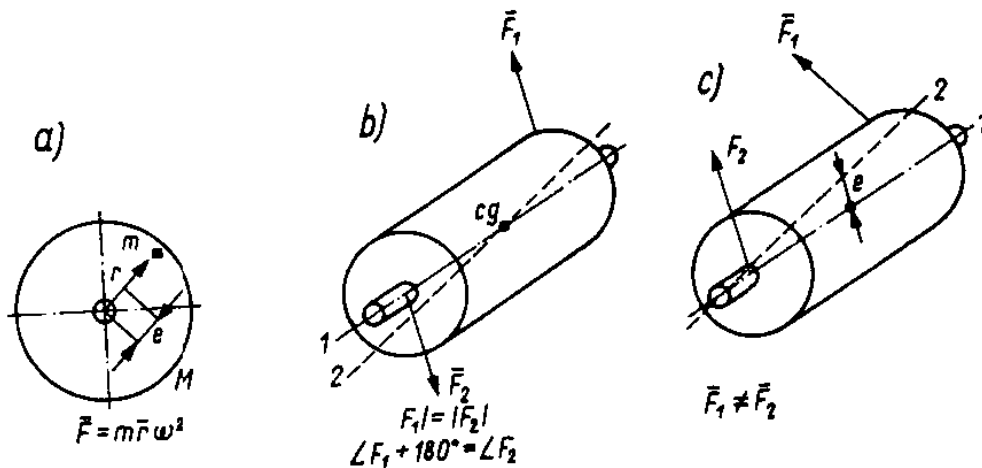


Fig. 4.5. Kinds of unbalance: a – static, b – couple of forces, c – dynamic, 1 – geometric axis, 2 – axis of inertia.

4.7. Forced vibration

There are different causes of forced vibration. In mining machines one of the common causes of forced vibration is the mass unbalance of their rotating elements (the problem of unbalance is considered in chap. 4.6.). The variable load generated by the machine's cutting tool can be another cause of forced vibration (chap. 4.5). To investigate the behaviour of a mechanical system in which forced vibration was generated by a variable periodic force, a system shown in fig. 4.29 was considered. As proved in chap. 4.6, the equation of motion for such a system is (after transformations):

$$M\ddot{x} + kx + C\dot{x} = me\omega^2 \sin(\omega t) \quad (4.123)$$

Phase shifts $\pi/2$ and π occur respectively between displacements x , velocities \dot{x} and accelerations \ddot{x} (chap. 4.1). The same phase shift will occur between the forces expressed by equation (4.123). These forces can be represented geometrically as shown in fig. 4.34 if the exciting force amplitude $me\omega^2$ is denoted as F_o and the vibrating mass amplitude as X . For different frequencies of exciting force ω , phase shift Φ will differ depending on ratio ω/ω_n , where ω_n is the eigenfrequency for a system with one degree of freedom, (4.4). On the basis of fig. 4.34a the following relation can be written

$$F_o^2 = (k - m\omega^2)^2 X^2 + C^2 \omega^2 X^2 \quad (4.124)$$

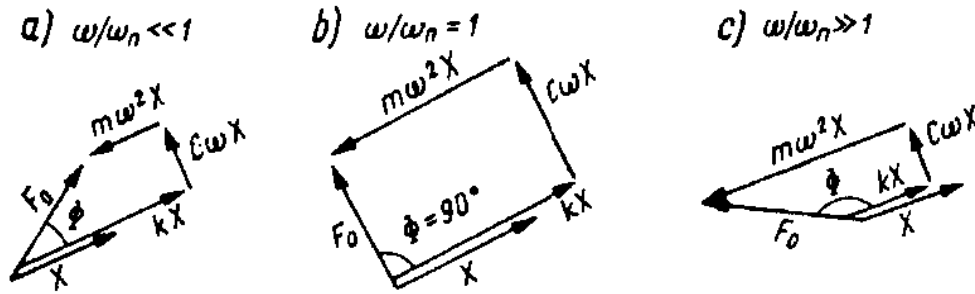


Fig. 4.1. Distributions of forces at vibration depending on ratio of exciting force frequency to eigenfrequency.

Using relation (4.124) the value of amplitude X can be calculated:

$$X = F_o/k1/\{[1 - (\omega/\omega_n)^2]^2 + (2\xi \omega/\omega_n)^2\}^{1/2} \quad (4.125)$$

This result can be obtained by using relations (4.4), (4.49) and (4.50). If (4.125) is reduced to a non-dimensional form, the above relation can be expressed as in fig. 4.35. As mentioned in chap. 4.3, the solution of differential equation (4.123) consists of a sum of solutions, i.e. the particular solution of the equation for which the vibration amplitude is given by (4.125) and the general solution of homogenous equation (4.56). Thus the solution of non-homogenous equation (4.123) can be written as follows

$$x(t) = F_o/k \sin(\omega t - \Phi) / \{ [1 - (\omega/\omega_n)^2]^2 + (2\xi \omega/\omega_n)^2 \}^{1/2} + X_1 \exp(-\xi \omega_n t) \sin(\omega_n \sqrt{1 - \xi^2} t + \Phi_1) \quad (4.126)$$

If the system is excited by a harmonically variable force and relation $\omega/\omega = 1$ holds, the system is in resonance and the vibration amplitude for under-critical damping is larger than the amplitude which excites the vibration.

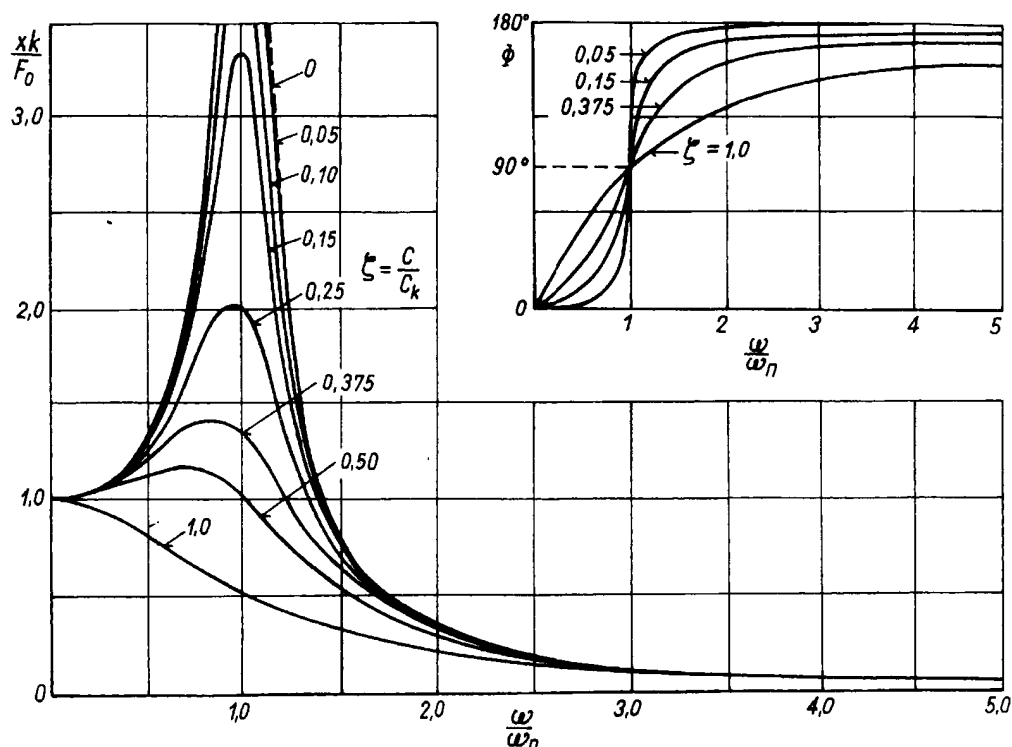


Fig. 4.2. Curves representing change in value of force xk in relation to amplitude of force F_0 as function of relative frequency; phase shift diagrams.

The system shown in fig. 4.5 was excited by the following force

$$F(t) = P + P d \sin(a_{ux} 2\pi) \quad (4.127)$$

where: P – an exciting force, N;

d – a coefficient of variation of force (0-1);

a_{ux} – an auxiliary value given by this formula

$$a_{ux} = \text{frac}(\varphi / 2\pi) \quad (4.128)$$

where *frac* stands for the fractional part of the expression in brackets.

Quantity

$$\varphi = \varepsilon t^2 / 2 \quad (4.129)$$

where: ε – has the dimension of angular acceleration, rad/s^2 ;

φ – angle of rotation, rad.

As a result, function $F(t)$ with a frequency-variable excitation component was obtained (fig. 4.36). Variation function φ is shown in fig. 4.37. Figs 4.38-4.39 show respectively: a plot of the sum of the stiffness force and the damping force in the system, a plot of the displacement of mass x and a plot of the velocity of mass \dot{x} . These are actually the beginnings of the plots for the general solution of the homogenous differential equation. This can be seen in more detail in fig. 4.40 where the plots exhibit eigenvibration. After 8 s from the beginning of excitation to vibration only the effect of forced vibration (at variable frequency) is visible. When the excitation frequency becomes equal to the eigenfrequency, resonance occurs. During the resonance the amplitude of the forces, the deflections and the velocities increases to the maximum.

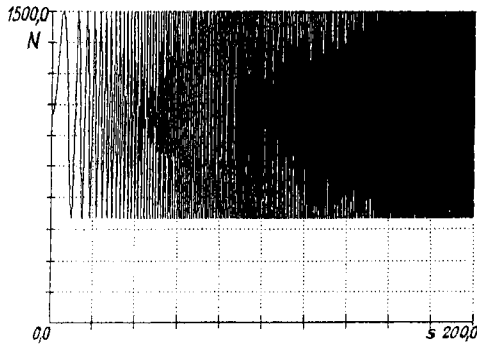


Fig. 4.3. Plot of exciting force with variable excitation frequency.

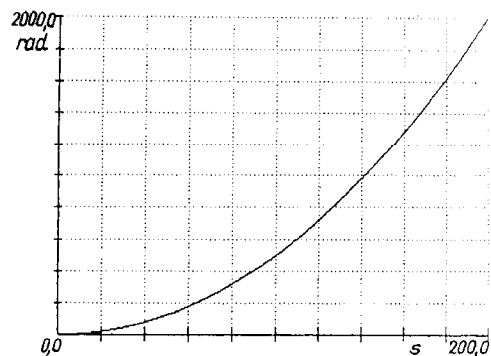


Fig. 4.4. Plot of angular displacement.

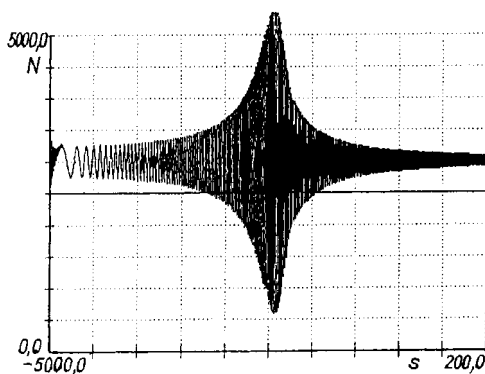


Fig. 4.5. Plot of sum of elastic force and viscous damping at changing exciting frequency; passage through resonance.

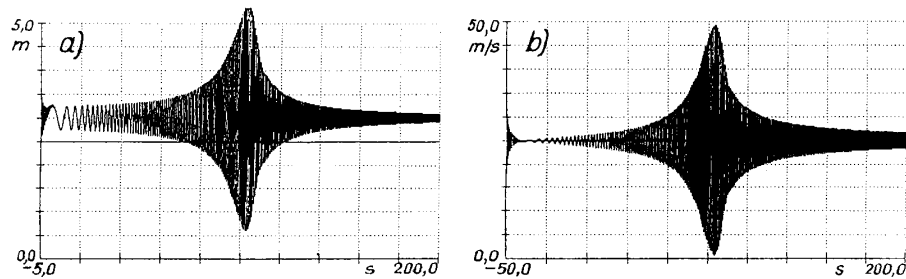


Fig. 4.6. Plot of deflection (a) and velocity (b) of mass of system excited by force with varying excitation frequency.

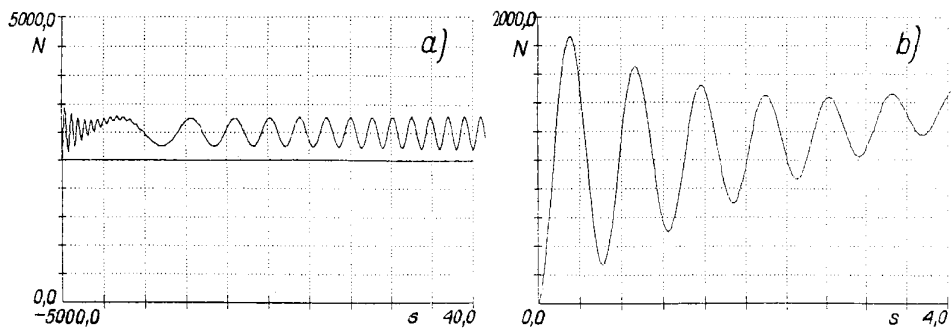


Fig. 4.7. Plot of sum of elastic and damping forces within: a – 40 s, b – 4 s.

The plots are periodic during resonance (fig. 4.41). As the system goes through resonance the amplitudes depend on ξ , i.e. on ratio C/C_k ; when ca. $C = 0.5C_k$, the vibration plots will be as shown in fig. 4.42. Excitations generated by changes in the machine's condition may be a step excitation.

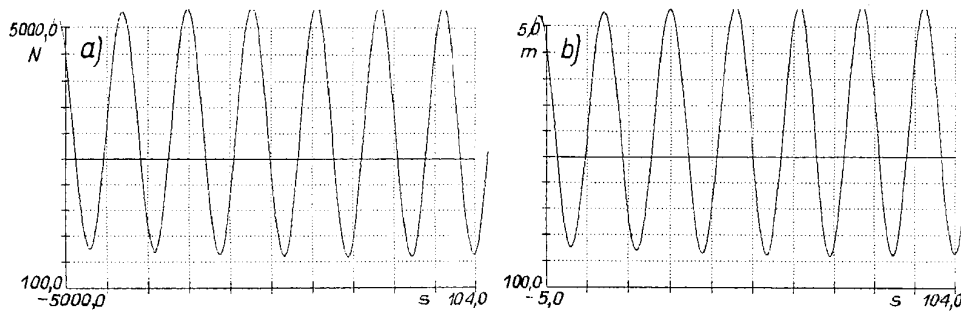


Fig. 4.8. Plots of elastic and damping forces (a) and mass deflection (b) as exciting force frequency goes through system resonance.

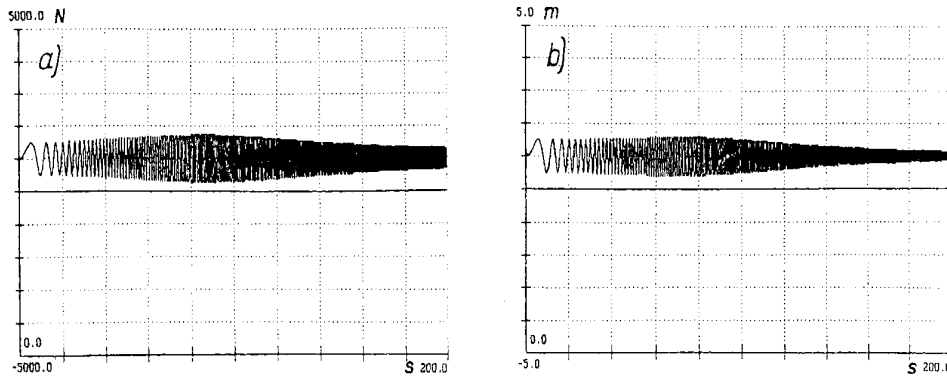


Fig. 4.9. Plots of sum of forces (a) and mass deflection (b) at increased damping.

An exemplary plot of step excitations is shown in fig. 4.43 and the system response to such excitations is shown in fig. 4.44 for mass deflection and in fig. 4.45 for vibration velocity.

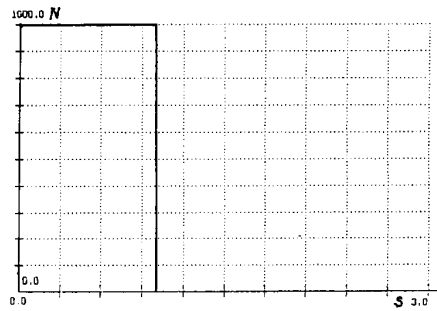


Fig. 4.10. Plot of two step excitations.

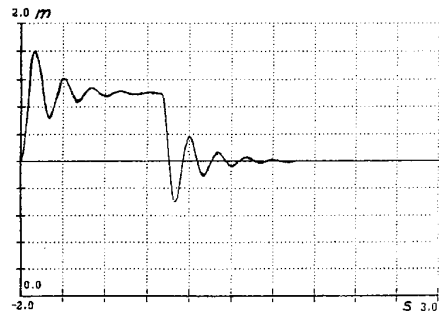


Fig. 4.11. Plot of mass deflection of system excited by step excitations as in fig. 4.43.



Fig. 4.12. Plot of velocity of system excited by step excitation as in fig. 4.43.

In a machine, such step excitations can occur as a result of an error in the mating of its parts, but these will not be step excitations with zero rise and decline time. The excitations are due to the mating of faulty parts and also to changes in the condition of machine parts. These problems will be discussed in the chapters devoted to the causes of vibration in the meshing of gearings and rolling bearings. The step excitation of vibration occurs in an audio frequency range up to 20 kHz (chap. 6, 7, 14, 15) as well as at ultrasonic frequencies and acoustic emission (chap. 10.4). The vibration carries diagnostic information and the utilisation of the latter will be discussed in chap. 6 and other chapters. Excitations of this kind are a primary source of information about the condition of machines.

4.8. References

- [4.1] Jakubowicz A., Orłoś Z.: Strength of Materials (in Polish), *WNT*, 1978.
- [4.2] Brmant A.F., Abramovich I.G.: Mathematical Analysis, *Mir Publishers*, Moscow, 1975.
- [4.3] Bartelmus W., Nosowicz B.: Relationship Between Vibroacoustics and Fundamental Machine Design (in Polish), *26th Open Seminar on Acoustics, Wrocław-Oleśnica 1979, Wrocław University of Technology*, 1979.
- [4.4] Bartelmus W.: Application of Some Vibration Signal Statistical Estimators as Criteria for Meshing Condition Assessment (in Polish), *Scientific Papers of Silesian Polytechnic, Mining*, No. 616, 1979.
- [4.5] Bartelmus W.: Vibration Condition Monitoring of Gearboxes, *Machine Vibration*, No. 1, pp. 178-189, 1992.
- [4.6] Bartelmus W.: Diagnostic Symptoms of Unstability of Gear Systems Investigated by Computer Simulation, *Proceedings of 9th International Congress COMADEM 96, Sheffield 1996, Sheffield Academic Press Ltd.*, 1996.
- [4.7] Broch T.: Mechanical Vibration and Shock Measurements, *Brüel-Kjear Publishers*, April 1984.

5. Modelling of power transmission system dynamics

A physical model of a one-step power transmission system is shown in fig. 5.1. The model is described in [5.1], [5.2] and its further expansion in chap. 6. The system in fig. 5.1 consists of an inertia which represents motor rotor inertia I_s , a toothed gear consisting of two gear wheels represented by two inertias I_{1p} and I_{2p} and a working machine represented by reduced inertia I_m . The reduction principles for the system are presented in chap. 4.5. The motor's characteristic is $M_s(\dot{\varphi}_1)$ where $\dot{\varphi}_1$ is the motor's angular velocity. The other quantities characteristic of the system in fig. 5.1 will be described as the system is represented by equations of motion. The principle of determining the inter-tooth force is illustrated in fig. 5.2 where meshing is represented by only one parameter – stiffness. If it is assumed that the meshing has stiffness k_z , the inter-tooth forces is

$$F = k_z(x_1 - x_2) \quad (5.1)$$

where: k_z – meshing rigidity, N/m;

x_1, x_2 – tooth deflections under moments M_1 and M_2 , m.

Since the deformation of the teeth is slight in comparison with radii r_1 and r_2 , the following relations can be written

$$x_1 = r_1 \varphi_1 \quad (5.2)$$

$$x_2 = r_2 \varphi_2 \quad (5.3)$$

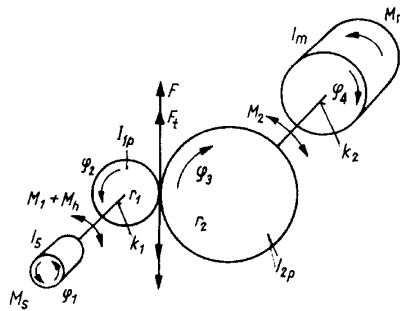


Fig. 5.1. Physical model of power transmission system with motor and one-step toothed gear.

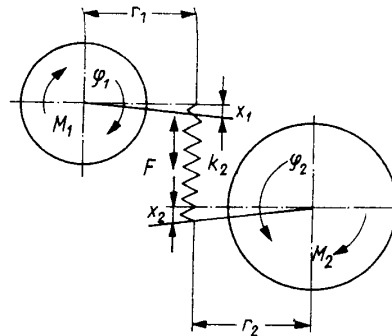


Fig. 5.2. Physical gear model for determining stiffness force.

hence the inter-tooth force is determined from relation

$$F = k_z(r_1 \dot{\varphi}_1 - r_2 \dot{\varphi}_2) \quad (5.4)$$

where: r_1, r_2 – radii of the base circles, m;

φ_1, φ_2 – angles of rotation of the gear wheels, rad.

If it is assumed that the inter-tooth film oil dampens vibration as a result of viscous friction, then the damping force is determined from this formula

$$F_t = C_z(r_1 \dot{\varphi}_1 - r_2 \dot{\varphi}_2) \quad (5.5)$$

where: C_z – a viscous damping coefficient, Ns/m;

$\dot{\varphi}_1, \dot{\varphi}_2$ – the angular velocity of the respective gear wheels, rad/s.

Taking into account forces F and F_t , the meshing will be described by two parameters: stiffness k_2 [N/m] and viscous damping C_z [Ns/m].

If Newton's second law is applied, the equations of motion for the system shown in fig. 5.1 are as follows:

$$I_s \ddot{\varphi}_1 = M_s(\dot{\varphi}_1) - (M_1 + M_h) \quad (5.6)$$

$$I_{1p} \ddot{\varphi}_2 = M_1 + M_h - r_1(F + F_t) \quad (5.7)$$

$$I_{2p} \ddot{\varphi}_3 = r_2(F + F_t) - M_2 \quad (5.8)$$

$$I_m \ddot{\varphi}_4 = M_2 - M_r \quad (5.9)$$

The forces and the torque moments are:

$$M_1 = k_1(\varphi_1 - \varphi_2) \quad (5.10)$$

$$M_2 = k_2(\varphi_3 - \varphi_4) \quad (5.11)$$

$$M_h = C_s(\dot{\varphi}_1 - \dot{\varphi}_2) \quad (5.12)$$

$$F = k_z(r_1 \dot{\varphi}_2 - r_2 \dot{\varphi}_3) \quad (5.13)$$

$$F_t = C_z(r_1 \dot{\varphi}_2 - r_2 \dot{\varphi}_3) \quad (5.14)$$

where: $\varphi, \dot{\varphi}, \ddot{\varphi}$ – an angle of rotation [rad], angular velocity [rad/s] and angular acceleration [rad/s²], respectively;

k_1, k_2 – torsional stiffness of the shafts, Nm/rad;

k_z, C_z – coefficients of rigidity [N/m] and a damping coefficient [Ns/m] for the meshing;

C_s – a viscous damping coefficient for the coupling linking the motor with the gear, Nms/rad.

The driving asynchronous motor's characteristic is shown in fig. 5.3a. To model dynamic phenomena, one can also use simplified characteristics (figs 5.3b and c). In further considerations a shortened, symbolic notation of the load characteristic, i.e. M_s (const/var), is used. This means that if the motor's characteristic is as that shown in fig. 5.3c, then the driving torque during starting (motion acceleration) will be denoted as M_s (const.).

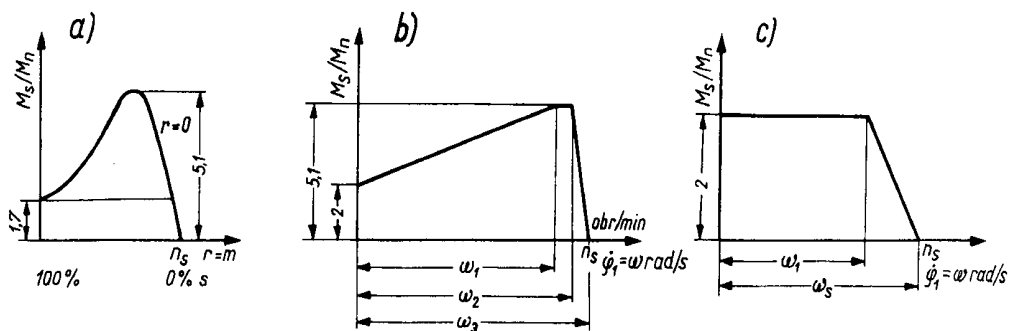


Fig. 5.3. Models of electric motor characteristics: a – actual characteristic of asynchronous electric motor, b – simplified model of asynchronous electric motor characteristic, c – model of electric motor with constant starting torque.

If the motor's characteristic is as shown in fig. 5.3b, then the driving torque during starting is M_s (var). Figs 5.4-5.19 show plots of the physical quantities (characteristics describing the power transmission system). The shape of the characteristics depends on the type of driving motor denoted as M_s (const/var), the external load and the condition of the system. The external load can be described as $M_r(w; r, p_w; r_p; k_r)$. This symbolic description of the load is presented in chap. 4.5. The relative load versus nominal motor torque M is shown in fig. 5.14.

The plot of the driving torque at M_s (const.) and M_r (0; 0; 0; 0; 0) is shown in fig. 5.4; in symbolic notation M_r , zero values mean that in the fourth period of operation (fig. 5.5) the system runs under a constant external load. Four periods can be distinguished in the motor driving torque plot:

- 1 – starting for M_s (const.),
- 2 – free motion of the system,
- 3 – running under a linearly increasing external load,
- 4 – running under external load M_r (0; 0; 0; 0; 0).

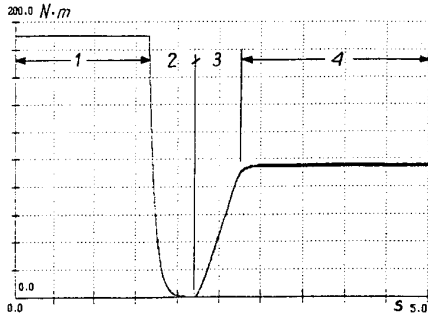


Fig. 5.4. Plot of electric motor torque for motor characteristic shown in fig. 5.3c: 1 ÷ 4 periods in system operation.

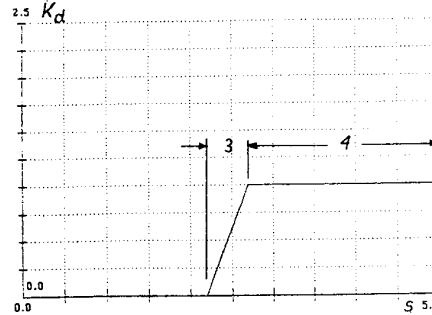


Fig. 5.5. Plot of relative machine load torque: 3 ÷ 4 periods in system operation.

In the first period at M_s (const.) the motor's torque overcomes the inertia of the power transmission system and the friction forces in the meshing (the meshing friction factor $\mu = 0.02$). In the second period there is no resistance to motion. In the third period the external load increases linearly from 0 to the rated value (fig. 5.5) and the fourth period applies to a case when the external load to nominal load ratio is 1. A plot of the relative external load is shown in fig. 5.5. A plot of the angular velocity under the assumptions made for M_s (const.) and M_r (0; 0; 0; 0; 0) is shown in fig. 5.6. A plot of the power consumption as a product of instantaneous values M_s and $\dot{\phi}_1$ (fig. 5.1) is shown in fig. 5.7.

$$N = M_s(\dot{\phi}_1) \dot{\phi}_1, \quad W \tag{5.15}$$

where: $M_s(\dot{\phi}_1)$ – the motor's torque, Nm;

$\dot{\phi}_1$ – the motor's angular velocity, rad/s;

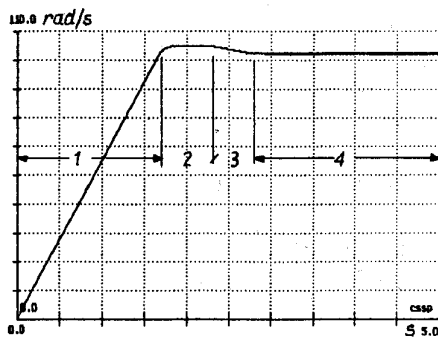


Fig. 5.6. Plot of motor angular velocity: 1 ÷ 4 as in fig. 5.4.

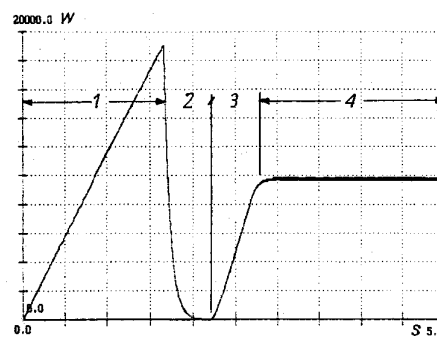


Fig. 5.7. Plot of power consumption by motor: 1 ÷ 4 as in fig. 5.4.

Plots of the power of the losses in the meshing for $\mu = 0.02$ are shown in fig. 5.8. Fig. 5.9 shows plots of instantaneous efficiency values defined as

$$\eta = (N_s - N_{str})/N_s \quad (5.16)$$

where: N_s – the motor's power, W;

N_{str} – the power of the losses due to friction in the meshing, W.

Plots of the above parameters when the gear is properly lubricated and the frictional resistance is defined by friction factor $\mu = 0.02$ are shown in figs 5.8 and 5.9. For comparison, plots of the power of the losses and efficiency plots for $\mu = 0.1$ are shown in figs 5.10 and 5.11. As it follows from fig. 5.9, efficiency is in a range of 0.098-1 and at $\mu = 0.1$ it ranges from 0.98 to 1 (fig. 5.11). A comparison of fig. 5.8 and 5.10 shows that for steady running (period 4) at μ varying from 0.02 to 0.1, i.e. at a fivefold increase in the value of the friction factor, the losses are respectively $N_{str} = 38$ W and 195 W and hence the loss ratio is $195/38 = 5$. Thus the fivefold increase in the friction factor corresponds to the fivefold increase in the power of the frictional losses.

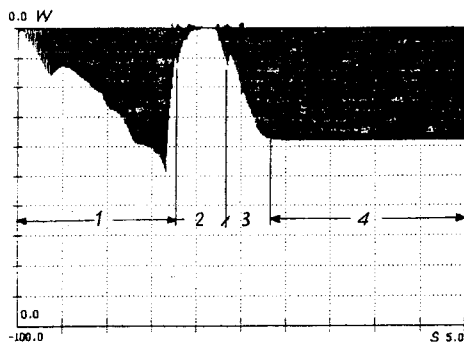


Fig. 5.8. Plot of power of system losses due to friction in meshing for $\mu = 0.02$: 1 ÷ 4 as in fig. 5.4.

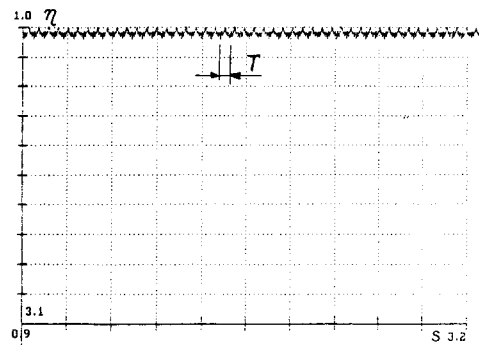


Fig. 5.9. Plot of instantaneous efficiency values for $\mu = 0.02$.

After the fivefold increase in the friction factor (fig. 5.11) the oscillations of efficiency coefficient η become more pronounced. The oscillations occur at the frequency of meshing. This corresponds to meshing period T . To get a closer look at η , it was plotted for a shorter time interval (fig. 5.12) whereby another cause of the variation became apparent: defects in the meshing. A simulation run is shown for meshing error E (0.5; 10; 0; 0), where 0.5 is a parameter characterising the shape of a resultant meshing error, 10 is the maximum value of the error (in μm). The other zero values in the symbolic notation will be described in chap. 6. Defects in meshing result in the impulse excitation of the system to eigenvibration as shown in fig. 5.12 (vibration period T_n). A study of a mechanical system subjected to step excitation is presented in

chap. 4.3. In the cases of both step and impulse excitation the system is excited to vibration at a natural frequency.

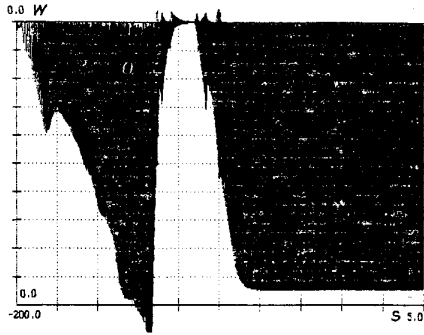


Fig. 5.10. Plot of power of system losses due to friction in meshing for $\mu = 0.1$.

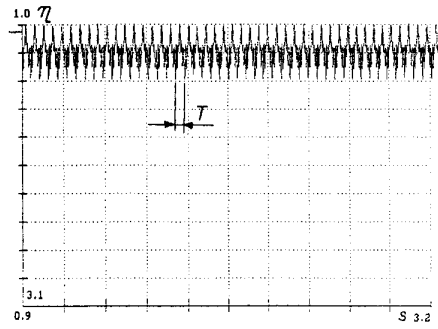


Fig. 5.11. Plot of instantaneous efficiency values for $\mu = 0.1$.

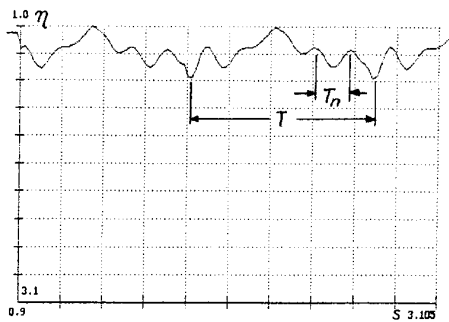


Fig. 5.12. Plot of instantaneous efficiency values within time interval of 0.005 s.

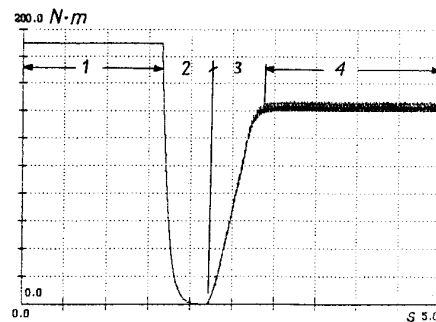


Fig. 5.13. Plot of electric motor torque for motor characteristic as in fig. 5.3c and external load as in fig. 5.14: 1 ÷ 4 as in fig. 5.4

A plot of the electric motor's driving torque for M_s (const.) and M_t (1; 0; 0.9; 0; 8) is shown in fig. 5.13. A plot of the relative torque for the external load is shown in figs 5.14 and 5.15. Oscillations in torque in period 4, due to oscillations in external load torque (fig. 5.14), are visible in fig. 5.13 (variation period T_r). Fig. 5.15 is a close-up of the plot of a relative external load increment from zero to a value corresponding to steady running. Oscillations in electric motor torque, whose period corresponds to external load variation period T_r , are shown in fig. 5.16 where a load averaging effect caused by the inertia of the electric motor's rotor is visible. The maximum external load torque value reduced to the shaft is 190 N · m and for $r = 1$ it ranges from 95 to

190 N · m. The corresponding electric motor torque (for steady running) is about 172 N · m (figs 5.13 and 5.16).

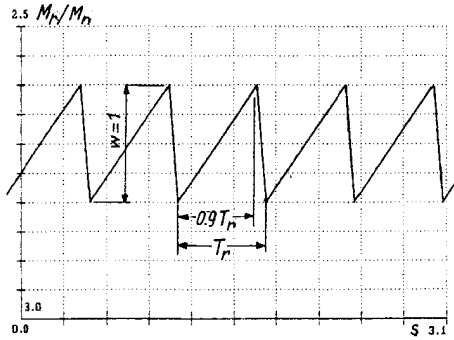


Fig. 5.14. Plot of relative variation in external load.

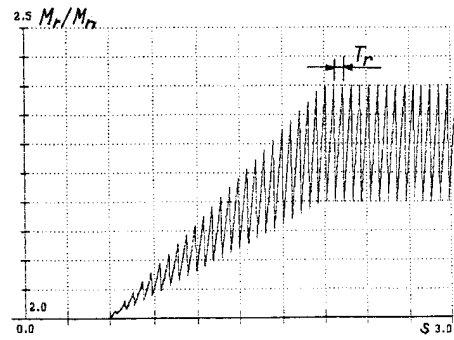


Fig. 5.15. Plot of relative increment in external load torque.

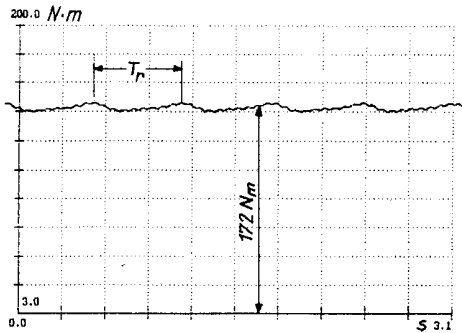


Fig. 5.16. Close-up of electric motor torque plot.

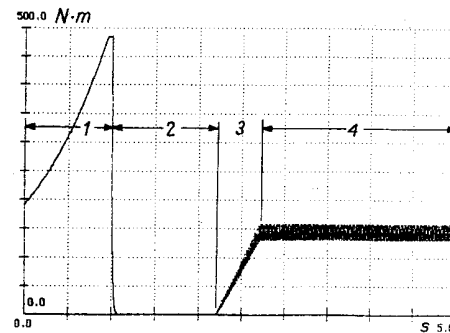


Fig. 5.17. Electric motor torque for characteristic as in fig. 5.3b: 1 ÷ 4 as in fig. 5.4.

Plots of the power transmission system's basic quantities for M_s (var) are shown in figs 5.17, 5.18 and 5.19. It appears that the motor's characteristic is as that shown in fig. 5.3b. The motor's driving torque during starting is not constant but changes non-linearly (period 1 in fig. 5.17). Figs 5.17, 5.18 and 5.19 represent the previously described periods. The external load is as shown in figs 5.14 and 5.15. A characteristic feature of this power transmission system is that $M_s(t)$, $\phi_1(t)$ and $N(t)$ increase non-linearly in the first running period when the motor overcomes the forces of inertia. Plots of η defined by expression (6.16) are shown in figs 5.9, 5.11 and 5.12. The plots exhibit periodicity related to the meshing period. The amplitude of the changes depends on the meshing condition expressed by coefficient μ . The plots have diagnostic

properties of the meshing condition. They represent a way of describing vibration in a dimensionless system and thus broaden the definition of vibration given in chap. 4.1.

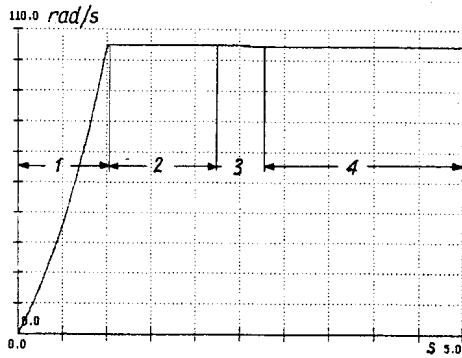


Fig. 5.18. Plot of motor rotational speed for driving motor whose characteristic is shown in fig. 5.3b: 1 ÷ 4 as in fig. 5.4.

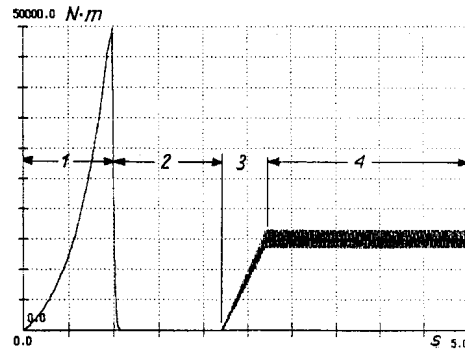


Fig. 5.19. Motor power consumption for characteristic shown in fig. 5.3b.

5.1. References

- [5.1] Bartelmus, W.: Computer Simulation of Vibration Generated by Meshing of Toothed Wheel For Aiding Diagnostic of Gearboxes, Condition Monitoring '94 Swansea Conference Proceedings, UK PINE-RIDGE PRESS, Swansea, UK.
- [5.2] Bartelmus, W.: Transformation of Gear Intertooth Forces into Acceleration and Velocity. Proceedings of the 7th International Symposium on Transport Phenomena and Dynamics of Rotating Machinery, Bird Rock Publishing House, Honolulu Hawaii, USA, February 1988.

6. Modelling of gear meshing dynamic behaviour

6.1. Introduction

To model the dynamics of gear meshing one needs some knowledge of gear meshing kinematics and of how friction forces and moments of friction arise during meshing. In chap. 5 the influence of a friction coefficient on the power of losses in gear meshing was considered but without getting to the core of the problem (its theoretical basis). Some principles of toothed gear modelling were presented in chap. 5 when discussing the dynamic properties of a power transmission system. In this chapter, further possibilities of modelling the state of gear intermeshing are presented. Intermeshing gear teeth are pictured in fig. 6.1. The geometric locus of consecutive points of contact between the teeth is a segment (denoted as N_1 , N_2 in the figure) of the line tangent to the two base circles. It follows from the properties of an involute gearing that when the involutes of both circles are ideal, the direction of the engagement line is constant in space. The friction forces are directed perpendicular to the engagement line determined for points from N_1 to N_2 .

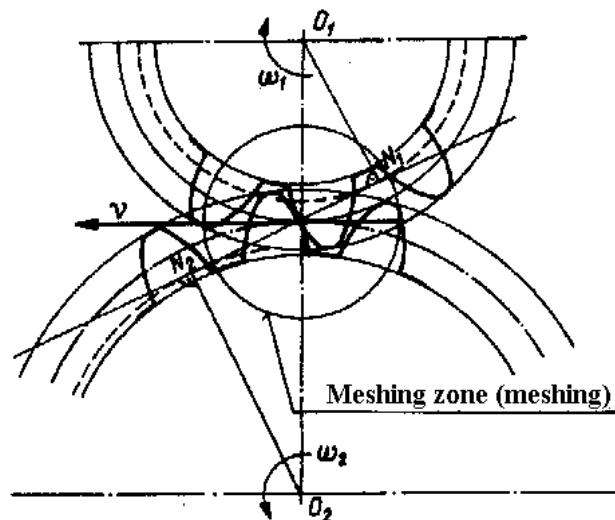


Fig. 6.1. Meshing of gear wheels

6.2. Distribution of velocities at point of instantaneous contact between two meshing teeth

The geometric locus of the points of contact between meshing teeth is a straight line tangent to the two basic circles. The velocity components for a contact point can be determined from the law of motion of a rigid body. The peripheral speed of any point of a body rotating with angular velocity ω is

$$v = \omega r_x \tag{6.1}$$

where r_x is the distance of the peripheral speed vector from axis of rotation, m.

The velocity distribution for point A is shown schematically in fig. 6.2. The linear velocities of point A for the first wheel – 1 and the second wheel – 2 are

$$v_1 = r_{x1} \omega_1 \tag{6.2}$$

$$v_2 = r_{x2} \omega_2 \tag{6.3}$$

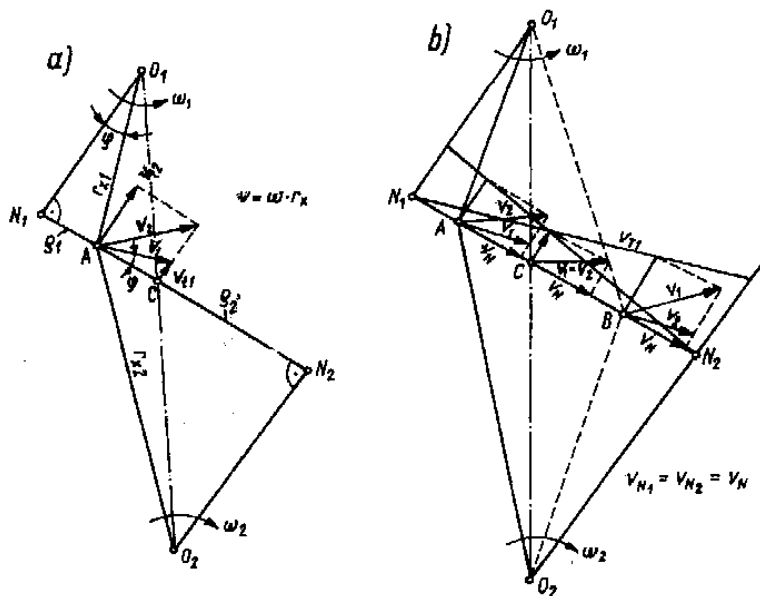


Fig. 6.1. Linear velocity distribution in intermeshing zone: a – at instantaneous contact point A, b – at instantaneous contact points A, B, C.

The velocities v_1 and v_2 can be decomposed into two components: one in the direction tangent to and the other in the direction normal to the tooth profile. According to fig. 6.2. tangential component v_{t1} perpendicular to engagement line is

$$v_{t1} = v_1 \sin \varphi = r_{x1} \omega_1 \sin \varphi \quad (6.4)$$

Since $r_{x1} \sin \varphi$ is equal to distance (N₁, A) denoted as ρ_1 ,

$$v_{t1} = \rho_1 \omega_1 \quad (6.5)$$

The above equation expresses one of the laws of motion of a rigid body, according to which the velocity of any point, perpendicular to a segment joining the considered point with a point relative to which the velocity is calculated, is a product of the distance between the two points and the angular velocity. This means that the tangent velocity of any point on the engagement line for both circles can be determined from this relation

$$v_{t1} = \rho_1 \omega_1; v_{t2} = \rho_2 \omega_2 = \rho_2 \omega_1 / u \quad (6.6)$$

where u is the gear ratio.

It follows from the above relations that the tangent velocities spread linearly: velocity $v_{t1} = 0$ for point N₁ and velocity $v_{t2} = 0$ for point N₂.

The decomposition of the velocities into directions tangent and normal to the engagement line is shown for three points (A, B, C) in fig. 6.2b. The velocities normal to the tooth profile when the continuity of meshing is preserved (no teeth separation) are the same at each contact point

$$v_{N1} = v_{N2} = v_N \quad (6.7)$$

On the basis of fig. 6.2b one can plot the tangent velocities along the engagement line (fig. 6.3).

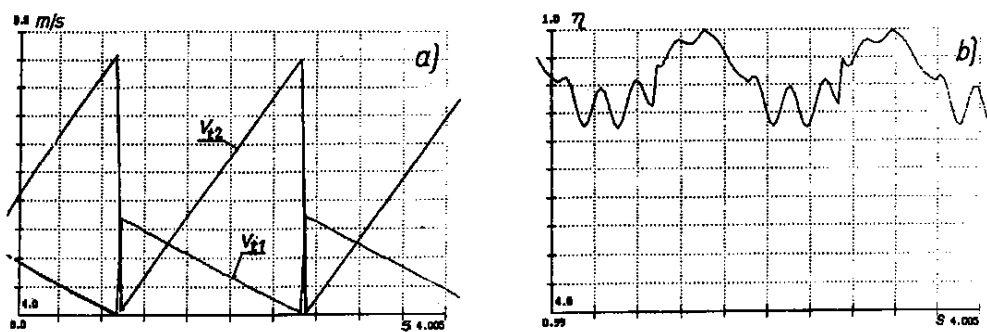


Fig. 6.2. Graph of tangent velocities at points of instantaneous contact (a) and plot of instantaneous values of meshing efficiency (b).

For point C velocities v_1 and v_2 are equal since

$$r_{x1} = r_{w1}; r_{x2} = r_{w2} \tag{6.8}$$

hence

$$r_{x1} \omega_1 = r_{w2} \omega_2 \tag{6.9}$$

where v is the peripheral speed of the gear wheels, m/s. This means that projections of velocity v onto the perpendicular to the contact line are the same and so the tangent velocity is the same for both gear wheels. At point C no linear relative motion of the contact points occurs and there is no slip, as shown by the tangent velocity graph (fig. 6.3). Since there are differences between the tangent velocities at the other points of meshing contact, slip occurs between the tooth profiles and friction forces arise. The difference in the velocity between the points of contact is called slipping velocity v_p (see fig. 6.4). The contact force (the intertooth force) acting along the engagement line (N_1, N_2) and the relative motion in the direction tangent to meshing produce a friction force acting in tangent direction $T - T$. It follows from fig. 6.5 that at point A, lying before rolling point C, driven tooth tangent velocity v_{t2} is higher than v_{t1} (slip occurs) for driving wheel tooth 1 and driven wheel tooth 2. The friction force is directed as shown in fig. 6.5.

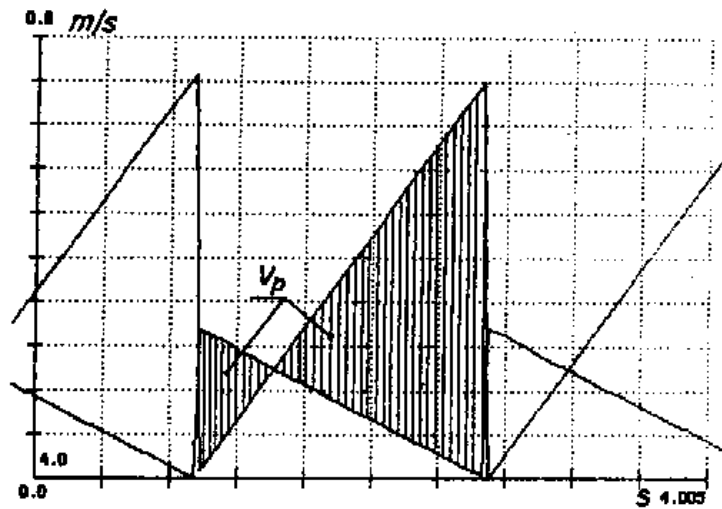


Fig. 6.3. Graph of slipping velocity at points of instantaneous contact

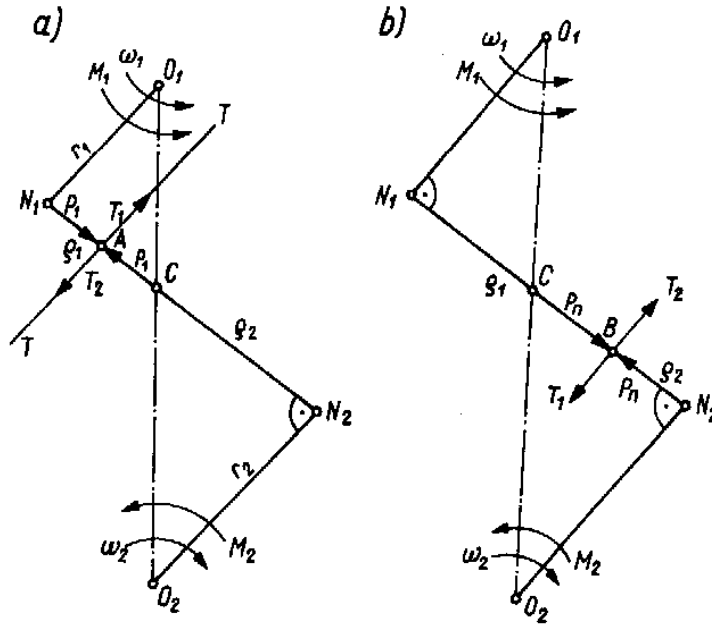


Fig. 6.4. Friction forces in meshing along contact line:
a – at point A,
b – at point B.

6.3. Friction forces and moment of friction in meshing

The friction force is denoted by T_1 for driving gear wheel 1 and by T_2 for driven gear wheel 2. The equations of equilibrium of the moments for point A are as follows:

$$M_1 - P_n r_1 + T_1 \rho_1 = 0 \quad (6.10)$$

$$-M_2 + P_n r_2 - T_2 \rho_2 = 0$$

if the second equation is multiplied by -1 , we get:

$$M_2 - P_n r_2 + T_2 \rho_2 = 0 \quad (6.11)$$

$$T_1 = T_2 = \mu P_n \quad (6.12)$$

After substituting T_1 and T_2 , we get for point A

$$M_1 - P_n r_1 + \mu P_n \rho_1 = 0 \quad (6.13)$$

$$M_2 - P_n r_2 + \mu P_n \rho_2 = 0 \quad (6.14)$$

After substituting T_1 and T_2 , we get for point B:

$$M_1 - P_n r_1 - \mu P_n \rho_1 = 0 \tag{6.15}$$

$$- M_2 + P_n r_2 + \mu P_n \rho_2 = 0$$

after multiplying the second equation by -1 , we get:

$$M_2 - P_n r_2 - \mu P_n \rho_2 = 0 \tag{6.16}$$

The moment of friction is a product of the friction force and distances ρ_1, ρ_2 . It follows from fig. 6.4 that friction forces T_1 and T_2 change their direction as a result of the change in the direction of the slipping velocity at midpoint C. Graphs of friction moment variation are shown in fig. 6.6.

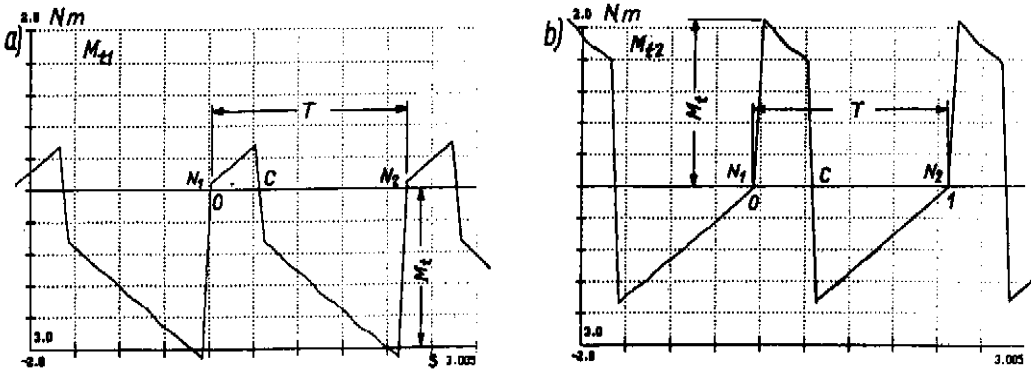


Fig. 6.1. Graphs of friction moments in meshing: a – moment of friction for first gear wheel, b – moment of friction for second gear wheel.

6.3.1. Friction power

The friction power is equal to a product of the slipping velocity and the friction force. The slipping velocity can be calculated as an absolute value of the difference between the tangent velocities

$$v_p = v_{i2} - v_{t1} \tag{6.16}$$

The instantaneous friction power is

$$M_{ct} = v_p \mu P_n \tag{6.17}$$

Plots of instantaneous friction loss are shown in figs 5.8 and 5.10 for different friction coefficient values: $\mu = 0.02$ and 0.1 .

6.4. Analytical description of changes in meshing stiffness, moments of friction, tooth errors, intertooth backlash, gear intertooth forces

A plot of changes in meshing stiffness in one period of relative length (0-1) is shown in fig. 6.7. The stiffness change values were calculated according to the principle given in [6.1] and [6.2], taking into account the defection of the teeth and their contact deformations. A simplified stiffness characteristic for a pair of helical gear wheels (fig. 6.7) was selected on the basis of computer calculations [6.2].

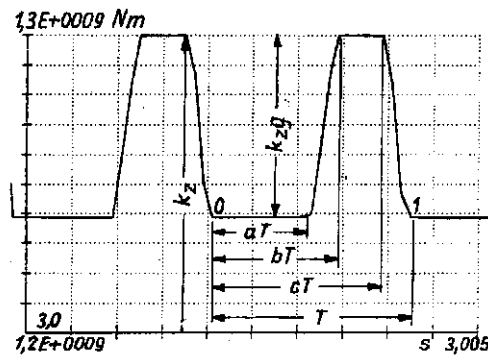


Fig. 6.1. Plot of changes in meshing stiffness.

This characteristic is repeated on the toothed wheel's circumference as many times as there are teeth. The wheel's arc corresponding to a one-period plot is

$$o_{kr} = 2\pi / z_1 \quad (6.18)$$

where z_1 is a number of teeth in the driving wheel.

When the wheels mesh, the position of the wheel on relative length (0-1) can be determined as follows

$$\text{frac}(\phi / o_{kr}) = a_{ux} \quad (6.19)$$

where a_{ux} is an auxiliary variable ranging from 0 to 1.

Function frac stands for a fractional part from ratio ϕ / o_{kr} where ϕ is the total angle of rotation of the wheel in arc measure.

Assuming maximum tooth stiffness k_z (fig. 6.7), meshing stiffness $k_z(a_{ux})$ within interval $[0, a]$ is

$$k_z(a_{ux}) = k_z(1 - g) \quad (6.20)$$

where: $k_z(a_{ux})$ – describes meshing stiffness as a function of value a_{ux} ,

g – a relative value of stiffness change, $g < 1$;

for segment [a, b] (taking into account the fact that the straight line passes through point (b, k_z):

$$k_z(a_{ux}) = gk_z/(b - a)(a_{ux} - b) + k_z = k_z[1 + g(a_{ux} - b)/(b - a)] \quad (6.21)$$

for segment [b, c]:

$$k_z(a_{ux}) = k_z \quad (6.22)$$

for segment (c, 1] the straight line passes through point (c, k_z)

$$k_z(a_{ux}) = -gk_z(a_{ux} - c)/(1 - c) + k_z = k_z[1 - g(a_{ux} - c)/(1 - c)] \quad (6.23)$$

6.4.1. Analytical description of changes in moments of friction

Relative length (0, 1) was used to describe changes in the moments of friction shown in fig. 6.6. Denoting the length of the path of contact as $(N_1, N_2) = d$ and assuming that approximately

$$d = 2\pi r_{w1}/z_1 = 2\pi r_1/z_1 \quad (6.24)$$

where:

r_{w1} – the radius of the first rolling wheel,

r_1 – the radius of the first base circle (fig. 6.8),

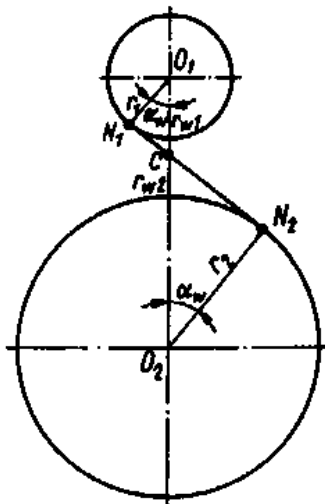


Fig. 6.1. Diagram aiding in division of contact line.

one can calculate the maximum friction moment which is

$$M_f = d \mu (F + F_f) \quad (6.25)$$

According to fig. 6.8:

$$u = r_{w2}/r_{w1} = r_2/r_1 \quad (6.26)$$

$$N_1 C = r_{w1} \sin(\alpha_w) \quad (6.27)$$

$$N_2 C = r_{w2} \sin(\alpha_w)$$

By dividing by sides, we get

$$N_1 C / N_2 C = r_{w1} r_{w2} = 1/u \quad (6.28)$$

$$N_1 C + N_2 C = N_1 N_2 \quad (6.29)$$

and substituting

$$N_1 C = N_2 C / u \quad (6.30)$$

$$N_2 C / u + N_2 C = N_1 N_2 \quad (6.31)$$

$$N_2 C = N_1 N_2 / (1 + 1/u) \quad (6.32)$$

if

$$N_1 N_2 = 1 \quad (6.33)$$

where 1 is the relative length of the path of contact, then we get

$$N_2 C = u / (u + 1) \quad (6.34)$$

and

$$N_1 C = 1 / (u + 1) \quad (6.35)$$

The linear function of changes in moments of friction, shown in fig. 6.6, for wheel 1 can be written in interval $[0, 1/(1 + u)]$ as

$$M_{t1} = M_t a_{ux} \quad (6.36)$$

in interval $[1/(1 + u), 1]$ as

$$M_{t1} = -M_t a_{ux} \quad (6.37)$$

for driving wheel 2 in interval $[0, 1/(1 + u)]$ as

$$M_{t2} = -M_t (a_{ux} - 1) = M_t (1 - a_{ux}) \quad (6.38)$$

in interval $[1/(1 + u), 1]$ as

$$M_{t2} = -Mt(1 - a_{uv}) \quad (6.39)$$

6.4.2. Analytical description of intertooth force with intertooth backlash taken into account

The intertooth force value is equal to a product of meshing stiffness coefficient k_z and tooth deflection values which amount to

$$\varphi_1 r_1 - \varphi_2 r_2 \quad (6.40)$$

According to 5.2, the intertooth force is equal to

$$F = k_z(\varphi_1 r_1 - \varphi_2 r_2) \quad (6.41)$$

A function illustrating changes in the values of the forces depending on relative wheel rotation $\varphi_1 r_1 - \varphi_2 r_2$ in the case when there is backlash l_u in meshing is shown in fig. 6.9. If we denote

$$x = \varphi_1 r_1 - \varphi_2 r_2 \quad (6.42)$$

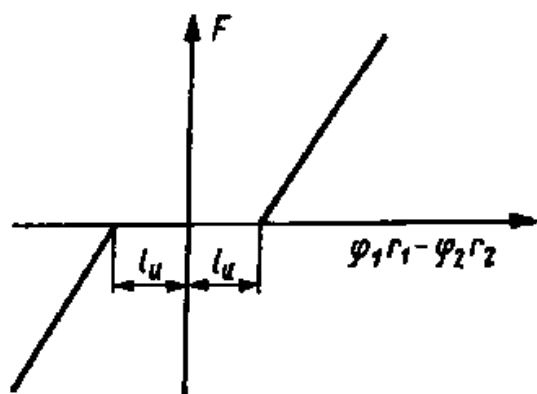


Fig. 6.1. Graph of changes in meshing stiffness with intertooth backlash

the equation of the force for $x \geq 0$ is as follows

$$F = k_z(x - l_u) = k_z(\varphi_1 r_1 - \varphi_2 r_2 - l_u) \quad (6.43)$$

for value $x < 0$

$$F = k_z[x - (-l_u)] = k_z(\varphi_1 r_1 - \varphi_2 r_2 + l_u) \quad (6.44)$$

For the computer simulation of the above relations it is necessary to define the following functions which will be written in Pascal as

FUNCTION min (a, b: real) : real;

```

BEGIN
  IF a<b THEN min :=a ELSE min := b
END;
FUNCTION max (a, b : real) : real;
  BEGIN
    IF a>b THEN max:=a ELSE max:=b
  END;

```

If the above functions are used, the intertooth force can be written as follows

$$F = k_z(a_{ux})\max(\varphi_1 r_1 - \varphi_2 r_2 - l_u, \min(\varphi_1 r_1 - \varphi_2 r_2 + l_u, 0)) \quad (6.45)$$

where: $k_z(a_{ux})$ – the stiffness change function described above,

$\varphi_1 r_1 - \varphi_2 r_2 - l_u$ – the equation of the stiffness characteristic for a positive intertooth force value,

$\varphi_1 r_1 - \varphi_2 r_2 + l_u$ – the equation of the stiffness characteristic for a negative intertooth force value.

6.4.3. Interpretation of intertooth force function notation

If $\varphi_1 r_1 - \varphi_2 r_2 - l_u > 0$

then $\min = 0$, since $a > b$

and $\max(\varphi_1 r_1 - \varphi_2 r_2 - l_u, 0)$

then $\max = \varphi_1 r_1 - \varphi_2 r_2 - l_u$

if $\varphi_1 r_1 - \varphi_2 r_2 + l_u < 0$

$a < b$

then $\min \varphi_1 r_1 - \varphi_2 r_2 + l_u$

then $\max(\varphi_1 r_1 - \varphi_2 r_2 - l_u, \varphi_1 r_1 - \varphi_2 r_2 + l_u)$

$\max = \varphi_1 r_1 - \varphi_2 r_2 + l_u$

since $a < b$

6.4.4. Analytical notation of error function

The error function is shown in fig. 6.10. It can be written analytically in interval [0, a] as follows

$$E_r(a_{ux}) = e/a a_{ux} \quad (6.46)$$

and in interval [a, 1]:

$$E_r(a_{ux}) = -e(p_{om} - 1)/(1 - a) = e(1 - a_{ux})/(1 - a) \quad (6.47)$$

where e is the maximum error value.

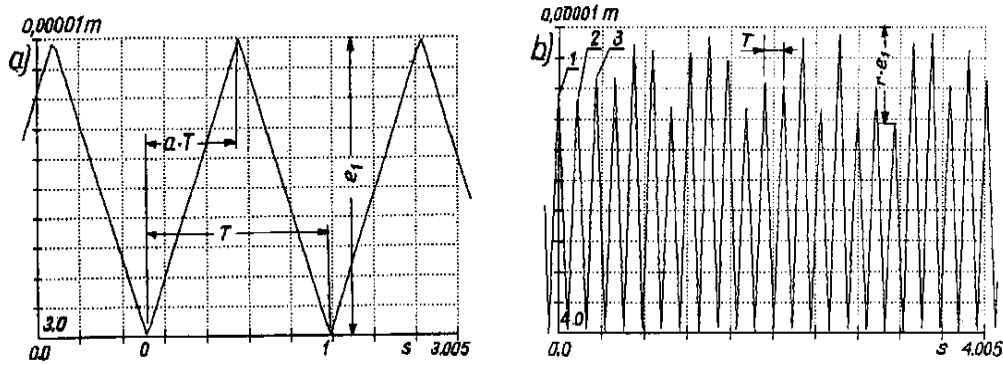


Fig. 6.1. Plots of gearing error function: a – constant plot of error function $E(0.5; 10; 0; 0)$, b – random plot of error function $E(0.5; 10; 0.3; 0)$.

For individual pairs of teeth, error values can be random; this randomness can be taken into account as follows

$$e(\text{random}) = [1 - r(1 - l_i)]e \quad (6.48)$$

where: e – the maximum gearing error value;

r – an error range coefficient, range (0 – 1);

l_i – a random number, range (0 – 1).

The variation of gearing errors is written symbolically as $E(a; e; r)$. The meaning of the parameters given in brackets, including that of parameter a specifying the position of the maximum value of error e , is explained in fig. 6.10a. An illustrative plot for $E(0.5; 10; 0.3)$ is shown in fig. 6.10b.

The value of the force for the joint impact of meshing stiffness variation, intertooth backlash and gearing errors when the max., min. functions are used is: follows

$$F = k_z(a_{ux}) \max(\varphi_1 r_1 - \varphi_2 r_2 - l_u + E_r(a_{ux}), \min(\varphi_1 r_1 - \varphi_2 r_2 + l_u + E_r(a_{ux}), 0)) \quad (6.48a)$$

Both elastic forces and damping forces act in meshing and so the total force is $F + F_t$.

It follows from the above that many factors affect the dynamics of a system incorporating a toothed gear. As mentioned (after [6.3], [6.4], [6.5]) in chap. 4.5, the factors can be divided into four groups:

- design factors – D.F.,
- production technological factors – PT.F., limit
- operational (motion) factors – O.F.,
- change-of-condition factors – C.C.

Using the symbols that were used to describe the gear dynamics model, D.F. are represented by: I_{p1} , I_{p2} , k_z , C_s , C_h , k_1 , k_2 , I_s , I_m , r_1 , r_2 , e_{lim} , a , l_{ulim} , μ_{lim} , where e_{lim} , l_{ulim} , μ_{lim} – a permissible/limit gearing error, backlash, friction coefficient value.

T.F. specify if the adopted design factors ($e \leq e_{lim}$, $l_u \leq l_{ulim}$) were or were not fulfilled when producing a given toothed gear.

O.F. are represented by: M_1 , M_2 , ϕ_1 , M_r .

C.C. are represented by $e > e_{lim}$, $\mu > \mu_{lim}$, $l_u > l_{ulim}$.

The listed above factors gives possibility for understanding the role of influence of design, technology, operation and the change of condition factors on condition monitoring signals. It leads to "Design, Production Technology, Operation, Condition Change, factors based diagnostics" (DPTOCC factors based diagnostics).

6.5. Dynamical model of toothed gear

This chapter summarises the considerations relating to a dynamical model of a gear consisting of two toothed wheels separated from a machine system (fig. 6.11) or constituting a self-contained system (fig. 5.1). In the dynamical model of a gear consisting of two toothed wheels, meshing is represented by stiffness k_z [N/m] (the arrow indicates that the stiffness is variable) which is analytically described by expressions (6.20), (6.21), (6.22), (6.23) and shown in fig. 6.7. Also damping parameter C_z [Ns/m] represents the meshing properties. The inter-tooth force is a sum of stiffness force (6.48) and damping force (5.5). The stiffness force includes variable meshing stiffness, intertooth backlash and changes of gearing error modes.

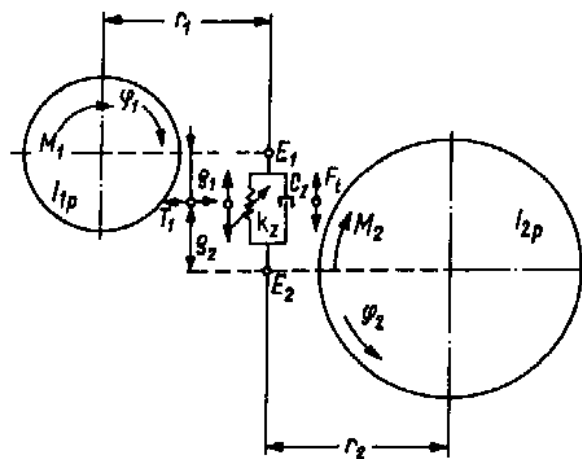


Fig. 6.1. Dynamical model of toothed gear.

Also friction force T , which produces moment of friction M_{t1} and M_{t2} respectively on the first and second wheel, and the direction in which the friction force acts when the meshing teeth are in contact at point A (fig. 6.5a) are marked in fig. 6.11. The moments of friction are the functions shown in fig. 6.6. A full description of the equations of motion for the two gear wheels is as follows

$$I_{1p} \ddot{\varphi}_1 = M_1 - r_1(F + F_t) + M_{t1} \quad (6.49)$$

$$I_{2p} \ddot{\varphi}_2 = r_2(F + F_t) - M_2 - M_{t2}$$

A mathematical model formed by the above equations describes the behaviour of the dynamical system consisting of the pair of gear wheels shown in fig. 6.11. This model was applied to the self-contained system (fig. 5.1) and used for computer simulations. The computer simulation results are presented in several chapters of this book and in many papers by the author [6.6]-[6.10]. The model can be also used to model multistage gears as described in papers [6.11], [6.12].

6.6. Inter-tooth forces and dynamical overload factor

The model shown in fig. 5.1, with the moments of friction acting in meshing (fig. 6.11) taken into account, was used for the simulation of intertooth forces and dynamical tooth overload factor K_d . The obtained results were compared with the experimental ones presented in [6.13]. The intertooth forces are represented by overload factor K_d defining the degree of tooth overload over the rated load specified in the design assumptions for the gear. Simulations of factors K_d were run assuming: $M_s(\text{const.})$, gearing errors E (0.5; 10; 0; 0) and external load $M_r(0; 0; 0; 0)$. These are reference parameters and they are not mentioned again when interpreting results unless this is needed to elucidate the text. The gear is driven by a motor whose characteristic is shown in fig. 5.3c. The gearing error function is shown in fig. 6.10a and the external load function – in fig. 5.5. A plot of K_d in the four gear meshing periods, as described in chap. 5 (fig. 5.4), is shown in fig. 6.12.



Fig. 6.1. Plot of factor K_d ; 1 ÷ 4 gear meshing periods.

Zooms of K_d plots for the fourth gear meshing period in two time intervals $\Delta t = 0.1$ and 0.005 and a plot of coefficient K_d for a selected pair of teeth (meshing period T [s]) are shown in fig. 6.13.

The results obtained on the test stand described in [6.13] are presented in fig. 6.14. They are for the fourth gear meshing period and for gear operation at a meshing frequency: below gear resonance, equal to gear resonance and above gear resonance. The results presented in figs 6.12 and 6.13 are for gear operation below resonance. A comparison of the results in fig. 6.13b with those in fig. 6.14 (gear operation below resonance represented by a solid line) shows that test-stand results agree with the simulation results.

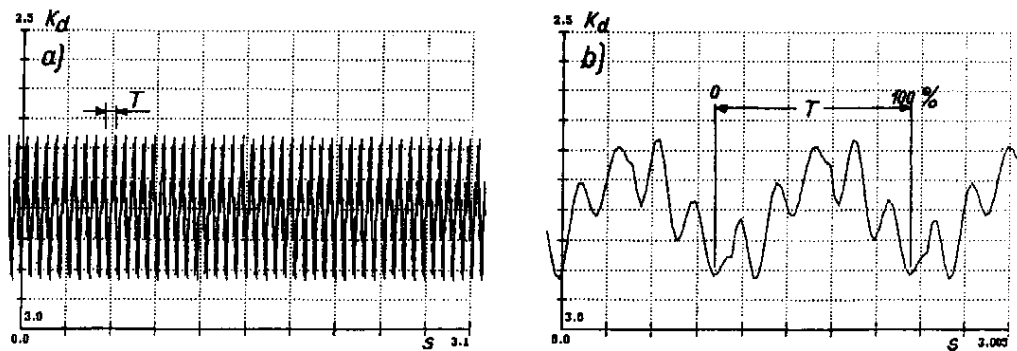


Fig. 6.2. Plot of coefficient K_d in time interval: a – 0.1 s, b – 0.005 s.

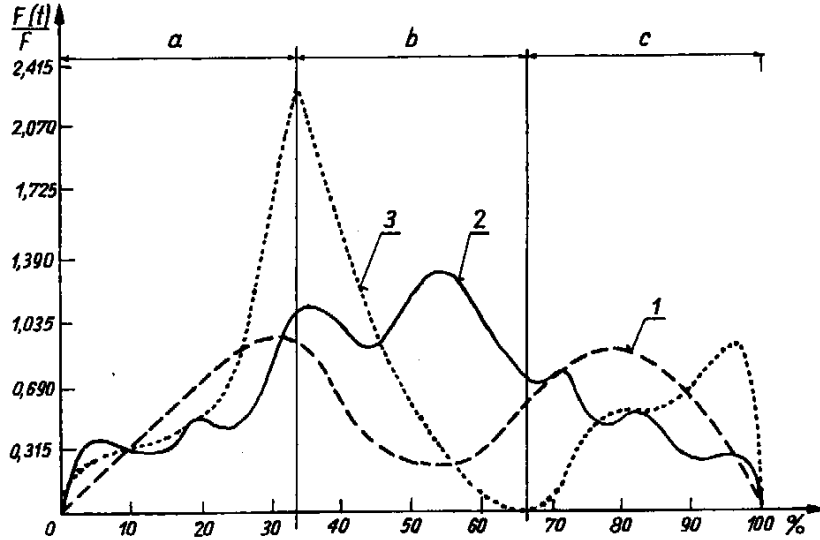


Fig. 6.3. Plot of coefficient K_d along contact line expressed in per cent, according to [6.13]: a – two-pair contact, b – one-pair contact, c – two-pair contact, 1 – above resonance, 2 – below resonance, 3 – at resonance.

As already mentioned, computer simulation results are influenced by such design factors as clutch damping C_s [Nms/rad]. The simulation studies of gear operation at the resonant velocity were conducted without damping, $C_s = 0$ and with damping $C_s = 1000$ Nms/rad. The influence of the system's free vibration on the intertooth forces is illustrated in fig. 6.15.

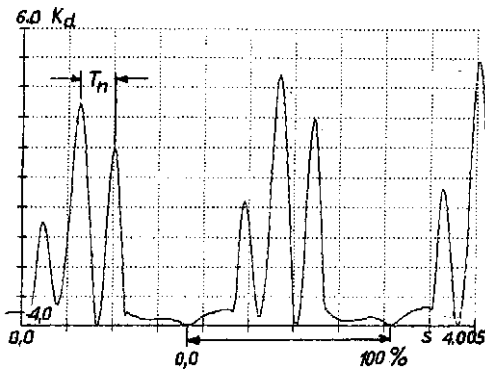


Fig. 6.4. Plot of coefficient K_d at gear subresonant rotational speed in time interval 0.005 s, 990 rev./min., $E (0.1; 10; 0; 0)$.

Natural period T_n can be read out from the figure and used to calculate a gear speed at which $T_n = T$, i.e. the meshing period is equal to the natural period of the gearing.

When the gear reaches its full rotational speed, it will run at resonance. Plots K_d for $C_s = 0$ are shown in figs 6.16 and 6.17 and for $C_s = 1000$ Nms/rad – in fig. 6.18. The influence of clutch damping on the plot of K_d is visible in the figures. A comparison of fig. 6.14, fig. 6.17 and fig. 6.18b shows agreement between the experimental results and the simulations.

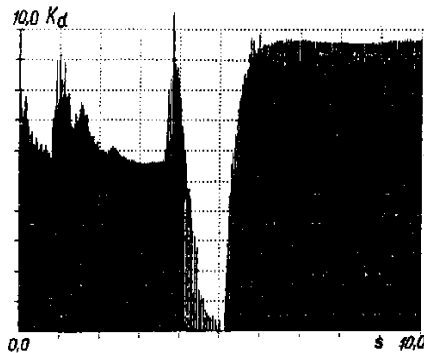


Fig. 6.5. Plots of coefficient K_d at gear resonant rotational speed.

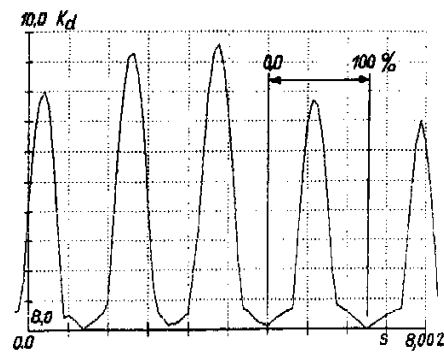


Fig. 6.6. Plots of coefficient K_d at gear resonant rotational speed in time interval of 0.002 s.

Figs 6.18-6.20 are for gear above resonance operation, fig. 6.19 for $C_s = 0$ and figs 6.18 and 6.20 for $C_s = 1000$ Nms/rad. The above investigations are described in [6.7].

Further simulations were run to study the influence of the error function's form on the dynamic forces. The modes of errors are described as follows:

- a) $E(0.1; e; 0; 0)$,
- b) $E(0.5; e; 0; 0)$,
- c) $E(0.5; -e; 0; 0)$.

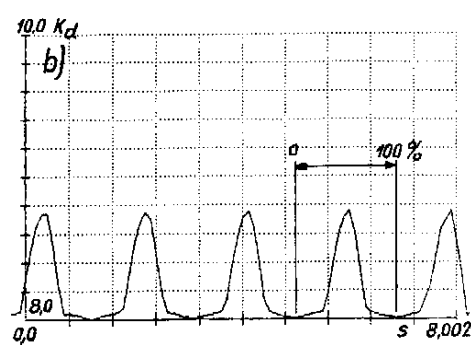
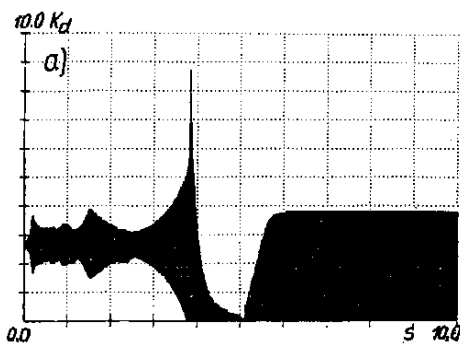


Fig. 6.7. Plot of coefficient K_d at gear over-resonance rotational speed: a – gear train with clutch damping of 1000 Nms, 6000 rev./resonant; b – in time interval of 0.002 s, 6000 rev./min.

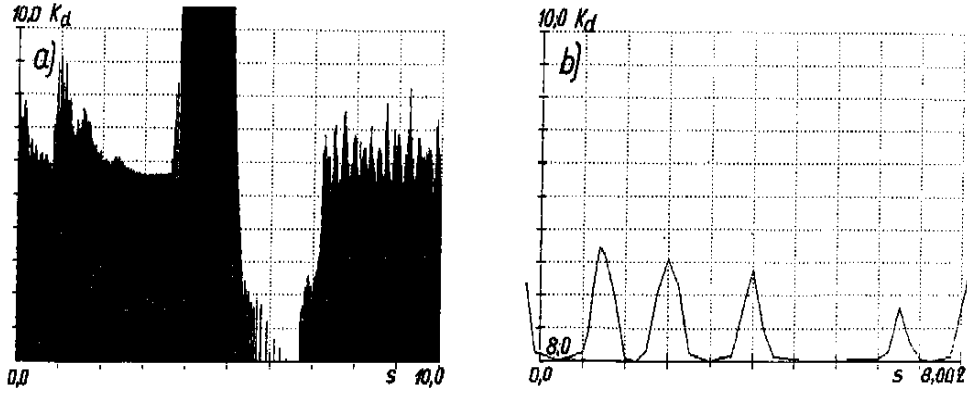


Fig. 6.8. Plot of coefficient K_d at gear above resonance rotational speed: a – 6000 rev./min., b – in time interval of 0.002 s, 6000 rev./min.

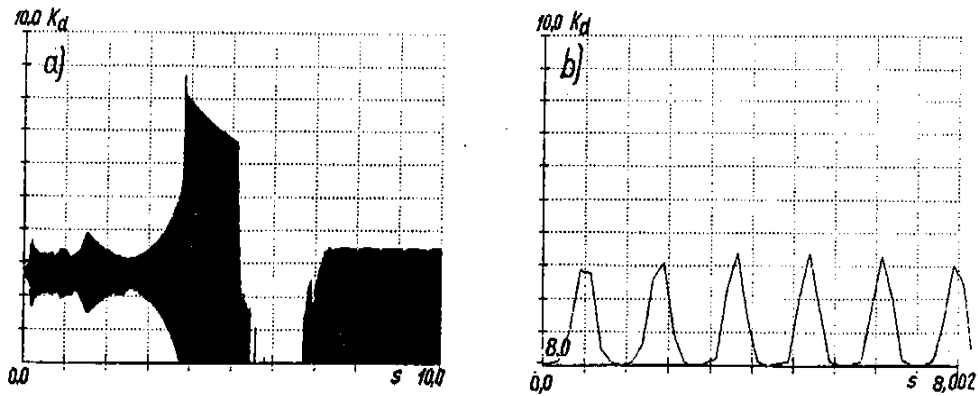


Fig. 6.9. Plot of coefficient K_d at gear over-resonance rotational speed: a – gear train with clutch damping of 1000 Nms, 6000 rev./min., b – in time interval of 0.002 s, 6000 rev./min.

The three error modes and error e [μm] as the variable factor were assumed in the simulations. Plots of the functions for $e = 10 \mu\text{m}$ are shown in fig. 6.21a, b, c. Then it was assumed that the described errors apply to a new gear – a), a run-in gear – b) and a gear damaged by pitting – c). Fig. 6.15 illustrates how coefficient a (a change of a from 0.5 to 0.1) affects the intertooth force plot. This is due to "sharp meshing" resulting in the stronger excitation of the gear to free vibration.

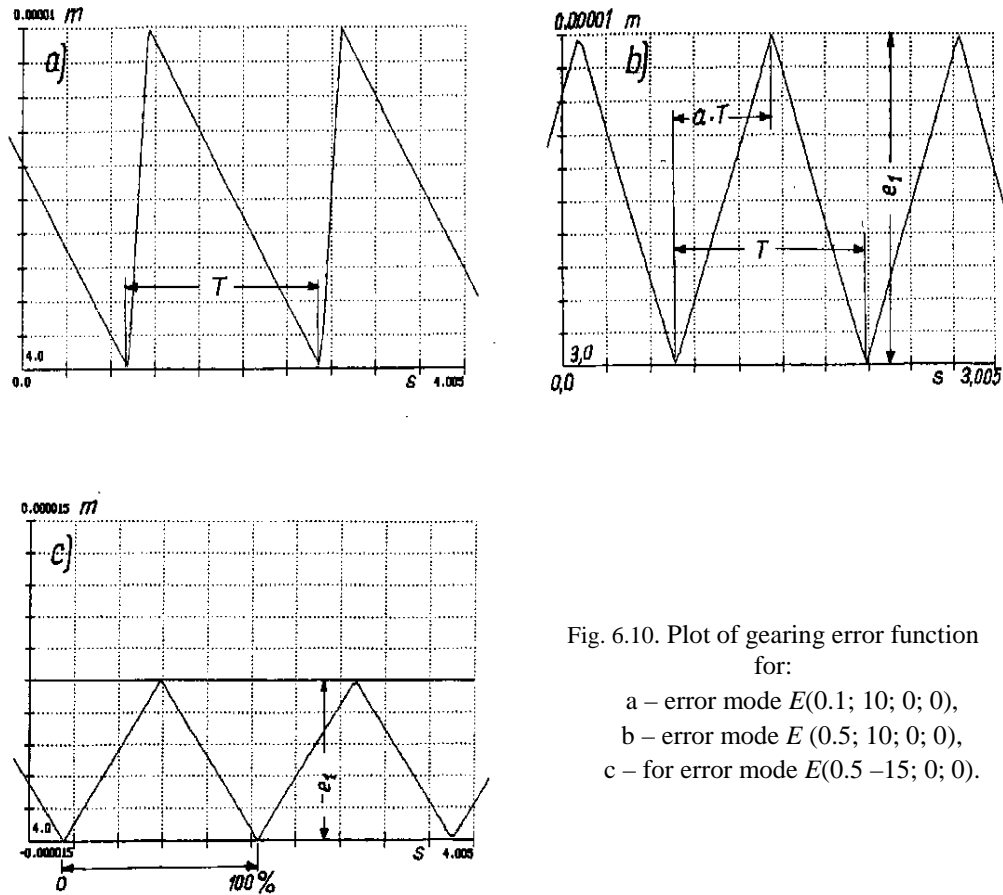


Fig. 6.10. Plot of gearing error function for:

- a – error mode $E(0.1; 10; 0; 0)$,
- b – error mode $E(0.5; 10; 0; 0)$,
- c – for error mode $E(0.5-15; 0; 0)$.

Max. K_d versus error e and versus error mode E (error modes a), b), c) in fig. 6.21) is shown in fig. 6.22a and b. One can see that K_d increases linearly up to $K_d = 2$ as e increases. At 2 a jump occurs – a symptom of the unstable operation of the gearing. As fig. 6.22 shows, the linear increase in K_d occurs at different slopes of the straight line. K_d increases most rapidly for error type a). This error mode occurs when the gearing is new or one of its rolling bearings is damaged and the contact between the teeth is uneven, which is accompanied by an increase in the value of e as compared with a new gearing. The effect of the uneven contact between the teeth on the diagnostic acceleration signal is shown in fig. 16.10 after [6.14], where a linear increase in vibration is visible (the measurements were taken in industrial conditions). In some cases the gear's operation became unstable (due to a gearing error) when the load increased. This is another corroboration of the results obtained by computer simulation.

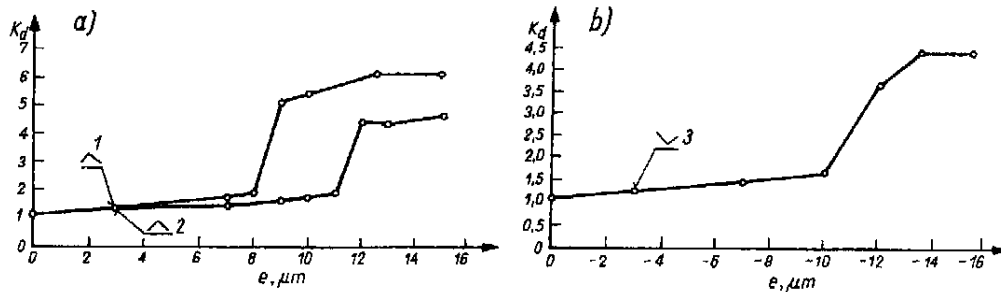


Fig. 6.11. Plot of maximum values of coefficient K_d versus error e for error modes:
 a) 1 – $E(0.1; e; 0; 0)$, 2 – $E(0.5; e; 0; 0)$; b) 3 – $E(0.5; -e; 0; 0)$.

6.7. Normalization of dynamic meshing forces

While determining dynamic force coefficient K_d the dynamic meshing forces were normalized relative to the value of nominal force F_n calculated from the rated moment transmitted by the toothed gear. Instantaneous force values can also be presented against other quantities. The aim of the normalization is to eliminate the effect of an external load on diagnostic signal plots which should reflect only the influence of design factors and of a change in condition on the diagnostic signal, excluding the simultaneous influence of load variation – an operating factor. Computer simulations were run assuming $M_s(\text{const})$; $E(0.5; 10; 0; 0)$; $M_r(1; 0; 0.9; 0; 8)$. The external load plots are shown in fig. 5.14. As coefficient $k_r = 8$ indicates, the external load changes periodically: period $T_r = 8T$ (T_r – a period of load variation, T – a meshing period). The computer simulation results are for the steady (fourth period) running of the gear (fig. 5.4). The following additional quantities describing normalization are defined:

$$K_{d1} = F(t)/F_1(t) \quad (6.50)$$

where: $F(t)$ – a current intertooth force,

$F_1(t)$ – a force twisting the first shaft, produced by torque $M_1 + M_h$ (fig. 5.1).

$$K_{d2} = F(t)/F_r(t) \quad (6.51)$$

where: $F_r(t)$ – a force changing in agreement with the external load

$$K_{d3} = F(t)/F_2(t) \quad (6.52)$$

$F_2(t)$ – a reduced-to-first-shaft force generated by the torsion of the shaft by torque M_2 (fig. 5.1).

$$K_{d4} = F(t)/F_s(t) \quad (6.53)$$

$F_s(t)$ – a force produced by averaged torque supplied by the electric motor (fig. 5.16).

The simulation results for the different normalizing forces are presented in figs 6.23-6.24. The influence of periodicity T_r in the signal (due to external load variation) is the slightest in fig. 6.24a. The gear overload values in fig. 6.23 are overrated, as compared with the average load supplied by the electric motor, since the normalization was performed relative to the nominal force.

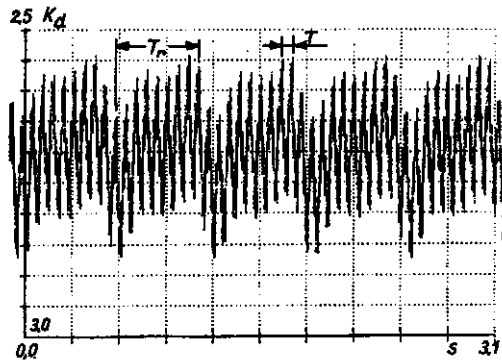


Fig. 6.1. Plot of coefficient K_d at under resonance rotational speed of gear in time interval of 0.1 s, 990 rev./min., $E(0.5; 10; 0; 0)$ and plot of external load $M_r(1; 0; 0.9; 0; 8)$.

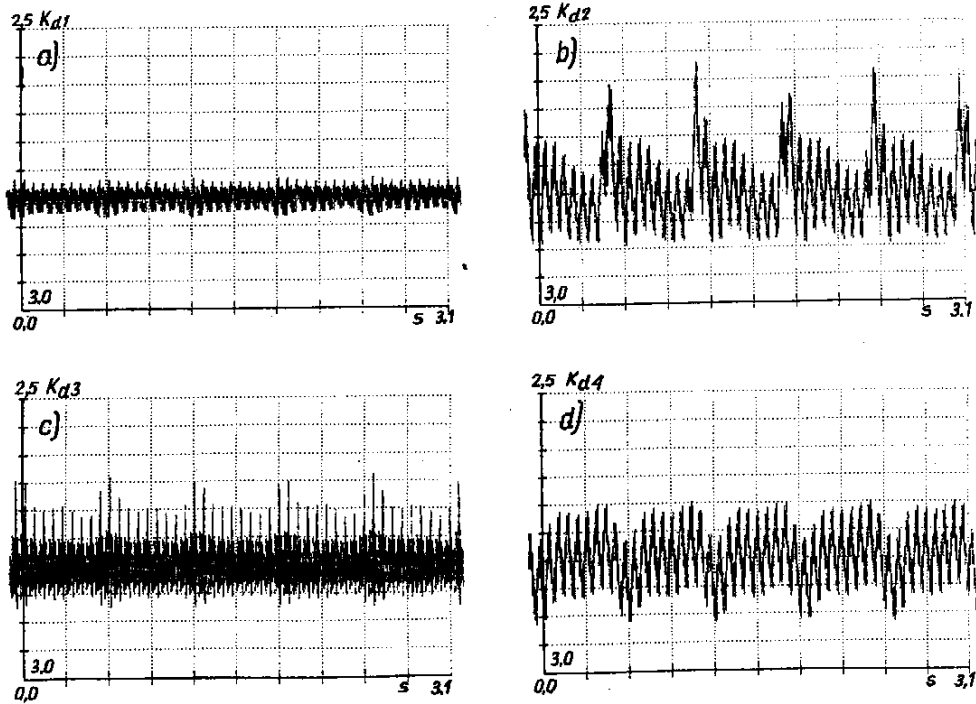


Fig. 6.2. Plots of coefficients: a – K_{d1} , b – K_{d2} , c – K_{d3} , d – K_{d4} at under resonance rotational speed of gear in time interval of 0.1 s, 990 rev./min., $E(0.5; 10; 0; 0)$ and plot of external load $M_r(1; 0; 0.9; 0; 8)$.

The shown K_d takes into account the joint effects of: the external load and factors related to the meshing properties. In gearing design/calculations these effects are separated by introducing two coefficients K_p and K_d , and their joint impact is defined as product $K_p K_d$ [6.15]. The overload value in relation to the torque supplied by the motor is given by coefficient K_{dt} (fig. 6.24d). From the diagnostic point of view a definition of K_{dl} is interesting. According to this definition, the vibration caused by the external load has the slightest influence on the course of this function.

6.8. Effect of changes in meshing stiffness and that of friction coefficient on meshing dynamics

Changes in meshing stiffness belong to design factors and they are described by coefficient g and other parameters (see fig. 6.7). A change in the meshing friction factor is caused by a change in the gearing condition or by improper lubrication. The influence of g and μ was studied under the following assumptions: M_s (const); $E(0; 0; 0; 0)$ and $M_r(0; 0; 0; 0; 0)$ – elements describing quantities invariable during a simulation. The variable elements are g and μ . Plots of driving wheel friction moments M_{t1} and driven wheel friction moments M_{t2} are shown in fig. 6.6. Plots of M_{t1} and M_{t2} for $\mu = 0.02$ and $g = 0$, obtained by computer simulation for E and M_r as assumed above, are shown in fig. 6.25a and b, respectively. The plots are for the steady running (4th period) of the gear (fig. 5.4). Plots of moments M_{t1} and M_{t2} for $\mu = 0.1$ and $g = 0$ are shown in figs 6.25c and d which illustrate only the influence of coefficient μ on the course of friction moments. Moments of friction M_{t1} and M_{t2} additionally influenced by gearing errors $E(0.5; 10; 0; 0)$ and $\mu = 0.02$ ($g = 0$) are shown in fig. 6.26.

The effect of changes in stiffness on coefficient K_d under the above assumptions and for $\mu = 0$, $g = 0.06$ (g is for a gear with helical teeth) is illustrated in fig. 6.27. The variation of meshing stiffness for $g = 0.06$ is shown in fig. 6.28. A plot of K_d for a combined effect of stiffness variation $g = 0.06$ and friction factor $\mu = 0.1$ is shown in fig. 6.29. A comparison of fig. 6.27 with fig. 6.29 shows that friction forces have a slight influence on the plot of coefficient K_d .

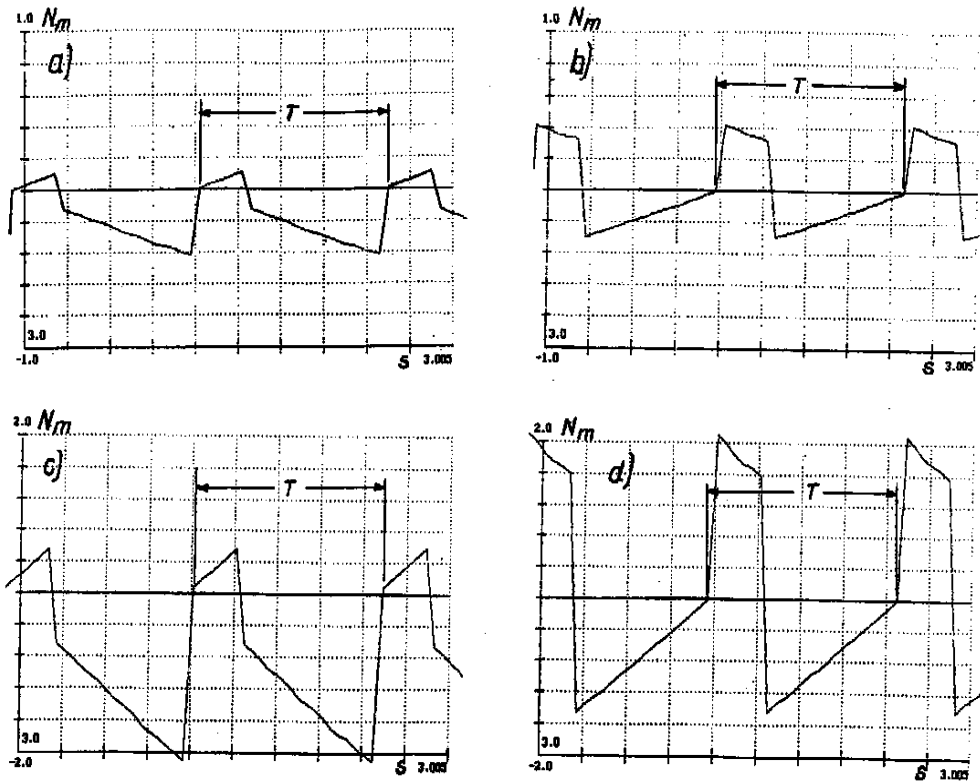


Fig. 6.1. Plots of friction moments for: a – pinion $\mu = 0.02$, b – wheel $\mu = 0.02$, c – pinion $\mu = 0.1$, d – wheel $\mu = 0.1$.

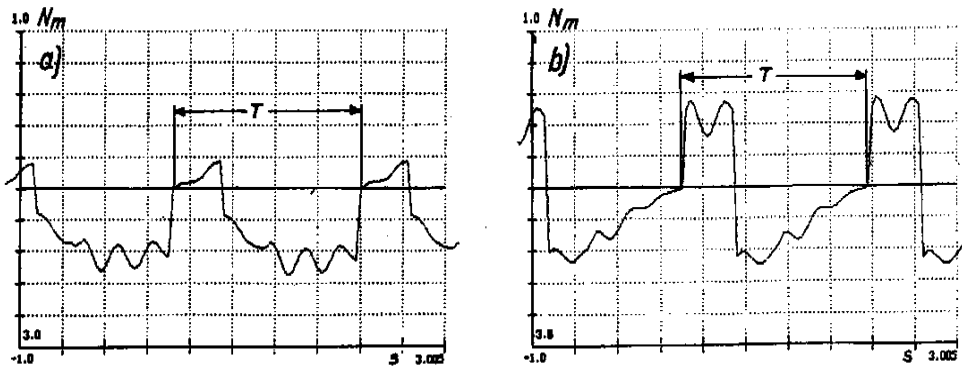


Fig. 6.2. Plots of friction moments for: a – pinion $\mu = 0.02$ at $E(0.5; 10; 0; 0)$, b – wheel $\mu = 0.02$ at $E(0.5; 10; 0; 0)$.

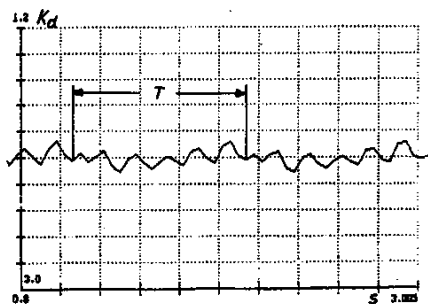


Fig. 6.3. Plot of coefficient K_d for influence of exclusively meshing stiffness variation coefficient $g = 0.06$.

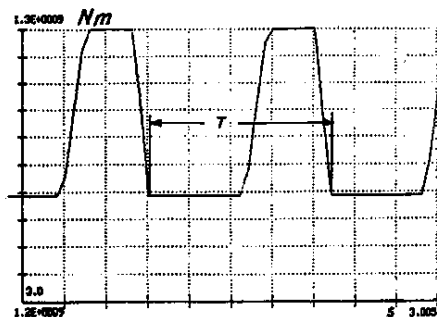


Fig. 6.4. Variation of meshing stiffness.

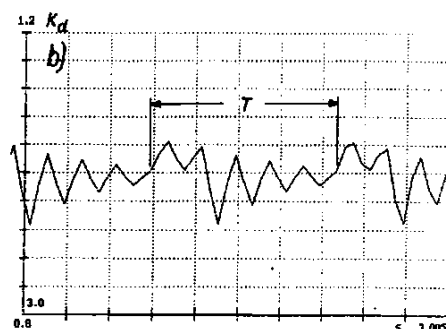
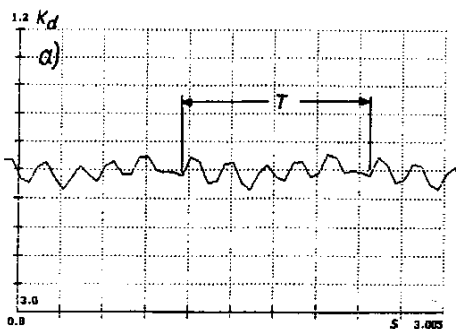


Fig. 6.5. Plot of coefficient K_d for influence of exclusively: a – meshing stiffness variation coefficient $g = 0.06$ and friction factor $\mu = 0.1$, b – friction factor $\mu = 0.5$, $g = 0.0$.

One should bear in mind that $\mu = 0.1$ corresponds to dry friction of steel against steel. If gear seizing occurs then $\mu = 0.5$, $g = 0.0$ is assumed to describe it. The computer simulation result is shown fig. 6.29b. The whole K_d plot for $\mu = 0.5$ and $g = 0.4$, where g is as for a spur gearing, is shown in fig. 6.30. The four gear operation stages (denoted 1 – 4) are marked in the figure. The intermeshing of the gearing for selected time intervals during the starting of the gear is described in detail in fig. 6.31a, b, c, d. The dynamic effect of the applied (during starting) motor driving torque double the value of the rated torque is shown in fig. 6.31a. Also the system's response to the abrupt application of a driving torque (cf. figs 4.10, 4.44 and 4.45) and period T decreasing with increasing rotational speed are visible. Fig. 6.30 shows that the total effect of stiffness variation $g = 0.4$ (for a spur gearing) and $\mu = 0.5$ (representing the intermeshing of the gears in seizing conditions) is a 25% increase (as compared to the rated load) in the intertooth forces (the fourth gear meshing period). The intermeshing of the gears for $g = 0.06$ and coefficient $\mu = 0.5$ (4th meshing period) is illustrated in fig. 6.32.

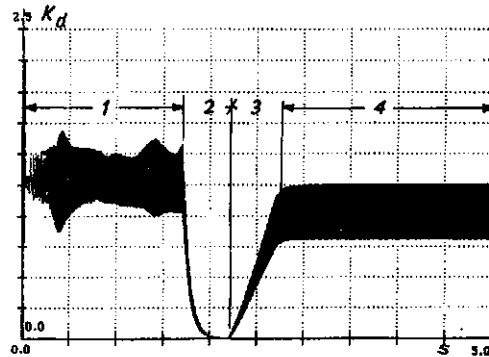


Fig. 6.6. Plot of coefficient K_d for influence of meshing stiffness variation coefficient $g = 0.4$ alone and friction factor $\mu = 0.5$ alone; 1+4 gear meshing periods.

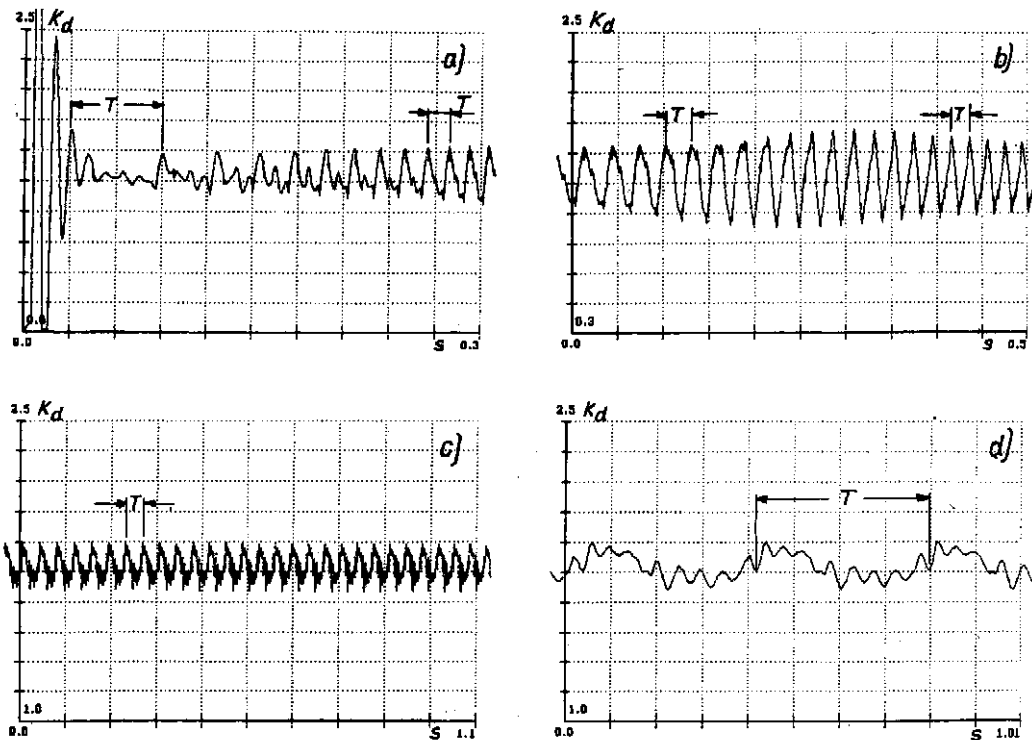


Fig. 6.7. Plot of coefficient K_d for influence of meshing stiffness variation coefficient $g = 0.4$ alone and friction factor $\mu = 0.5$ alone in starting time interval: a – $0 \div 0.3$ s, b – $0.3 \div 0.5$ s, c – $1 \div 1.1$ s, d – $1 \div 0.1$ s.

The plot is shown for a time interval of 0.005 s. Since the principal factor influencing intermeshing is a high coefficient of friction – $\mu = 0.05$, the plot is similar to

those for friction moment variation (fig. 6.25c, d). Figs 6.32-6.34 show plots of K_d and K_{d1} for $\mu = 0.5$ and $g = 0.4$.

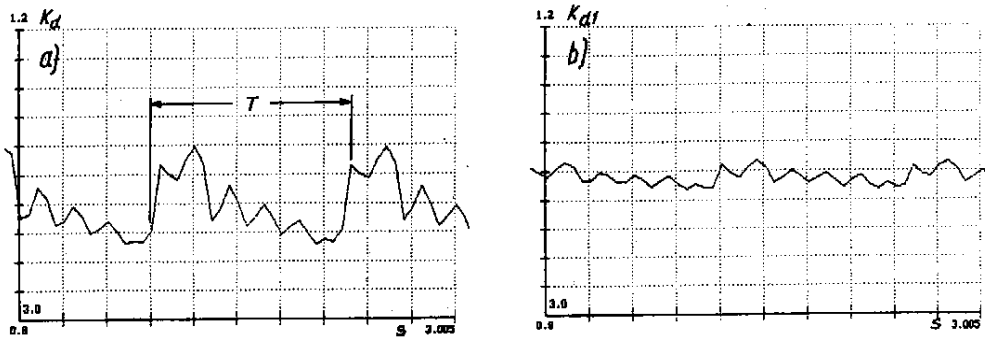


Fig. 6.8. Plot of coefficients: a – K_d , b – K_{d1} for influence of meshing stiffness variation coefficient $g = 0.06$ alone and friction factor respectively $\mu = 0.5$ and $\mu = 0.1$ alone in time interval of 0.005 s.

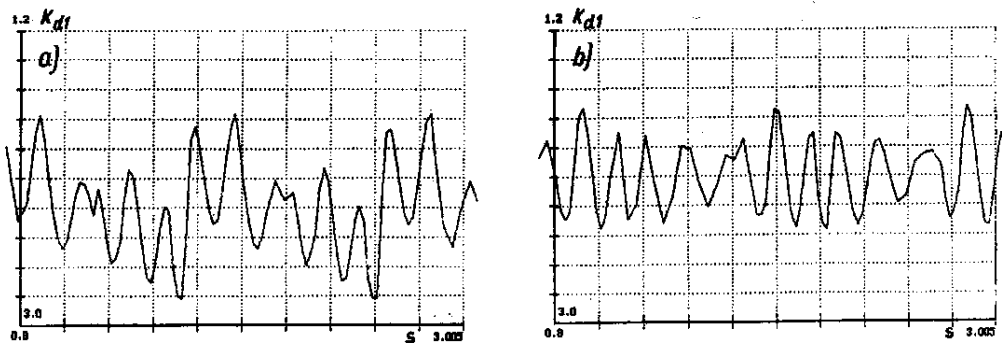


Fig. 6.9. Plot of coefficient K_{d1} for influence of meshing stiffness variation coefficient $g = 0.4$ alone and friction factor : a – $\mu = 0.0$, b – $\mu = 0.5$ alone in time interval of 0.005 s.

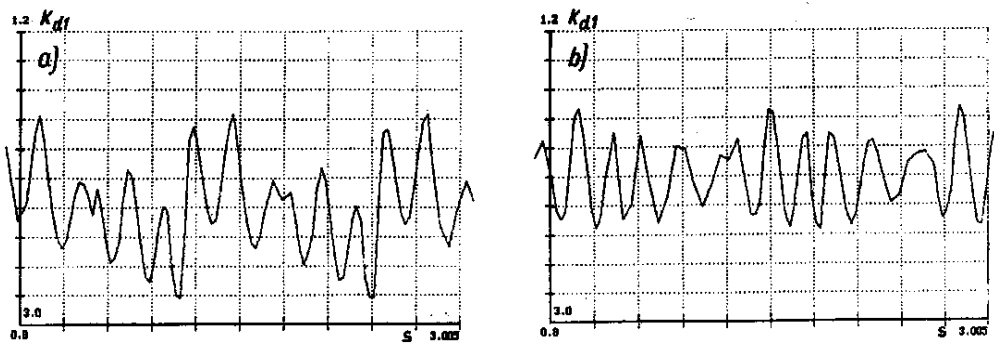


Fig. 6.10. Plot of coefficient K_d for influence of meshing stiffness variation coefficient $g = 0.4$ alone and friction factor: a – $\mu = 0.0$, b – $\mu = 0.5$ alone in time interval of 0.005 s.

For K_{dl} in fig. 6.33a and fig. 6.33b the combined effect of $\mu = 0.5$ and $g = 0.4$ can be distinguished from that of $\mu = 0$ and $g = 0.4$. This effect cannot be distinguished for K_d in figs 6.34a and b. In this way K_{dl} again has proved to be more useful.

6.9. Relationship between intertooth forces and relative acceleration of gear wheels

So far intertooth forces being a direct measure of the condition of intermeshing have been considered. It is intertooth forces which determine the durability of a gearing. It is very difficult, sometimes impossible, to assess the condition of a gearing directly. Accelerations are measured in order to diagnose gears. Accelerations can be measured directly on gear wheels, but this is rather difficult to do. In diagnostic practice, vibration accelerations are measured on the gearbox wall.

In this section the relationship between intertooth forces and relative accelerations of gear wheels is presented. This relationship can be determined by tests described in chap. 1 (fig. 1.13 – the test stand). The accelerations are transmitted to the gearbox wall via the rolling bearings. Since very good agreement between the test results and the computer simulation results had been found (chap. 6.5), computer simulation was used to determine the relationships between intertooth forces and gear wheel accelerations. The simulations were run for the following conditions $E(0.5; 10; 0; 0)$; $M_r(0; 0; 0; 0; 0)$; $M_s(\text{const})$. The effect of viscous damping (a design factor) in clutch C_s on the above relationship was investigated. For the first few simulations it was assumed that the system shown in fig. 5.1 incorporates a clutch for which $C_s = 1000$ Nms/rad. A plot of intertooth forces $F + F$ for the above conditions defined by E ; M_r and M_s is shown in fig. 6.35.

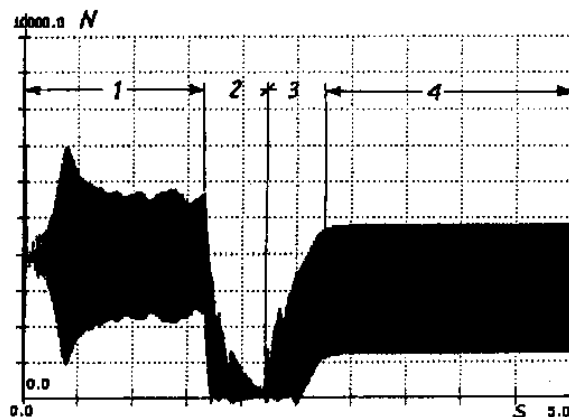


Fig. 6.1. Plot of intertooth forces (sum of elastic and damping forces): 1÷4 gear meshing periods.

A zoom of the plot of intertooth forces for the same conditions is shown in fig. 6.36a. This fragment is for the fourth gear meshing period – the gearing operates under a rated steady load. A zoom of the wheel acceleration difference $\ddot{\varphi}_3 - \ddot{\varphi}_2$ plot is shown in fig. 6.36b. Acceleration $\ddot{\varphi}_3$ corresponds to the angular acceleration of the driven wheel and $\ddot{\varphi}_2$ to the angular acceleration of the driving wheel.

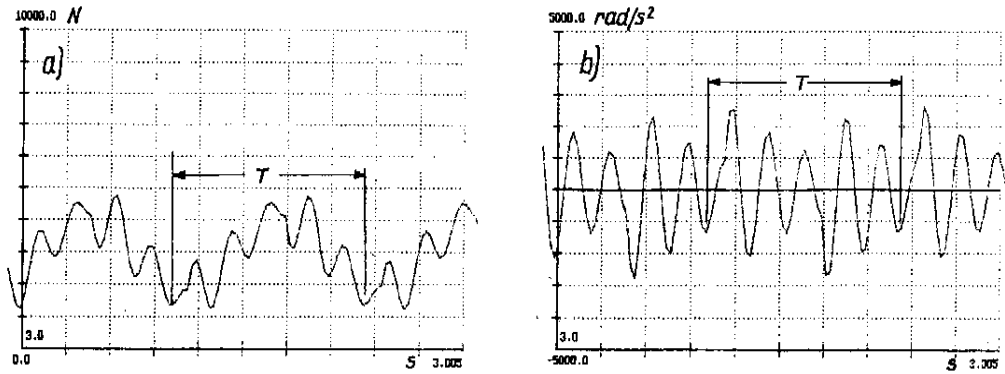


Fig. 6.2. Plot of intertooth forces (sum of elastic and damping forces) (a) and accelerations of torsional vibration of gear wheels (b) for time interval of 0.005 s.

A comparison of fig. 6.36a and fig. 6.36b shows a similarity between the plots of these physical quantities; the average value of the acceleration plot is equal to zero. But this similarity is not full. A plot of accelerations in the four meshing periods (described in chap. 6.5) is shown in fig. 6.37. Plots of the intertooth forces and those of the acceleration difference for increasing rotational speed of the gear (the first period) are shown respectively in fig. 6.38a and b. As one can see in fig. 6.38b, the acceleration plot differs from the intertooth force plot. The acceleration difference changes with a frequency corresponding to half of the meshing period ($1/2T$). Changes associated with the frequency of the free vibration of the gearing and a variation in the intertooth force plot are clearly visible. Variation period $T = 0.00368$ s corresponds to a rotational speed of 9.713 rev./s for $t = 1$ s from the moment when the system starts spinning. Figs 6.39a and b illustrate the intertooth forces and the acceleration difference for $E(0.1; 10; 0; 0); M_r(0; 0; 0; 0; 0)$ – parameter a changed from 0.5 to 0.1. This change of parameter a can be due to a change in the condition of the rolling bearing resulting in edgewise intermeshing. A zoom of the intertooth force plot and a zoom of the acceleration difference $\ddot{\varphi}_3 - \ddot{\varphi}_2$ plot for this condition of the gear for a time interval of 0.005 s are shown respectively in fig. 6.40a and fig. 6.40b.

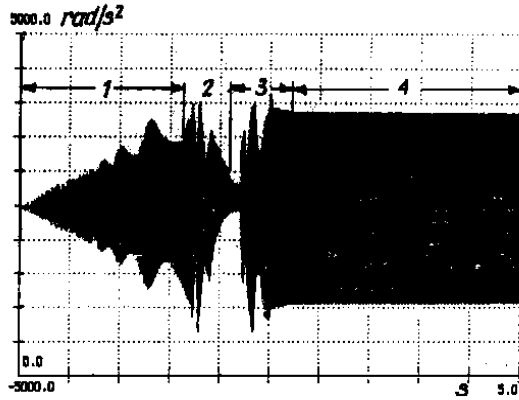


Fig. 6.3. Plot of acceleration of gear wheel torsional vibration: 1÷4 gear meshing periods.

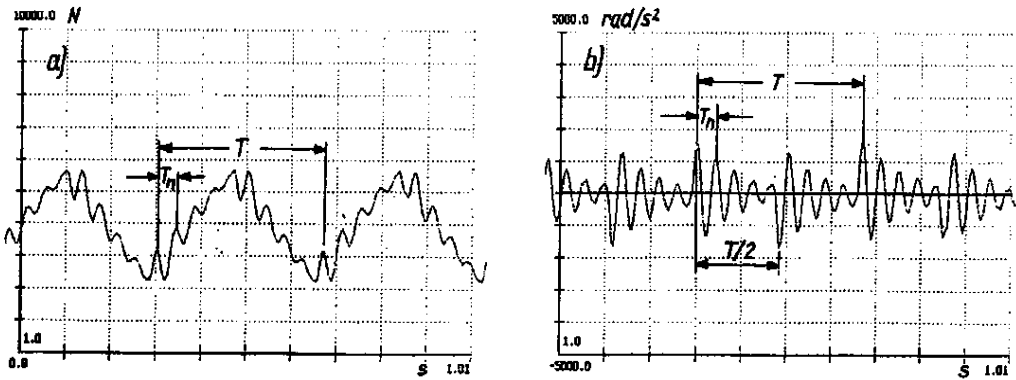


Fig. 6.4. Plot of intertooth forces (sum of elastic and damping forces) (a) and gear wheel torsional vibration acceleration plot (b), for time interval of (1÷1.01 s).

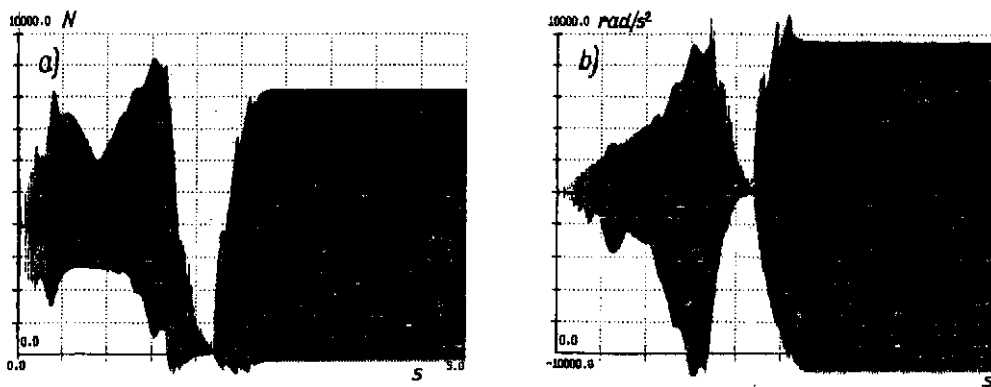


Fig. 6.5. Plot of intertooth forces (sum of elastic and damping forces) (a) and gear wheel torsional vibration acceleration plot (b), for $E(0.1; 10; 0; 0)$

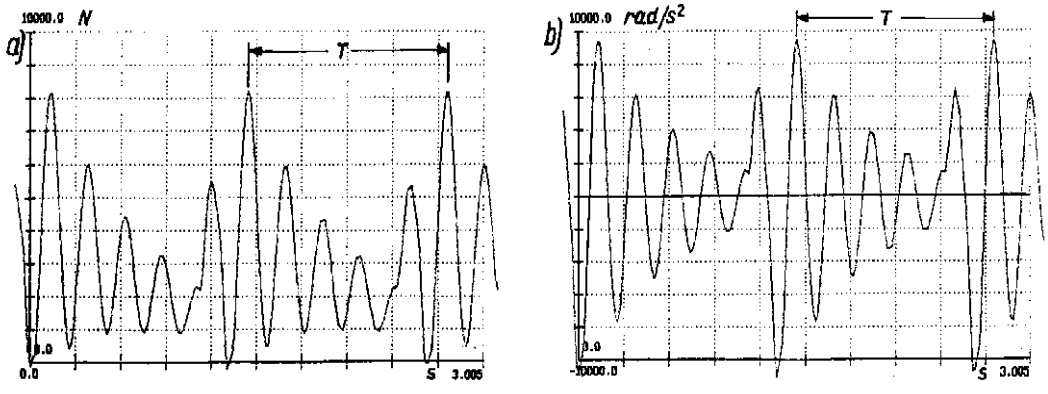


Fig. 6.6. Plot of intertooth forces (sum of elastic and damping forces) (a) and gear wheel torsional vibration acceleration plot (b), for $E(0.1; 10; 0; 0)$ and time interval of 0.005 s.

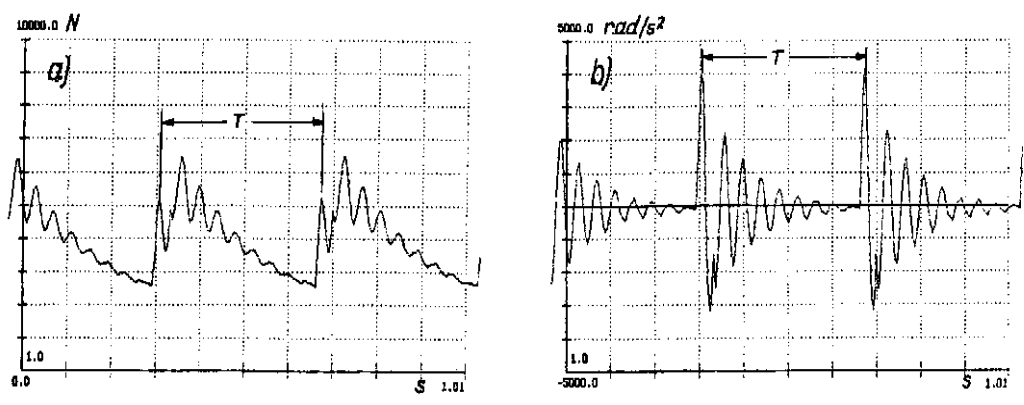


Fig. 6.7. Plot of intertooth forces (sum of elastic and damping forces) (a) and gear wheel torsional vibration acceleration plot (b), for $E(0.1; 10; 0; 0)$ and time interval of (1-1.01 s).

Good agreement (close similarity) between the plots is observed. This means that vibration accelerations faithfully reflect the state of intermeshing. Simulations were run for $C_s = 1000$ Nms/rad. The intertooth force plot and the gear wheel acceleration difference plot after the first second of gear running are shown respectively in fig. 6.41a and b. The acceleration plot is only to some degree similar to the intertooth force plot. The differences are probably due to, among others, the influence of the clutch, i.e. to the C_s value. In further simulations $C_s = 0$ was assumed. The full acceleration and intertooth force plots are shown in figs 6.42 and 6.43 for the four gear meshing periods.

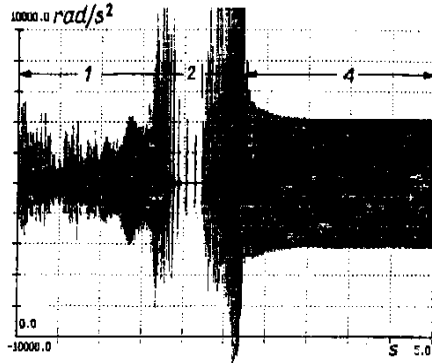


Fig. 6.8. Plot of gear wheel torsional vibration acceleration for $E(0.5; 10; 0; 0)$ for system incorporating clutch with damping of 1000 Nms.

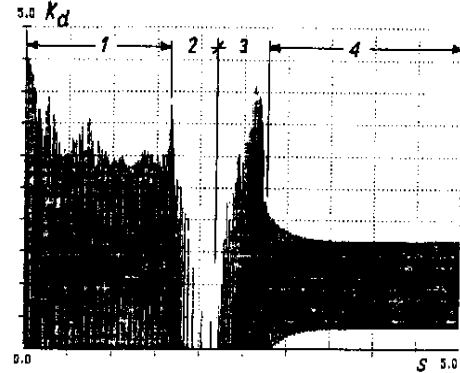


Fig. 6.9. Plot of coefficient K_d for $E(0.5; 10; 0; 0)$.

Zooms of the plots in a time interval of 0.005 s are shown in figs 6.44a (acceleration difference) and b (intertooth forces). Plot of K_d is shown in fig. 6.45a. A strong similarity between the forces and the accelerations, stronger than the similarity between figs 6.36a and b when the gear was operating at the same parameters E and M_I but with a clutch characterized by damping $C_s = 1000$ Nms/rad., can be seen in figs 6.45b and c. This means that the degree of similarity between the intertooth force plot and the acceleration plot depends on the damping in the clutch and it is the greater, the better the condition of the gearing. Plots of K_d after the first second of gearing operation are shown in figs 6.45b and c. The intertooth forces do not change with period T but with period T_I which is about 4 times longer than period T (the simulation was run for $C_s = 0$). The stiffness of the clutch has an influence on the obtained result.

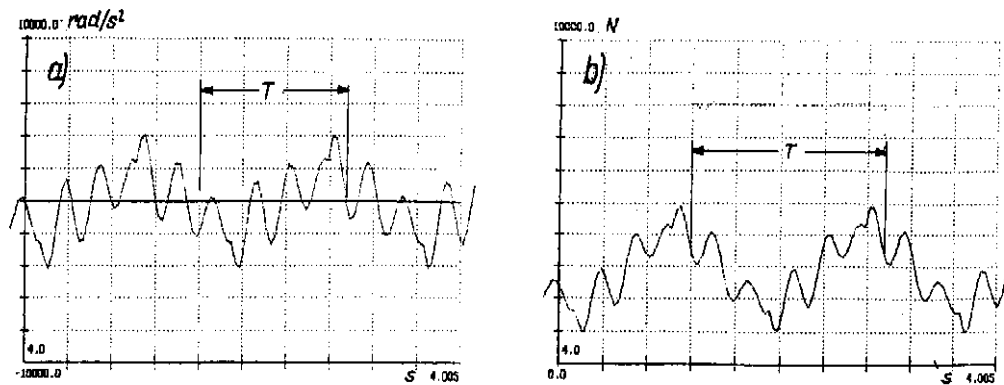


Fig. 6.10. Gear wheel torsional vibration acceleration plot (a) and plot of intertooth forces (sum of elastic and damping forces) (b) for $E(0.5; 10; 0; 0)$ and time interval of 0.005 s.

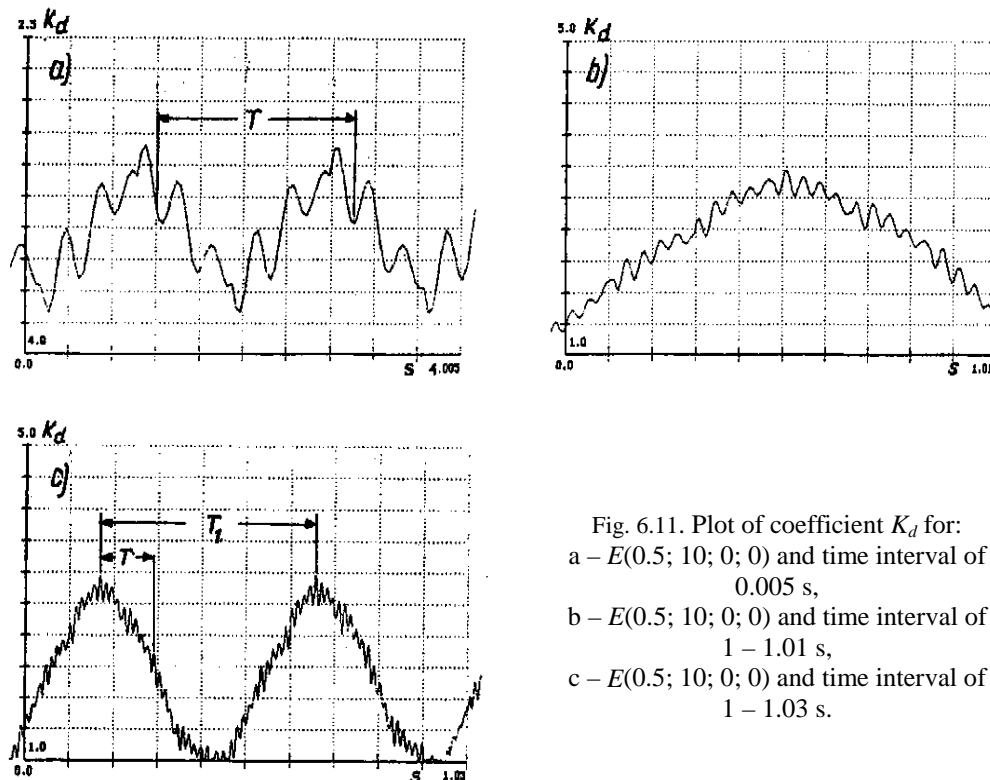


Fig. 6.11. Plot of coefficient K_d for:
 a – $E(0.5; 10; 0; 0)$ and time interval of 0.005 s,
 b – $E(0.5; 10; 0; 0)$ and time interval of 1 – 1.01 s,
 c – $E(0.5; 10; 0; 0)$ and time interval of 1 – 1.03 s.

A physical model and a mathematical model of a gear incorporated into a power transmission system (fig. 5.1) were presented in this chapter. Results of computer simulations were reported and shown to be in agreement with test-stand results [6.13] and industrial test results [6.14]. Computer simulations revealed the basic dynamic properties of the investigated systems. The considered example of a power transmission system with a toothed gear showed that simulations can be used to determine the relationship between design factors, changes in condition (wear) and motion parameters (operating factors), which in the course of the operation of a machine become symptoms of the machine's condition. From these symptoms the condition of the machine can be diagnosed. Various other relationships between the above factors and the form of the diagnostic signal are presented in the next chapters. It became obvious that the problems involved in the analysis of the relationship between the condition of a machine and signals – symptoms of this condition – are complex. To facilitate the use of methods of engineering diagnostics, expert systems are being developed. The latest expert systems incorporate neural networks. This will be discussed in chap. 19.

6.10. References

- [6.1] Müller L.: Gearboxes, Dynamics (in Polish), Warsaw, WNT, 1986.
- [6.2] Wilk A. et al.: Software for Determining Meshing Stiffness of Spur, Helical and Herringbone Gears (in Polish), Gliwice, Silesian Polytechnic, 1992 (unpublished).
- [6.3] Bartelmus W., Nosowicz B.: Relationship between Vibroacoustic Diagnostics and Machine Design Fundamentals (in Polish), 26th Open Seminar on Acoustics, Wrocław-Oleśnica 1979, Wrocław University of Technology, 1979.
- [6.4] Bartelmus W.: Application of Some Statistical Estimators of Vibration Signal as Criteria for Assessing Gearing Condition (in Polish), *Scientific Papers of Silesian Polytechnic, Mining*, No. 616, 1979.
- [6.5] Bartelmus W.: Vibration Condition Monitoring of Gearboxes, *Machine Vibration*, No. 1, pp. 178-189, 1992.
- [6.6] Bartelmus W.: Computer Simulation of Vibration Generated by Meshing of Toothed Wheel for Aiding Diagnostic of Gearboxes, Conference Proceedings Condition Monitoring '94 Swansea, UK Pine-Ridge Press, Swansea, UK.
- [6.7] Bartelmus W.: Diagnostic Symptoms of Unstability of Gear Systems Investigated by Computer Simulation, Proceedings of 9th International Congress COMADEM 96 Sheffield, July 1996, Sheffield Academic Press Ltd., 1996.
- [6.8] Bartelmus W.: Visualization of Vibration Signal Generated by Gearing Obtained by Computer Simulation, Proceedings of 14th IMEKO World Congress 1997, Finnish Society of Automation, 1997.
- [6.9] Bartelmus W.: Influence of Random Outer Load and Random Gearing Errors on Vibration Diagnostic Signals Generated by Gearbox Systems, Proceedings of 10th International Congress COMADEM '97, Sheffield Academic Press Ltd., 1997.
- [6.10] Bartelmus W.: Transformation of Gear Intertooth Forces into Acceleration and Velocity, Proceedings of the 7th International Symposium on Transport Phenomena and Dynamics of Rotating Machinery, February 1998.
- [6.11] Bartelmus W.: Introduction For Developing Individual Vibration Severity Criteria for Gearbox Maintenance, *Third International Symposium on Mine Mechanization and Automation, Golden Colorado, USA, Colorado School of Mines*, Vol. 2, pp. 17-13 to 17-24, June 1995.
- [6.12] Bartelmus W.: Modelling of Working Machine Gear Dynamics as Aid to Diagnostics (in Polish), Proceeding of Conference on Diagnostics of Earthmoving Machines and Vehicles, Bydgoszcz, Academy of Technology and Agriculture, pp. 15-20, 1994.
- [6.13] Rettig H.: Innere Dynamische Zusatzkräfte bei Zahanadgetrieben, *Ant. Antriebstechnik 16 (1977)*, No. 11, pp. 655-663.
- [6.14] Bartelmus W.: Vibration Condition Monitoring of Gearboxes, *Machine Vibration*, No. 1, pp. 178-189, 1992.
- [6.15] Müller L.: Toothed Gears, Design (in Polish), WNT, Warsaw, 1979.

7. Modelling of kinematics and dynamics of rolling bearings

One of the key components of mining machines is the rolling bearing. In engineering diagnostics the rolling bearing is treated as an assembly of elements (an outer ring, an inner ring, a rolling element and a cage).

Rolling bearings are subject to all forms of bearing capacity loss [7.1]. One form of this kind of loss is a fatigue failure, which is initiated by a single hollow/cavity in the race or in the rolling element. The rolling element as it passes over such a defect generates damped vibration of natural frequency. A plot of the vibration is shown in fig. 4.21. The frequency with which the rolling element passes over a damaged spot or the frequency with which the damaged ball contacts the race can be determined from the kinematics of the reciprocal motions of the bearing's components assuming that the defect occurs in the inner race – the fixed race. The distribution of instantaneous velocities is shown in fig. 7.1.

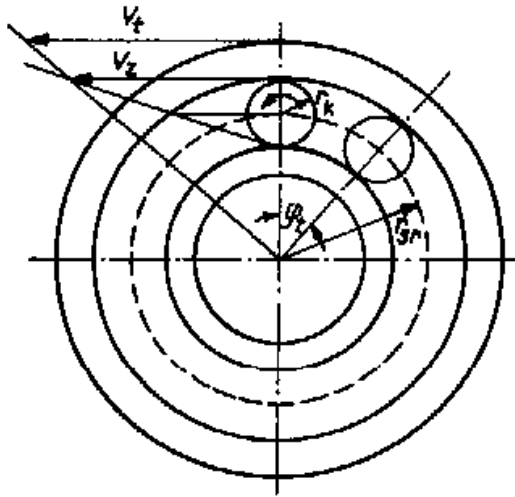


Fig. 7.1. Distribution of velocities in rolling bearing with fixed inner ring.

This situation corresponds to the kinematics of a bearing mounted on the axle of a belt conveyor roller. The velocity of the belt corresponding to the tangential velocity of the roller shell is denoted by v_f . It is assumed that no slip occurs between the components shown in fig. 7.1. If velocity v_f is known, actual velocity v_z of the contact be-

tween the rolling element (ball) and the bearing outer race as well as roller angular velocity ω can be determined. If the roller angular velocity is known, tangential velocity v_z can be calculated from this formula

$$v = \omega(r_{sr} + r_k), \text{ m/s} \quad (7.1)$$

where: r_{sr} – an average radius, m (fig. 7.1);
 r_k – the radius of the ball, m.

It follows from fig. 7.1 that the peripheral speed of the cage's centre is

$$v_{ko} = v_z/2 \quad (7.2)$$

and the angular velocity of the cage is

$$\omega_{ko} = v_{ko}/r_{sr} = v_z/(2r_{sr}), \text{ rad/s} \quad (7.3)$$

Putting v_z into the above formula we get:

$$\omega_{ko} = \omega(r_{sr} + r_k)/(2r_{sr}) \quad (7.4)$$

If the bearing has l_k balls, then after each revolution of the cage by this angle

$$\varphi_p = 2\pi/l_k \quad (7.5)$$

a ball passes over the damaged spot causing vibration. There is the following relationship between the angular velocity and the cage revolution frequency

$$\omega_{ko} = 2\pi f_{ko} = 2\pi/T_{ko} \quad (7.6)$$

where T_{ko} is a period of one cage revolution, s.

The period corresponding to the passage of a ball over the damaged spot in the inner race is

$$T_p = T_{ko}/l_k = 2\pi/(l_k \omega_{ko}) \quad (7.7)$$

Thus the frequency of passage over the damaged spot in the fixed inner race is

$$f_{pw} = 1/T_p = l_k \omega_{ko}/(2\pi) = l_k \omega(r_{sr} + r_k)/(4\pi r_{sr}) \quad (7.8)$$

Since $\omega = 2\pi f$, where f is the frequency of the revolutions of the bearing in the roller, then

$$f_{pw} = l_k f(r_{sr} + r_k)/(2\pi r_{sr}) = l_k f(1 + r_k/r_{sr})/2 \quad (7.9)$$

Taking into account the contact angle of the bearing, the ball contacts the race on radius r_s (fig. 7.2), i.e. the frequency of its passage over the damaged spot is

$$f_{pw} = l_k f(1 + r_k/r_{rs} \cos \alpha)/2 \quad (7.10)$$

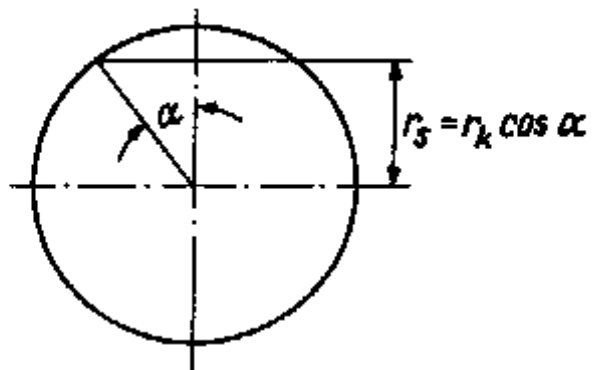


Fig. 7.2. Contact angle of rolling bearing.

The distribution of velocities for the kinematic pairs of the bearing in a case when the inner ring rotates, which corresponds to the operation of a bearing in a gearbox, is shown in fig. 7.3a. If it is assumed that the outer ring is damaged (the damaged spot is consistent with the direction of the force acting on the bearing), then on the basis of fig. 7.3a one can write the following relations

$$v_w = \omega (r_{sr} - r_k) \quad (7.11)$$

$$v_{ko} = v_w / 2 \quad (7.12)$$

$$\omega_{ko} = v_{ko} / (2r_{rs}) \quad (7.13)$$

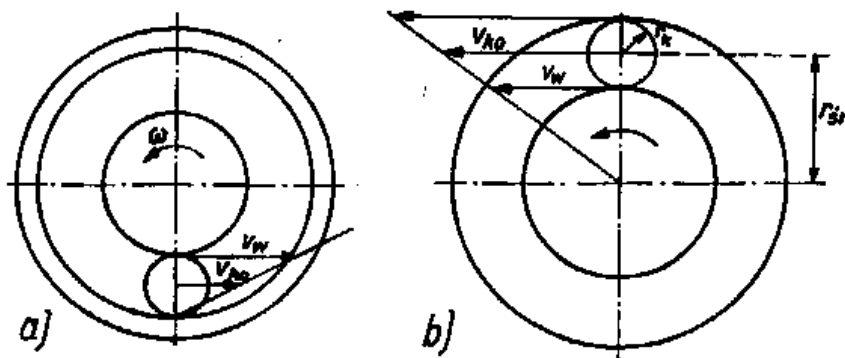


Fig. 7.3. Distribution of velocities in rolling bearing:
 a – for fixed outer ring,
 b – for movable inner and outer rings.

Putting (7.11) into expression (7.13) we get

$$v_w = \omega (r_{sr} - r_k)/(2r_{rs}) \quad (7.14)$$

Similar reasoning as above leads to a formula for the frequency of passage over a damaged spot in the outer race when the inner race revolves

$$f_{pz} = l_k f (1 - r_k/r_{sr})/2 \quad (7.15)$$

Taking into account the contact angle of the bearing, we get

$$f_{pz} = l_k f (1 - r_k/r_{sr} \cos \alpha)/2 \quad (7.16)$$

where l_k is a number of rolling elements in the bearing.

To take into account the effect of a bearing defect on the generation of a diagnostic signal, a relation describing angles of rotation φ between the components of a rolling bearing is needed. If the inner race is damaged (the bearing works in a belt conveyor roller), then by putting $\omega_{ko} = d\varphi_{ko}/dt$ and $\omega = d\varphi/dt$ into relation (7.10) we get

$$d\varphi_{ko}/dt = d\varphi/dt (r_{sr} - r_k)/(2r_{rs}) \quad (7.17)$$

Hence after integration by sides we get

$$\varphi_{ko} = \varphi (r_{sr} - r_k)/(2r_{rs}) \quad (7.18)$$

If the inner ring revolves, the following relationship between the angles of rotation is obtained:

$$\varphi_{ko} = \varphi (r_{sr} + r_k)/(2r_{rs}) \quad (7.19)$$

Also the angular velocities of the ball can be determined from figs 7.1 and 7.3a. And so when the outer ring revolves (as in the case of a roller), we get

$$\omega_k = v_z/(2r_k) = \omega (r_{sr} + r_k)/(2r_k) \quad (7.20)$$

The relation for the angles of rotation is as follows

$$\varphi_k = \varphi (r_{sr} + r_k)/(2r_k) \quad (7.21)$$

Similar relations for the case when the inner ring revolves (fig. 7.3a) are as follows

$$\omega_k = v_w/(2r_k) = \omega (r_{sr} - r_k)/(2r_k) \quad (7.22)$$

and for the angles of rotation

$$\varphi_k = \varphi (r_{sr} - r_k)/(2r_k) \quad (7.23)$$

In some cases both races can revolve – as shown in fig. 7.3b. The absolute velocity of the cage is

$$v_{bko} = (v_z + v_w)/2 = \omega_{bko} r_{sr} \quad (7.24)$$

hence

$$\omega_{bko} = (v_z + v_w)/(2r_{sr}) \quad (7.25)$$

The peripheral speed of the cage relative to the inner ring is

$$v_{wko} = (v_z - v_w)/2 = \Delta v_z/2 \quad (7.26)$$

where Δv_z is the velocity of the outer ring relative to that to the inner ring.

The relative velocity of the outer ring can also be calculated from this relation

$$\Delta v_z = \Delta \omega (r_{sr} + r_k) \quad (7.27)$$

The relative angular velocity of the cage is

$$\omega_{wko} = \Delta v_z/(2r_{sr}) = \Delta \omega (r_{sr} + r_k)/(2r_{sr}) \quad (7.28)$$

Taking into account $\Delta \omega = 2\pi \Delta f$, the frequency of passage over a damaged spot in the inner race is

$$f_{pw} = l_k \Delta f (1 + r_k/r_{sr})/2 \quad (7.29)$$

where l_k is a number of elements.

Also the frequency at which the system is excited to vibration when a ball is damaged can be determined. The length of the line of the vibration-producing contact between the ball and the inner ring is equal to the ball's circumference, i.e.

$$\varphi_{pko}(r_{sr} - r_k) = 2\pi r_k \quad (7.30)$$

The relationship between the angle of rotation of the cage and that of the bearing is expressed by

$$\varphi_{pko} = \varphi_p (r_{sr} + r_k)/(2r_{sr}) \quad (7.31)$$

according to (7.19). After putting the above into (7.30) we get

$$\varphi_p (r_{sr} + r_k)/(2r_{sr}) (r_{sr} - r_k) = 2\pi r_k \quad (7.32)$$

From (7.32) one can calculate

$$\varphi_p = 4\pi r_k r_{sr}/(r_{sr}^2 - r_k^2) \quad (7.33)$$

The number of impulses per one revolution of the bearing is

$$2\pi/\varphi_p = (r_{sr}^2 - r_k^2)/(2r_k r_{sr}) \quad (7.34)$$

If the bearing rotates at f [rev./s], then the frequency with which the ball comes in contact with the race is

$$f_p = f/(2r_k r_{sr}) (r_{sr}^2 - r_k^2) \quad (7.35)$$

Taking into account the contact angle of the bearing, we get

$$f_p = f/(2r_k r_{sr}) (r_{sr}^2 - r_k^2 \cos^2 \alpha) = f/2r_k/r_{sr} (1 - r_{sr}^2/r_k^2 \cos^2 \alpha) \quad (7.36)$$

A dynamical model of the rolling bearing is essential for the proper understanding of the engineering diagnostics of rolling bearings. A mathematical model in the form of differential equations is adopted to describe the motion of the rolling bearing. The rotary motion of the bearing is described by the following equation of rotary motion

$$I_k \ddot{\varphi} = M_s(\dot{\varphi}) \quad (7.37)$$

where: I_k – a mass moment of inertia, $\text{kg} \cdot \text{m}^2$;

$\dot{\varphi}$ – the angular velocity of the rolling bearing, rad/s ;

$\ddot{\varphi}$ – the angular acceleration of the bearing, rad/s^2 ;

$M_s(\dot{\varphi})$ – the torque driving the rolling bearing, $\text{N} \cdot \text{m}$.

The point of contact of the two rolling bearing elements (the ring and the ball) is characterised by rigidity k [N/m]. As a result of a defect the system having mass m_k vibrates as the rolling bearing rotates (7.37). The second equation of motion for this system is

$$m_k \ddot{y} = -k(y - E) \quad (7.38)$$

where: m_k – the system's mass, kg ;

y – a variable describing the displacement of the mass, m ;

E – a function describing the plot of the race damage.

One period of the former function, having relative length (0-1), is described (according to fig. 7.4) by the following relations:

for interval (0, b)

$$E = (g/b)a_{ux} \quad (7.39)$$

where: g – the depth of the damage, m ;

b – half of the damage width, m ;

for interval (b, 1-b)

$$E = g \quad (7.40)$$

for interval (1-b, 1)

$$E = - (g/b)(a_{ux} - 1) \quad (7.41)$$

Auxiliary value a_{ux} is calculated from the formula given below and the graph of the function is shown in fig. 7.5. The driving system characteristics for torque $M_s(\dot{\phi})$ and $\dot{\phi}(t)$ are shown in figs 7.6 and 7.7.

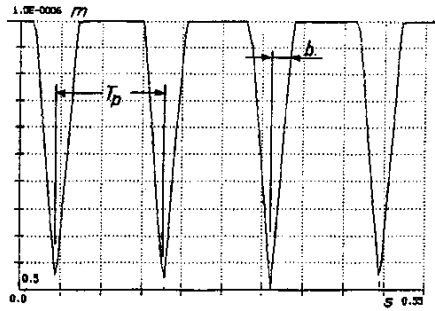


Fig. 7.4. Plot of rolling bearing damage function.

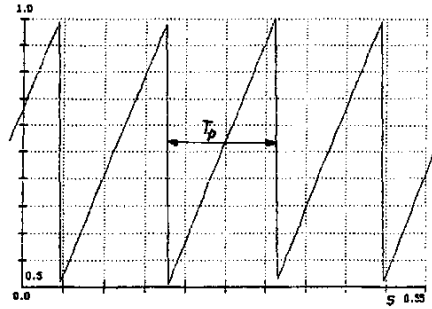


Fig. 7.5. Plot of auxiliary function.

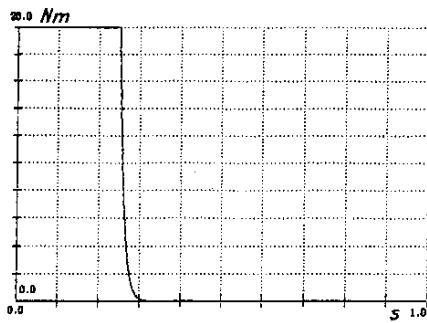


Fig. 7.6. Plot of starting torque.

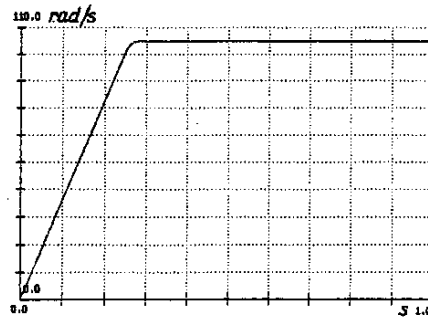


Fig. 7.7. Plot of angular velocities.

To model the effect of a bearing defect on the diagnostic signal one must know the relationship between the angle of rotation of the bearing's shaft and the angle of rotation of the bearing's cage. When the outer ring revolves, the latter is (according to (7.19))

$$\varphi_{ko} = \varphi (r_{sr} + r_k)/(2r_{rs}) \tag{7.42}$$

where: φ_{ko} – the angle of rotation of the cage, rad;

φ – the angle of rotation of the bearing.

Value a_{ux} is calculated from the following formula

$$a_{ux} = \text{frac}(\varphi_{ko} l_k / (2\pi)) \tag{7.43}$$

where: l_k – the number of balls in the bearing,

frac – the fractional part of the expression in brackets.

Illustrative plots of bearing force $S = k(y - E)$ are shown in fig. 7.8a and b. Fig. 7.8a shows the whole plot from the moment of starting and fig. 7.8b is a zoom of the plot for the steady running of the bearing. Characteristic traces of the impulses generated by the passage of a ball over the damaged spot are shown in fig. 7.8b.

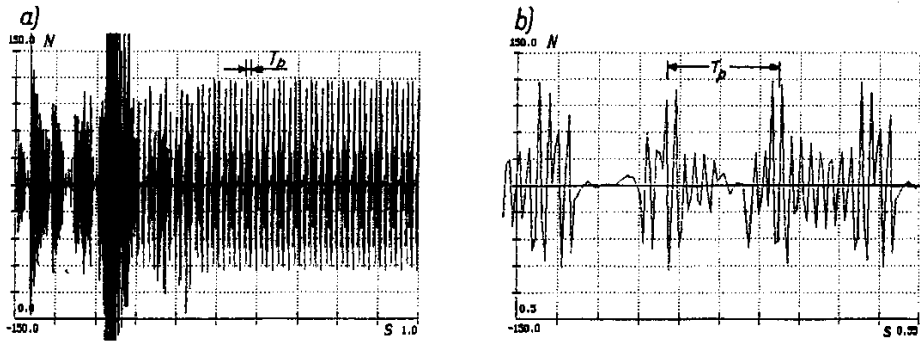


Fig. 7.8. Plot of forces between rolling element and rolling bearing race (a) and zoom of plot (b).

Having an appropriate mathematical model of the rolling bearing one can study the effect of design factors, operating factors and change-of-condition factors on the form of the diagnostic signal – as demonstrated for a gearing in chap. 6.

7.1. References

- [7.1] Bartelemus W.: Choice of Design Features for Large-Size Rim Bearings, *Górnictwo Odkrywkowe*, No. 6, 1987.

8. Modelling of belt conveyors

8.1. Modelling of forces in belt

Mathematical modelling and computer simulation are used to get a better insight into the dynamic phenomena which occur in the belt conveyor. The traditional modelling of the dynamic phenomena occurring in the belt conveyor focuses mainly on the effect of the motion factors involved in the starting and braking of the belt conveyor. For computer-aided diagnostics a new mathematical model describing in more detail (for the particular rollers) the dynamic phenomena is needed (see sect. 8.2). Nevertheless, to better understand the modelling of dynamic phenomena which occur in the belt conveyor a mathematical model representing the traditional approach (e.g. [8.1]) is presented in this section.

A model of the belt conveyor is assumed as a system consisting of a driving drum and a return drum – actually there may be several driving drums but they are reduced to one drum and a power transmission system (consisting of a motor and a gearbox) is reduced to this drum. The conveyor's top and bottom belts are substituted by concentrated masses. Ten masses are assumed for the (driving) top strand and six masses for the (driven) bottom strand. Also a two-parameter model of the belt, consisting of stiffness k [N/m] and damping C [Ns/m] is assumed. Dynamic modulus of elasticity $E_d = 2.1 \cdot 10^6$ N/m is assumed for the belt.

The following relation holds for the two-parameter model of the belt:

$$\sigma = E_d(\varepsilon + \tau \dot{\varepsilon}) \quad (8.1)$$

where: σ – the stress in the belt, N/m;

ε – relative strain;

τ – relaxation time, s ($\tau = 2$ s is assumed for calculations);

$\dot{\varepsilon}$ – the rate of relative strain.

The notation used for the forces is shown in fig. 8.1. The equation of motion for the driving drum assumes this form:

$$\ddot{\varphi}_1 = (M_s(\dot{\varphi}_1) + (-S_l - S_{lt} + S_{ls} + S_{l8t})r_b - S_t(\dot{\varphi}_1)M_{olt})/I_{b1} \quad (8.2)$$

If

$$S_{118} = (-S_I - S_{I_t} + S_{I8} + S_{I8t})$$

then

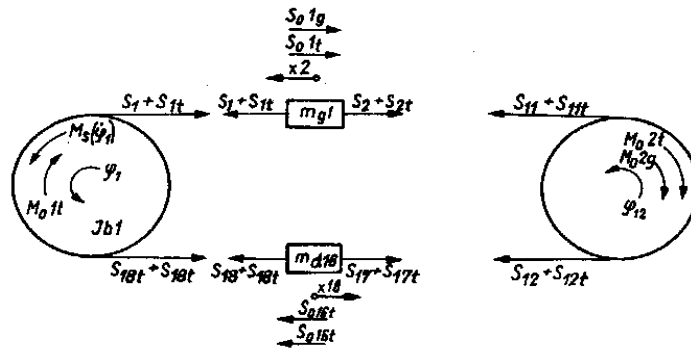


Fig. 8.1. Physical model of belt conveyor

$$\ddot{\varphi}_1 = (M_s(\dot{\varphi}_1) + S_{118} r_b - S_f(\dot{\varphi}_1) M_{o1}) / I_{b1}$$

Function $S_f(\dot{\varphi}_1)$ fulfils the following conditions:

$$\text{If } \dot{\varphi}_1 = 0, \text{ then } S_f(\dot{\varphi}_1) = 0$$

$$\text{If } \dot{\varphi}_1 > 0, \text{ then } S_f(\dot{\varphi}_1) = 1 \quad (8.3)$$

$$\text{If } \dot{\varphi}_1 < 0, \text{ then } S_f(\dot{\varphi}_1) = -1$$

The values of the particular damping and elastic forces can be calculated from the following relations:

$$S_I = k_I(\varphi_1 r_b - x_2) + S_o \quad (8.4)$$

$$S_{I_t} = C_I(\dot{\varphi}_1 r_b - \dot{x}_2)$$

where: $\ddot{\varphi}_1$ – angular acceleration, rad/s²;

$\dot{\varphi}_1$ – angular velocity, rad/s;

$M_s(\dot{\varphi}_1)$ – a function describing the characteristic of the motor reduced to the drum's shaft (a simplified characteristic of the motor is shown in fig. 8.2);

S_I, S_{I_t} – respectively the elastic force and the damping force running onto the drum, N;

S_{I8}, S_{I8t} – respectively the elastic force and the damping force running off the drum, N;

r_b – the drum's radius, m;

$S_f(\dot{\varphi}_1)$ – a function describing the direction of the friction force depending on the value and direction of the velocity (the function assumes the values given above);

M_{ol} – the moment of friction resistance on the driving drum, Nm;
 I_{bl} – the mass moment of inertia of the driving drum, kgm^2 ;
 S_o – the pre-tensioning force, N.

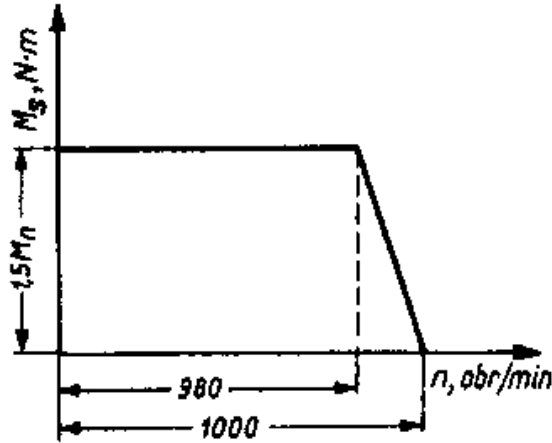


Fig. 8.2. Characteristic of motor driving belt conveyor.

The equation of motion for first mass m_{g1} in the driving strand is as follows:

$$\ddot{x}_2 = (S_1 + S_{1t} - S_2 - S_{2t} - S_t(\dot{x}_2)S_{ol} - S_{olg})/m_{g1} \quad (8.5)$$

If we denote

$$S_{12a} = S_1 + S_{1t} - S_2 - S_{2t} \quad (8.6)$$

then

$$\ddot{x}_2 = (S_{12a} - S_t(\dot{x}_2)S_{ol} - S_{olg})/m_{g1} \quad (8.7)$$

where S_1, S_{1t} as above and

$$S_2 = k_2(x_2 - x_3) + S_o \quad (8.8)$$

$$S_{2t} = C_2(\dot{x}_2 - \dot{x}_3) \quad (8.9)$$

\ddot{x}_2 – the linear acceleration of the first mass, m/s^2 ;
 $\dot{x}_2 - \dot{x}_3$ – the linear velocity of respectively the first and second mass, m/s ;
 S_{ol} – the friction force produced by the resistance of the rollers, N;
 m_{g1} – the mass of the first belt section, kg;

For example, the equation of motion for tenth mass m_{g10} assumes this form

$$\ddot{x}_{11} = (S_{1011} - S_t(\dot{x}_{11})S_{o10} - S_{o10g})/m_{g10} \quad (8.10)$$

where:

$$S_{1011} = S_{10} + S_{10t} - S_{11} - S_{11t} \quad (8.11)$$

$$S_{10} = k_{10}(x_{10} - x_{11}) + S_o \quad (8.12)$$

$$S_{10t} = C_{10}(\dot{x}_{10} - \dot{x}_{11}) \quad (8.13)$$

$$S_{11} = k_{11}(x_{11} - r_b \varphi_{12}) \quad (8.14)$$

$$S_{11t} = C_{11}(\dot{x}_{11} - r_b \dot{\varphi}_{12}) \quad (8.15)$$

(the same notation as above).

The equation of motion for the return drum is

$$\ddot{\varphi}_{12} = (S_{1112} r_b - S_t(\dot{\varphi}_{12})M_{o2t} - M_{o2g})/I_{b2} \quad (8.16)$$

where:

$$S_{1112} = S_{11} + S_{11t} - S_{12} + S_{12t} \quad (8.17)$$

and forces S_{11} , S_{11t} , S_{12} , S_{12t} as above

M_{o2t} – the reduced moment of resistance to motion on the return drum, Nm;

M_{o2g} – the reduced-to-the-return-drum gravitational force for the rectilinear segment of the belt conveyor, Nm;

I_{b2} – the moment of inertia of the return drum, kgm^2 .

A simplified model of the driving motor's characteristic is shown in fig. 8.2. Since the drive is reduced to the drum's shaft, the drum moment increases by the transmission ratio and the revolutions appropriately decrease by this ratio.

Let us model the possibility of slip on the driving drum between the drum and the belt. If we denote

$$P_1 = S_1 + S_{1t} \quad (8.18)$$

$$P_2 = S_{18} + S_{18t} \quad (8.19)$$

the condition of possible transmission of limit forces between the driving strand and the driven strand can be written as follows

$$P_1/P_2 = \exp(\mu \alpha) \quad (8.20)$$

If the circumferential force in the belt is denoted by P_o , slip will occur when

$$(P_2 + P_o)/P_2 > \exp(\mu \alpha) \quad (8.21)$$

$$P_o = M_s/r_b \quad (8.22)$$

After transformations we get the following slip occurrence condition

$$P_2 < M_s / [r_b (\exp(\mu \alpha) - 1)] \quad (8.23)$$

which means that the torque value transposed from the motor to the drum is

$$M_s = r_b P_2 (\exp(\mu \alpha) - 1) \quad (8.24)$$

This condition was introduced into the equations of motion of the belt conveyor.

The computer simulation results are shown in fig. 8.3a and b. The plots of driving drum angular velocity (rad/s) $\dot{\phi}_1$ and return drum angular velocity $\dot{\phi}_{12}$ and a plot of linear velocity \dot{x}_5 for the fourth mass in the driving strand of the belt are shown in fig. 8.3a. The belt conveyor was loaded up to 60% of its rated power. The plots represent the starting and braking of the belt conveyor. The plots of running-onto-drum force P_1 and running-off-drum force P_2 and the plot of electric motor driving torque M_s are shown in fig. 8.3b.

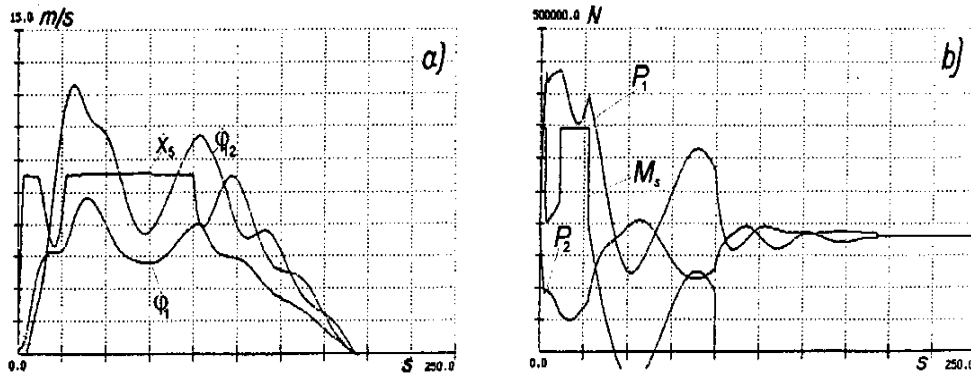


Fig. 8.3. Plots of driving and return drum velocities and fourth top-strand mass (a) and plots of driving-drum tightening and running-off forces and driving torque (b), for starting and braking at 60% loading of belt conveyor.

8.2. Dynamical model of belt conveyor route section

In sect. 8.1 a conventional model describing the dynamical properties of the belt conveyor was presented. Here a new dynamical model of a belt conveyor route section, which can be used to study the influence of the condition of the belt conveyor's elements (design factors and change-of-condition factors) on the vibration of the belt conveyor, is introduced [8.2], [8.3].

To determine the interactions between the rollers and the belt, taking into account the frame and the transported winning, a new physical model (fig. 8.4) has been developed. A corresponding mathematical model is described by equations of motion.

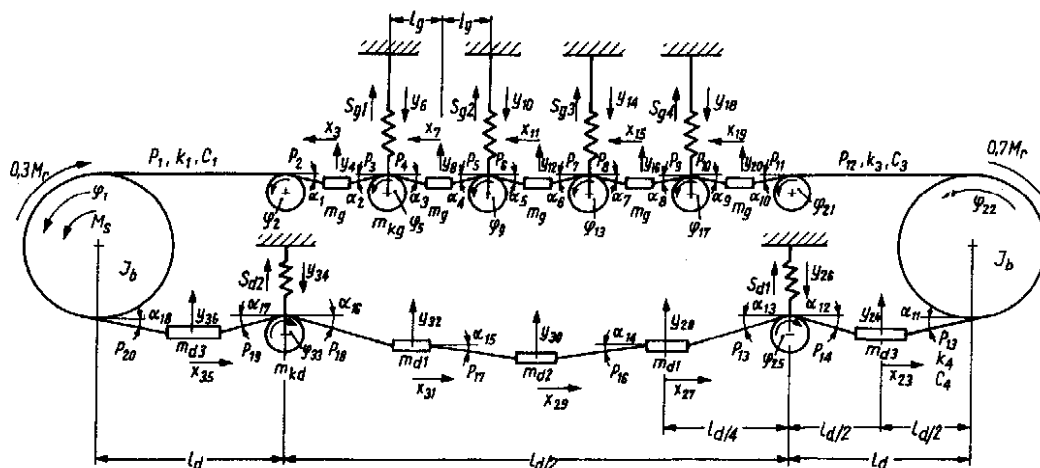


Fig. 8.1. Physical model of conveyor belt route section.

The motion dynamics of the model are described by 36 variables denoted as: x – horizontal displacements, y – vertical displacements and φ – revolutions. It is assumed that the system is driven by a motor with known driving torque characteristic $M_s(\dot{\varphi}_1)$ where $\dot{\varphi}_1$ is the angular velocity of the driving drum (fig. 8.2). Using the symbols from fig. 8.4, the equations of motion for the particular masses and inertias are as follows:

$$I_b \ddot{\varphi}_1 = M_s(\dot{\varphi}_1) - r_b(P_1 - P_{20}) - 0.3S_t(\dot{\varphi}_1)M_r \quad (8.25)$$

$$I_g \ddot{\varphi}_2 = r_g(P_1 - P_2) \quad (8.26)$$

$$m_g \ddot{x} = P_2 - P_3 \quad (8.27)$$

where: $\ddot{\varphi}, \ddot{x}$ – respectively angular acceleration (rad/s^2) and linear acceleration (m/s^2);
 I_b – the moment of inertia of the drum, $\text{kg} \cdot \text{m}^2$;
 P_1, P_{20}, P_2, P_3 – the tensioning forces in the belt, N;
 r_b, r_g – the drum's radius and the top roller's radius, m;
 M_r – the resistance-to-motion moment, $\text{N} \cdot \text{m}$;
 with 0.3 of the resistance motion value concentrated on the first drum and 0.7 on the second drum.

Function $S_t(\dot{\varphi})$ is defined as follows:

$$\begin{aligned} \text{If } \dot{\varphi} &= 0, \text{ then } S_t(\dot{\varphi}) = 0 \\ \text{If } \dot{\varphi} &> 0, \text{ then } S_t(\dot{\varphi}) = 1 \end{aligned} \quad (8.28)$$

If $\dot{\varphi} < 0$, then $S_t(\dot{\varphi}) = -1$

The further equations are:

$$m_g(\ddot{y}_4 - 1/2 \ddot{y}_6) = -(P_2\alpha_1 + P_3\alpha_2) \quad (8.29)$$

$$(I_g + m_{kg}e_2)\ddot{\varphi}_5 = r_g(P_3 - P_4) \quad (8.30)$$

$$m_{kg}\ddot{y}_6 = 3F_{w1} + P_3\alpha_2 + P_4\alpha_3 - S_{g1} \quad (8.31)$$

where: \ddot{y} – vertical accelerations of the belt, m/s²;

m_g – the mass of the belt section and winning between two rollers, kg;

m_{kg} , m_{kgr} – the mass of the top roller and the mass of the moving part of the top roller, kg;

e_2 – the shift of a roller's centre of gravity relative to the axis of rotation, m;

F_w – forces due to the unbalance of a roller, N.

$$m_g\ddot{x}_7 = P_4 - P_5 \quad (8.32)$$

$$m_g[\ddot{y}_8 - (\ddot{y}_{10} + 1/2(\ddot{y}_6 - \ddot{y}_{10}))] = -(P_4\alpha_3 + P_5\alpha_4) \quad (8.33)$$

$$(I_g + m_{kgr}e_2)\ddot{\varphi}_9 = r_g(P_5 - P_6) \quad (8.34)$$

$$m_{kg}\ddot{y}_{10} = 3F_{w2} + P_5\alpha_4 + P_6\alpha_6 - S_{g2} \quad (8.35)$$

$$m_g\ddot{x}_{11} = P_6 - P_7 \quad (8.36)$$

Only the first 11 differential equations describing eleven variables and only a part of the mathematical model are written above. The possibilities of using the mathematical model to study the effect of various design factors on the magnitude of vibration are presented in [8.3].

The computer simulation results are shown in figs 8.5-8.13. They illustrate the effect of different design factors on the vibration velocity for the steady motion of the belt conveyor running at a speed of 5.75 m/s. Run-out and unbalance of the rollers affect the vibration of the belt conveyor's elements. In the simulations a run-out of 0.9 mm and 1.6 mm was assumed for respectively the top and bottom rollers. An identical gravity-centre shift of 0.8 mm was assumed for all the rollers. The obtained simulation results are shown in figs 8.5-8.7. Then complex non-circularity of the rollers, causing 50 and 30 Hz vibration, was assumed. The two frequencies are the eigenfrequencies of the bottom and top rollers, respectively. The simulation results under this assumption are shown in figs 8.8-8.10.

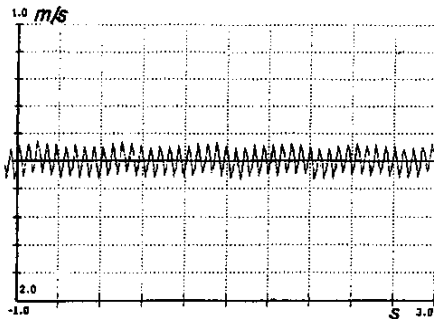


Fig. 8.2. Plot of vibration variation rate for frame at point of support of top roller (variable y_{10}), $gs5$.

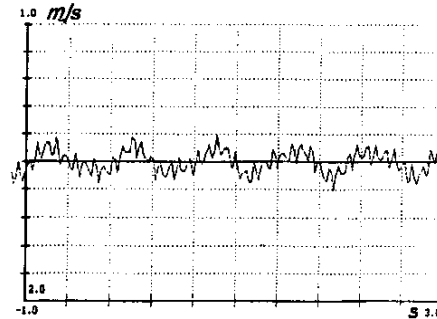


Fig. 8.3. Plot of vibration velocity for middle of belt between two top rollers (variable y_{12}), $gs5$.

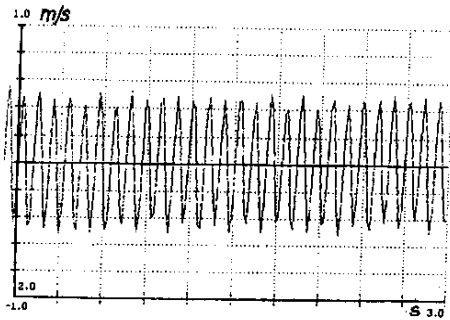


Fig. 8.4. Plot of vibration variation rate for frame at point of support of bottom roller (variable y_{26}), $gs5$.

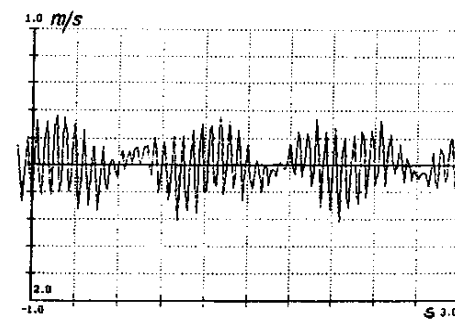


Fig. 8.5. Plot of vibration variation rate for frame at point of support of top roller (variable y_{10}), $gs7$.

These are plots of the actual conveyor element vibration velocity values for different variables describing the vibration (the variables are denoted in fig. 8.4). A plot of vibration velocity for variable y_{10} , being a measure of the impact of the roller on the belt conveyor's frame, is shown in fig. 8.5. One component with frequency $f = 50$ Hz features in the plot which is slightly modulated by a component having the roller revolutions frequency. A plot of the velocity for the middle of the belt under the rated load is shown in fig. 8.6. The plot features two vibration components having approximate frequencies: 10 and 50 Hz. The effect of the roller on its bottom suspension is illustrated by the plot of velocity for variable y_{26} in fig. 8.7. The plot features mainly vibration with a frequency of 30 Hz caused by the free vibration of the support. A slight influence of the vibration of the belt is visible. A plot of vibration velocity when the excitation due to top roller non-circularity was 50 Hz is shown in fig. 8.8. This resulted in a complex form of vibration featuring: a 50 Hz component – a resonant component coinciding with the excitation frequency, a 10 Hz component due to roller run-out and a 5 Hz component due to the vibration of the bottom section belt. The plot of

velocity in fig. 8.9 features 30 Hz components originating from the free vibration excited by the 30 Hz roller non-circularity component. Also the effect of the vibration of the bottom section of the belt is visible – the frequency of 2.5 Hz. A hypothetical noise spectrum with marked selected low-frequency vibration components: 5, 30 and 50 Hz and high-frequency components: 800, 1000, 1200 and 1500 Hz is shown in fig. 8.11. The frequencies of 800 and 1000 Hz are shown with side modulating components originating from the low frequencies.

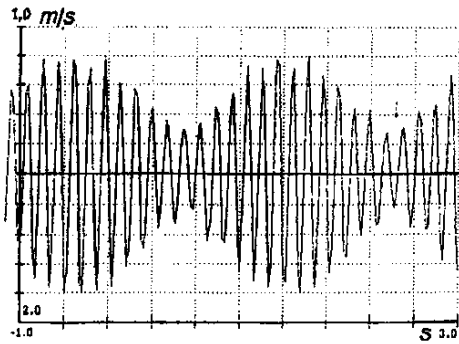


Fig. 8.6. Plot of vibration variation rate for frame at point of support of bottom roller (variable y_{10}), $gs7$.

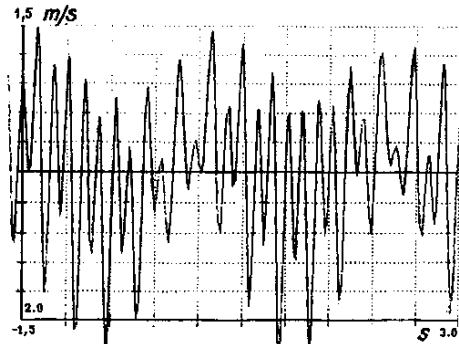


Fig. 8.7. Plot of vibration velocity for middle of belt between two bottom rollers (variable y_{30}), $gs7$.

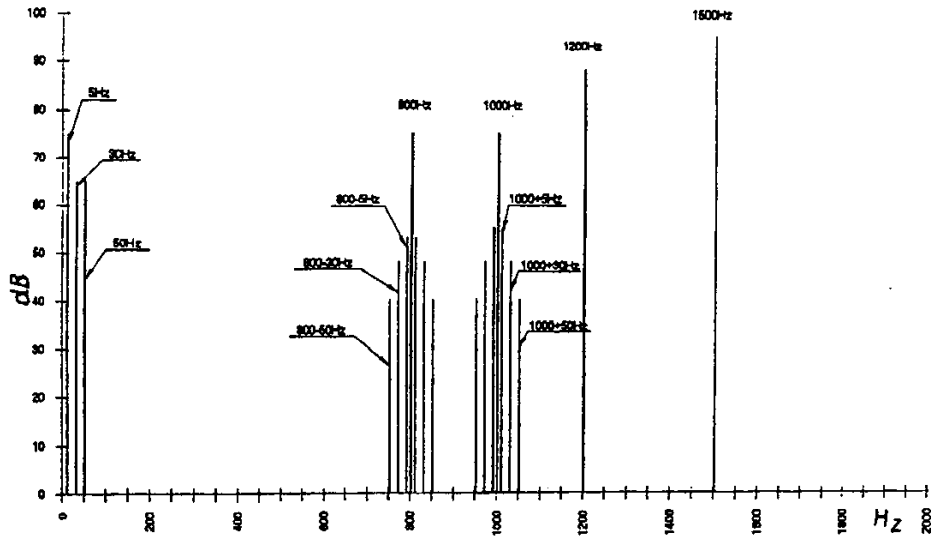


Fig. 8.8. Structure of noise spectrum for section of belt conveyor.

Fig. 8.11 is only an approximate representation of the structure of the noise emitted by the belt conveyor. The probable cause of the generation of high-frequency vibrations are surface irregularities of the belt or the variation in its stiffness. A plot of vibration velocity when the vibration (1000 Hz) is excited by periodic belt surface irregularities (amplitude of irregularities $b = 0.1$ mm) is shown in fig. 8.12a.

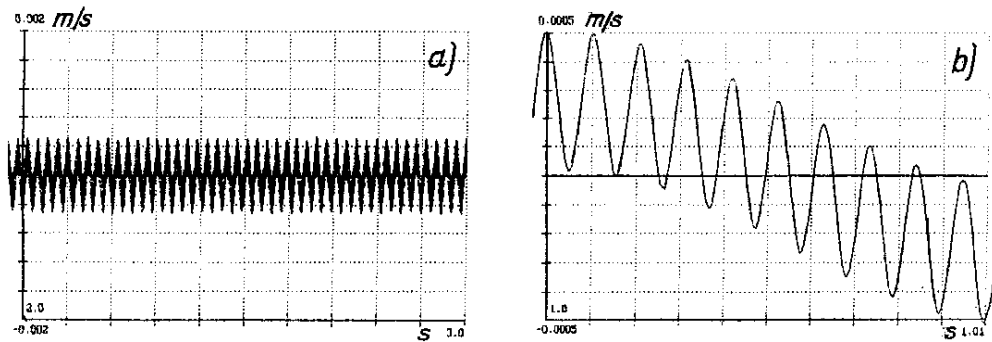


Fig. 8.9. Plot of vibration velocity (variable y_{12}) for belt midpoint and amplitude of surface irregularities $b = 0.1$ mm (a) and zoom of plot (b).

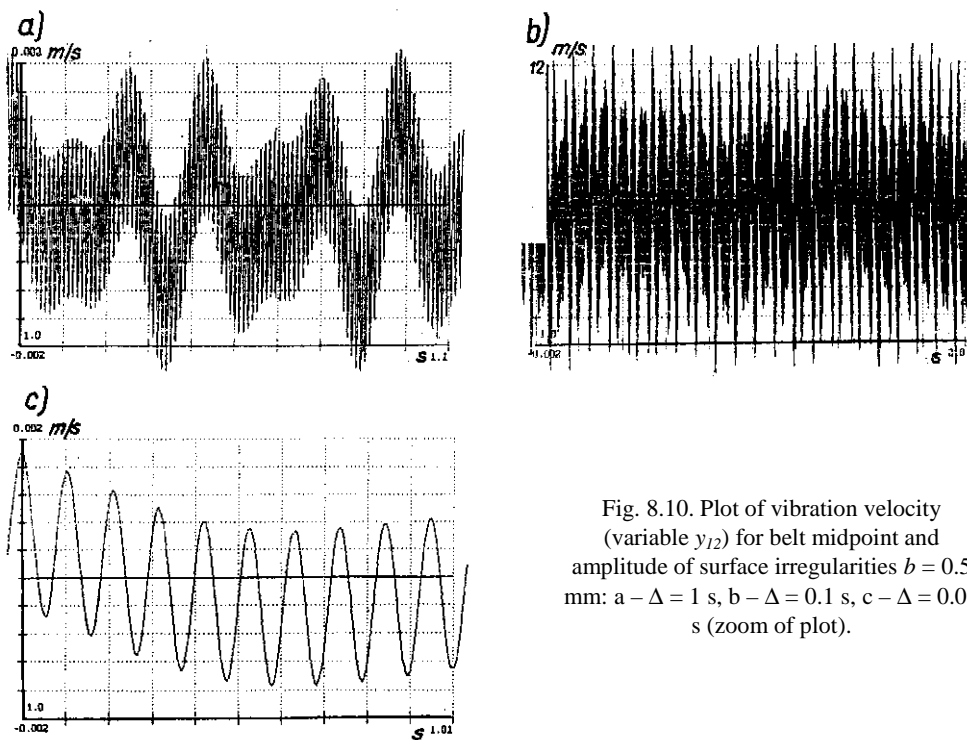


Fig. 8.10. Plot of vibration velocity (variable y_{12}) for belt midpoint and amplitude of surface irregularities $b = 0.5$ mm: a - $\Delta = 1$ s, b - $\Delta = 0.1$ s, c - $\Delta = 0.01$ s (zoom of plot).

This figure features a 50 Hz component and a high-frequency (1000 Hz) component. To identify the latter a zoom of the vibration velocity plot is shown in fig. 8.12b. The plots are for variable y_{12} , i.e. for the vibration of the conveyor belt midpoint. The vibration plots for variable y_{12} when the amplitude of belt surface irregularities is increased to 0.5 mm are shown in fig. 8.13a and b. The plot in fig. 8.13a is for time interval $\Delta = 1$ s, the one in fig. 8.13b for interval $\Delta = 0.1$ s and the one in fig. 8.13c for interval $\Delta = 0.01$ s. The figures show a complex form of vibration excited by periodic belt surface irregularities.

This chapter does not cover all the factors influencing belt conveyor vibration. This would require a very extensive treatment, e.g. to take into account the condition of the rolling bearings it would be necessary to modify the model of the belt conveyor route section and incorporate the rolling bearing model presented in chap. 7 into it.

8.3. References

- [8.1] Bartelmus W.: Modelling of Dynamics of Belt-Pipe Conveyor Subassemblies (in Polish), *Scientific Papers of Silesian Polytechnic, Mechanics*, No. 1230, pp. 19-26, Gliwice, 1994.
- [8.2] Bartelmus W., Gładysiewicz L., Sawicki W.: Structure of Conveyor Route Noise Spectrum (in Polish), *Scientific Papers of the Institute of Mining, Wrocław University of Technology*, No. 80, pp. 31-38, 1996.
- [8.3] Bartelmus W., Gładysiewicz L., Sawicki W.: Causes of Belt Conveyor Noise (in Polish), *Scientific Papers of the Institute of Mining, Wrocław University of Technology*, No. 79, pp. 15-22, 1996.

9. Forms of wear of mining machine elements

Changes in the condition of machines are due to the wear of their elements which make up kinematic pairs or joints. The following forms of wear of machine elements can be distinguished: abrasive wear, adhesion, pitting, seizing, corrosion, fretting and erosion. The forms of wear vary depending on the loading, the kind of kinematic pair and the environment in which the machine operates. In the considered case the strip mine is the operating environment. Area, linear and point contacts and sliding, rolling and concurrent sliding and rolling motions occur between the elements of kinematic pairs. The classification of kinematic pairs in the theory of mechanisms is based on the kind of motion and the kind of contact between kinematic pair elements. For example, rolling motion occurs when a rolling element mates with the races of a rolling bearing, concurrent rolling and sliding motions occur in a meshing toothed gearing. The distribution of motion velocities at a point of instantaneous contact between two meshing teeth is shown in sect. 6.2. The intermeshing of a pair of gear teeth can be compared to the mating (rolling and sliding) of two rolls with changing radii ρ_1 and ρ_2 (fig. 6.2). If sliding motion occurs between the elements of a kinematic pair, then also friction occurs between them. The magnitude of the frictional resistance depends on the condition of the surfaces (the height of surface irregularities), the kind of material and the loading determined by design and operating factors. An illustrative plot of the moments of friction arising during meshing is shown in fig. 6.6a and b. To reduce frictional resistance a lubricating medium (grease, oil) is introduced between the mating surfaces of a kinematic pair. The lubricant separates the mating elements and reduces the frictional resistance. The mating elements of a kinematic pair are separated to a different degree. Hence different forms of friction are distinguished:

- fluid friction – the elements of a kinematic pair are separated by a film of lubricant,
- semi-fluid friction – the elements of a kinematic pair are partially separated,
- dry friction – the elements of a kinematic pair are not separated by a lubricating medium.

The kind of friction can be determined by diagnostic methods, e.g. by the SPM (Shock Pulse Method) method described in chap. 15. The basics of this method are presented in figs 15.8-15.11. The conditions for the occurrence of fluid friction are described by the hydrodynamic theory of lubrication [9.1]. The occurrence of fluid friction depends on design and operating factors (determining the relative velocities of the elements), the loading and the condition of the mating surfaces. Also the environment influences the condition of a machine since impurities: solid (sand) particles and

water get into the lubricating medium from it. The kinds of particles which may get into the lubricating medium are described in chap. 10.2. As a result of the reciprocal motion of the elements of a kinematic pair the irregularities of their surface are truncated, particularly during running in. A new surface obtained by grinding and the same surface after running in are shown in fig. 9.1 (after [9.1]) and fig. 9.2 (after [9.1]), respectively. If they are not lubricated, the surfaces after running in may undergo adhesion during starting. Adhesion will occur depending on the state of lubrication and the machine's state of operation (starting). Once certain limit values determined by the design and operating (motion) factors are exceeded, the mating surfaces start seizing. An image of a surface (after [9.1]) on which seizing began is shown in fig. 9.3.

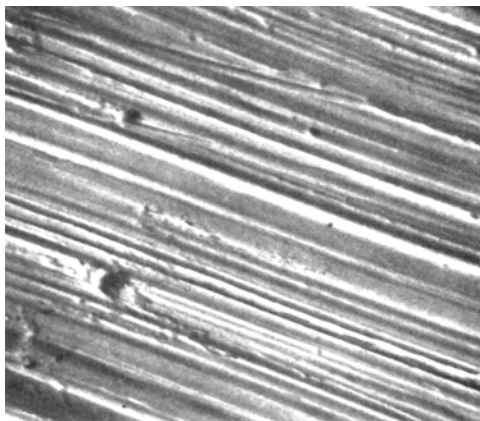


Fig. 9.1. Electron microscope image of ground surface, magnification of 1000x [9.1].

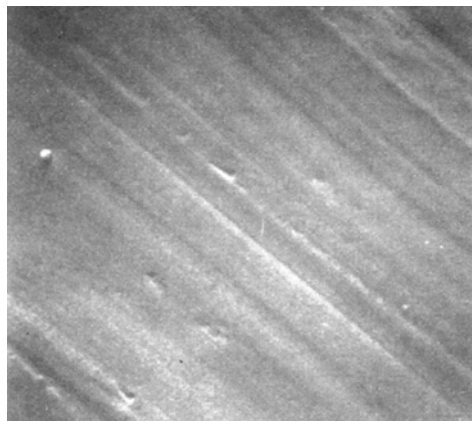


Fig. 9.2. Electron microscope image of ground and run in (through mating of kinematic pair elements) surface, magnification of 1000x [9.1].

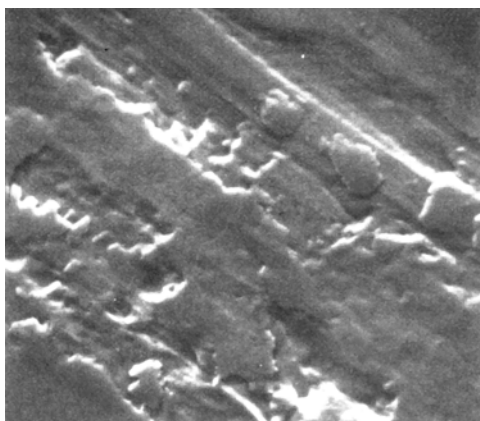


Fig. 9.3. Electron microscope image of surface damaged by seizing (in its initial stage), magnification of 1000x [9.1].

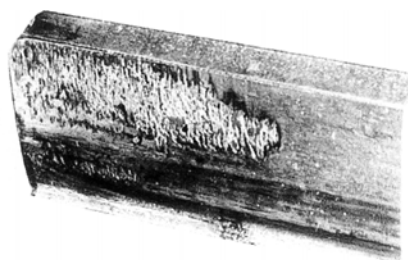


Fig. 9.4. Image of surface damaged by gear tooth seizing (resulting from out-of-parallel meshing of teeth) [9.2].

An image of severe damage (visible to the naked eye) resulting from seizing is shown in fig. 9.4. The seizing was caused by a secondary factor: a change in the condition due to the improper mounting of the motor relative to the gearbox. A similar image will be obtained if damage to one of the rolling bearings in a gear results in the nonaxial operation of the gear wheels' teeth (fig. 9.4 after [9.2]). Highly intensive seizing may occur in the case of tooth interference. An image of this condition is shown in fig. 9.5 after [9.2].

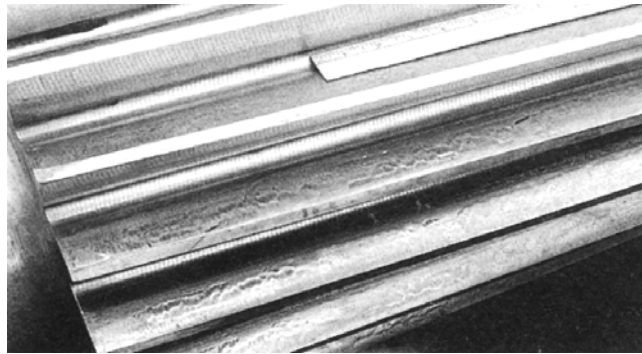


Fig. 9.5. Image of intensive wear of gear teeth due to their seizing [9.2].

Tooth interference may be due to mismatched design features or to the influence of technological factors (improperly cut teeth of the gear wheels). The surface of the mating elements of kinematic pairs may also be damaged as a result of metal surface fatigue. The wear of and damage to gear teeth are described in standard [9.3]. Changes in the condition of gearing caused by surface fatigue manifest themselves initially as stains (which may be transitory) on the surface of the teeth. The latter may be damaged severely by destructive pitting as shown in figs 1.15 and 10.20. Tempering chips and other kinds of damage may also occur on the tooth surface (more information can be found in standard [9.3]). When friction occurs in a corrosive environment, chemical reaction proceed on the surfaces of the mating elements of kinematic pairs. The products of the chemical reactions are generally weakly bound with the base and as a result of friction they are removed from it. A form of abrasive-corrosive wear is fretting which occurs when the surfaces of the contacting elements execute small oscillatory motions. Fretting may occur in thermocompression, bolted and riveted joints. It is a form of adhesion wear combined with corrosion.

To sum up, the occurrence of one or several of the phenomena described above is understood to constitute a change in the condition of the machine due to wear.

Erosion is defined as the destruction of a surface, accompanied by material loss, as a result of the flow of a solid-particles-carrying liquid or a gas around the surface. Cavitation is a form of erosion. Cavitation occurs in liquids in which bubbles filled with the vapour of the liquid form. Close to the walls the bubbles burst under the pres-

sure of the liquid. The implosion of the bubbles results in local high-velocity micro-jets hitting the inner walls of the machine's elements and removing material particles from their surface. The aim of engineering diagnostics is to detect such phenomena through the measurement of the physical quantities which reflect the corresponding changes in the condition. If physical quantities being symptoms of a change in the condition are measured, then methods of engineering diagnostics are applied to determine the changes in the condition. The phenomena described above generate characteristic wear particles which are identified and on this basis the condition of the machine is determined. More information about forms of wear can be found in, for example, [9.1].

9.1. References

- [9.1] Barwell F.T.: Bearing Systems, Principles and Practice, Oxford University Press, 1979.
- [9.2] Kress D.F.: The Good Girth Guide, World Mining Equipment, Vol. 21, No. 3, 1997.
- [9.3] Polish Standard PN-67/M-88506 Toothed Gears, Wear and Damage, Names and Definitions (in Polish).

10. Description of secondary processes accompanying operation of machine as carrier of information about its condition

10.1. Basic description of vibroacoustic signal

Functions describing dynamic variables can be presented in different forms, i.e. versus different independent variables. Sinusoidal plots of physical quantities, describing instantaneous values of displacement, velocity, and vibration acceleration are shown in fig. 4.2. For a particular physical quantity such functions can be characterized by period T [s] or its inverse, i.e. frequency f [Hz], amplitude X (for different physical quantities) and phase shift ϕ [rad.]. A signal can be also visualized as a spectrum. A sinusoidal plot and its spectrum (as a function of frequency) are shown in fig. 10. Sinusoidal functions can be out of phase which means that beside an amplitude spectrum one needs a phase spectrum to describe a signal fully.

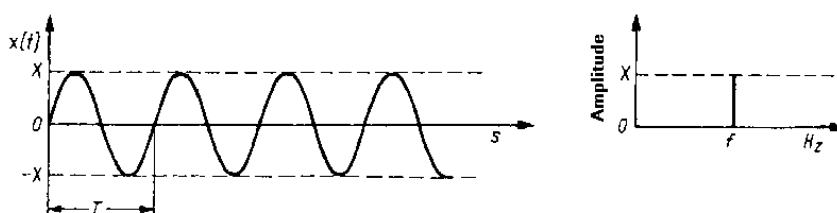


Fig. 10.1. Plot of sinusoidal signal and its spectrum.

Any periodic signal can be presented in the form of a spectrum. Examples of complex periodic signals in the time form and in the spectrum form are shown in fig. 10.2. The signals are determinate since their value can be determined at any instant. Not all signals are periodic. A classification of determinate signals, according to [10.1], is presented in fig. 10.3. A spectrum of a polyharmonic signal and that of an almost periodic signal are shown in figs 10.4 and 10.5, respectively. A periodic signal can be de-

composed into simple sinusoidal components by applying the Fourier transform. If a signal as a function of time is denoted by $x(t)$ then by applying the Fourier series it can be expressed as

$$x(t) = \frac{1}{2} a_0 + \sum_{n=1}^{\infty} (a_n \cos(2\pi n f_1 t) + b_n \sin(2\pi n f_1 t)) \quad (10.1)$$

where:

$$f_1 = \frac{1}{T_p} \quad (10.2)$$

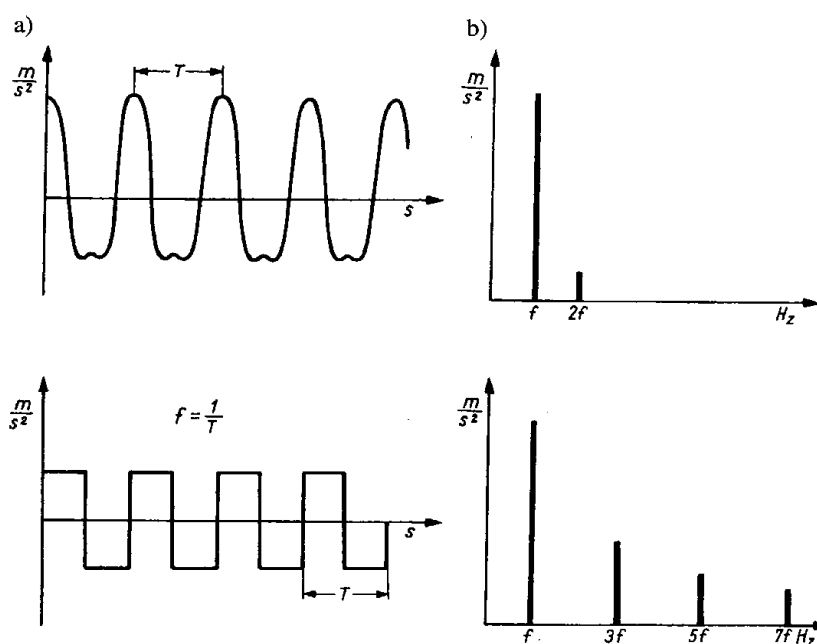


Fig. 10.2. Examples of polyharmonic signals and their spectra: a – signal in time domain, b – signal in frequency domain.

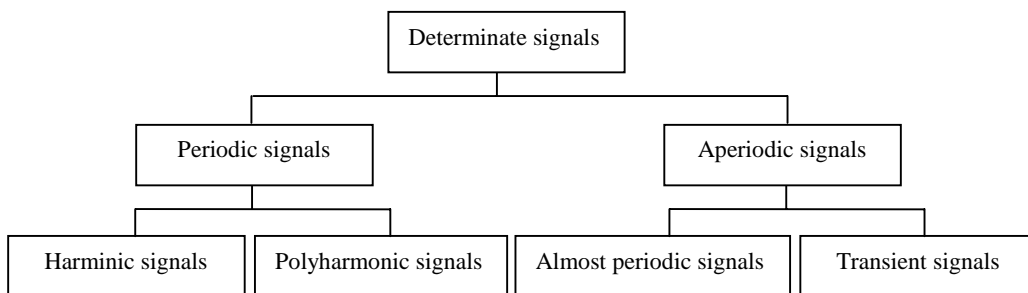


Fig. 10.3. Classification of determinate signals [10.1].

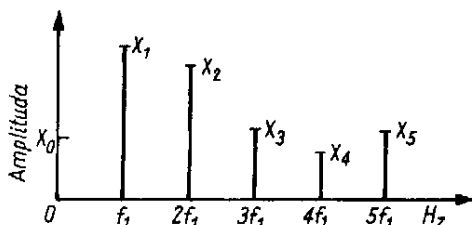


Fig. 10.4. Spectrum of polyharmonic signal.
Amplitude

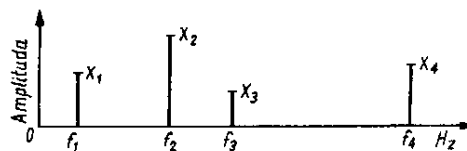


Fig. 10.5. Spectrum of almost periodic signal.

$$a_n = \frac{2}{T_p} \int_0^{T_p} x(t) \cos(2\pi n f_1 t) dt, \quad n = 0, 1, 2, 3, \dots \quad (10.3)$$

$$b_n = \frac{2}{T_p} \int_0^{T_p} x(t) \sin(2\pi n f_1 t) dt, \quad n = 0, 1, 2, 3, \dots \quad (10.4)$$

where T_p is the fundamental period of the signal.

Another kind of notation can be used for the Fourier series in the case of a polyharmonic signal:

$$x(t) = X_0 + \sum_{n=1}^{\infty} X_n \cos(2\pi n f_1 t - \theta_n) \quad (10.5)$$

where:

$$X_0 = \frac{1}{2} a_0 \quad (10.6)$$

$$X_n = \sqrt{a_n^2 + b_n^2} \quad n = 1, 2, 3, \dots \quad (10.7)$$

$$\theta_n = \arctg \frac{b_n}{a_n} \quad n = 1, 2, 3, \dots \quad (10.8)$$

As mentioned above, if values X_n are expressed as functions with discrete domain $f_1 n$, a signal spectrum is obtained; if phases θ_n are also expressed as functions in domain $f_1 n$, a signal phase spectrum is obtained. The amplitude spectra of signals are often described in the form of dB levels. A dB level is expressed as follows

$$L = 10 \log_{10} \left(\frac{a}{a_0} \right)^2 = 20 \log_{10} \left(\frac{a}{a_0} \right) \quad (10.9)$$

where: a – the amplitude of a signal (acceleration, velocity, displacement) for a given frequency f , Hz;

a_0 – a reference amplitude according to ISO1683.

The levels of amplitudes according to ISO1683 are as follows:

for accelerations – 10^{-6} ms^{-2} ,

for velocities – 10^{-9} ms^{-1} ,

for displacements – 10^{-12} m .

Transients form an important class of signals. Examples of such signals with their mathematical description are shown in fig. 10.6. Transients a and b can describe the response of a system to step excitations (see figs 4.10 and 4.11). One can also find spectra for transients. Unlike periodic signals, the spectra are continuous (see fig. 10.7). The actual traces of physical quantities are only approximately determinate. In engineering diagnostics we deal with signals which are a “sum” of determinate and random signals. A classification of random signals according to [10.1] is presented in fig. 10.8. Illustrative time plots of a random signal are shown in fig. 10.9. The signals are thermal noise signals.

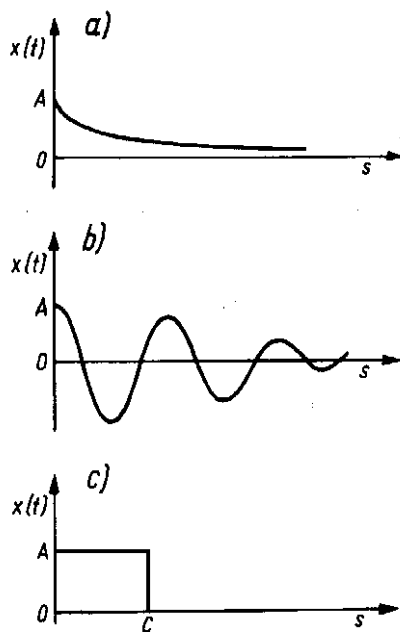


Fig. 10.6. Examples of transients: a – fading signal, b – fading periodic signal, c – impulse signal.

Analyses of diagnostic signals show that rolling bearings in good condition generate vibration which can be described by broadband noise. A defect of a rolling bearing results in the generation of periodic signals caused by impulse excitation (fig. 7.8). A periodic signal providing information about a change in condition is masked by a broadband noise signal.

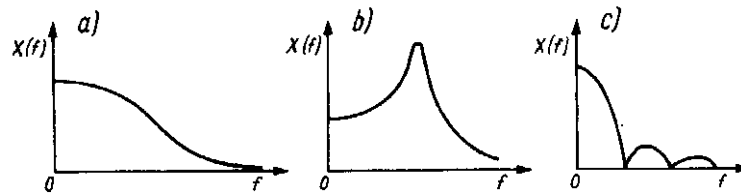


Fig. 10.7. Spectra of transients (fig. 10.6): a – spectrum of fading signal, b – spectrum of fading periodic signal, c – spectrum of impulse signal.

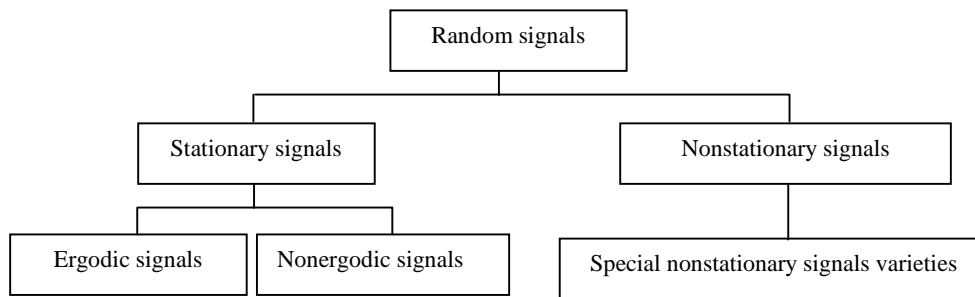


Fig. 10.8. Classification of random signals [10.2].

Hence engineering diagnostics deals with methods of detecting signals in noise. In some cases it is assumed that the diagnostic signal is a random signal to which stochastic signal analysis methods are applicable. Stochastic signals are described by estimators.

Vibroacoustic signal description estimators will be discussed assuming signal ergodicity [10.1].

An ergodic signal can be described uniquely on the basis of one process realization, which in the case of vibroacoustic processes is random function in time domain $s(t)$. A random process is described by nonrandom parameters (referred to as process characteristics). Theoretical parameters are calculated for realization $s(t)$ of infinite duration, i.e. $T \rightarrow \infty$. A parameter calculated for finite T is called an estimator of this parameter or in short: estimator. The accuracy with which the estimator is calculated depends on, among others, duration T . Besides the above limitation of signals to ergodic ones, another constraint is introduced: to describe fully a stochastic process it is enough to find statistic moments of the first and second kind. The above nonrandom parameters and estimators of diagnostic signal can be described in time domain τ [s], frequency domain f [Hz] or amplitude domain s [mm], [mm/s], [mm/s²] depending on a physical quantity.

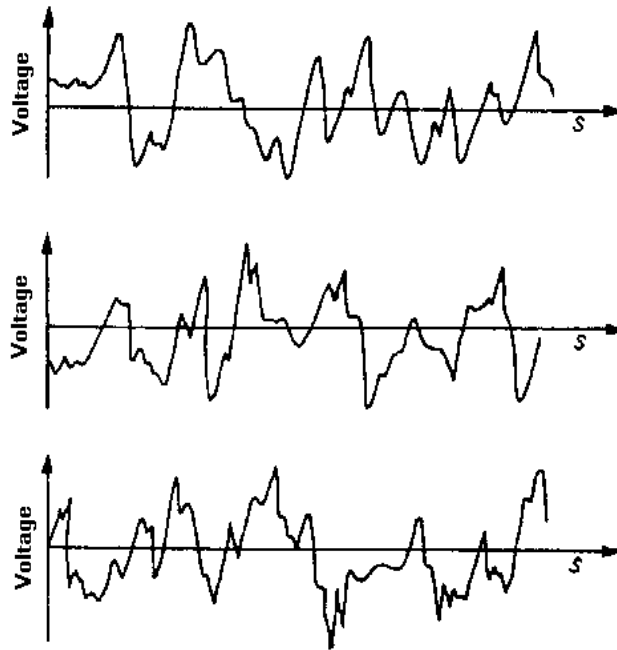


Fig. 10.9. Realizations of output signals of thermal noise generators

Under the above constraints imposed on the description of a stochastic process it is enough to find the parameter (or its estimator) of: the autocorrelation function and the related signal power spectral density function or the probability density function.

The basic stochastic process parameters under the above constraints imposed on the kind (class) of a stochastic process are presented below.

The square mean value is

$$\Psi_s^2 = \lim_{T \rightarrow \infty} \frac{1}{T} \int_0^T s^2(t) dt \quad (10.10)$$

where: $s(t)$ – a stochastic process realization;

T – realization duration, s ;

t – time, s .

The mean value is

$$\mu_s = \lim_{T \rightarrow \infty} \frac{1}{T} \int_0^T s(t) dt \quad (10.11)$$

for considered machine wall vibration $\mu_s = 0$.

The process variance is

$$\sigma_s^2 = \lim_{T \rightarrow \infty} \frac{1}{T} \int_0^T [s(t) - \mu_s]^2 dt \quad (10.12)$$

The following relation holds

$$\sigma_s^2 = \Psi_s^2 - \mu_s^2 \quad (10.13)$$

If for the considered processes $\mu_s = 0$, then

$$\sigma_s^2 = \Psi_s^2 \quad (10.14)$$

The probability density function is

$$p(s) = \lim_{\Delta S \rightarrow 0} \frac{1}{\Delta S} \left[\lim_{T \rightarrow \infty} \frac{T_s}{T} \right] \quad (10.15)$$

where: ΔS – the width of the amplitude change window,

T_s – residence time at given level s within limits ΔS (fig. 10.10). There are the following relationships between the estimators:

$$\mu_s = \int_{-\infty}^{\infty} sp(s) ds \quad (10.16)$$

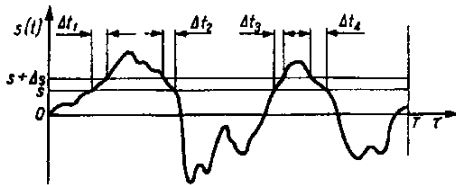


Fig. 10.10. Illustration of probability measurement.

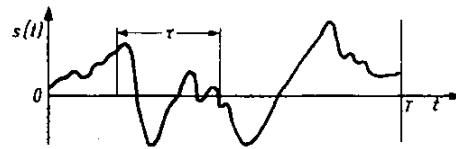


Fig. 10.11. Illustration of autocorrelation measurement.

$$\Psi_s^2 = \int_{-\infty}^{\infty} s^2 p(s) ds \quad (10.17)$$

The signal autocorrelation function (fig. 10.11) has the following form

$$\psi(\tau) = \lim_{T \rightarrow \infty} \frac{1}{T} \int_0^T s(t)s(t-\tau)dt \quad (10.18)$$

and function $\psi_s(t)$ has the following properties

$$\psi_s(-\tau) = \psi_s(\tau) \quad (10.19)$$

$\psi_s(0) \geq \psi(\tau)$ for all τ .

The following relations hold:

$$\mu_s = \sqrt{\psi_s(\infty)} \quad (10.20)$$

$$\Psi_s^2 = \psi_s(0) \quad (10.21)$$

Illustrative autocorrelation functions for different signals are shown in fig. 10.12. As mentioned above, a spectrum is used to describe signals, whereas random signals are described by a spectral power density function.

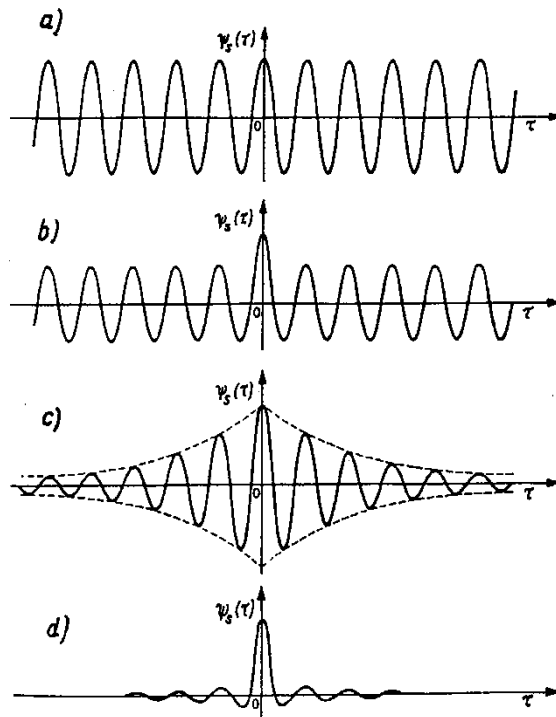


Fig. 10.12. Plots of autocorrelation function for: a – sinusoidal signal, b – sinusoidal signal with random noise, c – narrowband random noise, d – broadband random noise.

The spectral power density function (unilateral) is as follows

$$W_s(f) = \lim_{\Delta f \rightarrow 0} \frac{1}{\Delta f} \left[\lim_{T \rightarrow \infty} \frac{1}{T} \int_0^T s^2(t, f, \Delta f) dt \right] \quad (10.22)$$

where Δf is a bandwidth in Hz, $s^2(t, f, \Delta f)$ is a frequency of function $s(t)$ for any frequency f and in its neighbourhood Δf . A spectral signal power density function is shown in fig. 10.13.

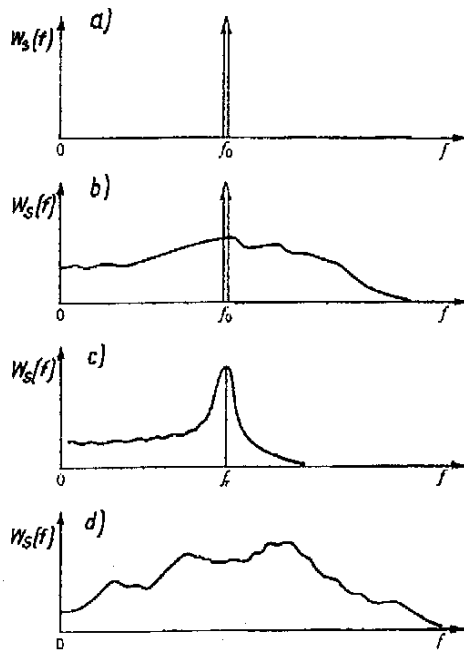


Fig. 10.13. Plots of spectral power density function for:

- a – sinusoidal signal,
- b – sinusoidal signal with random noise,
- c – narrowband random noise,
- d – broadband random noise

The following relations hold:

$$W_s(f) = 2 \int_{-\infty}^{\infty} \psi(\tau) e^{-j2\pi f \tau} d\tau \quad (10.23)$$

$$\mu_s = \sqrt{\int_{-0}^{+0} W_s(f) df} \quad (10.24)$$

$$\psi^2 = \int_0^{\infty} W_s(f) df \quad (10.25)$$

Besides the above parameters for one process, it is also essential to know the joint parameters for the two processes. The main parameters for a class of ergodic processes are given below.

The joint probability density function is

$$p(s_1, s_2) = \lim_{\substack{\Delta s_1 \rightarrow 0 \\ \Delta s_2 \rightarrow 0}} \frac{1}{\Delta s_1 \Delta s_2} \lim_{T \rightarrow \infty} \frac{T_{s_1 s_2}}{T} \quad (10.26)$$

the denotations as in fig. 10.14.

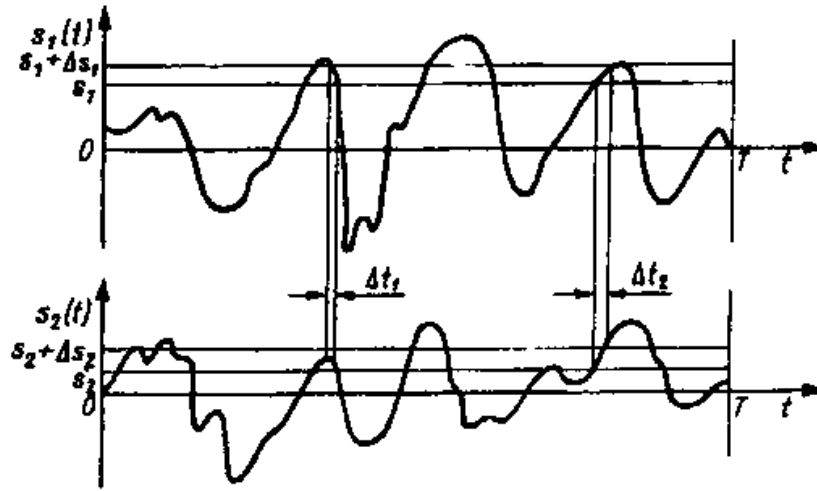


Fig. 10.14. Illustration of joint probability measurement.

If the processes are stochastically independent, the following relation holds

$$p(s_1, s_2) = p(s_1) p(s_2) \quad (10.27)$$

for probability functions $p(s_1, s_2)$ and $p(s_1), p(s_2)$.

$$\psi_{s_1 s_2}(\tau) = \lim_{T \rightarrow \infty} \frac{1}{T} \int_0^T s_1(t) s_2(t + \tau) dt \quad (10.28)$$

This function has the following properties:

$$\psi_{s_1 s_2}(-\tau) = \psi_{s_1 s_2}(\tau) \quad (10.29)$$

$$|\psi_{s_1 s_2}(f)|^2 \leq \psi_{s_1}(0) \psi_{s_2}(0) \quad (10.30)$$

Plots of two functions $s_1(t)$ and $s_2(t + \tau)$ are shown in fig. 10.15.

For an analysis of the interdependences between two signals the following reciprocal spectral density function is defined

$$W_{s_1 s_2}(f) = C_{s_1 s_2}(f) - iQ_{s_1 s_2}(f) \quad (10.31)$$

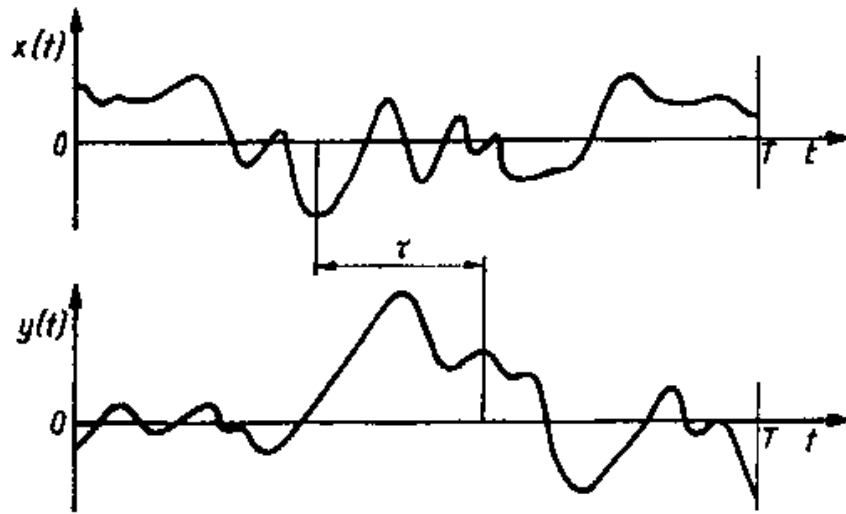


Fig. 10.15. Illustration of intercorrelation measurement

where: $i = \sqrt{-1}$,

$$C_{s_1 s_2}(f) = \lim_{\Delta f \rightarrow 0} \lim_{T \rightarrow \infty} \frac{1}{T \Delta f} \int_0^T s_1(t, f, \Delta f) s_2(t, f, \Delta f) dt \quad (10.32)$$

$$Q_{s_1 s_2}(f) = \lim_{\Delta f \rightarrow 0} \lim_{T \rightarrow \infty} \frac{1}{T \Delta f} \int_0^T s_1(t, f, \Delta f) s_2^*(t, f, \Delta f) dt \quad (10.33)$$

Function $s_2^*(f, t, \Delta f)$ is shifted by $\frac{1}{4}$ period: $\tau = \frac{1}{4} f$. Function $W_{s_1 s_2}(f)$ is a complex function.

The relationship between functions $W_{s_1 s_2}(f)$ and $\Psi_{s_1 s_2}(\tau)$ is as follows (also a reverse relation holds)

$$W_{s_1 s_2}(f) = \int_{-\infty}^{\infty} \psi_{s_1 s_2}(\tau) e^{-i2\pi f \tau} d\tau \quad (10.34)$$

To determine the interrelations between signals one can also use a coherence function. Its square is given by this formula

$$\gamma_{s_1 s_2}^2(f) = \frac{|W_{s_1 s_2}(f)|^2}{W_{s_1}(f)W_{s_2}(f)} \quad (10.35)$$

The numerical parameters are given by formulas: (10.10)-(10.12), (10.14), (10.16), (10.17), (10.20), (10.21), (10.25). The functional parameters are given by: (10.15), (10.18), (10.22), (10.23), (10.26), (10.28), (10.31)-(10.35). The numerical parameters of a process are represented by one number. The process functional parameters are written as functions in the amplitude domain (10.15), (10.26), the time domain (10.18), (10.28) and the frequency domain (10.22), (10.23), (10.31)-(10.35).

Practically only parameter estimators or derivative parameter estimators can be found. A derivative parameter or its estimator is defined as a parameter or an estimator subjected to a simple mathematical operation, such as squaring or extraction of a roots.

10.1.1. Process estimators and their application to vibroacoustic diagnostics

Vibroacoustic process $\{s(t, 0)\}$ is represented by its realization $s(t, 0)$ (this is possible under the above constraints). It is a function of current time (measurement time) in neighbourhood t_0 in which diagnosis is being made and of machine's lifetime Θ (service time). A vibroacoustic process for variable time Θ is nonstationary and thus nonergodic. In our considerations $\Theta = \text{const}$. Thus the realizations are represented by $s(t)$.

Mean value estimator

$$\hat{\mu}_s = \frac{1}{T} \int_0^T s(t) dt = 0 \quad (10.36)$$

The length of time T is finite and it depends on the accuracy with which a given estimator denoted by $\hat{\mu}$ should be calculated.

Quadratic mean estimator

$$\hat{\Psi}^2 = \frac{1}{T} \int_0^T s^2(t) dt \quad (10.37)$$

$$\Psi^2 = \sigma_s^2 \text{ if } \mu_s = 0$$

Absolute mean estimator

$$\left| \hat{\mu}_s \right| = \frac{1}{T} \int_0^T |s(t)| dt \quad (10.38)$$

Root-mean-square value estimator (derivative estimator)

$$\hat{\Psi}_s = \sqrt{\frac{1}{T} \int_0^T s^2(t)} \quad (10.39)$$

From the above examples of numerical and derivative estimators one can infer how to effect a transition from a parameter to a parameter estimator.

As mentioned above, the accuracy with which numerical estimators are calculated depends on realization time T . In the case of functional estimators, the accuracy with which they are calculated is also affected by: bandwidth Δf or “window” width Δs . The longer the realization time T , the higher the accuracy of estimation of point parameters, whereas for functional estimators: the higher the product $\Delta f T$ or $\Delta s T$, the higher the accuracy.

Cepstrum power function estimator

The cepstrum function was defined in [10.2]. Power cepstrum is defined as the power density of logarithmic signal $s(t)$ power spectrum. It is a “quefrequency” function – a number of cycles/Hz, i.e. a function in the time domain. To explicate this, the mathematical operations leading to the cepstrum power function are described below.

The realization of process $s(t)$ determinate in interval $0 \leq t \leq T$ is used to find this Fourier transform

$$F_s(f) = \int_0^T s(t) e^{-i2\pi ft} dt \quad (10.40)$$

The transform is used to find the following power density function

$$W_s(f) = 2 \frac{1}{T} [F_s(f)]^2 \quad (10.41)$$

The cespstrum power function is expressed by this formula

$$C(\tau) = \left| \int_0^T \log W_s(f) e^{-i2\pi f \tau} df \right|^2 \quad (10.42)$$

It has been proved that the cepstrum power function is a function of time having the same physical meaning as the time in the autocorrelation function. The proof is in [10.2] where one can learn how the phase shift between original signal $s(t)$ and its echo shifted by τ_0 and amplified or attenuated, which can be written as $s(t - \tau_0)$, can be found on the basis of the cepstrum power function.

The usefulness of the cepstrum power estimator can be presented as follows:

$x(t)$ – a signal emitted in the signal source,

$y(t)$ – a signal received in the machine's wall,

$h(t)$ – a signal transition impulse function – a function describing the properties of the signal transition path.

Between the spectra of the signals one can find the following relationship:

$$W_y(f) = H^2(f)W_x(f) \quad (10.43)$$

$H(f)$ is transmittance, i.e. a Fourier transform of function $h(t)$. After finding the logarithm (10.43) (see [10.3], we get

$$\log W_y(f) = 2 \log H(f) + \log W_x(f) \quad (10.44)$$

Instead of product $|H(f)|^2 W_x(f)$ we obtain a logarithmic sum. If functions $H(f)$ and $W_x(f)$ have different frequency ranges, i.e. function $H(f)$ has a frequency range narrower than that of function $W_x(f)$, then the two functions become separated in the time domain on the graph of the cepstrum power function [10.3] and thus the influence of $H(f)$ on the result of the diagnosis, reflected by spectrum $W_x(f)$, is eliminated.

The separability of the spectrum can be illustrated by the following example. If a signal is recorded at two different measuring points (fig. 10.14), then this signal is influenced by transition function (transmittance function) $h(t)$ reflecting this signal spectrum (fig. 10.16), but the form of $C(\tau)$ remains unaffected (see fig. 10.16) (according to [10.3]).

Synchronous summation function spectrum

By applying synchronous summation one can “filter off” a determinate or coherent signal from the incoherent noise background. This operation is represented by the following expression

$$W_s(f) = |H(f)|^2 W_x(f) + \frac{1}{m} |H(f)|^2 W_n \quad (10.45)$$

where: m – a number of full summation cycles,

$W_n(f)$ – an incoherent signal density spectrum.

If m is sufficiently large, the term with spectrum $W_n(f)$ decreases and an amplified spectrum of signal $x(t)$ is obtained. In the case of synchronous summation the signal is totalled in time with the rotary motion of the machine.

Examples of synchronous and asynchronous summation are shown in fig. 10.17. Depending on what is to be the information signal one can perform synchronous summation and obtain the picture shown in fig. 10.17a or perform asynchronous summation and obtain the picture shown in fig. 10.17b.

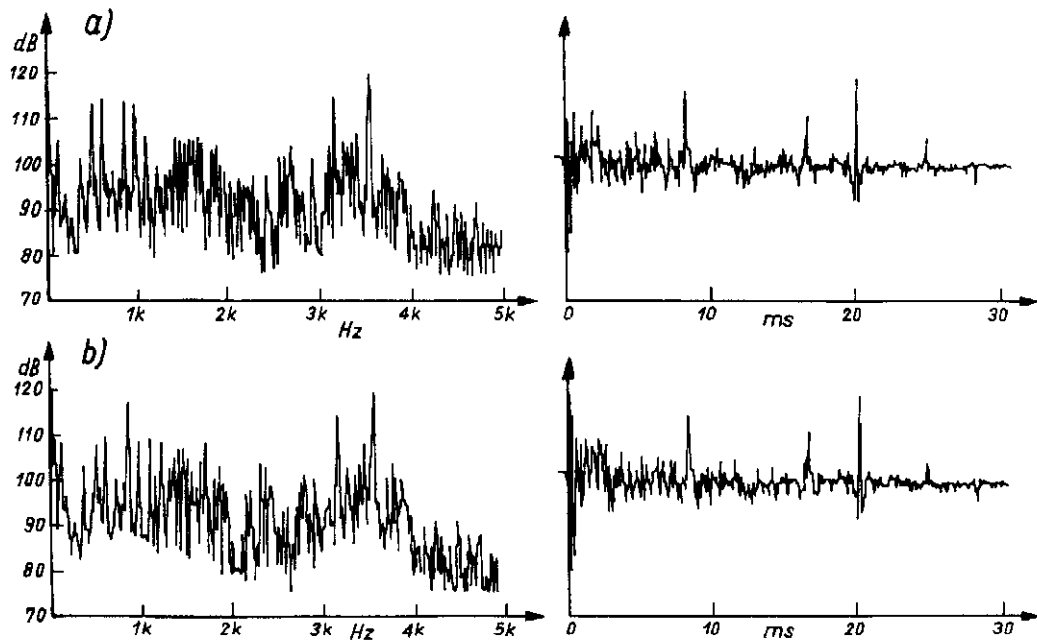


Fig. 10.1. Spectra of signals generated by gears and their cepstra for two signal reception points a and b.

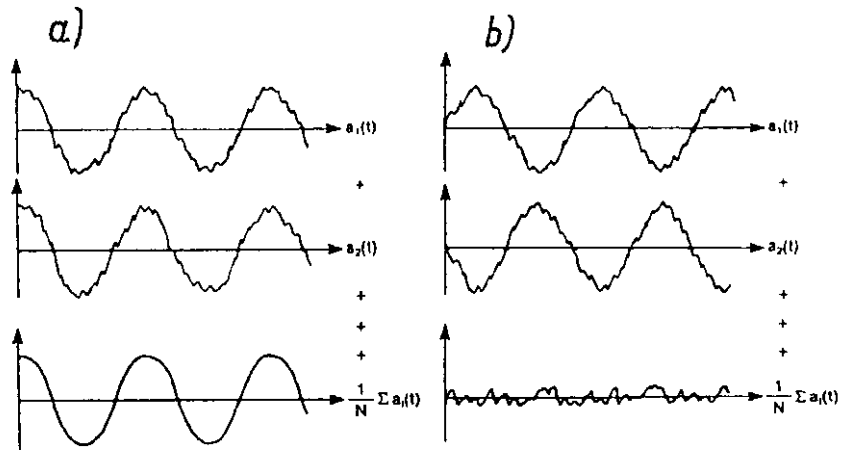


Fig. 10.2. Synchronous time averaging (a) and asynchronous time averaging (b).

Bispectrum function

A statistical moment of the third order is the base of the bispectrum function. For Gaussian noise this moment is equal to zero and in the case of a sum of signals consisting of a determinate process and Gaussian noise, it is different from zero. The bispectrum can be treated as a discriminator of a determinate process hidden in Gaussian noise.

Bicoherence functions are written as

$$\gamma(f_1, f_2) = \frac{B_s(f_1, f_2)}{[W_s(f_1)W_s(f_2)W_s(f_1 + f_2)]^{\frac{1}{2}}} \leq 1 \quad (10.46)$$

where $B_s(f_1, f_2)$ is a bispectrum.

The bispectral function was employed to assess the condition of gear meshing [10.4]. The way in which the function can be used is shown in fig. 10.18.

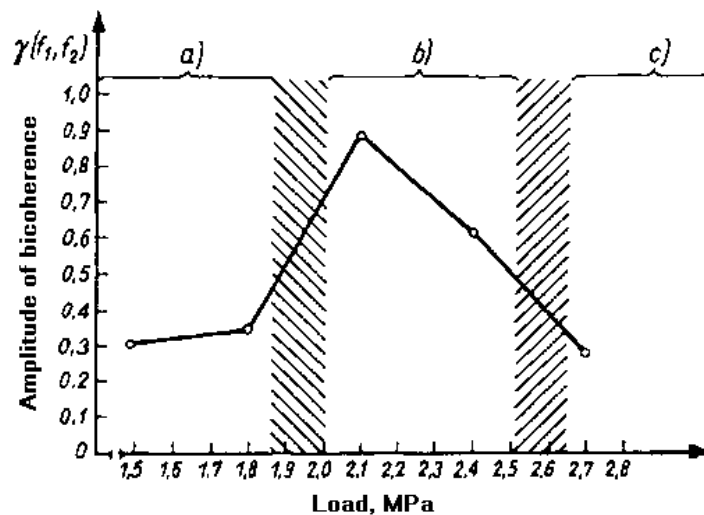


Fig. 10.3. Bicoherence values as function of gear loading and condition [10.4]: a – light load, b – normal operation, c – wear of teeth.

Coherence function

Theoretical considerations and research on the use of the coherence function in gear meshing diagnostics are treated extensively in [10.5]. The condition of gear meshing is assessed on the basis of the reception of a signal from several points on the gear's walls (fig. 1.13). The coherence function's narrowband components are determined for characteristic frequencies. It is assumed that the signals received from several points on the gear's wall consist of broadband incoherent noise and coherent components generated in the bands with characteristic frequencies.

The principle of diagnostic inference says: by measuring signals the difference between them can be determined as differentiating process $z(t)$. Thus signals $s_1(t)$ and $s_2(t)$ received from two points on the wall of a machine consist of a correlated (coherent) part of the processes, which are denoted by $y_1(t)$, $y_2(t)$ and differentiating part $z(t)$. Signals $s_1(t)$ and $s_2(t)$ can be written as:

$$s_1(t) = y_1(t), s_2 = y_2(t) + z(t) \quad (10.47)$$

The spectra of signals (10.47) are described by the following formulas (signals $y_1(t)$, $y_2(t)$ are assumed to be correlated):

$$\begin{aligned} W_{s_1 s_2}(f) &= W_{y_1 y_2}(f) \\ W_{s_1 s_1}(f) &= W_{y_1 y_1}(f) \\ W_{s_2 s_2}(f) &= W_{y_2 y_2}(f) + W_{zz} \end{aligned} \quad (10.48)$$

By putting formula (10.48) into formula (10.35) we get:

$$\gamma_{s_1 s_2}^2(f) = \frac{|W_{y_1 y_2}(f)|^2}{[W_{y_2 y_2}(f) + W_{zz}(f)]W_{y_1 y_1}(f)} \quad (10.49)$$

If $W_{zz}(f) = 0$, then $\gamma_{s_1 s_2}^2(f) = 1$, since $|W_{y_1 y_2}(f)|^2 = W_{y_1 y_2}(f)W_{y_2 y_2}(f)$ when signals $y_1(t)$, $y_2(t)$ are correlated. However, if

$$W_{y_1 y_2}(f) = 0, \text{ then } \gamma_{s_1 s_2}^2(f) = 0$$

$$W_{zz}(f) > 0, \text{ then } 0 < \gamma_{s_1 s_2}^2(f) < 1 \quad (10.50)$$

Relations (10.50) show how values $\gamma_{s_1 s_2}^2(f)$ can change with the condition of gear meshing. The share of the process which differentiates the two processes received from the gear's wall is the larger, the better the condition of the machine. And vice versa, for condition regarded to be poor, the differentiation process's share is the smaller, the poorer the machine's condition. Condition parameters range from 0 to 1.

Illustrative spectrum components after [10.5] are shown in fig. 10.19. The components denoted 1-6 correspond to the gear meshing harmonic frequencies. The picture shown in fig. 1.16 was obtained by considering the components as the components of a vector and determining its length and angle φ relative to the vector whose length was shortest. To determine the angle and the length of the vectors the following formulas are used:

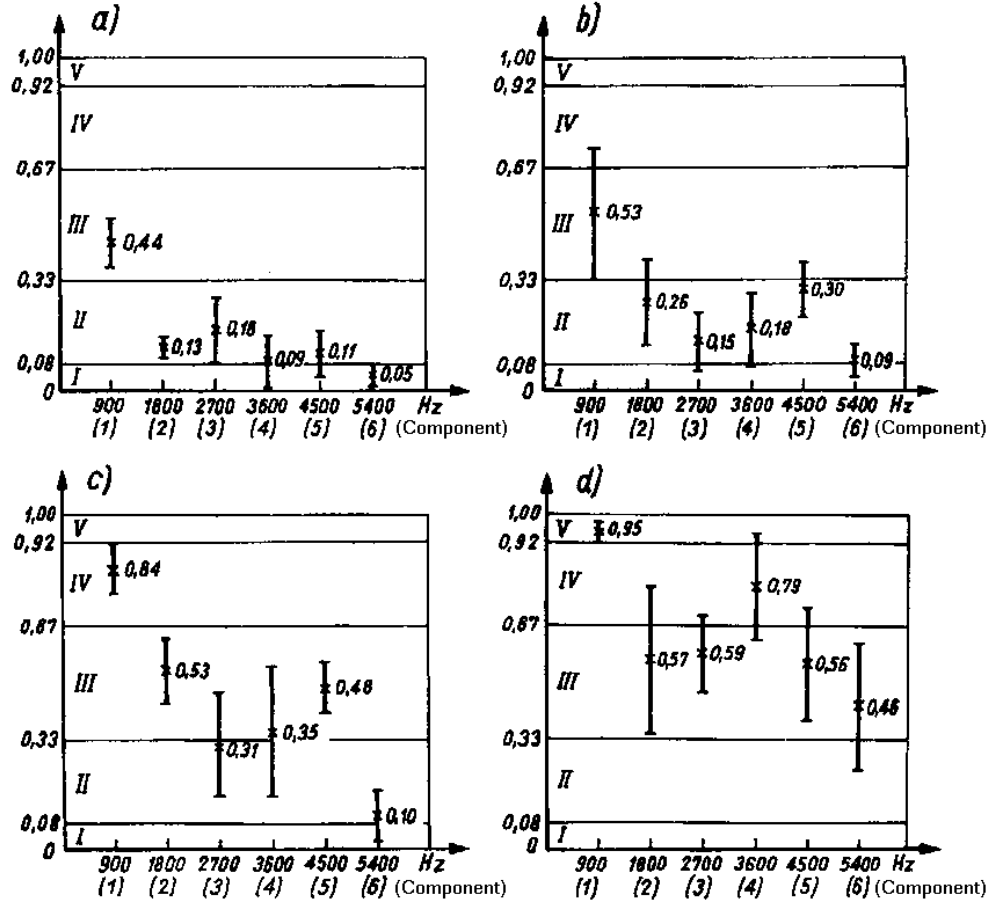


Fig. 10.4. Gear meshing components for wheels: a – $w_1(h)$, $4_1(h)$, mod $0.4t_z$, b – $w_1(h)$, $O_1(h)$, c – $9_p^p(h)$, $9_p^p(m)$, d – $5_p^p(m)$, $5_p^p(m)$.

$$\cos \varphi = \frac{[\gamma_w^2(f_1, \Delta f_1)][\gamma^2(f_1, \Delta f_1)] + \dots + [\gamma_w^2(f_6, \Delta f_6)][\gamma^2(f_6, \Delta f_6)]}{\left| \bar{V} \right| \left| \bar{W} \right|} \quad (10.51)$$

$$\left| \bar{W} \right| = \sqrt{\sum [\gamma_w^2(f_i, \Delta f_i)]^2} - \text{the module of the basic vector} \quad (10.52)$$

$$\left| \bar{V} \right| = \sqrt{\sum [\gamma^2(f_i, \Delta f_i)]^2} - \text{the module of the vector for a given pair of wheels} \quad (10.53)$$

$$[\gamma_w^2(f_i, \Delta f_i)] - \text{the components of the basic vector } (i = 1, 2 \dots 6) \quad (10.54)$$

$$[\gamma^2(f_i, \Delta f_i)] - \text{the components of the vector for a given pair of wheels} \quad (10.55)$$

Damage to gear wheels caused by pitting is shown in fig. 10.20, the gear meshing condition components – in fig. 10.19d and the influence of design features on the length and angle of the signal vector in fig. 1.16. In the case of gear wheels damaged by pitting, angle φ increases and ranges from 37 to 48°. Angle φ for modified wheels is about 10° and for unmodified but damaged by pitting wheels it amounts to about 42°. This is mainly due to an increase in the share of higher-frequency components.

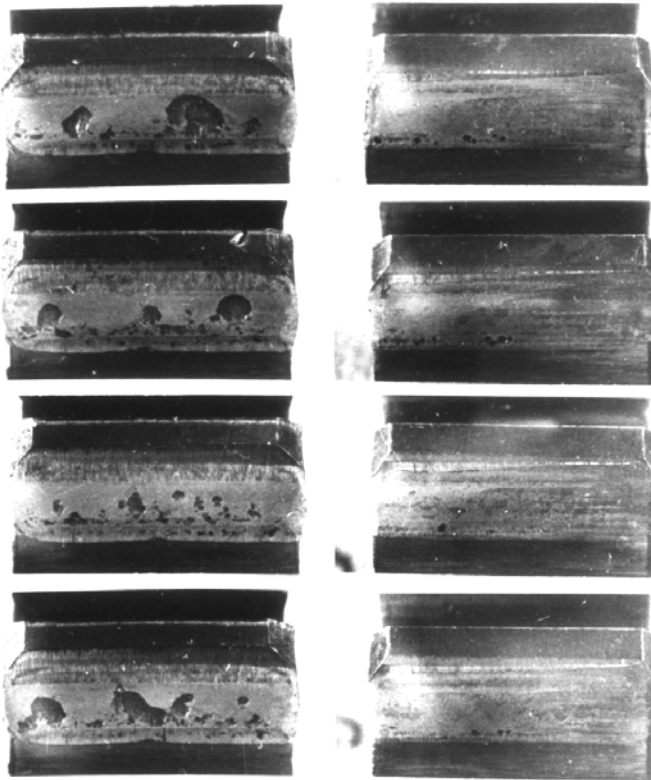


Fig. 10.5. Picture of fatigue pitting for $S_p^p(m)$, $S_p^p(m)$.

Envelope spectrum

To obtain an envelope spectrum, the Hilbert transform is used:

$$\chi[s(t)] = \tilde{s}(t) = \frac{1}{\pi} \int_{-\infty}^{\infty} s(\tau) \frac{1}{1-\tau} d\tau \quad (10.56)$$

To obtain a signal envelope, the notion of an analytical signal is introduced

$$z(t) = s(t) + i\tilde{s}(t) \quad (10.57)$$

which can also be written as

$$z(t) = A(t)e^{i\phi(t)} \quad (10.58)$$

where $A(t)$ is called a signal envelope and $\phi(t)$ – an instantaneous signal phase.

In order to obtain a signal envelope spectrum, the analytical signal is subjected to the Fourier transform according to [10.40]. Signal envelope $A(t)$ is calculated as the positive root of this expression

$$A(t) = \sqrt{x^2(t) + \tilde{x}^2(t)} \quad (10.59)$$

Function $\phi(t)$ is referred to as a signal of instantaneous values of the phase which is calculated from this formula

$$\phi(t) = \text{tg}^{-1} \left[\frac{\tilde{x}(t)}{x(t)} \right] \quad (10.60)$$

Illustrative forms of signals $x(t)$, $\tilde{x}(t)$ and $A(t)$ are shown in fig. 10.21.

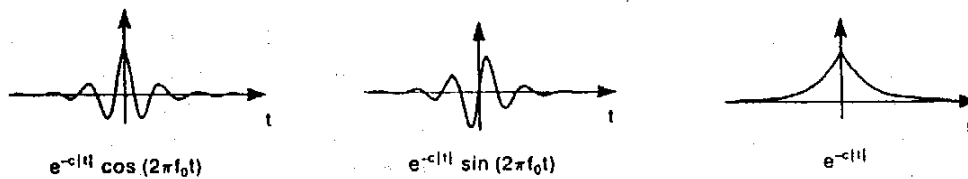


Fig. 10.6. Conversion of signal into envelope.

Gabor transform, Gabor spectrum

The disadvantage of the Fourier transform is that information in the time domain may be determined for the whole length of signal $s(t)$. This is due to the fact that the spectrum is obtained on the basis of an integral calculated in an interval from $-\infty$ to $+\infty$. The acquired information is averaged in the whole interval of length of signal $s(t)$. If at any signal time local vibration occurs which provides special information, the latter will influence the Fourier transform, but its location on the time (t) axis will be lost because of the operation of the Fourier transform. There is no way of detecting if particular component f in the Fourier transform stems from the components occurring in the whole period of function $s(t)$ or it originates from one or several selected periods. This inconvenience can be avoided by applying the Gabor transform or the wavelet transform [10.6]. The Gabor transform consists in the application of the Fourier transform jointly with an appropriate time window imposed on the considered fragment of the signal. The window's shape corresponds to the Gaussian function.

The Gabor spectrum for function $s(t)$ is defined in the time domain and the frequency is given by this formula

$$G(f, t) = \int_{-\infty}^{\infty} s(\tau) g^*(\tau - t) \exp(-2\pi f \tau) d\tau \quad (10.61)$$

where: $g^*(t)$ is a conjugate function of Gaussian window $g(t)$ in the following form

$$g(t) = \frac{\sigma}{\sqrt{\pi}} \exp(-\delta^2 t^2) \quad (10.62)$$

where σ is a constant.

The Gabor spectrum circumscribes the Fourier transform of signal $s(t)$ around time t .

Wavelet transform

The wavelet transform of signal $s(t)$ can be written as

$$W(a, b) = \frac{1}{\sqrt{a}} \int_{-\infty}^{\infty} s(t) h^* \left(\frac{t-b}{a} \right) dt \quad (10.63)$$

where a and b are an extension and a shift of transform kernel $h(t)$. Coefficient $1/\sqrt{a}$ is used to normalize the signal. Shift b specifies the location of the kernel in time and extension a ($a > 0$) defines the kernel's width and scale. Thus the result of local transform $W(a, b)$ can be considered in a time domain (scale) in which short-duration but high-frequency events are on a small scale and long-duration and low-frequency events are on a large scale. The properties of the local transform can be exploited by selecting a kernel suitable for a particular problem.

10.2. Wear products as signal of machine's condition

The causes for which machine elements are replaced are shown in fig. 10.22 ([10.7]) according to which 70% of the cases represent damage to the surface of the mating elements, 50% of which is due to wear and 20% due to corrosion. Wear results from abrasion, adhesion, fatigue and erosion (chap. 9). The changes in the condition of the surface are accompanied by the generation of characteristic wear and corrosion products (Z_u, K). An illustrative classification of wear products, corrosion products and impurities (Z_u, K, Z_a) is shown in fig. 10.23 after [10.8]. Particles (Z_u, K, Z_a) can be characterized by: shape, colour, density/porosity, index of refraction, edge sharpness or roundness, hardness, structure, volume and chemical composition.

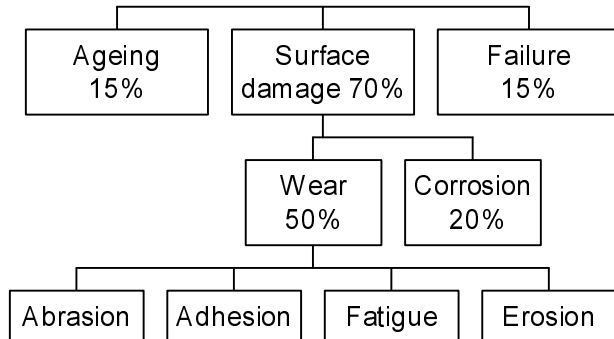


Fig. 10.1. Causes for replacement of machine elements [10.7].

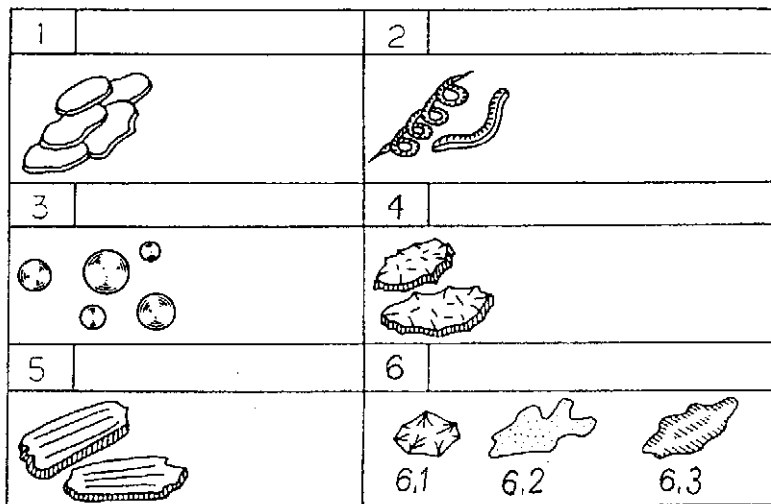


Fig. 10.2. Forms of particles (Z_u , K , Z_a): 1 – normal wear particles: flat, smooth surface, dimensions $0.5-5 \mu\text{m}$; 2 – abraded particles: chips, dimensions $25 \div 100 \mu\text{m}$; 3 – spherical particles: dimensions $1 \div 5 \mu\text{m}$; 4 – surface fatigue (pitting) particles: rough surfaces and edges, dimensions $> 20 \mu\text{m}$; 5 – interference particles: rough surfaces (surface irregularities running in parallel), dimensions $> 20 \mu\text{m}$; 6 – other particles: 6.1. – sand, 6.2 – plastic, 6.3 – rust.

The condition of a machine can be determined on the basis of the above measurable characteristics. Much information can be gained from analytical ferrography [10.9]-[1.16]. This method enables the separation of wear products/particles (Z_u , K , Z_a) from the oil, which are then distributed depending on their size on a transparent base (e.g. glass) and observed under an optical or electron microscope. The machine element wear products on a transparent base become distributed under the action of a

strong electromagnetic field. The analytic ferrographic equipment manufactured by Foxboro was used for the first time to assess the condition of machines in 1972 [10.9]. Thus ferromagnetic diagnostics makes it possible to determine the condition of a machine through the monitoring of the products of wear of its elements, which reflect the mechanism of the wear. The probability of a failure depends on the form of wear of the surfaces of the mating elements (fig. 10.24). On the basis of the experience in the use of analytical ferrography simplified ferrographic methods have been developed [10.12]. They make it possible to assess the concentration of machine element wear products/particles (Z_u , K , Z_a) in the oil. The simplified ferrography is used to continuously monitor the concentration of wear products represented by numerical values [10.13].

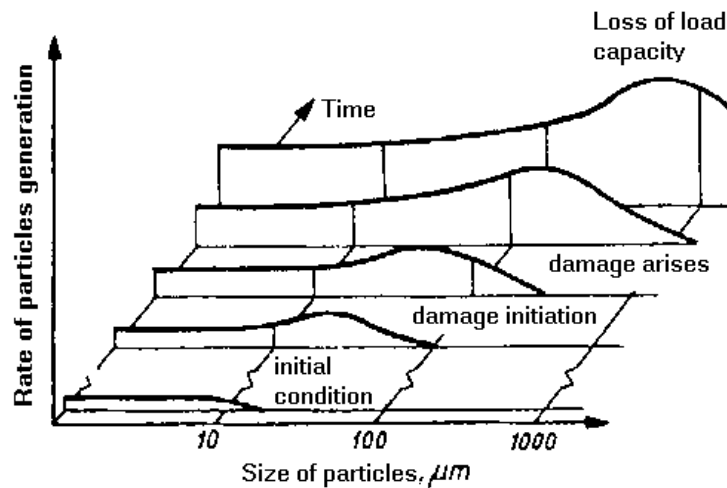


Fig. 10.3. Rate of particles generation.

Analytical ferrography apparatus and method

The basic unit of the apparatus is a ferromagnetic analyzer (fig. 10.25 after [10.12]) which consists of a magnet and a casing in which a transparent base – a plate with deposited element wear products, i.e. particles (Z_u , K , Z_a) circulating in the oil – is secured. A sample of diluted oil is fed by a pump onto the plate fixed on a slant whereby the oil trickles down along the plate. The delivery of the pump is as low as 0.2 ml/min to enable the settling of wear products in the form of metallic (mainly magnetic) particles (iron, nickel, cobalt) or nonmetallic particles. The rate of flow of oil through the magnetic field is such that the particles settle beginning with the largest (at oil inflow) to smallest (at oil outflow). The particles range from a few to a few hundred micrometers in size. After the sample has been pumped through, the particles are rinsed and the remaining oil is washed away. The particles adhere to the plate. The washing liquid evaporates rapidly and the plate with the adhering particles becomes dry.

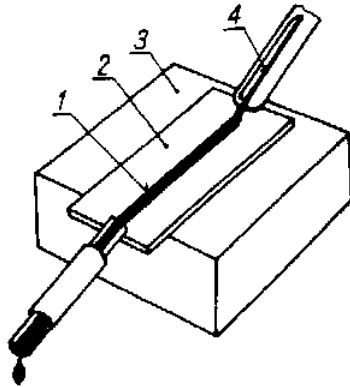


Fig. 10.4. Diagram of analytic ferrograph:
 1 – trickle of oil in magnetic field,
 2 – ferrogram plate,
 3 – magnet casing,
 4 – oil inflow.

The time needed for the pumping through of the oil sample is 5 min and the rinsing of the particles and their adhering to the plate take from 5 to 10 min. The particles firmly adhere to the plate. A typical 3 ml oil sample is mixed with 1 ml of a sticking substance. If the concentration of wear products in the sample is high, the sample is diluted with pure oil of the same type.

Ferrographic examinations are made using a dichromatic microscope called a ferriscope (fig. 10.26). The ferriscope has two independent light sources. Light beams from one of the light sources pass through a red filter and the light is directed, via a lens with magnifications similar to those of a metallographic microscope, towards a ferrogram.

Light from the second light source passes through the green filter and lights the ferrogram from below. The use of two contrasting colours makes it possible to distinguish the light passing through the ferrogram from the reflected light. Non-transparent particles reflect light and they are seen as red. Particles which to a certain degree dampen light are seen as different shades of yellow and green. The microscope can be equipped with a reader enabling readouts of the density of particles on the ferrogram and thus the determination of the percentage of the area covered with particles. The particles in the ferrogram can also be observed with an electron microscope.

To sum up, a set of apparatus and ferrographic diagnostic (analytic ferrography) aids should include:

- an analytical ferrograph,
- a dichromatic microscope (ferriscope) (green light passed through, red light reflected) optionally with an attachment for taking colour photographs and an attachment for measuring the density of particles,
- a catalogue of typical forms of wear (according to current views, a separate catalogue should be compiled for each device),
- aids for taking oil samples, e.g. syringes, bottles made of transparent glass with appropriate stoppers insoluble in oil, transparent plates for ferrograms.

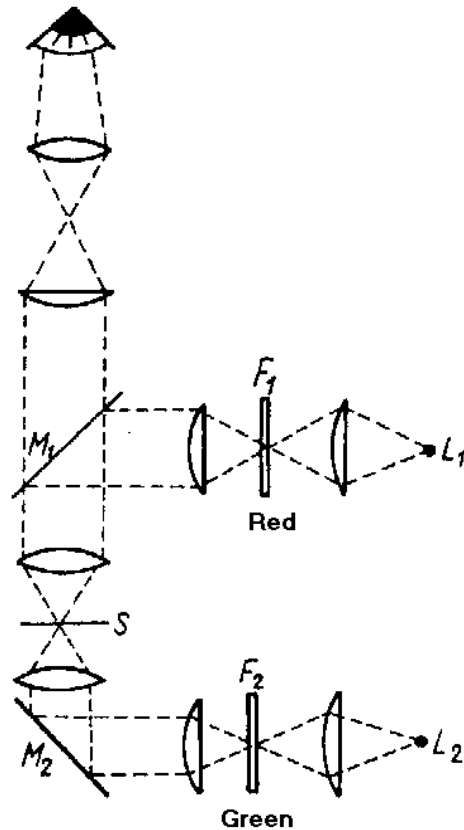


Fig. 10.5.
Diagram of dichromatic microscope –
ferriscope:
 L_1, L_2 – light sources,
 M_1, M_2 – mirrors,
 F_1, F_2 – filters,
 S – sample.

Principles of sampling

During the normal operation of a lubrication system or a hydraulic system, the concentration of machine element wear products in the oil reaches an equilibrium for given operating parameters of the machine. Since the wear products are continuously generated in an operating mechanical system, the equilibrium of particle concentration implies that the particles are removed in the same amount as they are generated. The known and presumable losses of particles are due to (according to [10.13]):

- filtration,
- deposition,
- adhesion to stationary walls,
- crushing during repeated passage through the zone of contact between elements,
- chemical action,
- oil loss.

Having in mind the above principle of particle concentration, when taking oil samples the following rules should be observed:

- samples should be taken from one place in the system (different parts of the system may have different particle concentration);
- one should try to take samples at a location before oil filtration in the lubrication system;
- if samples are taken during the operation of the machine, they should be taken at comparable operating parameters (operating/motion factors) of the machine;
- if samples are taken after the machine has been turned off, then the particle settling rate should be taken into account;
- taken samples should be placed in glass bottles with at least 15 ml volume;
- experience shows that a high percentage of failures occurs during the starting of a new machine, therefore the frequency of sampling in this period should be increased (acc. to [10.10] it is recommended to take samples at every few hours);
- after wear (running-in) products stabilize, the following oil sampling rates are recommended:
 - aircraft gas turbines: every 10÷200 h,
 - aircraft hydraulic systems: every 20÷200 h,
 - Diesel engines: every 100÷500 h,
 - heavy transmissions: every 100÷500 h,
 - other hydraulic systems: every 50÷500 h.

Application of ferrography to wear products monitoring

Experiments presented in paper [10.14] prove that the wear products/particles (Z_u , K , Z_a) deposited on the ferrogram reflect the wear mechanism occurring on the surface of mating machine elements. A surface damaged by micropitting is shown in fig. 10.27. One can see that the surface is covered with elements in the shape of flat "tongues". The ferrogram of this area shows the particles to be slightly different (fig. 10.28). Ferrography makes it possible to trace the development of wear products and to compare microscopic images with known images contained in a catalogue of possible forms of wear. A failure hazard is assigned to the particular forms of wear. The amount and distribution of wear products are determined by optical measurements. When the wear product density readouts from consecutive oil samples are constant values this means that the machine operates normally and wear products are produced at a constant rate.

A sudden increase in the rate of production of wear products, particularly an increase in the ratio of large to small particles indicates dangerous element wear leading to a failure.

Metal particles even as small as 1 μm reflect red light. Particles generated by friction and particles resulting from adhesion which are found in the oil of a machine have the shape of flakes and they are an indicator of normal, allowable wear of the machine

elements (fig. 10.28). Micropitting wear products can reach a size of 50 μm and a thickness of 0.25-0.5 μm . According to [10.15] and [10.16] such particles are similar to wear products referred to as rubbing wear particles. Particles as they are rubbed off or sheared (10.29) assume the shape of miniature spirals, loops or bent wires.

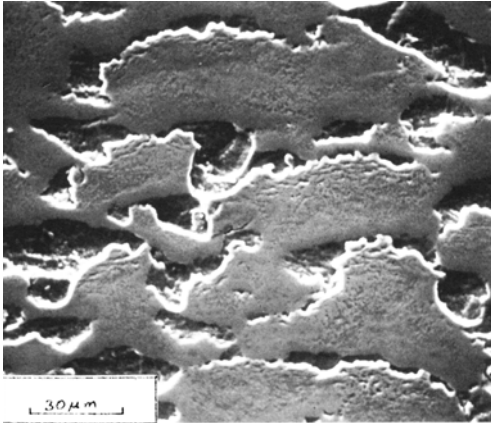


Fig. 10.6. Surface of gear wheel tooth damaged by micropitting [10.11].

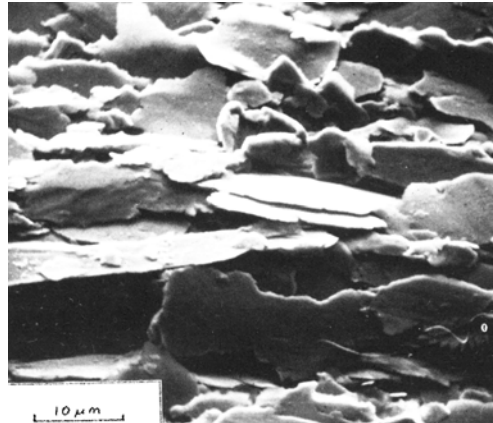


Fig. 10.7. Micropitting particles in form of flakes [10.15].



Fig. 10.8. Sheared products of wear of mating surfaces [10.15].

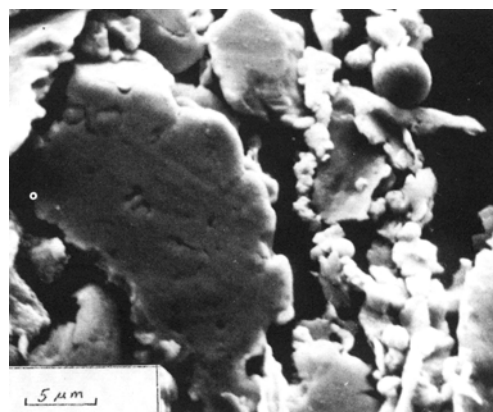


Fig. 10.9. Particles originating from worn out rolling bearing [10.15] (visible characteristic spherical element).

Their occurrence and degree of concentration indicate a dangerous abrasive form of wear of the elements and a sudden increase in their concentration should be treated as a warning signal of an impending failure. Spherical steel particles in the case of rolling contact (rolling bearings) are characteristic of the development of a fatigue fracture. A concentration of spherical elements is a sign of the development of a fatigue crack (fig. 10.30).

Also the products of wear of a slide bearing can be observed. In fig. 10.31 one can see particles of a copper-tin alloy with an antimony addition and characteristic wear products in the form of balls. The occurrence of spherical elements in a microscopic image is not always a reflection of the condition of a rolling bearing or a slide bearing – in fig. 10.32 one can see dust particles which were present around the revolving shaft.

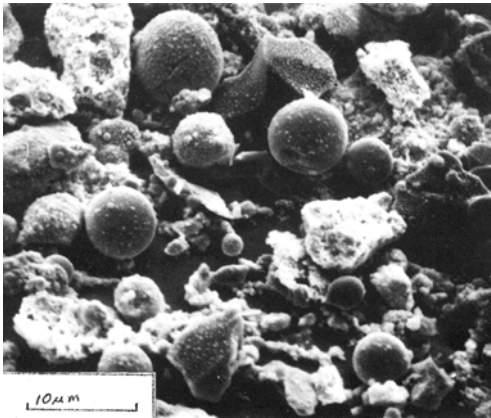


Fig. 10.10. Particles from wear of slide bearing (particles of copper-tin alloy with antimony addition) [10.15].

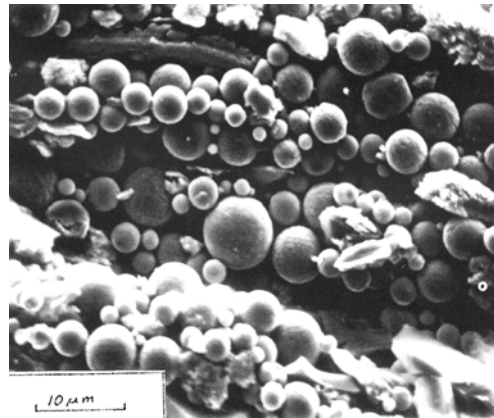


Fig. 10.11. Microscopic image of dust particles around revolving shaft.

Electron microscope images of wear products are shown in figs 10.28-10.33. In practice, a microscope, called a ferriscope, with a resolution similar to a metallographic microscope is used for such observation.

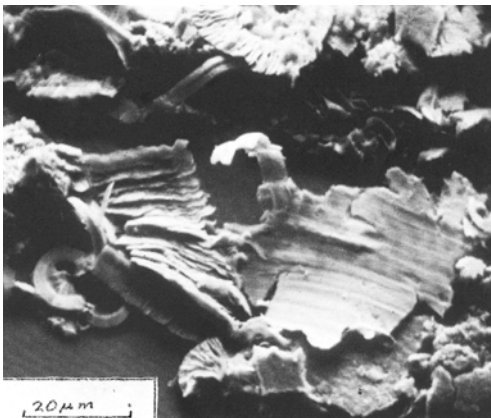


Fig. 10.12. Image of gearing damage (scuffing) particles [10.15].

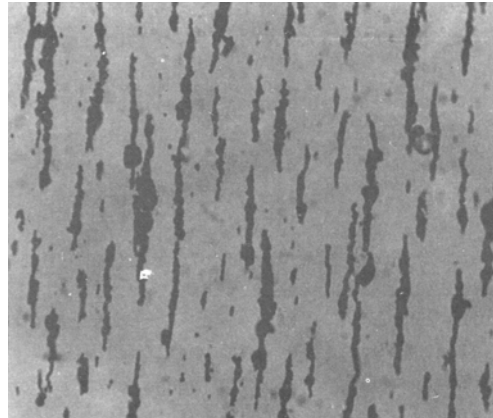


Fig. 10.13. Ferrogram of wear products from toothed gear after 1678 h of operation.

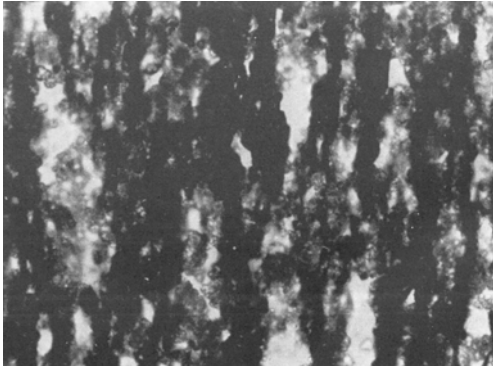


Fig. 10.14. Ferrogram of wear products from gear after 3669 h of operation.

Friction products with polymer inclusions and a ferrogram of products of wear of toothed gear operating for 1678 h are shown in figs 10.33 and 10.34, respectively. A ferrogram of products of wear of a toothed gear operating for 3669 h, including wear products with polymer inclusions, is shown in fig. 10.35 (the size of the largest particles is 10-15 μm).

Other methods of detecting particles (Z_u , K , Z_a)

The following methods are used to detect particles (Z_u , K , Z_a):

The measurement of the variation in the electrical resistance of the flow of particles (Z_u , K , Z_a) through a throat (fig. 10.36a). The volume of a particle can be determined in this way when it flows through a throat and the electric resistance of the liquid in the throat changes.

The measurement of electroacoustic properties (fig. 10.36b). The liquid is subjected to the action of a changing electric field whose frequency changes (the frequency band in MHz). The size of a particle is determined on the basis of the measured angle of diffraction of the waves generated by the particles. Measurements at a high concentration of particles – from 0.5 to 40% – are possible [10.17].

- The measurement of the pressure drop caused by the settling of particles (Z_u , K , Z_a) on a filter (fig. 10.36c). Several filtration membranes of different porosity can be used to determine the particle size.
- The measurement of inductance (fig. 10.36d). A working medium flows through a coil whose inductance changes when the liquid with particles flows through it. The sensitivity of the method depends on electrical interference screening.
- The measurement of changes in the magnetic flux due to the settling of particles (fig. 10.36e). Only ferromagnetic particles can induce changes in the magnetic flux.
- The measurement of optical quantities – by measuring Fraunhofer rings (fig. 10.36f). It is possible to detect particles from 0.1 μm up. Several detectors

placed in a light flux receive deflected light beams depending on the particle size – the smaller the particle, the larger the deflection.

- The measurement of the degree to which particle (Z_u , K , Z_a) screens light – fig. 10.36g.
- The measurement involving the use of a spinning light flux – fig. 10.36h.

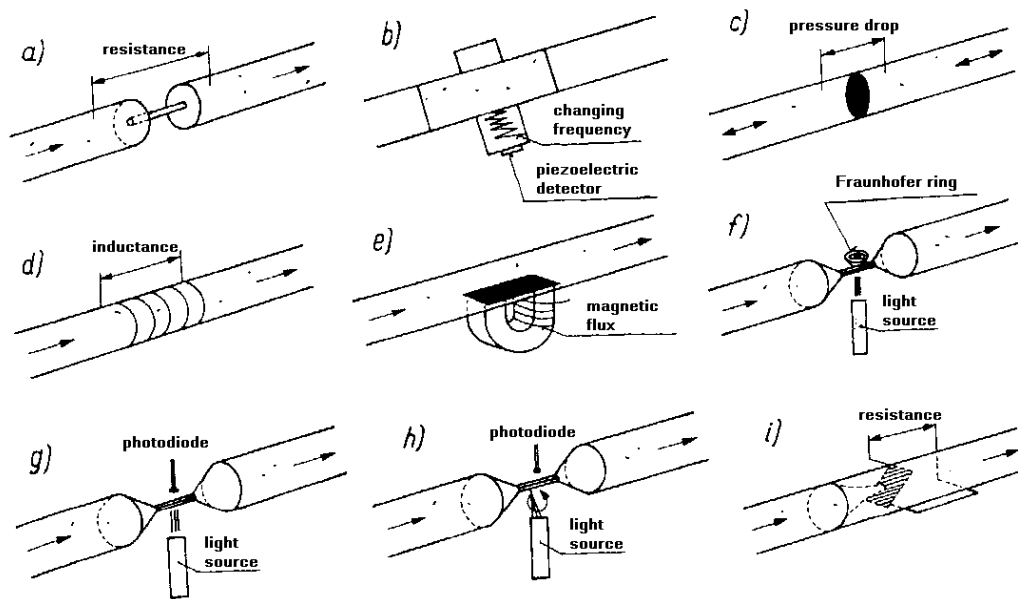


Fig. 10.15. Methods of detecting particles: a – resistance method, b – electroacoustic method, c – pressure drop method, d – induction method, e – magnetic method, f – Fraunhofer lines method, g – optical method, i – Fulmer resistance method [10.21].

10.3. Thermal effects as signals of machine's condition

Some of the energy supplied to the machine is lost – converted into thermal energy. This is one of the processes which accompany the operation of the machine. How much energy is lost depends on the condition of the machine. The energy is lost due to friction. As a result the efficiency of the machine decreases.

The problem of friction in gear meshing was considered in chap. 5 (figs 5.8, 5.9, 5.10 and 5.11) and in chap. 6 in which expression (6.17) gives the instantaneous values of power lost (converted into heat) through friction. How much energy is lost through friction in a gear depends on the lubrication of the kinematic pairs (gear meshing, the rolling element–the bearing race, the shaft–the seal). How much energy

is lost in the kinematic pairs depends on the mating of the elements, i.e. on the quality of lubrication, which in turn, is determined by the condition of the mating surfaces (the height of the surface irregularities) allowing an oil wedge to form between the elements. A damage to the bearing results in edgewise intermeshing. As the local pressures increase, the continuity of the oil film in the gearing is disrupted, the friction factor increases and so do the losses in the form of the emitted heat and the temperature of the mating elements rises. As a result of the abnormal mating of the elements the oil heats up. However, the assessment of the condition of meshing based on the rise of the temperature of the oil in the gear box is highly imprecise since other factors, such as the condition of the mating of the rolling bearings and the condition of the seal, may contribute to the temperature rise through the generation of heat as a result of the rubbing of the shaft against the seal. The released heat causes an increase in the temperature of the bearing casing at the places where the shafts and the seal mate (the inlet and outlet of the gear transmission shafts). This may happen also in the case of other subassemblies, such as pumps, electric motors, runners and so on. The temperature of the elements or its distribution can be monitored by a contact or noncontact method. For contact monitoring it is necessary to install a temperature sensor in a place where the temperature will be representative for the condition of the mating of a given kinematic pair or to use a portable temperature gauge. Thermography can be applied to determine the temperature distribution. As they heat up, the machine's elements emit heat in the form of visible- and invisible-range waves. The invisible heat radiation is called infrared radiation. The temperature distribution monitored by thermographic devices is displayed in the form of a two-dimensional colour image. Thermography is used to assess the condition of the bearings of conveyor belt rollers, which is described in sect. 16.3.

10.4. Ultrasounds and acoustic emission as machine condition signal

10.4.1. Ultrasounds

Ultrasounds are sounds whose frequency in an interval of 20kHz-100kHz. Vibrations within this range are referred to as ultrasound vibrations. The latter are exploited in rolling bearing diagnostics as presented in [10.18] and described in more detail in chap. 15. A vibration band around 32 kHz was chosen for rolling bearing diagnostics. Vibrations emitted by a damaged or improperly lubricated rolling bearings are called shock pulses (SP). Sensors which measure the condition of rolling bearings bear symbol SPM (Shock Pulse Method).

The above mentioned states of machines can be monitored by means of only one measuring instrument to which different diagnostic signal receivers can be attached.

Ultraprobe™ 2000 manufactured by UE Systems INC. is an example of such a versatile diagnostic instrument. Typical recommended frequencies to which the instrument is set depending on the diagnosed kinematic pair or a machine subassembly are given in tab. 10.1 in [10.19]. For some applications it is recommended to use a constant frequency or tune to a specified frequency. As it follows from tab. 10.1. ultrasounds or ultrasound frequency range vibrations can be used to determine the condition of:

- steam traps,
- valves,
- compressor valves,
- rolling bearings,
- leakage in pressure and underpressure vessels,
- electric arcing in electric equipment,
- gear wheel meshing,
- pump cavitation,
- pipeline leaktightness,
- condensers,
- heat exchangers.

The flow of an air stream from a vessel to the environment when there is overpressure or underpressure in the vessel is shown respectively in figs 10.37a and 10.37b. As a stream of gas or liquid flows in or out ultrasounds are generated. The wave generation frequency depends on the width of the port. Ultrasounds are characterized by directivity whereby it is easy to locate the origin of an ultrasonic wave. Most of the diagnostic instruments employ a heterodyne to convert the signal by converting its frequency, i.e. the high-frequency signal is converted into a signal in the audible frequency range. The converted signals are received by a headset. The Ultraprobe™2000 instrument includes an indicator, a heterodyne and a headset.

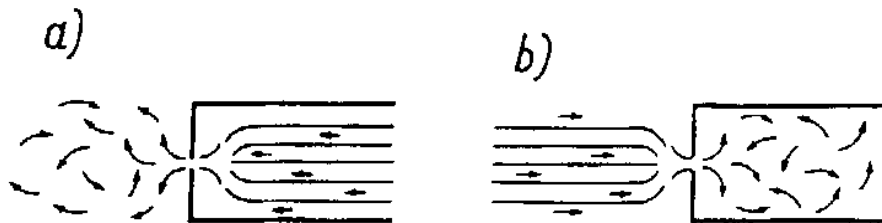


Fig. 10.1. Turbulences generating ultrasounds: a – during outflow of gas to environment, b – during inflow of gas to subpressure vessel.

One of important applications of ultrasonic vibration is the assessment of the leak-proofness of valves (fig. 10.38). For this purpose an instrument with a contact probe is used. Ultrasonic vibration is also exploited to assess the operation of the valves in compressors.

| | Constant frequency | Frequency range | | | | | | | |
|----|--------------------|-----------------|--------|--------|--------|--------|--------|--------|---------|
| | | 20 kHz | 25 kHz | 28 kHz | 32 kHz | 40 kHz | 50 kHz | 60 kHz | 100 kHz |
| 1 | - | x | - | - | - | x | - | - | - |
| 2 | x | - | x | - | - | - | - | x | x |
| 3 | x | - | - | x | x | - | - | - | - |
| 4 | x | - | - | - | - | x | - | - | - |
| 5 | x | - | - | - | - | x | - | - | - |
| 6 | - | x | x | - | - | - | - | - | - |
| 7 | x | x | x | - | - | - | - | - | - |
| 8 | x | x | - | - | - | x | - | - | - |
| 9 | x | - | - | - | - | x | - | - | - |
| 10 | x | - | - | - | - | - | - | - | - |

Fig. 10.2. Recommended frequencies of ultrasonic signal reception: 1 – valves, 2 – compressors (valves), 3 – rolling bearings, 4 – leaks, 5 – electric breakdowns, 6 – gear meshing, 7 – pumps (cavitation), 8 – pipework, 9 – condensers, 10 – heat exchangers; [10.19].

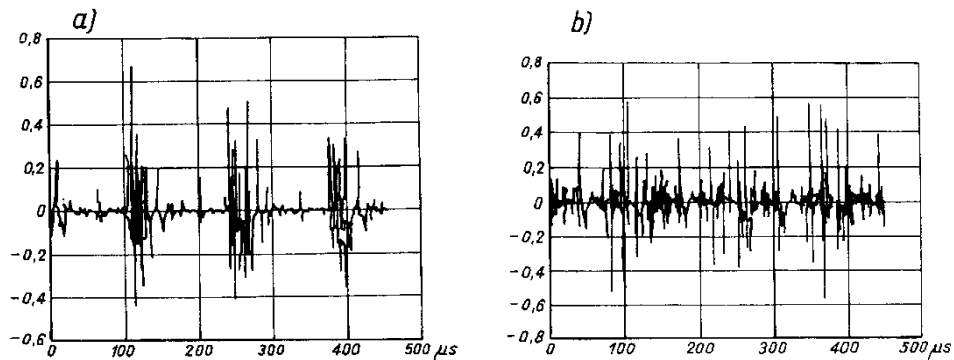


Fig. 10.3. Valve condition signal: a – normal operation of valve, b – abnormal operation of valve.

The closing and opening of valves is accompanied by vibration impulses whose plots are shown in fig. 10.39. The normal operation of the valve is shown in fig. 10.39a, whereas its abnormal operation is shown in fig. 10.39b.

10.4.2. Acoustic emission

Acoustic emission (AE) is sometimes referred to as stress wave emission (SWE). As the energy accumulated in machine elements is released elastic waves are generated. The sources of acoustic emission can be put into four categories:

1. dislocations in the crystal structure (defects in the crystal lattice),
2. phase changes,
3. friction mechanisms,
4. appearance of fatigue cracks and their propagation.

The generated signals can be roughly grouped into:

- continuous and
- transient.

Continuous signals have the character of broadband noise. Transient signals are fading sinusoidal signals generated by resonances in the system and in the converters. Images of similar signals are shown in figs 4.10, 4.20, 4.21, 4.45 and 10.6. The energy liberated by displacements in the crystal lattice caused by structural defects and the generated acoustic emission are too low to be detected by the existing instruments for measuring acoustic emission (AE). Many defects (dislocations) in the crystal structure produce the domino effect and generate a continuous emission signal. A typical martensite transformation in carbon steel produces a transient signal every time a steel grain undergoes transformation. Fatigue cracks on the surface of a material and inside it generate transient signals which are partly transformed into an AE signal. Fracturing is also accompanied by friction phenomena which emit a signal of the transient type.

Propagation of acoustic emission waves

A source of acoustic emission can be compared to a radio antenna with specific radiation for different (shearing, compressive) waves, but the particular properties of the AE signal are described only for special cases. If the source emits a spherical wave it will propagate unimpeded only in a homogenous isotropic medium infinite in size and having perfectly elastic properties. In a true medium (machine element) the propagation of waves will be affected by the surface limitation resulting in the reflection of waves and the formation of surface (Rayleigh, Lamb) waves. The inhomogeneities due to the welds will also produce reflections and interference in the wave front.

Such factors make it very difficult to investigate the mechanisms of the propagation of the AE signal. The formation of a wave caused by a micro-crack and the associated formation of a surface wave are shown schematically in fig. 10.40.

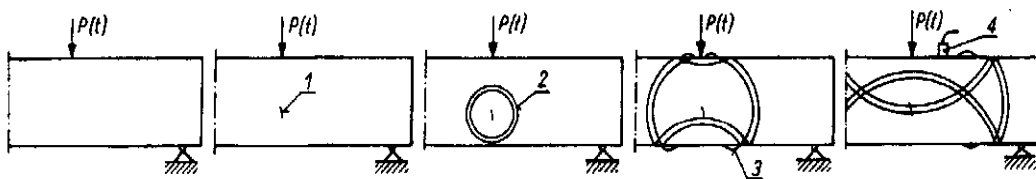


Fig. 10.1. Propagation of stress waves: 1 – micro-crack, 2 – stress wave, 3 – surface wave; AE signal reception transducer.

Fig. 10.41 illustrates, after [10.20], methods of assessing the intensity of AE signal impulses. The methods are:

- a) the measurement of the size of the surface areas demarcated within the assumed level;

- b) the measurement of the sum of the surface areas between the marked levels; this quantity is called a weighted total;
- c) the determination of the number of times a given level is exceeded.

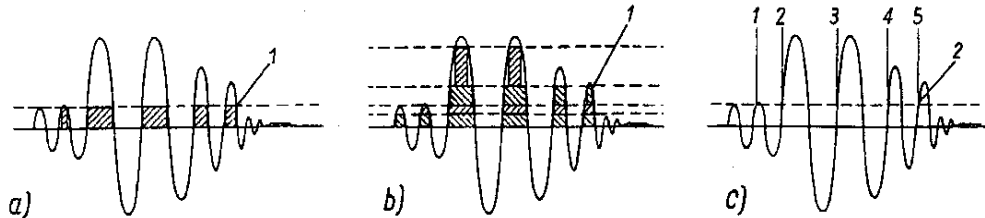


Fig. 10.2. Methods of assessing AE signal intensity: 1 – measured surface area, 2 – exceeded levels, 3 – 1'+5' – number of times level is exceeded.

The measurements of the AE signal generated by a specimen during a tension test are shown in fig. 10.42, after [10.20]. The tested specimen was a metal alloy with a 60% Cu and 40% Zn content. The tensile force, the peak values of the particular impulses (fig. 10.42a) and the weighted sum (fig. 10.42b) were registered in accordance with the adopted principle of measurement (fig. 10.41.b). As the figures show, no AE signal is emitted when stress passes the yield point.

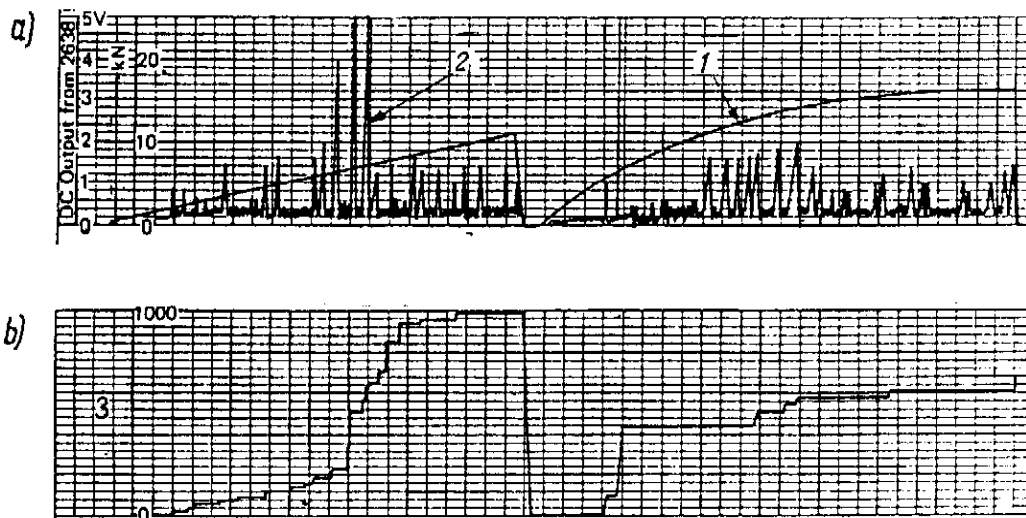


Fig. 10.3. Plot of tensile force and AE signal (a) and plot of total weighted value (b): 1 – tensile force in time, 2 – AE signal, 3 – weighted value according to fig. 10.41b.

10.5. Corrosion monitoring

The mine environment and the fluids used in machines cause corrosion of their elements. In some cases corrosion may lead to irreparable damage to the machine (fig. 1.2). Different electrical methods are used to monitor corrosion, such as:

- The **resistance method** in which a thin wire is introduced into the fluid. As the wire corrodes, its cross-section decreases and its electric resistance increases. This resistance can be measured by a bridge system and continuously monitored. The obtained results are a measure of the fluid's corrosivity.
- The **polarization method**. Corrosion is an electrochemical reaction. There is a relation which expresses the reaction rate through the slope of a curve representing a function between the applied potential and the current intensity.
- The **potential method**. The electric potential between the monitored machine and a reference electrode is a measure of the corrosion rate.

The very simple weight method consists in the periodic weighing of a tester (a steel coupon) kept in the same environment as the monitored element. On the basis of the changes in the weight of the tester one can indirectly determine the corrosion induced changes in the monitored element's thickness. Corrosion induced changes in the thickness of machine elements can also be determined by means of ultrasonic waves.

10.6. References

- [10.1] Bednar J., Piersol A.: Methods of Analyzing and Measuring Random Signals (in Polish), PWN, Warsaw, 1976.
- [10.2] Bogart B.P. et al.: The Quefrency Analysis of Time Series for Echoes: Cepstrum, Pseudo-Autocovariance, Cross-Cepstrum and Saphe Cracking, *Proceedings of the Symposium on Time Series Analysis by M. Rosenblatt, Wiley, N.Y.*, pp. 209-243, 1963.
- [10.3] The Application of Cepstrum Analysis to Machine Diagnostics, *Briuel & Kjeaar BA materials*, 7076-12.
- [10.4] Sato T. et al.: Real-Time Bispectral Analysis of Gear Noise and Its Application in Contactless Diagnosis, *J. Acoustic. Soc. Am.*, Vol. 62, No. 2, pp. 382-387, 1977.
- [10.5] Bartelmus W.: Application of Some Statistical Estimators of Vibration Signal as Criteria for Assessment of Gear Meshing Condition (in Polish), *Scientific Papers of Silesian Polytechnic, Mining*, No. 616, 1979.
- [10.6] Newland D.: An Introduction to Random Vibrations, Spectral and Wavelet Analysis, *Longman*, Singapore, 1993.
- [10.7] Day M: Condition Monitoring of Hydraulic Systems, *Handbook of Condition Monitoring, Elsevier Science LTD*, pp. 209-252.
- [10.8] Kurahashi M.: Applications of Ferrography to Iron and Steel Making Plant Maintenance, *Proceedings of an International Conference on Condition Monitoring Swansea 1984, Pineridge Press U.K.*, pp. 537-549.
- [10.9] Foxboro company materials.

- [10.10] Foxboro Analytical: Ferrographic Oil Sampling Techniques, 1979.
- [10.11] Scott D., Seifert W., Westcott V.C.: Ferrography – an Advanced Design Aid for the 80s, *Wear*, Vol. 34, pp. 251-260, 1975.
- [10.12] Levis D.S.: Machinery Health Monitoring Evaluation at Mining Research and Development Establishment, *Condition Monitoring 84*, University College of Swansea, pp. 470-484, 1984.
- [10.13] Mason A.R.: The Development, Proving and Application of an In-Line Metal Particle Detector (MPD), *Condition Monitoring 84*, University College of Swansea, *Pineridge Press U.K.*, pp. 637-659, 1984.
- [10.14] Reda A.A., Bowen R., Westcott V.C.: Characteristics of Particles Generated at the Interface Between Sliding Steel Surfaces, *Wear* 34, pp. 261-273, 1975.
- [10.15] Yarrow A.S., Gadd P.: The Role of Ferrography in the Monitoring of Helicopter Assemblies, *Condition Monitoring 84*, University College of Swansea, *Pineridge Press U.K.*, pp. 503-524, 1984.
- [10.16] Bowen E.R., Westcott V.C.: Wear Particle Atlas Prepared for the Navel Air Engineering Centre, Lakehurs, July 1976.
- [10.17] Hunt T.: Condition Monitoring of Mechanical and Hydraulic Plant, *Chapman & Hall*, 1996.
- [10.18] Sohoel E.: Shock Pulse as a Measure of the Lubricant Film Thickness in Rolling Element Bearings, Proceedings of an International Conference on Condition Monitoring, Swansea, *Pineridge Press U.K.*, 1984.
- [10.19] Mohr G.: Technology Overview: Ultrasonic Detection, *P/PM Technology*, August 1995.
- [10.20] Broch T.: Mechanical Vibration and Shock Measurements, *Brüel & Kjaer*, 1984.

11. Diagnostic inference from vibroacoustic signal

So far several examples of the relation between the machine condition and the generated signal have been given. Signals were presented versus time as in, e.g., figs 6.36-6.45. Signals can be transformed as described in chap. 10.1 or represented as a function of frequency f [Hz]. Certain frequencies characteristic of the relationship between the machine condition and the intensity of the vibration signal can be distinguished in the spectral frequency ranges. The relationship between the diagnostic signal and the vibration frequencies is described by different authors (cited tab. 11.1 from [11.1]). To make a diagnosis, a proper component must be detected in the spectrum and the hazard must be determined. This is specified in proper standards and classifications, e.g. standard [11.2] discussed in chap. 13. It is also necessary to monitor the trends of physical quantities/symptoms. A continuous increase in vibration as shown in fig. 11.1 can be taken as the first approximation. It was mentioned in chap. 6 that in certain meshing states instability occurs and vibration increases rapidly up to a certain limit after which no upward tendency is observed (fig. 6.22a and b). This is one of the symptoms indicating that the condition of the gearing should be checked.

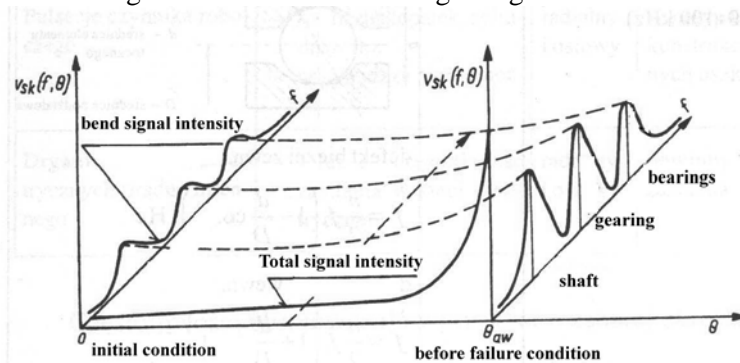


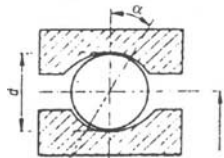
Fig. 11.1. Diagnostic signal trend in time θ and frequency f

Table 11.1 shows that frequency f_0 occurs most often. It is calculated from this relation:

$$f_0 = n/60 \text{ Hz} \quad (11.1)$$

where: f_0 – a fundamental frequency, Hz;
 n – a rotational speed, rpm, rev./min.

Tab. 11.1. Characteristic vibration frequencies.

| Defect description | Vibration frequency | Direction of vibration | Notes |
|--|--|------------------------|--|
| 1 | 2 | 3 | 4 |
| unbalance of rotating element | | radial | common cause of vibration in machines, amplitude proportional to unbalance |
| shaft nonalignment or bending | usually | radial axial | if amplitude of component $2f_0$ (axial) exceeds 75% of component f_0 (radial), such damage may cause machine failure |
| damaged rolling bearing element | impulses with frequencies f associated with rotation and kind of damaged element; also vibration in high frequency band (20 ÷ 100 kHz) | radial and axial | <p>impulse frequencies associated with defect:</p> <p>β – contact angle</p> <p>n – number of rolling elements,</p> <p>f_r – relative revolutions frequency of bearing race in Hz (inner to outer race)</p>  <p>α – contact angle of bearing,</p> <p>d – diameter of rolling bearing element</p> <p>D – pitch diameter</p> <p>defect of outer race $f = n/2f_r(1 - d/D \cos \alpha)$</p> <p>defect of inner race $f = n/2f_r(1 + d/D \cos \alpha)$</p> <p>defect of one rolling element $f = D/df_r(1 - (d/D)^2 \cos^2 \alpha)$</p> <p>cage run-out, slackness $f = 1/2f_r(1 - d/D \cos \alpha)$</p> <p>race or shaft run-out $f = f_r$</p> |
| slackness in bearing mounting | $1/2 f_0$; $1/3 f_0$ rotation subharmonics | radial | such slackness appears only at certain rotation and temperature (e.g. in turbogenerators) |
| instability of oil filter in slide bearing | from 0.42% to 0.48% | mainly radial | always below $1/2 f_0$ often occurs in high-speed turbines |
| damaged or worn out gears | $n \cdot f_0$ harmonics n – number of teeth | radial and axial | sidebands around meshing frequency indicate eccentricity of gear wheels (detectable only by $\Delta f = \text{const.}$ narrowband analysis) |
| slackness in couples of rotations | $2 \cdot f_0$ | radial or axial | usually combined with unbalance and nonalignment ($3f_0$) |
| damaged driving belt | $1 \cdot f_0$ of belt pulley $2 \cdot f_0$ of belt pulley $3 \cdot f_0$ of belt pulley $4 \cdot f_0$ of belt pulley | radial | damage easily detectable in stroboscopic light |

| 1 | 2 | 3 | 4 |
|---|---|------------------|--|
| unbalance forces and moments in to-and-fro motion | $1 \cdot f_0$ and higher harmonics dependent on unbalance magnitude | mainly radial | inseparably associated with machine operation, can only be reduced through changes in design or vibration insulation |
| working medium pulsations | f_0 – number of blades, cylinders, etc. and higher harmonics | radial and axial | if coincide with structure resonances, can cause serious damage |
| vibrations of a.c. machines | 1 or 2 – mains frequency | radial and axial | should disappear after current is switched off |

The gearing shaft rotation/revolution frequency is calculated from this formula:

$$f_{o1} = n_1/60, \text{ Hz} \quad (11.2)$$

$$f_{o2} = n_2/60 = n_1/(60u), \text{ Hz} \quad (11.3)$$

where: f_{o1}, f_{o2} – respectively the driving and driven shaft frequency, Hz;

n_1, n_2 – respectively the driving and driven shaft rotational speed, rev./min.,

$u = n_1/n_2$ – a gear ratio.

The meshing frequency is calculated from this formula:

$$f_z = nz/60 = n_1z_1/60 = n_2z_2/60 = f_{o1}z_1 = f_{o2}z_2, \text{ Hz} \quad (11.4)$$

where: f_z – the meshing frequency, Hz,

z – the number of teeth,

z_1, z_2 – respectively the driving and driven wheel tooth number.

Components f_{o1}, f_{o2} occur also as modulation components $f_z + f_0, f_z - f_0, f_z + 2f_0, f_z - 2f_0$, etc. in the signal spectrum. A narrowband spectroscopic analysis (zoom) reveals also other side components (in the gearing spectrum); their origin can be traced as follows: each entrance into tooth contact results in an excitation the system responds to which are shown as coefficient K_d in fig. 14.16 and depending on a gearing error – in fig. 14.14. One may ask a question: after how many rotations do the same teeth meet producing a similar excitation? If this number is denoted by N and multiplied by number of teeth z_1 , then the number of excitations after which the excitation cycle will be repeated is obtained. Number N corresponds to the number of revolutions of the pinion after which the same teeth will meet again. It is calculated from ratio z_1/z_2 , e.g. 38/50, and after the elimination of common divisors a ratio of 19/25, where $N = 25$, is obtained. Thus the same teeth meet after 25 revolutions of the pinion. The duration of one excitation is

$$\tau_1 = 1/f_z = 60/(n_1z_1), \text{ s} \quad (11.5)$$

Meshing generates a sequence of recurrent excitations with period

$$T_p = \tau_1 N z_1 = 60N/n_1, \text{ s} \quad (11.6)$$

A sequence of excitations forms a function whose repetition rate is

$$f_p = 1/T_p = n_1/(60N), \text{ Hz} \quad (11.7)$$

A zoom of a sequence of impulses is shown in fig. 14.16. If a signal spectrum for this function is found, then components if_z (where i – an integer larger or equal to 1) together with a complex structure of modulation components dependent on the distribution of errors on the particular teeth will be obtained. An increase in the nonuniformity of error distribution in meshing is a measure of wear of the gear teeth. In tab. 11.1. one can also find relations which can be used to determine the frequencies associated with damage to the race, to a rolling element of a bearing. The principle of determining the frequencies is described in chap. 7. To determine the condition of kinematic pairs it is necessary to know the component frequencies and their intensity. The degree of danger is specified in proper condition classes the interpretation of which is given in chap. 13.1.

In the diagnostics of machines used in surface mines it is essential to determine the meshing rate for planetary gears. The latter are used in bucket wheel drives and to drive caterpillar undercarriages (fig. 17.7). A diagram of a one-stage planetary gear used in surface mine machinery drives is shown in fig. 11.2. The gear consists of three gear wheels denoted as 1, 2 and 3. Wheels 1 and 2 are external and wheel 3 – internal gears. Wheel 1 is called a middle wheel or a solar (sun) wheel and wheel 2 – a satellite wheel. Driving power is transmitted from the engine to wheel 1 and via wheels 2 and 3 to the yoke. Wheel 1 rotates with rotational speed n_1 [rev./min.], wheel 2 – with rotational speed n_2 and the yoke – with rotational speed n_j . The distribution of instantaneous rotational speed values for the gear is shown in fig. 11.2 for inner wheel tangential velocity $n_3 = 0$. Knowing rotational speed n_1 one can calculate angular velocity $\omega_1 = \pi n_1/30$. If angular velocity ω_1 is known, then the tangential velocity of wheel 1 is

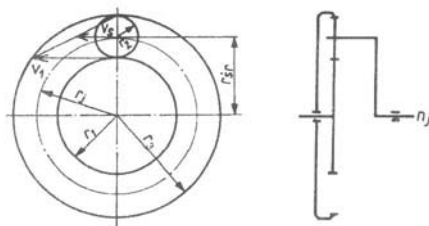


Fig. 11.2. Schematic of planetary gear showing distribution of peripheral velocities.

$$v_1 = \omega_1 r_1 \quad (11.8)$$

where r_1 is the radius of rolling wheel 1, m.

From the distribution of instantaneous peripheral velocity values we get the following peripheral velocity of the centre of wheel 2:

$$v_s = v_l/2 \quad (11.9)$$

Velocity v_s is equal to the peripheral velocity of the yoke on radius r_j . The yoke angular velocity is

$$\boldsymbol{\omega}_j = v_s/r_j = v_l/(2r_j) = \boldsymbol{\omega}_l r_l/(2r_j) \quad (11.10)$$

The gear ratio of the planetary gear shown in fig. 11.2 is a ratio of angular velocity ω_l to angular velocity ω_j and it can be calculated from (11.10)

$$u = \boldsymbol{\omega}_l/\boldsymbol{\omega}_j = 2r_j/r_l \quad (11.11)$$

The planetary gear ratio expressed by formula (11.11) can be rearranged to a form with gear wheel tooth numbers. The radii of the gear wheels can be calculated on the basis of the modulus and the number of teeth as follows:

$$r_1 = z_1 m/2; \quad r_2 = z_2 m/2; \quad r_3 = z_3 m/2 \quad (11.12)$$

Since radius $r_j = r_3 - r_2$ and $r_2 = (r_3 - r_1)/2$ after putting these terms in (11.11) we get the following expression for the planetary gear ratio

$$u = 1 + r_3/r_1 = 1 + z_3/z_1 \quad (11.13)$$

To determine the rate of meshing for a pair of wheels 1 and 2 one must determine the angular velocities relative the yoke. The latter are:

$$\boldsymbol{\omega}_{1j} = \boldsymbol{\omega}_l - \boldsymbol{\omega}_j; \quad \boldsymbol{\omega}_{2j} = \boldsymbol{\omega}_2 - \boldsymbol{\omega}_j \quad (11.14)$$

By dividing the angular velocity values by 2π we get the rates of rotation of the wheels relative to the yoke. The spectral frequency originating from the meshing of the kinematic pair of wheels 1 and 2 is

$$\begin{aligned} f_{12} &= z_1(\boldsymbol{\omega}_l - \boldsymbol{\omega}_l r_l/(2r_1)) = n_l/60 z_1(1 - r_l/(2r_1)) = n_l/60 z_1((r_1 + 2r_2)/2(r_1 + r_2)) = \\ &= n_l/60 z_1(z_3/(z_3 + z_1)) \end{aligned} \quad (11.15)$$

We can also find that the rate of meshing between wheels 2 and 3 which generates system vibrations is $f_{12} = f_{23}$.

In this way additional frequencies, which should be monitored to determine changes in the condition of planetary gears, are obtained. The frequencies are not included in table 11.1. Meshing frequency (11.4) and its harmonics occur in the meshing signal spectrum. An illustrative spectrum for a gearing vibration acceleration signal, obtained by computer simulation, is shown in figs 11.3a and b. The signal is generated by gear meshing. A plot of the signal is shown in fig. 6.36b and the meshing error function – in fig. 6.10a. The coefficient of meshing stiffness variation for spiral tooth meshing is $g = 0.06$. The cause of the generation of vibration are gearing production errors represented by an error function, as shown, e.g., in fig. 6.10a. Thus the gearing in the mechanical system of a machine converts the error function into a diagnostic signal. The conversion is affected by the machine properties described by design fea-

tures (chap. 6.4). The diagnostic signal can be represented as a plot (e.g. fig. 6.36) or a spectrum. An error spectrum corresponds to a given error function. An illustrative error spectrum (for the error function in fig. 6.10a) is shown in figs 11.4a and b. In the latter figure (a zoom of the error spectrum with only ten first harmonics) odd harmonics are clearly visible. A spectrum in a range of 0-50 000 Hz is shown in fig. 11.2a. A zoom of this spectrum up to 3000 Hz is shown in fig. 11.3b. The meshing frequency is about 460 Hz. As one can see in figs 11.3a and b, the fifth harmonic is the dominant component – due to its proximity to the meshing eigenfrequency. If only the error function is subject to spectrum conversion, then the first harmonic dominates (figs 13.4a and b). If the rotational speed of the gear is changed so that the third harmonic is close to the meshing eigenfrequency, then the third harmonic is dominant (figs 11.6a and b). This spectral pattern confirms the effect of eigenfrequency on the intensity of spectral meshing components.

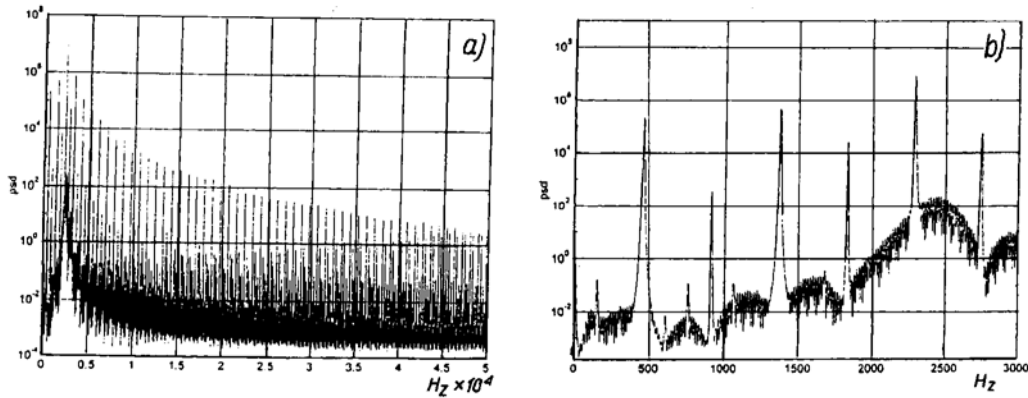


Fig. 11.3. Gear signal spectrum (a) and its zoom (b), signal was obtained by computer simulation.

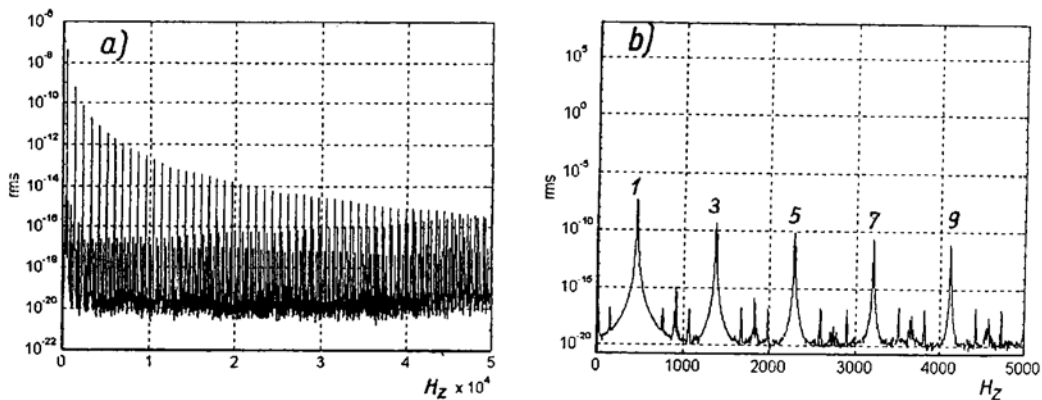


Fig. 11.4. Gearing production error signal spectrum (a) and its zoom (b) for E(0.5, 10, 0, 0): 1, 3...9 – harmonic components.

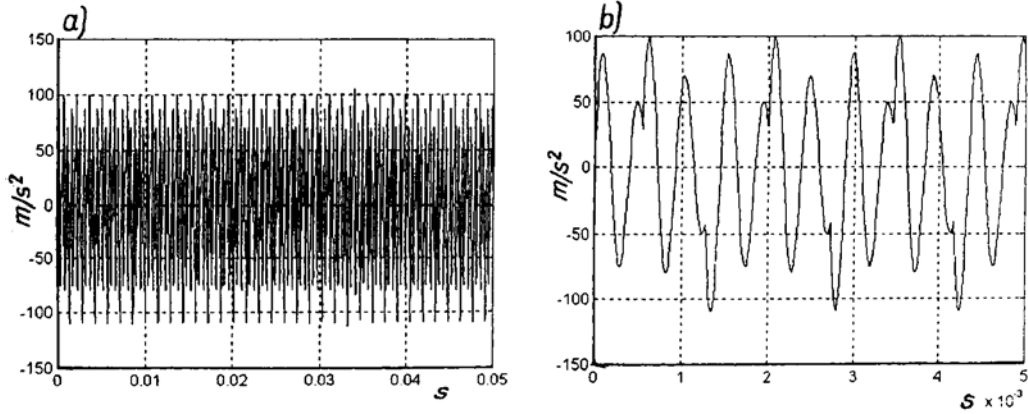


Fig. 11.5. Plot of signal (a) – gearing operates at rotational speed $n_1 = \text{rev./min.}$, gearing production error $E(0.5,10,0,0)$; zoom of gear signal plot (b) for time interval of 0.005 s.

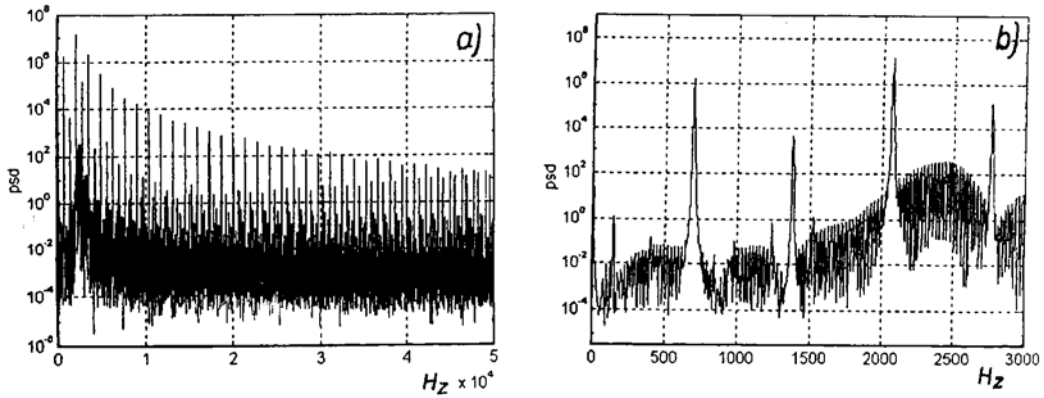


Fig. 11.6. Signal spectrum (a) and its zoom (b) for signal shown in fig. 11.5.

Odd components dominate in the spectrum (fig. 11.3b) – due to the effect of the error function shape.

Also a change in the gearing stiffness (fig. 6.7) affects the diagnostic signal trace/plot. The change may contribute to the intensification of the odd components in the spectrum. It has been shown so far that gearing production errors e have a dominant effect on the diagnostic signal (cf. fig.6.36 and fig. 6.40). In the literature on gearing dynamics, changes in gearing stiffness are mentioned as having a significant effect on the diagnostic signal. Gearing stiffness changes most in spur gears. The change can be described by coefficient g (the effect of g on changes in gearing stiffness is described in chap. 6.6) which for a spur gearing is about 0.4. A plot of accelerations for a gearing for which $g = 0.4$ is shown in fig. 11.7 and a gearing production error function is plotted in fig. 6.10a. A comparison of the maximum acceleration am-

plitudes – figs 6.36 and 11.7 shows that the amplitudes are nearly identical and they amount to about 83 m/s^2 . Thus the effect of a change from $g = 0.06$ to 0.4 did not manifest itself in the maximum value amplitude but the trace/plot changed (cf. fig. 6.36 and fig. 11.7). Also the acceleration signal spectrum changed slightly (when $g = 0.4$ and the error function as shown in fig. 6.10a) – see fig. 11.8. A comparison of the spectrum in fig. 11.3b and the one in fig. 11.8 reveals an effect of changes in stiffness $g = 0.4$ in the even spectral components, which confirms the prediction of this effect.

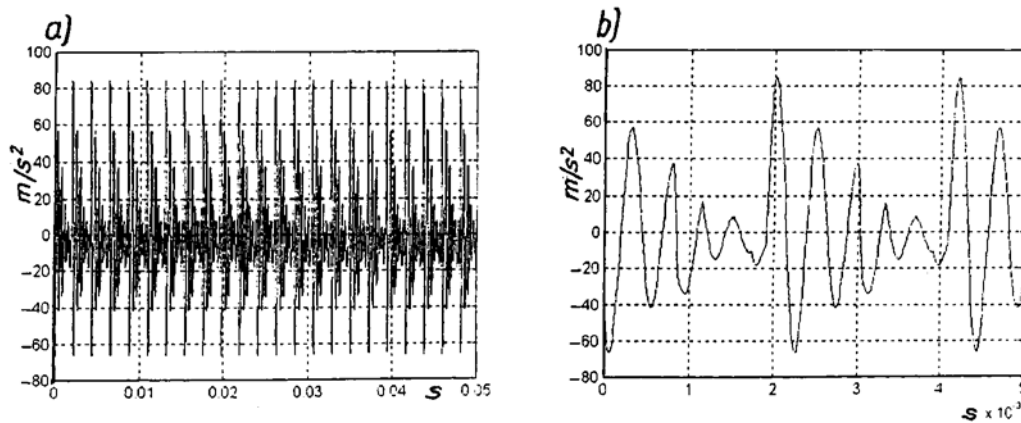


Fig. 11.7. Plot of signal (a) and its zoom (b) at increased stiffness change coefficient $g = 0.4$ and $E(0.5,10,0,0)$.

A trace/plot of the acceleration signal when one tooth of the driving wheel is broken is shown in fig. 11.9a and b. A spectrum corresponding to this signal is shown in fig. 11.10a and b. It follows from the figures that the vibration intensity increased significantly in the fifth harmonic which is within the gear resonance. Only the first, third and fifth spectral components are clearly visible – the other components are hidden in the background of the vibration spectrum. The intensity of the spectrum background increased notably in comparison with the spectrum for the gearing without a broken tooth (fig. 11.8).

Besides the frequency and intensity of the spectral components also monitoring of the increment in signal intensity aimed at determining the trend is used (fig. 11.1). One should consider a possibility of the occurrence of discontinuities in the trend of physical quantities (fig. 6.22a and b). A method of representing signal as a plot obtained by synchronous summation of the vibration signal is highly promising. This will be described in chap. 14.

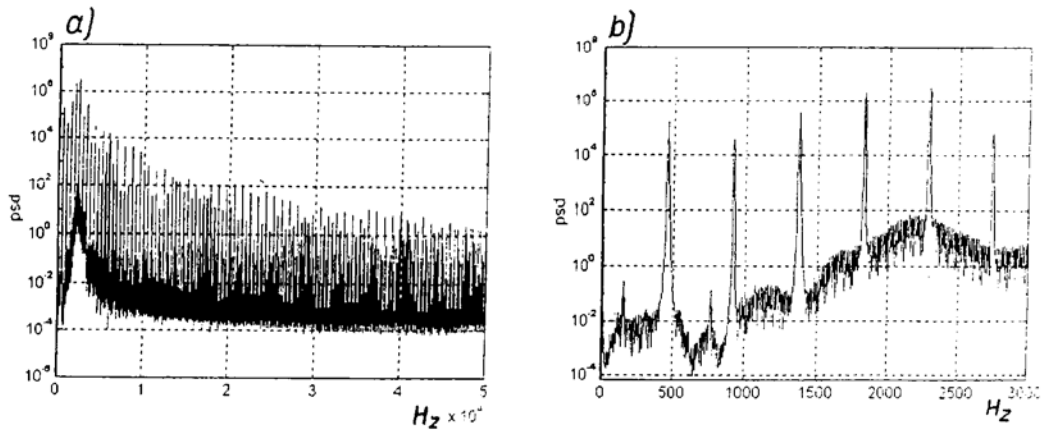


Fig. 11.8. Signal spectrum for signal plot shown in fig. 11.7 (a) and its zoom (b).

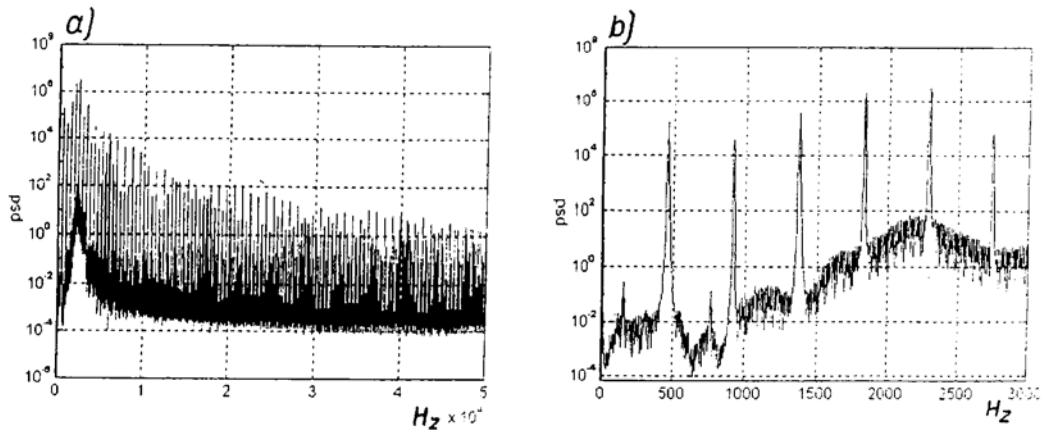


Fig. 11.9. Plot of signal for gearing with broken tooth (a) and for tooth immediately after broken tooth (b).

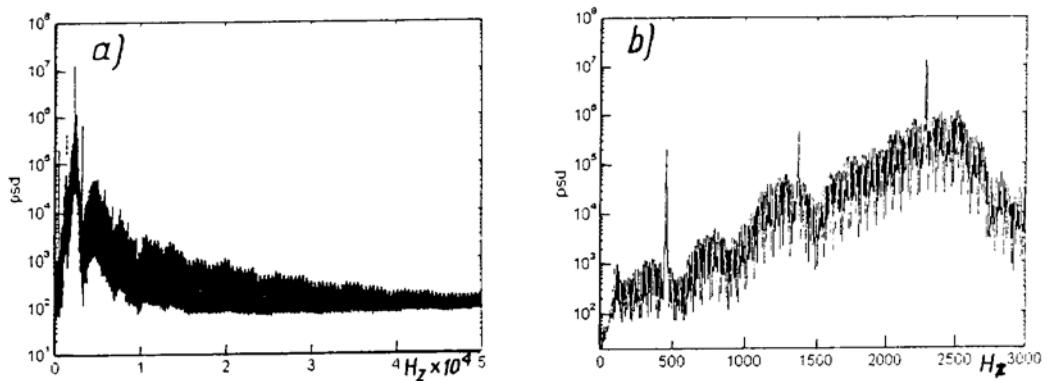


Fig. 11.10. Signal spectrum for gearing with broken tooth (a) and its zoom (b); signal obtained by computer simulation.

Components originating from gearing runout may occur in the gear signal. A plot of the acceleration signal for a gear which both wheels are mounted slightly eccentrically is shown in fig. 11.11a. Zooms of the signal for the steady running of the gear are shown in fig. 11.11b, c and d. They are for decreasing time intervals: 0.5 s, 0.05 s and 0.005 s. The effect of the runout of the two gear wheels can be noticed. It follows from fig. 11.11d that the intermeshing of individual pairs of teeth is similar to that for a gearing without runout. A signal spectrum for this gear is shown in fig. 11.12a and b.

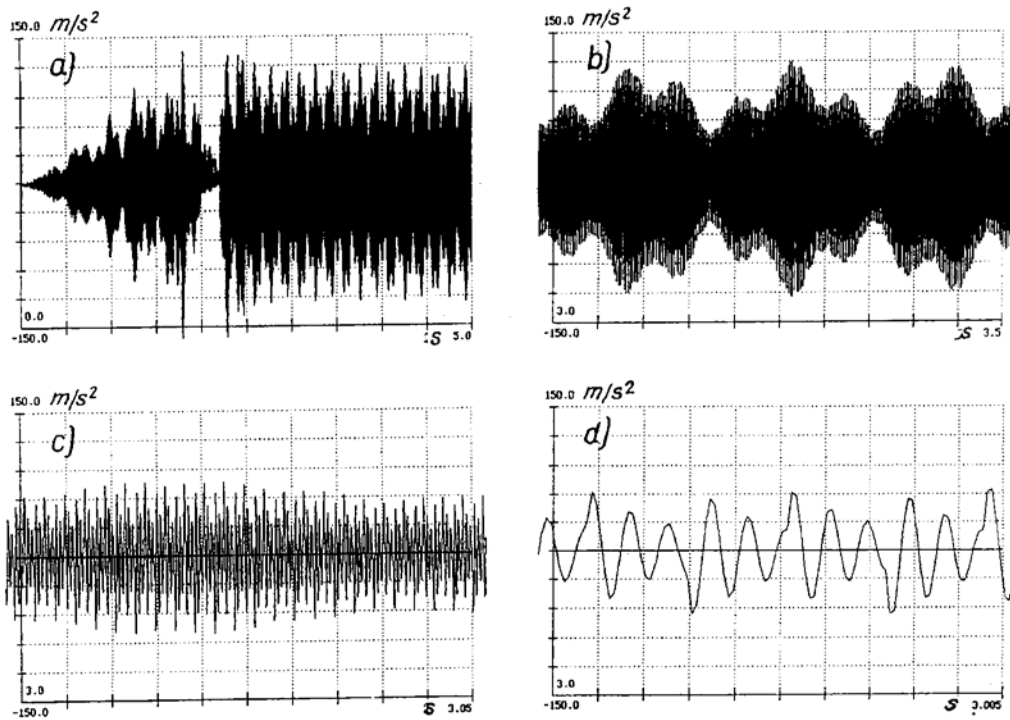


Fig. 11.11. Plot of signal for gear with eccentrically mounted teeth (a): in time interval of 0.5 s, c – in time interval of 0.05 s and d – in time interval of 0.005 s.

Gearing meshing components (the first harmonic of 456 Hz is shown separately in fig. 11.3) and modulation components with gearing runout frequencies are visible in the spectrum. All the components are modulated. The modulation of the fifth harmonic is shown in fig. 11.14. The frequency of the modulation components is calculated from (11.2) and (11.3).

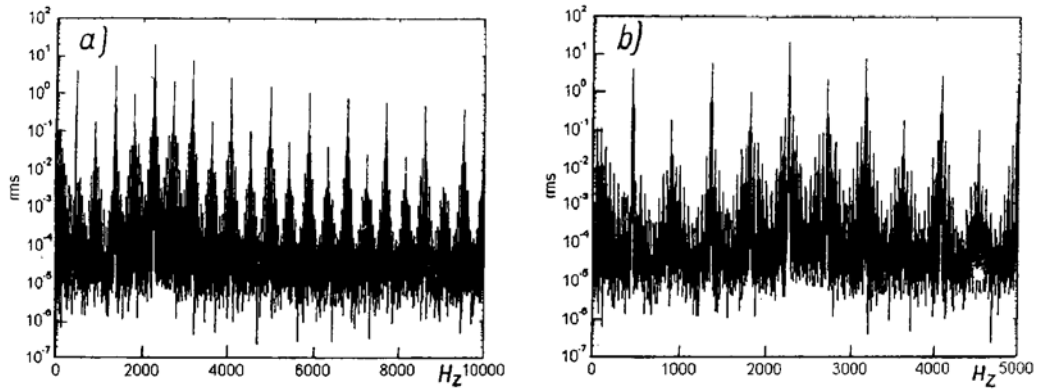


Fig. 11.12. Spectrum of gear for plot shown in fig. 11.11 (a) and its zoom (b).

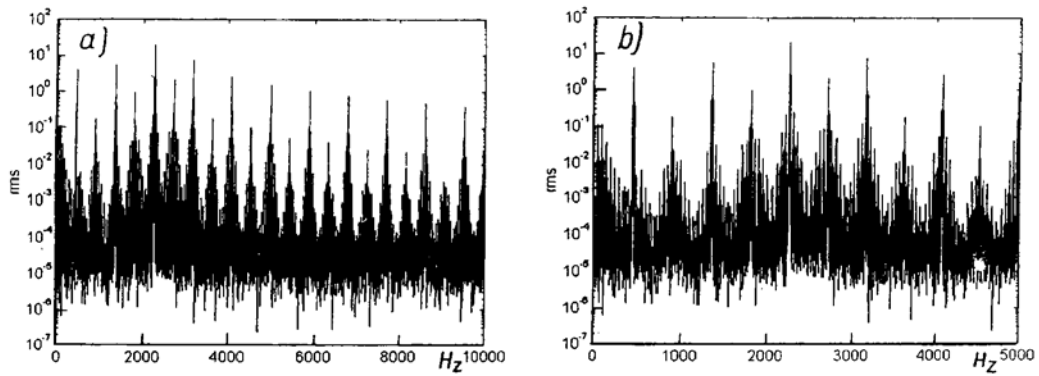


Fig. 11.13. Spectral component 456 Hz together with modulation components for spectrum in fig. 11.12.

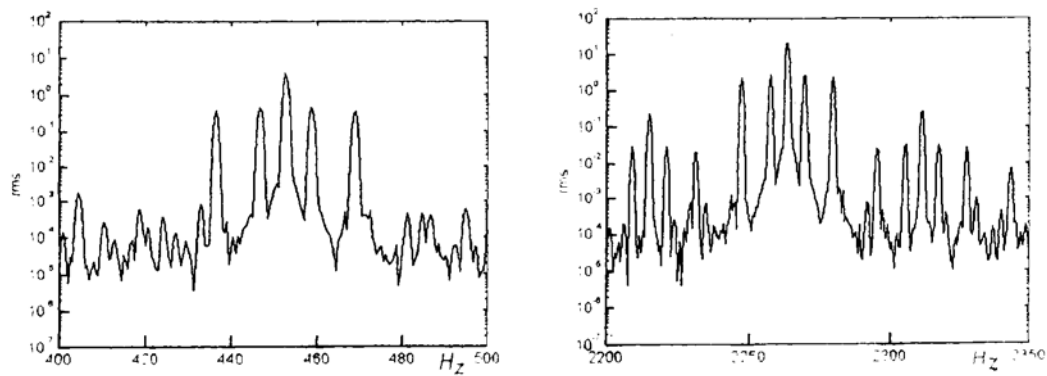


Fig. 11.14. Fifth harmonic and gearing runout modulation components (11.2) and (11.3).

11.1. References

- [11.1] Cempel C.: Fundamentals of Machine Vibroacoustic Diagnostics, Warsaw, WNT, 1982.
- [11.2] ISO 3945 – 1997: Mechanical Vibration of Large Rotating Machines with Speed Range from 10-200 rev/s., Measurement and Evaluation of Vibration Severity in Site.

12. Integrated diagnostic inference from vibration signal and wear products

Integrated inference is described in [12.1]. In chap. 11 a vibration signal trend was mentioned. Three periods can be distinguished in the trend, as shown in fig. 12.1, i.e. running-in, normal operation and intensive wear. Characteristic symptoms are associated with the periods. In the running-in period the intensity of vibration decreases, the error characteristic changes and form *a* changes to *b* (fig. 6. 21a and b).

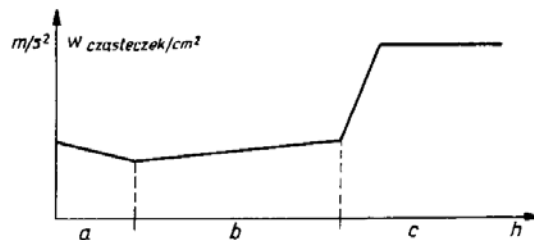


Fig. 12.1. Trend of condition change; a - running-in, b - normal operation, c - intensive wear

The generation of wear particles, intensive in this period, gradually diminishes. The particles produced in the running-in period have small dimensions $< 10 \mu\text{m}$. The particles are described in chap. 10.2 – fig. 10.23 item 1 and fig. 10.24. They are particles resulting from the mutual running in of the elements and micropitting particles. The period of normal and moderate wear is characterized by a very slow increase in the number of generated particles; also the intensity of vibrations increases but slowly. Increments in vibration can be observed at certain frequencies or in certain frequency bands. If external pollution is present, intensive wear of rolling bearings occur which affects intermeshing and leads to a rapid increase in the level of vibration. The increase may be even abrupt, particularly in areas of instability, due to the reasons described in chap. 6 (fig. 6.22a and b). As a result of interference also characteristic particles over $20 \mu\text{m}$ in size are generated. The particles are described in chap. 10.2 – fig. 10.23 item 5 and can be seen in ferrographic images in chap. 17 – fig. 17.9b. Their size can reach $50 \mu\text{m}$. The condition of the gearing's surface is shown in fig. 9.4. The intensification in vibration is due to the impulse character of excitations generated by intermeshing. Plots of the responses to the excitations caused by gearing execution errors and changes in the gearing stiffness are shown in fig. 6.36 for normal intermeshing and in fig. 6.40 for abnormal intermeshing. The excited free vibrations, described in chap. 4.3, have damped character. If a gear operates with a meshing fre-

quency lower than the meshing resonance frequency, the pattern of impulses is as that shown in the figures mentioned above. As the intermeshing error increases, vibration impulses and the excitation of vibration in the resonance frequency intensify (fig. 6.15). If vibration intensifies as a result of edge-wise intermeshing caused by a failure of one of the bearings, then uniform impulses are generated which may cause unstable run the gear. If the gearing is being worn out nonuniformly, signal modulation components are generated, which manifests itself in side components in the signal spectrum (chap. 11) and in nonuniform vibration excitations given in the traces/plots obtained by synchronous summation (chap. 14, fig. 14.18 and 14.20). The plots of the response to the excitations may become distorted under the influence of the different factors described in chap. 14.

The complex of symptoms described above can be defined as a gearing meshing condition syndrome. Intermeshing is accompanied by heat release and an increase in temperature – an additional gearing condition symptom in the gearing meshing syndrome. It is extremely difficult to exploit directly the phenomenon of an increase in temperature resulting from a change in the gearing meshing condition.

12.1. References

- [12.1] Bartelmus W.: Integration of Methods of Diagnosing Belt Conveyor Drive Gears (in Polish), Scientific Papers of Institute of Mining, no. 78, Wrocław University of Technology, 1995.

13. Standardization and classification of machine states

13.1. Introduction

To facilitate diagnostic inference, machine state parameters (symptoms) have been standardized (assuming certain standard limits for states), classified and interpreted in technical-economic terms. As in [13.1], the parameters are divided into classes on the basis of:

- appropriate permissible vibration and noise levels posing hazards to people (users) [13.2]; the classes do not apply directly to machine diagnostics;
- permissible parameter values stemming from technical advisability [13.3], determined from standard machine vibration data obtained from careful observations conducted in accordance with technical documentation;
- technically and economically advisable, permissible parameter values taking into account faults during operation.

13.2. Standardization in vibration diagnostics

The most widely used classification in vibration diagnostics seems to be a classification based on the ISO 3945 recommendations [13.4] (fig. 13.1), according to which the root-mean-square value of vibration velocity in the 10÷1000 Hz band is a diagnostic measurement parameter. Machine states are termed: good, satisfactory, unsatisfactory, im-permissible. A similar interpretation is given in IRD [13.5] where the categories are: exceptionally uniform, uniform, very good, permissible, rather dangerous, dangerous and very dangerous. Classes of states for the mating of bearing elements are interpreted in [13.6] similarly as above using such terms as: good, deteriorated and bad mating conditions (the latter correspond to a failure of the bearing). The terms are meant to reflect the operating conditions of the bearing such as: the arrangement of the subassemblies in the machine, lubrication, the fitting of the bearing and a failure of the bearing. A wide range of state interpretations can be found in [13.7]. The interpretations can be classified as stemming from technical and economic advisability, from decision categories relating to the date of renovation or repair and from condition description categories. The particular state classes are denoted by letter symbols: AA, A and D, where D – good condition and AA – condition dangerous for machine operation.

| | | | |
|-----------------------------------|--|--|--|
| impermissible, | impermissible, | impermissible, | impermissible, |
| permissible, | permissible, | permissible, | permissible, |
| satisfactory, | satisfactory, | satisfactory, | satisfactory, |
| good – small machines up to 15 kW | good – medium class machines: 15÷75 kW or up to 300 kW on special foundation | good – large machines on rigid and heavy foundation whose natural frequency exceeds machine rotational speed | good – large, heavy machines whose rotational speeds exceed foundation natural frequency (e.g. turbine sets) |
| group K | group M | group G | group T |

Fig. 13.1. Classification of machine states [13.4].

Classification of vibration state for four turbomachines based on ISO 3945

RMS value of vibration velocity amplitude mm/s

According to [13.7], the following terms based on economic advisability are adopted for the particular classes:

- AA – dangerous,
- A – correction urgent,
- B – correction profitable,
- C – correction unprofitable,
- D – faultless.

The terms which can be assigned to technical advisability are:

- AA – danger,
- A – acute fault,
- B – some fault,
- D – no fault.

The classes in decision categories relating to a date of correction are interpreted as follows:

- AA – danger, immediately put out of operation;
- A – extreme fault, correction within 48 hours;
- B – some fault, correction within 21 days;
- C – minor fault, do not correct;
- D – without fault, do not correct.

The physical interpretation of the classes given in [13.7] is as follows:

- AA – destroyed (unrecoverable) oil film, metallic contact between elements, seizing of bearings, breaking of gear teeth possible at any instant;

| CONDITION | DECISION |
|------------------|------------------------------------|
| ✓ good | ✓ regularly monitor vibration |
| ✓ profitable | ✓ fix within next weeks |
| ✓ permissible | ✓ fix within next days |
| ✓ dangerous | ✓ immediately put out of operation |
| ✓ catastrophic | ✓ shut-down at once |

The term *profitable* in classification [13.7] is not synonymous with that in [13.8]. Neither it is fully explained. As a result it is difficult to use the classifications.

The term *profitable* in [13.7] should probably be understood as follows: if state parameters correspond to this class, correction should be made at appropriately low expenditures. If state parameters correspond to the next states, then the machine worktime will be only slightly longer but the expenditures on regeneration will be high. In the classification given in [13.8], the term *profitable* should probably be understood as follows: if state parameters correspond to this class, then proper machine durability and the related benefits are obtained.

Proper interpretation of the classes facilitates inference and making decision on, e.g., whether a given object, despite a certain degree of danger, can continue operating, if it is necessary for production reasons. The physical interpretation of classes given in [13.7] now can be validated by ferrographic methods. There are other classifications besides the ones mentioned above, e.g. in [13.1] one can find a classification and an interpretation of classes based on a coherence function (10.49). The possibility of applying the coherence function to the assessment of gearing meshing condition is presented in chap. 10. A classification and its interpretation for the assessment of gearing meshing condition are given in chap. 16.2. A classification of the condition of rolling bearings according to SKF is presented in chap. 15.

13.3. Diagnostics standardization based on analysis of wear products

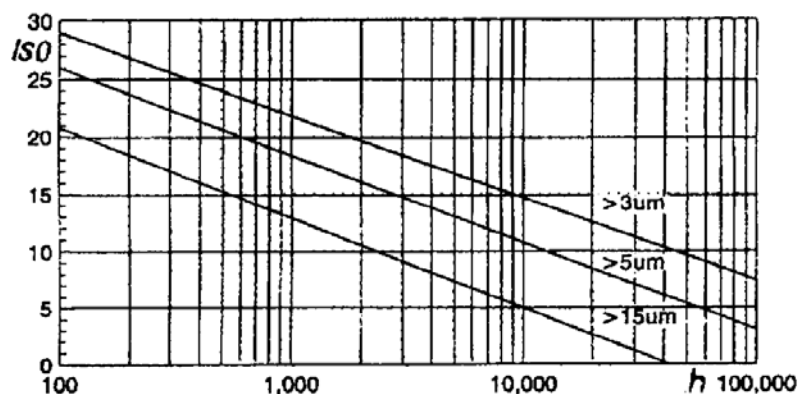
Wear products together with external pollution contaminate machine oil. This problem is described in chap. 10.2. Degrees of oil contamination are classified according to standard ISO 4406. 28 levels are assumed. The standard applies mainly to particles below 5 μm . The classes, the levels and the corresponding numbers of particles are given in table 13.1. The minimum and maximum number of particles per 1 ml of oil are given. It should be noted that the purity of oil, particularly oil used in hydraulic systems cannot be assessed with the naked eye since the human eye distinguishes particles above 40 μm and faults in hydraulic systems can generate particles as large as 5÷15 μm .

Tab. 13.1. Classification of oil contamination according to ISO 4406.

| ISO code | Minimum number of particles per [ml] | Maximum number of particles per [ml] |
|----------|--------------------------------------|--------------------------------------|
| 1 | 0.01 | 0.02 |
| 2 | 0.02 | 0.04 |
| 3 | 0.04 | 0.08 |
| 4 | 0.08 | 0.16 |
| 5 | 0.16 | 0.32 |
| 6 | 0.32 | 0.64 |
| 7 | 0.64 | 1.3 |
| 8 | 1.3 | 2.5 |
| 9 | 2.5 | 5 |
| 10 | 5 | 10 |
| 11 | 10 | 20 |
| 12 | 20 | 40 |
| 13 | 40 | 80 |
| 14 | 80 | 160 |
| 15 | 160 | 320 |
| 16 | 320 | 640 |
| 17 | 640 | 1300 |
| 18 | 1300 | 2500 |
| 19 | 2500 | 5000 |
| 20 | 5000 | 10000 |
| 21 | 10000 | 20000 |
| 22 | 20000 | 40000 |
| 23 | 40000 | 80000 |
| 24 | 80000 | 160000 |
| 25 | 160000 | 320000 |
| 26 | 320000 | 640000 |
| 27 | 640000 | 1300000 |
| 28 | 1300000 | 2500000 |

Even 2 μ m particles can cause a malfunction of a hydraulic system. By preserving the purity of oil in hydraulic systems one increases their durability and that of other systems. The relationship between durability and the number of particles specified by ISO code numbers is illustrated in fig. 13.2 after [13.9]. The figure shows that if the number of particles corresponds to code number 20 and their size is 15 μ m, then the

predicted life is 100 h, but if the code number decreases from 20 to 5, then the durability increases to 10000 h, i.e. 100 times.



Tab. 13.2. Average durability of machine versus particle size (Z_w , K , Z_a).

13.4. References

- [13.1] Bartelmus W.: Application of Some Statistical Estimators of Vibration Signal as Gearing Meshing Condition Assessment Criteria (in Polish). *Scientific Papers of Silesian Polytechnic, Mining* 1979, No. 616.
- [13.2] SN 626 – 66, Soviet Health Standard (in Polish).
- [13.3] Dietrych J. et al.: Fundamentals of Machine Design, Part 1 (in Polish), *WNT*, Warsaw, 1969.
- [13.4] ISO 3945 – 1997: Mechanical Vibration of Large Rotating Machines with Speed Range from 10-200 rev/s., Measurement and Evaluation of Vibration Severity in Site.
- [13.5] IRD Mechanoanalysis Inc.: Special Treatments of Vibrations Sources to Reduce Plant Noise, Technical Paper, No. 110, 1976.
- [13.6] SKF Bearing Detector TMED1 Handbook.
- [13.7] Blake M.: Vibration Standards for Maintenance: Hydrocarbon Processing and Petroleum Refinery, Vol. 43, (January) 1964, pp. 111-114.
- [13.8] Cempel C.: Handbook of Vibration Diagnostics (in Polish), *Eksploatacja i Dozór*, No. 4, 1980.
- [13.9] Day M.: Condition Monitoring of Hydraulic Systems, Handbook of Condition Monitoring, *Elsevier Science LTD*, 1966.

14. Fundamentals of gear transmission diagnostics

14.1. Gear transmission loading and gearing condition, life of gearing

A gear tooth loading plot for one cycle is shown [after 14.1] in fig. 6.14. Load cycle plots for different gear transmission states (stemming from the design features) and changes in condition caused by the wear of the bearings and the gearing are shown in figs 6.15, 6.40. The gear transmission's durability is affected mainly by its rolling bearings and gear wheels (gearing) and so primarily these elements are subject to diagnostic assessment. The gearing is usually assumed to have unlimited life as shown in table 14.1 [14.2]. This is possible when the gearing is in proper condition and under constant (constant-amplitude) external loading. Unlimited durability can also be achieved at the narrow-band loading amplitude. If the gearing's life is limited, the number of load cycles must be determined by identifying the changes in the load in relation to the mean load.

Tab. 14.1. Relationship between form of loading and life.

| External load | Gearing load | Gear condition | | Gearing load | Gearing lifetime |
|-------------------------|---|----------------|----------------------------|-------------------------------|------------------|
| Stable | Stable-amplitude from zero oscillatory | Proper | $K_d K_r < l_m^*$ | Stable-amplitude | Unlimited |
| | | Improper | $K_d K_r > l_m$ pitting | Stable-amplitude wide-band | Limited |
| Variable narrow-band | Variable amplitude | Proper | $K_d K_r < l_m$ | narrow-band | Unlimited |
| | | Improper | $K_d K_r > l_m$ pitting | narrow-band wide band | Limited |
| Variable wide-band | Variable amplitude | Proper | $K_d K_r < l_m$ | wide-band | Limited |
| | | Improper | $K_d K_r > l_m$ pitting | wide-band wide-band | Limited |

* l_m = limit

A change in the load crossing the mean value line upwards and downwards represents one load cycle. Despite the fluctuations, the plot (full line) in fig. 6.14 can be regarded as representing one load cycle. Whereas the plot in fig. 6.15 shows marked changes in the load. The variation depends on the faults/errors in the produc-

tion/machining of the gearing and on their form (fig. 6.22). Considering the relationship between the load and the durability of the gearing, the following states of loading can be distinguished:

- constant-amplitude loading of the teeth (constant external loading of the gear transmission) – the “aa” form or loading with variable amplitude corresponding to narrow-band noise (one load maximum per one crossing of the mean value line by the load at the equivalent load [14.3] smaller than the load corresponding to the limit fatigue strength – the material behaviour described by broken line *a* in fig. 14.1);
- variable-amplitude (wide-band) loading – the “bb” form (more than one load maximum per one crossing of the mean value line by the load – the material behaviour described by straight line *b* in fig. 14.1);
- variable-amplitude loading as above (the “bb” form) and the gearing with a notch caused by pitting or other damage (the behaviour of the material under the load is described by straight line *c* in fig. 14.1).

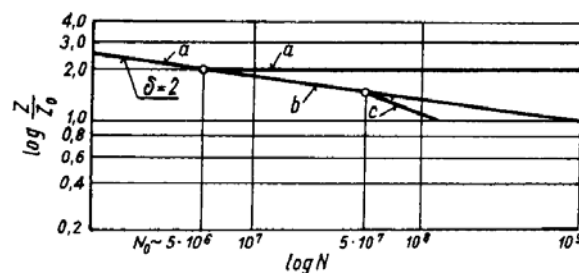


Fig. 14.1. Fatigue properties of gearing depending on its loading: δ – factor of safety, N – number of load cycles, Z – fatigue strength, Z_0 – fatigue strength for N_0 load cycles.

The load forms corresponding to the above description are shown as intertooth force plots in figs 6.14, 6.15, 6.40 and 14.18.

Partial loss of load capacity by one of the rolling bearings may change the state of gearing loading, mainly because of the nonuniform contact between the teeth. As a result, the state of loading changes from “aa” to “bb” (figs 6.15 and 6.40). The state of loading may also change due to the nonuniform wear of the teeth (the form of loading shown in fig. 14.18). The form of a change in loading, resulting from both a change in the condition of the bearing and the nonuniform wear of the teeth, is shown in fig. 14.20. Besides the natural fatigue of the material, also the adverse effect of the strip-mine environment contributes to a change in the condition of the rolling bearings in gear transmissions.

Impurities get into the rolling bearings and accelerate the abrasive or fatigue wear of their surfaces [14.4, 14.5]. This change in the condition of the bearings causes a change in meshing and consequently, in the form of loading (compare fig. 6.13 with fig. 6.15).

So far the life of rolling bearings has been assumed to be limited [14.5]. Recently it has been reported [14.6] that it can be assumed to be unlimited. This is due to the use of new, better materials, the meeting of the bearing hydrodynamic lubrication condition and the assumption that external factors do not affect the operation of the bearings. If it is assumed that the life of the bearings in a gear transmission is limited, then damage to a bearing affects meshing, changes the intertooth contact trace and so increases the load intensity along the engagement line, which results in damage shown in fig. 9.4. The nonuniformity of the tooth load along the flank line is expressed by coefficient K_r [14.7, 14.8]. Also dynamic coefficient K_d changes. Product K_r, K_d (tab. 14.1) was assumed, according to [14.7, 14.8], as the measure of the combined effect of the above factors. If this product exceeds a boundary value, the durability of the gearing will become limited. The factors contributing to the limited life of the gearing are detected by means of diagnostic methods. It is especially important to detect durability limiting factors which act in conjunction, e.g. an increase in the intertooth load and a change in the form of the load (transition from narrow-band to wide-band loading).

14.2. Description of change in gear transmission condition and effect of design, technological and operational factors on form of signal

In a description (tab. 14.2) of gear transmission condition and its effect on the form of the signal one can distinguish: design, production technology and operational factors [14.9, 14.10] and a change in the condition of the gear transmission as a result of its operation (fatigue of the materials, wear and the effect of the environment).

Tab. 14.1. Relationship between design, production technology, operation and change-of-condition factors and form of signal.

| | Gear transmission condition | Form of signal |
|--|---|---|
| Design factors | (1,2); (2,2); (3,2); (6,2); (8,2) Effect within permissible error limits | (1,1); (2,3); (3,3); (6,3) |
| production technology/manufacture factors | (5,2); (2,2); (3,2); (6,2); (8,2) Effect beyond permissible manufacture error limits | (5,3); (2,3); (3,3); (6,3); (8,3) |
| Operational factors | v – peripheral velocity of wheels Δv – changes in velocity P – load ΔP – changes in load | (1,3) (8,3) (1,3) (6,3) |
| Change in gear transmission condition as a result of operation (fatigue of materials, effect of environment) | (3,1); (4,2); (7,2); (9,2); (10,2); (11,1) | (3,3); (4,3); (7,2); (9,3); (10,3); (11,3) |

The above factors are described in chap. 6. The interrelations between the factors, the description of gear transmission condition and the form of the signal are represented in tab. 14.3. The design factors include: the stiffness of elements (4.23), particularly that of the gearing (fig. 6.7, formulas 6.20-6.23), the accuracy of elements within permissible error limits; description of gearing errors (6.46) and (6.47). The main production technology/manufacture factor is a failure to stay within the accuracy classes imposed by the design factors. Operational factors include: wheel peripheral velocity v and Δv and load P and ΔP (changes in the external load are described in chap. 4.5, figs 4.24, 4.26a). In gear transmission calculations, design and operational factors are taken into account through coefficient K representing the nonuniformity of loading along the engagement line. The coefficient is a function of the condition described in tab. 14.3, i.e. $K_r = f[2, 2]$ where numerals (2, 2) stand for respectively: the number of the row and the number of the column in table 14.3. Besides coefficient K_r , also coefficient $K_d = f[(2, 2); (8, 2), v]$, where v is the tangential velocity of the gear wheels, is taken into account. As mentioned above, the total effect of the design and operational factors is taken into account as product $K_r K_d$. When a change in condition occurs as a result of operation, then $K_r K_d = f[(2, 2); (3, 2); (8, 2); (9, 2); v]$. If this product is greater than the boundary value, a change in condition will affect the durability of the gear transmission (tab. 14.1). In further considerations relating to computer simulation results, the effect of the above factors is represented by one coefficient – K_d .

14.3. Vibroacoustic diagnostics, properties of vibroacoustic signal generated by gear transmission; sources of gear transmission vibroacoustic processes

As described in chap. 6 and 14.2, the operation of a gear transmission is accompanied by mechanical vibration and noise, which together constitute the so-called vibroacoustic process. The source of vibration in a gear transmission are rolling or slide bearings and the gearing. If synchronous summation of the vibration signal is performed (chap. 10.1), a synchronous signal in the time domain, as shown in fig. 6.44, will be obtained. A comparison of fig. 6.44 with fig. 6.14 shows an explicit relationship between the state of loading and the vibration signal. This means that changes in the vibration pattern, when the loading conditions and the rotational speed of the gear wheels remain unchanged, indicate a change in the condition of the gear transmission. The relationship between the condition and the form of the signal is described in columns 2 and 3 in tab. 14.3. The description of the signal in tab. 14.3 is for a constant external load and a constant rotational speed. As figs 11.3 and 11.6 show, the gear transmission generates a polyharmonic signal. Column 3 (rows 1, 2, 3, 4, 9) in tab. 14.3. illustrates how the form of the polyharmonic signal changes with gear transmis-

sion condition. Changes in the condition also result in the modulation of the frequency and amplitude of the signal [14.11, 14.12, 14.13]. Ways of detecting changes in condition through the representation of the signal as: a cepstrum, an envelope spectrum, a zoom and a synchronous summation are given in tab. 14.3. The above terms are defined in chap. 10.1.

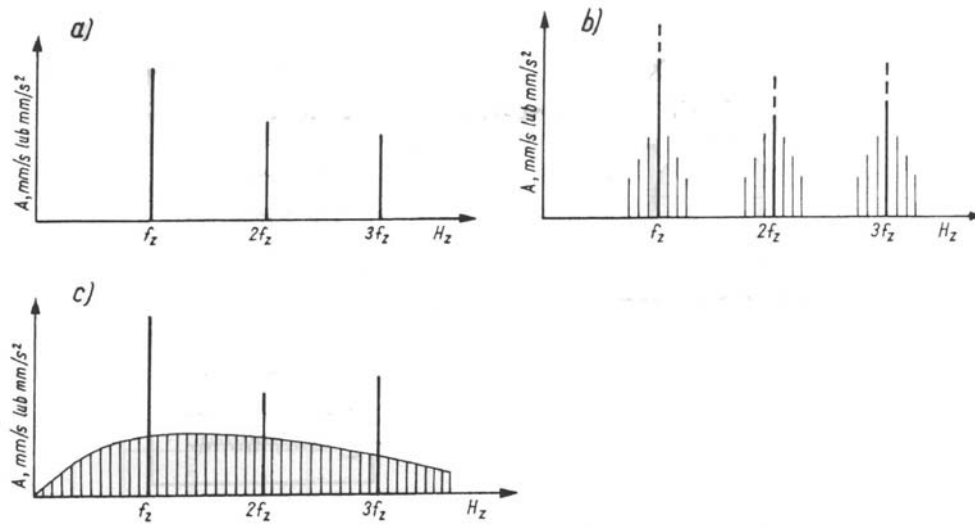


Fig. 14.1. Spectra of signal generated by gearing:
 a – polyharmonic signal with basic frequency f_z ,
 b – polyharmonic signal at frequency or amplitude modulation
 c – amplitude modulation caused by single damage to gearing.

A simplified spectrum of the signal generated by gearing is shown in fig. 14.2. The actual polyharmonic signal is more complex as a result of the superimposition of the different causes of signal generation. This is due to the simultaneous modulation of the amplitude and the frequency and impulse modulation (phenomena that occur per revolution of the gear wheel (cf. fig. 11.6 and fig. 11.10)). Modulation by periodic signals is shown in figs 11.13 and 11.14. Modulation caused by a signal generated by single damage to a tooth is shown in fig. 11.10. A change in the load or in the rotational speed during measurement causes additional amplitude or frequency modulation. Random influences (resulting in amplitude and frequency modulation) which may affect the form of the signal can be eliminated through signal sampling combined with synchronous summation [14.13, 14.14]. The complexity of a signal spectrum increases in the case of a multistage gear when the signal spectra generated by the particular stages overlap. According to [14.14], a plot for a given kinematic pair of gear wheels, with the effects of the particular gear stages eliminated, can be obtained through synchronous summation. This principle is illustrated in fig. 14.3. The syn-

chronous summation picture may be disturbed by the occurrence of component f_m reflecting the kinematic properties of the kinematic chain of the machine tool used for the machining of the gear wheel (tab. 14.3 row 5 column 2) – this represents a technological-factor influence. The component is shown in fig. 14.4a. It may occur in close proximity to the meshing frequency and cause beating affecting the picture obtained through synchronous summation and thus making it difficult to assess the condition of the gearing (fig. 14.4a and b).

It is shown in [14.9, 14.15], by means of the coherence function (10.49) for determining the condition of intermeshing, that the power of the polyharmonic signal generated by a high-quality transmission is low in comparison with that of the noise generated by the gearing itself and by the rolling bearings (if the signal is analyzed in a certain frequency band, e.g. 6% of the relative bandwidth).

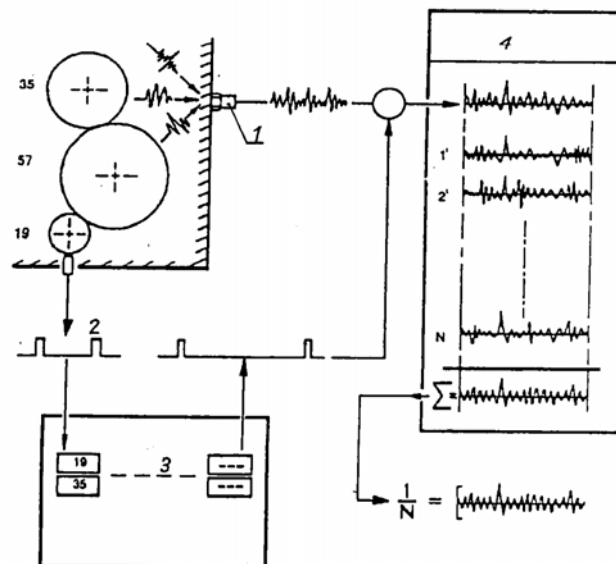


Fig. 14.2. Diagram illustrating principle of averaging gear transmission signal: 1 – piezoelectric transducer, tachometric signal, 3 – electronic gear, 4 – signal averaging, 1', 2' ... N – number of averaged signal samples, 19, 35 – number of gear wheel teeth.

If the condition changes and a persistent error occurs, intermeshing will deteriorate and both the power of the polyharmonic component and the values of the coherence function components will increase (10.49). The causes of this change in the condition of the gear transmission are given in table 14.3. (items 2,2, 3,2 and 4,2). The power of the polyharmonic signal may also increase if most of the teeth are damaged by pitting (item 9,2 in tab. 14.3). Then the signal is narrowband noise and the coherence function component increases (as shown in [14.9 and 14.15]). If bicoherence function (10.46) is used to measure the condition of intermeshing, then, according to the interpretation

given in [14.16], the random component is eliminated from the signal and the value of the bicoherence function is close to unity (it ranges from 0 to 1). This happens when the gear transmission operates under a load close to the nominal one and the polyharmonic signal predominates (the random signal has been removed by processing). If most of the gear transmission's teeth are damaged by pitting, the gear transmission generates Gaussian noise and the bicoherence function's value decreases markedly in relation to its value when the signal generated by the gearing was a determinate, periodic, polyharmonic signal. According to [14.16], a change in condition corresponding to item 9,2 in table 14.3 can be detected by means of the bicoherence function. In the table, synchronous summation is listed as one of the ways of representing signals. In the author's opinion, it is one of the most important forms of representing the gear transmission diagnostic signal.

Computer simulations (see chap. 6 and 14) can be helpful in interpreting the actual gear transmission results.

This chapter has provided a summary of the relationship between the condition of the gear transmission, the form of the signal generated by this condition and the different forms of the signal obtained through its transformation.

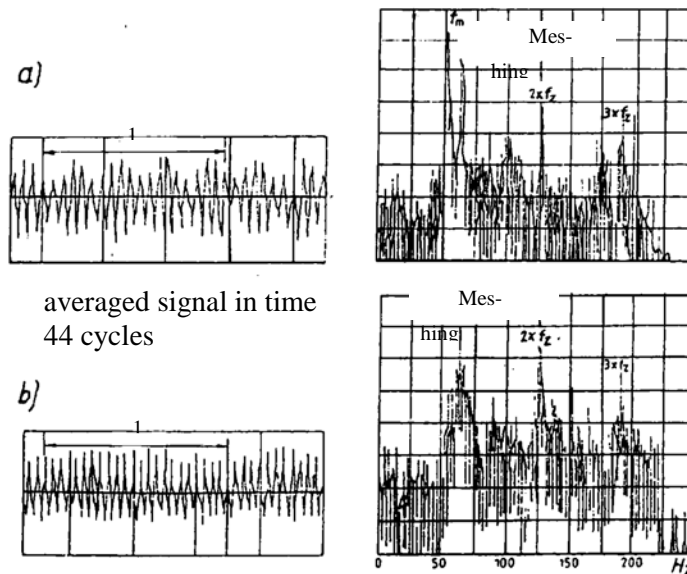


Fig. 14.3. Synchronous summation signal and its spectrum [18]: a – initial condition, b – condition of transmission before failure.

Tab. 14.3. Relationship between condition of transmission, form of signal and signal detection mode.

| Number of row/column | Condition of transmission | | Form of signal | Signal detection mode** | | | | | | |
|----------------------|-------------------------------|--|--|-------------------------|------|-----------|-------------|----------|-------------------|-----------------------|
| | Condition of rolling bearings | Condition of gearing | | Spectrum | Zoom | Coherence | Bicoherence | Cepstrum | Envelope spectrum | Synchronous summation |
| 1 | 1 | 2 | 3 | 4 | 5 | 6 | 7 | 8 | 9 | 10 |
| 1 | | teeth yielding under load | Polyharmonic signal with basic frequency f_z (meshing frequency) | (1,4) | | (1,6) | | | | (1,10) |
| 2 | | Persistent pressure angle error or nonuniform tooth contact | Polyharmonic signal with basic frequency f_z (component with higher intensity as compared with (1.3)) | (2,4) | | (2,6) | | | | (2,10) |
| 3 | Damaged bearing race | Nonuniform tooth contact | As above | 3,4) | | 3,6) | | | | (3,10) |
| 4 | | Uniform initial wear of teeth | Polyharmonic signal with basic frequency f_z , increased intensity in 2 nd and higher harmonics | (4,4) | | (4,6) | | | | (4,10) |
| 5 | | Persistent error in manufacture of teeth, stemming from properties of kinematic chain of machine tool used for cutting teeth | Occurrence of spectral component f_m with frequency close to frequency f_z | (5,4) | | | | | | |

14.4. Unit damage to gearing

Unit damage to the teeth is a partial or total fracture of a tooth, a fatigue crack or extensive damage to one of the teeth in a gear wheel. The application of synchronous summation to the detection of tooth fractures in the gear transmission is described in [14.14]. A signal obtained through synchronous summation is shown in fig. 14.5 [14.14]. The signal for a case when the gear transmission has all its teeth intact and for a case when one of its teeth is broken is shown in fig. 14.5a and 14.5b, respectively.

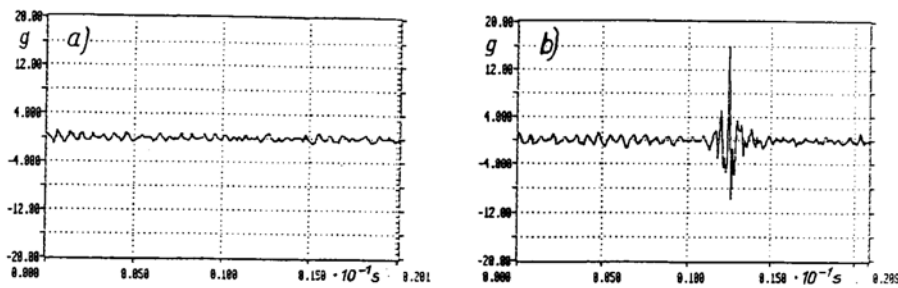


Fig. 14.1. Gear transmission condition signal obtained through synchronous summation: a – undamaged transmission, b – transmission with broken tooth [14.14], g – gravitational acceleration.

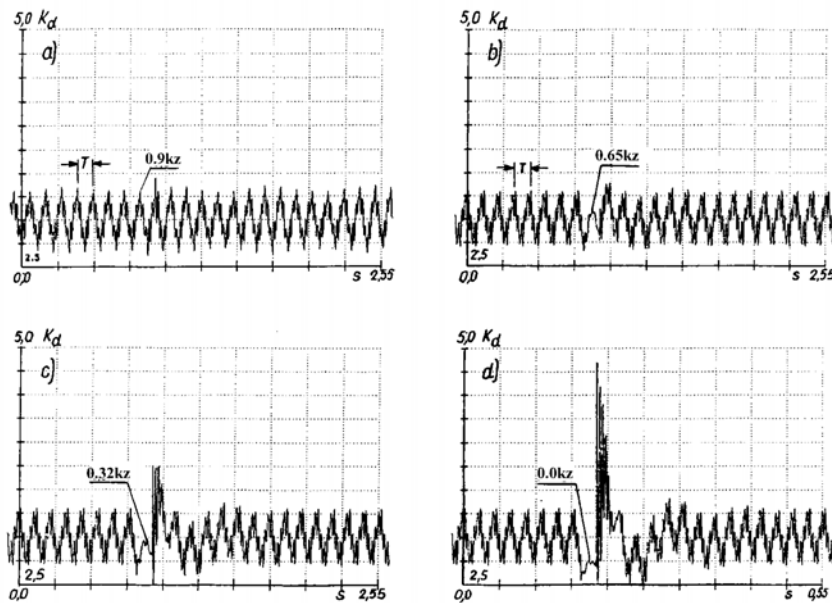


Fig. 14.2. Gearing condition signal in form of coefficient K_d (signal obtained by computer simulation) and changes in gearing rigidity: a – to $0.9 k_z$, b – to $0.65 k_z$, c – to $0.32 k_z$, d – to $0.0 k_z$ (broken tooth).

To study the forms of the diagnostic signal more closely, simulations were run for the following basic parameters: $M_r(0; 0; 0; 0)$; $E(0.5; 10; 0; ?0)$. The symbolic notation for state of loading M_r and for form of error E is given in chap. 4.5 and 6.4, respectively. The influence of changes in the stiffness k_z (6.20) to (6.23) of one of the teeth until fracture (stiffness, $k_z = 0$) was studied. The results of the computer simulations are shown in fig. 14.6a, b, c and d.

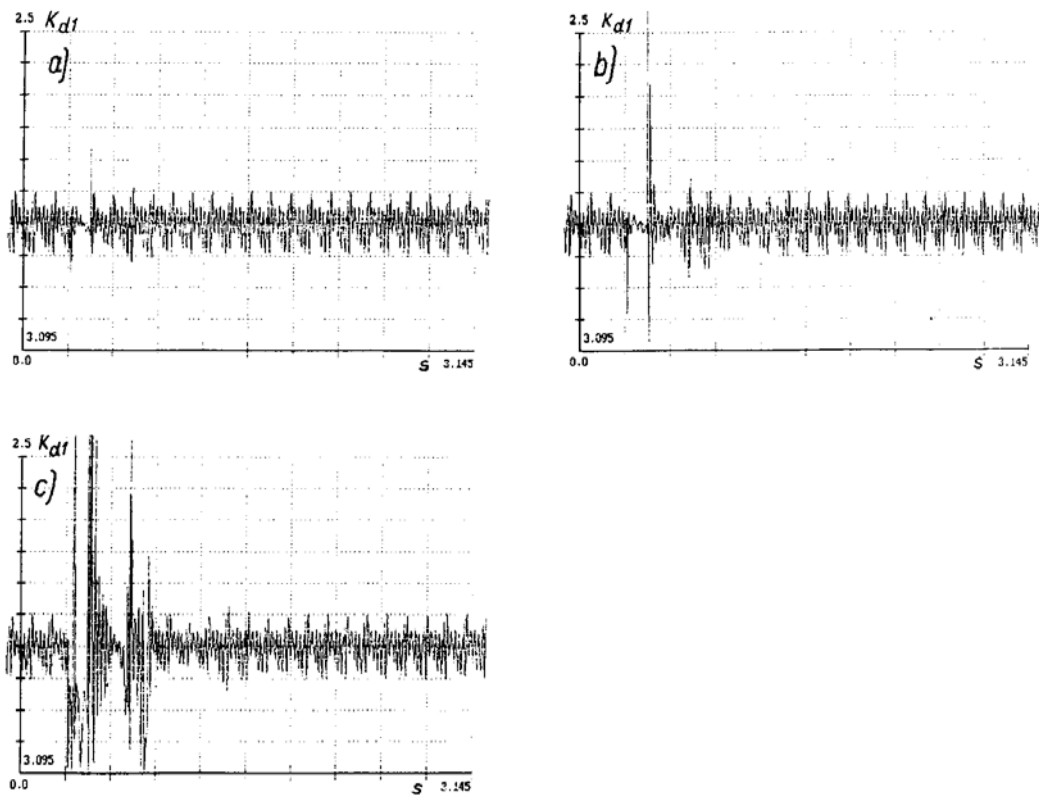


Fig. 14.3. Gearing condition signal in form of coefficient K_{d1} (signal obtained by computer simulation) and changes in gearing rigidity: a – to $0.65 k_z$, b – to $0.32 k_z$, c – to $0.0 k_z$ (broken tooth).

If k_z denotes the total stiffness of the gearing, the results are, respectively, for the following stiffness: $0.9 k_z$, $0.65 k_z$, $0.32 k_z$ and $0.0 k_z$ (a tooth missing). Plots of function K_{d1} (defined in chap. 6.7) when one of the teeth had rigidity $0.65 k_z$, $0.32 k_z$ and $0.0 k_z$, respectively, and when $M_r(0; 0; 0; 0)$, $E(0.5; 10; 0; 0)$ are shown in fig. 14.7. Then simulations were run for a changing external load and the state of external loading was described by $M_r(0.3; 0; 0.9; 0; 8)$ and $M_r(1; 0; 0.9; 0; 8)$. The signal was represented as function K_{d1} which, as shown in chap. 6.7, makes it possible to minimize the influence of changes in the state of loading on the form of the signal. Function K_{d1} for

load change coefficients $w = 0.3$ and $w = 1$, respectively, is shown fig. 14.8. A zoom of plot K_{dl} for a time interval of 0.005 s is shown in fig. 14.9. Plots K_{dl} for a case when one of the teeth is damaged (by pitting), which is described by unit error on one tooth $e = -10 \mu\text{m}$, are shown in fig. 14.10. To eliminate the influence of changes in the mean load on the results of the computer simulations for load $M_r(1; 0; 0.9; 0)$ also function K_{d4} (defined in chap. 6.7) was used.

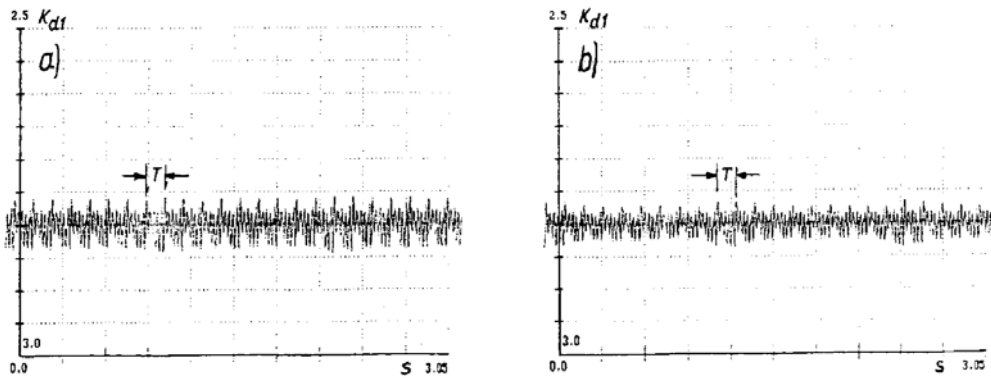


Fig. 14.4. Gearing condition signal in form of coefficient K_{dl} (signal obtained by computer simulation) for changing external load: a – $M_l(0.3; 0; 0.9; 0; 8)$, b – $M_l(1; 0; 0.9; 0; 8)$.

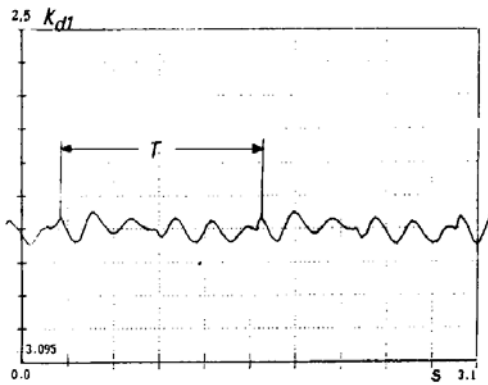


Fig. 14.5. Zoom of gearing condition signal in form of coefficient K_{dl} (signal obtained by computer simulation) for changing external load $M_l(0.3; 0; 0.9; 0; 8)$ and signal time interval of 0.005 s.

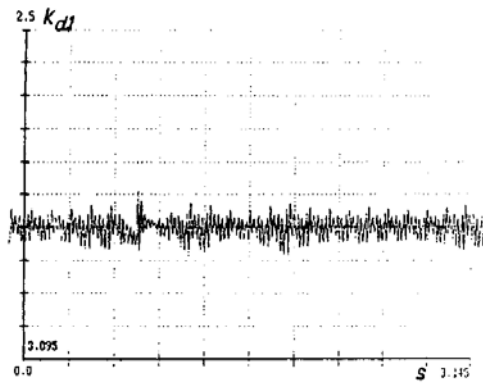


Fig. 14.6. Gearing condition signal in form of coefficient K_{dl} (signal obtained by computer simulation) for changing external load $M_l(0.3; 0; 0.9; 0; 8)$ and one tooth damaged by pitting $e = -10 \mu\text{m}$.

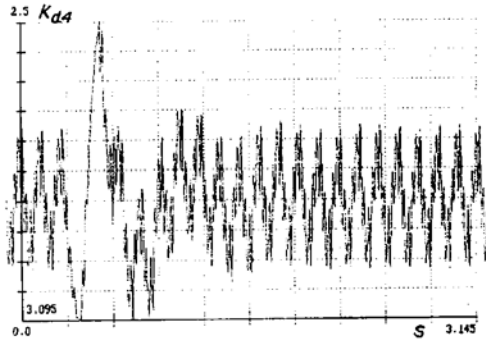


Fig. 14.7. Gearing condition signal in form of coefficient K_{d4} (signal obtained by computer simulation) for invariable external load $w = 0$ and one tooth damaged by pitting $e = -10 \mu\text{m}$.

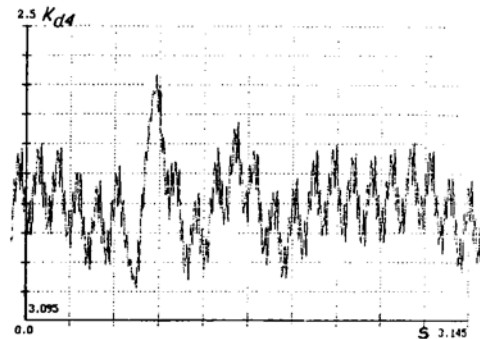


Fig. 14.8. Gearing condition signal in form of coefficient K_{d4} (signal obtained by computer simulation) for changing external load $M_r(1; 0; 0.9; 0; 8)$ and one tooth damaged by pitting $e = -10 \mu\text{m}$.

The influence of unit error $e = -10 \mu\text{m}$ for $w = 0$ was investigated. As shown in fig. 14.11 the error exerts a marked influence on the diagnostic signal. The signal for both error $e = -10 \mu\text{m}$ and external load $M_r(1; 0; 0.9; 0)$ (i.e. $w = 1$) is shown in fig. 14.12. A comparison of figs 14.11 and 14.12 shows an influence of variability parameter $w = 1$ which may reduce the effect of error $e = -10 \mu\text{m}$ on the result of the computer simulation, i.e. on a gearing condition assessment. Similar lowering of sensitivity to changes in condition ($e = -10 \mu\text{m}$) due to the influence of $w = 1$ can be noticed if figs 14.10 and 14.13 are compared. Computer simulations show that a diagnostic signal plot for gearing with a tooth partially damaged by a fatigue crack is similar to a signal plot for a case when pitting occurs on one of the teeth – compare fig. 14.7a or b with fig. 14.13. The influence of unit damage to gearing on the form of the signal is also considered in [14.17] and [14.18].

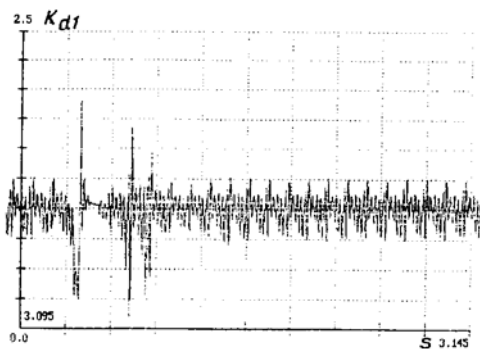


Fig. 14.9. Gearing condition signal in form of coefficient K_{d1} (signal obtained by computer simulation) for invariable external load $w = 0$ and one tooth damaged by pitting $e = -10 \mu\text{m}$.

14.5. Influence of gearing error randomness and external load randomness on diagnostic signal

The influence of gearing manufacture/execution error randomness, changes in condition and external load randomness on the form of the diagnostic signal is described in [14.20]. The gearing manufacture error is given as $E(a; e_j; r; r_a)$. Quantities a and e_j have constant values for a given simulation experiment. Parameters r and r_a , specifying the range of variation, are also constant. The error value for each successive pair of teeth is different and given by formula (6.48) in chap. 6.4. The randomness of the gearing error is specified by random variable l_i . The variable is fitted to z_1 successive teeth of the first (driving) gear wheel. An illustrative error function is shown in fig. 14.14 for $E(0.5; 10; 0.3; 0)$, i.e. the maximum error values for $r = 0.3$ can vary by 30%. In the extreme case (for $r = 1$), the maximum error value varies by 100%. One can assume approximate value $r = 0$ for new gearing, $r = 0.3$ for accidental initial wear of gearing and $r = 1$ for worn down gearing.

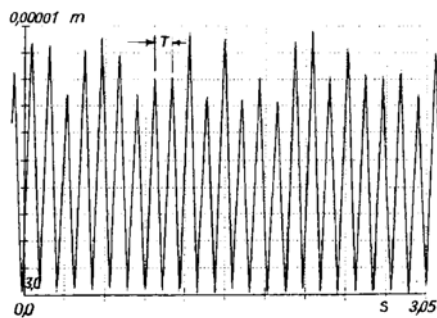


Fig. 14.1. Form of gearing error for $E(0.5; 10; 0.3; 0)$.

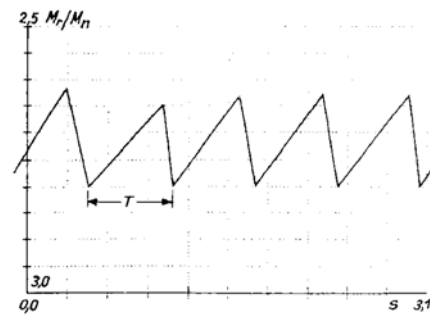


Fig. 14.2. Form of relative external load $M_r(1; 0.3; 0.9; 0; 8)$.

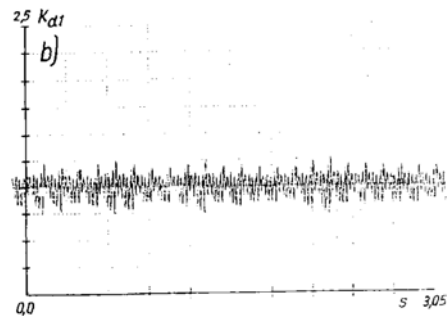
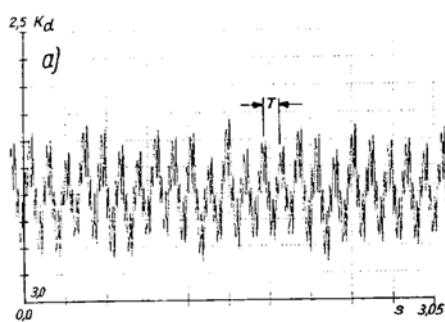


Fig. 14.3. Plot of coefficient: a – K_d , b – K_{d1} for random form of gearing error $E(0.5; 10; 0.3; 0)$ and constant load $M_r(0; 0; 0; 0)$.

The external load was described as $M_r(w; r; p_w; r_p, k_r)$, where parameters r and r_p describe the limits of variation of respectively quantity w and p_w . This is expressed by formulas (4.116) and (4.117) in chap. 4.5. A plot of the relative value of changes in the external load described by $M_r(1; 0.3, 0.9; 0; 8)$, i.e. when increments in the external load values vary by 30% for $r = 0.3$, is shown in fig. 14.15. According to chap. 6.7 and 14.4, the defined coefficients K_d and K_{dl} (definition (6.50) in chap. 6.7) should be used for plotting the diagnostic signal. The results of investigations into the influence of random gearing error values and random external load values on the signal are presented in the form of plots of K_d and K_{dl} versus time t [s]. The plot of K_d and K_{dl} for the error form described by $E(0.5; 10; 0.3; 0)$ (fig. 14.14) and that of K_{dl} are shown in respectively fig. 14.16a and 14.16b. The load form is described by $M_r(0; 0; 0; 0; 0)$, i.e. the external load is fixed and the gear transmission operates in the 4th period (fig. 6.12). A plot of gearing errors in the form of $E(0.5; 10; 1; 0)$ and the corresponding functions K_d and K_{dl} are shown in fig. 14.18. A new error form: $E(0.1; 10; 1; 0)$ (parameter a has changed from 0.5 to 0.1) and the corresponding functions K_d and K_{dl} are shown in fig. 14.19 and fig. 14.20, respectively. The above figures show a distinct relationship between the form of the signal and the condition of the gearing. The simulation results are shown in fig. 14.21 and they obtained under the random condition of load change given in fig. 14.21. No influence of the external load is visible. The influence of random changes in the load can be eliminated by choosing a proper fragment of the diagnostic signal plot (this is the more difficult, the lower the value of coefficient $k_r = T_r/T$ – see chap. 4.5). If this is impossible, an attempt can be made to determine the relationship between the condition of the gearing and the diagnostic signal for the case when the transmission operates without any external load and the overcoming of the system's inertial resistance constitutes the only load (fig. 14.22). Further figures show the relationship between the form of the error and the form of the diagnostic signal described by function K_d (figs 14.23-14.28). The plots correspond to the signal during the running up (one second after the latter begins) of the system (period 1 in fig. 6.14). The influence of free vibration on the diagnostic signal plot is shown in figs 14.24 and 14.26. This influence is the more marked, the higher the values of the impulses generated due to gearing errors and the steeper the error function curve (compare figs 14.23 and 14.25 with figs 14.24 and 14.26).

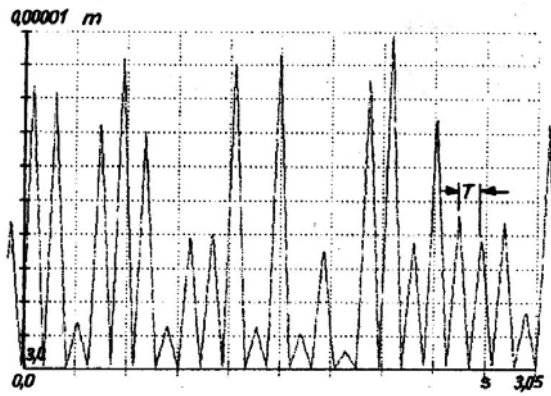


Fig. 14.4. Form of gearing error $E(0.5;10;1;0)$.

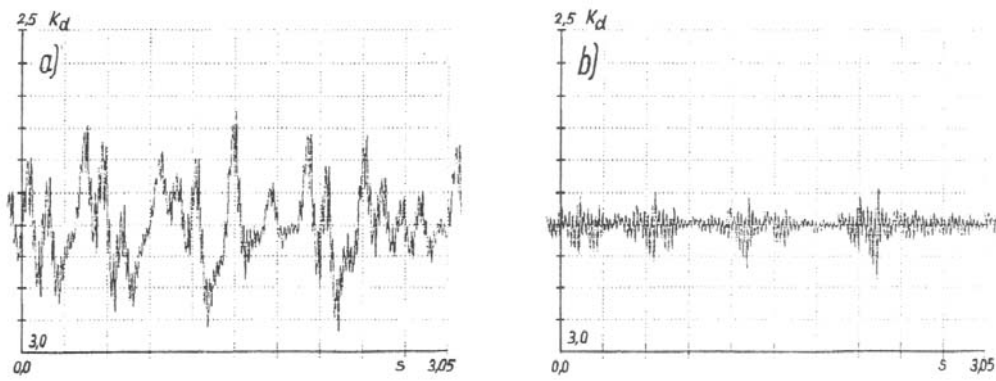


Fig. 14.5. Plot of coefficient: a) K_d and b) K_{d1} for random gearing error $E(0.5;10;1;0)$ and constant load $M_1(0;0;0;0)$.

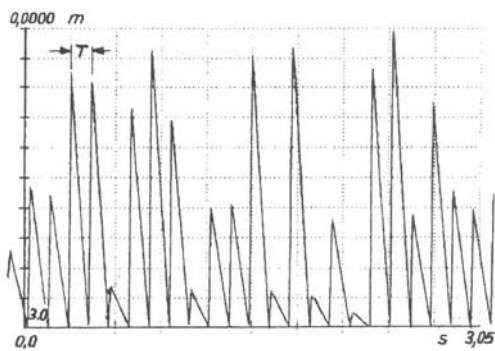


Fig. 14.6. Form of gearing error $E(0.1;10;1;0)$

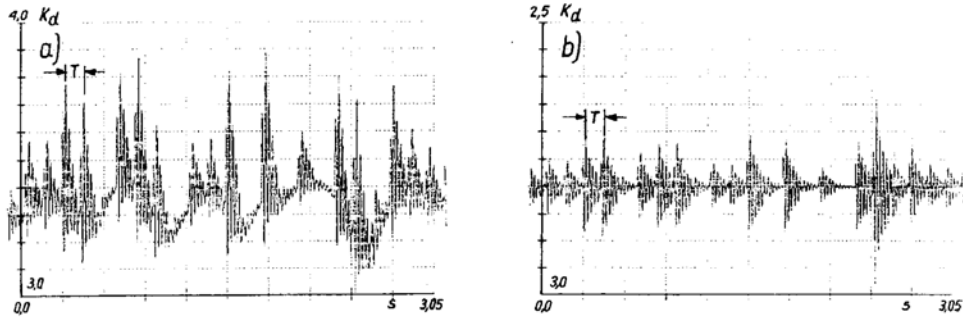


Fig. 14.7. Plot of coefficient: a) K_d and b) K_{d1} for random gearing error $E(0.1;10;1;0)$ and load $M_l(1;1;0.9;0;8)$.

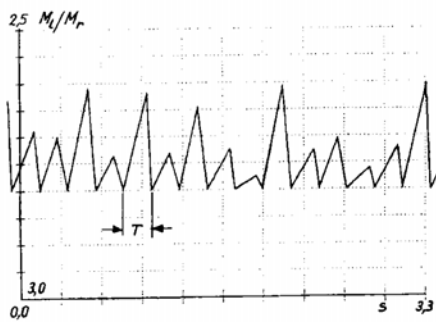


Fig. 14.8. Plot of random external load $M_l(1;1;0.9;0;8)$.

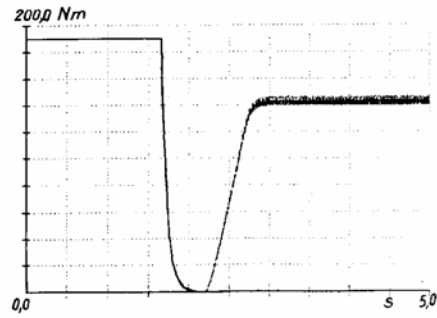


Fig. 14.9. Plot of electric motor's driving torque

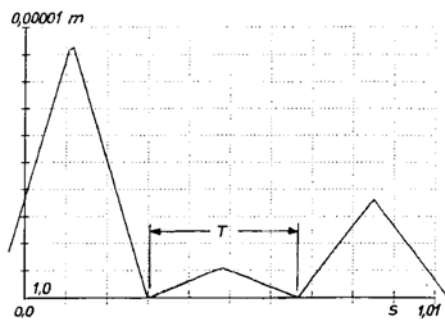


Fig. 14.10. Random from of error $E(0.5;10;1;0)$ in three pairs of gearing teeth.

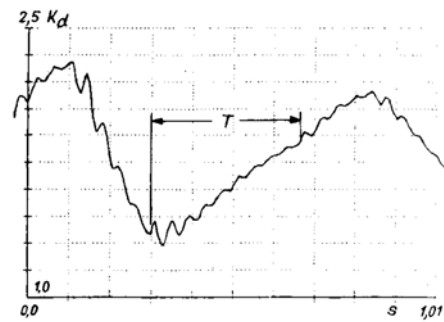


Fig. 14.11. Plot of coefficient K_d during starting of gear transmission in time interval of 1-1.01 s for $E(0.5;10;1;0)$ in fig. 14.23.

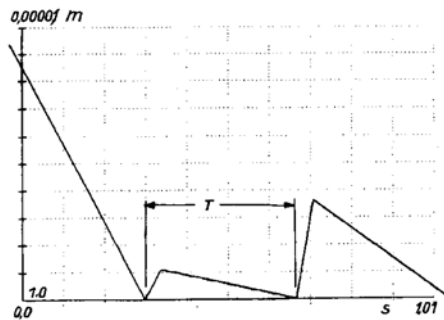


Fig. 14.12. Random form of error $E(0.1;10;1;0)$ in three pairs of gearing teeth.

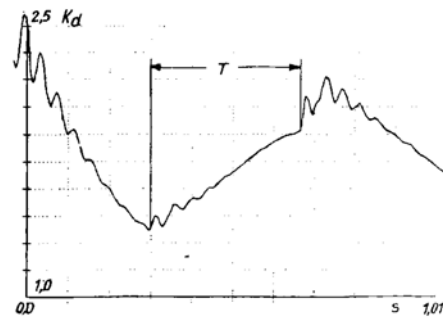


Fig. 14.13. Plot of coefficient K_d during starting of gear transmission in time interval of 1-10.1 s for $E(0.1;10;1;0)$ in fig. 14.25.

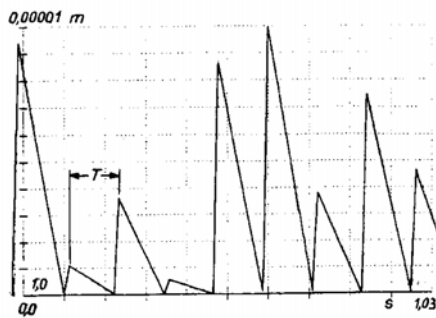


Fig. 14.14. Random form of error $E(0.1;10;1;0)$ in several pairs of gearing teeth.

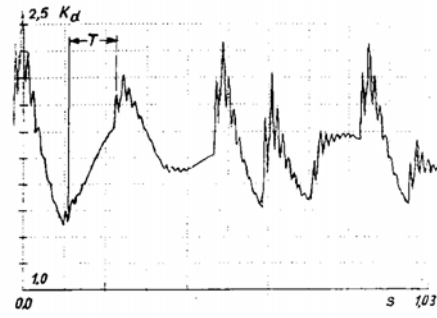


Fig. 14.15. Plot of coefficient during starting of gear transmission in time interval of 1-1.03 s for $E(0.1;10;1;0)$ in fig. 14.27.

14.6. References

- [14.1] Rettig H.: Innere Dynamische Zusatzkräfte bei Zahnadgetrieben. Ant. Antriebstechnik 16(1977) No. 11, pp. 655-663.
- [14.2] Bartelmus W.: Diagnostics of Toothed Gears (in Polish), Górnictwo Odkrywkowe, No. 2, 1991.
- [14.3] Bartelmus W.: Fundamentals of Gear Calculations for Toothed Gear Life, 1st International Conference on Reliability and Durability of Machines and Machinery Systems in Mining, Szczyrk, Gliwice, Silesian Polytechnic, 1986.
- [14.4] Nedimovic B.: Influence of Difficult Operation Conditions on Pitting Appearance and Reduced Bearing Capacity of Individual Parts and Constructions of the Mining Machinery in the Contact, Zagadnienia Eksploatacji Maszyn, No. 1 (65), 1986.
- [14.5] FAG Catalogue of Rolling Bearings, Basic Program (in Polish).

- [14.6] Joannides E., Harris T.A.: A New Fatigue Life Model for Rolling Bearings, *Ball Bearing Journal*, Vol. 224, pp. 2-22, 1985.
- [14.7] Niemann G.: *Maschinenelemente. II Band Getriebe*, Springer Verlag, Berlin, 1960.
- [14.8] Muller L: *Toothed Gears – Design* (in Polish), WNT, Warsaw, 1979.
- [14.9] Bartelmus W.: Application of Some Statistical Estimators of Vibrational Signal As Gearing Condition Assessment Criteria (in Polish), *Scientific Papers of Silesian Polytechnic, Mining*, No. 616, 1979.
- [14.10] Bartelmus W.: *Vibration Condition Monitoring of Gearboxes*, *Machine Vibration 1*: 178-189, Springer-Verlag London Limited, 1992.
- [14.11] Mark D. W.: Analysis of the Vibratory Excitation of Gear Systems: Basic theory, *J. Acoust. Soc. Am.* 63/5, pp. 1409-1430, May 1978.
- [14.12] Kohlar H. K. et al.: Dynamics and Noise of Parallel-Axis Gearing, *Proc. Inst. Mech. Engrs.*, Vol. 184, Pt 30., 1969-1970.
- [14.13] Randall R. B.: A New Method of Modelling Gear Faults, *An ASME Publication 81 – DE – 10*.
- [14.14] Penter, A. J.: A Practical Diagnostic Monitoring System, *Proceedings of an International Conference on Condition Monitoring*, Erding, Germany, Pineridge Press, pp. 79-96, 1991.
- [14.15] Bartelmus W.: Application of Some Statistical Estimators of Vibration Signal as Criteria of Assessment of Mesh State, *Proceedings of an International Conference on Condition Monitoring*, University College of Swansea, April 1984.
- [14.16] Sato T. et al.: Real-time Bispectral Analysis of Gear Noise and Its Applications in Contactless Diagnosis, *J. Acoustic. Soc. Am.*, Vol. 62, No. 2, pp. 382-387, 1977.
- [14.17] Bartelmus W.: Visualisation of Vibration Signal Generated by Gearing Obtained by Computer Simulation. *Proceedings of XIV IMEKO World Congress*, 1997.
- [14.18] Bartelmus W.: Transformation of Gear Intertooth Forces into Acceleration and Velocity, *Proceedings of The 7th International Symposium on Transport Phenomena and Dynamics of Rotating Machinery*, February 1998.
- [14.19] Bartelmus W.: Diagnostic Symptoms of Unstability of Gear Systems Investigated by Computer Simulation, *Proceedings of 9th International Congress COMADEM 96 Sheffield*, July 1996, Sheffield Academic Press Ltd., 1996.
- [14.20] Bartelmus W.: Influence of Random Outer Load Change and Random Gearing Faults to Vibration Diagnostic Signal Generated by Gearbox Systems, *Proceedings of 10th International Congress COMADEM 97 Espoo, Finland*, June 1997.

15. Diagnostics of rolling bearings

As mentioned in chap. 7, damaged rolling bearings generate impulses which cause damped vibration of a structure. The impulses repeat themselves depending on the frequency of rotations of the shaft on which the bearing rotates and on the rolling bearings' geometrical quantities – formulas in chap. 7 and tab. 11.1. The formulas are used to determine the frequencies that indicate defective places: the outer race, the inner race, a ball or the cage. The vibration components of the frequencies can be found in the spectrum if the measurement is made in a wide dynamics range. The intensity of the vibrations generated by a defective rolling bearing is low and so the vibrations generated by the damage may be hidden in the general noise produced by the bearing. The intensity of the vibrations generated by the gearing of a gear transmission is much higher than that of the vibrations generated by the rolling bearing. Vibration accelerations are measured to assess the condition of the rolling bearings. The measured vibrations are used to search for different measures of rolling bearing condition such as RMS vibration and peak vibration. The two measures are characterized in fig. 15.1. Also relative measures are used for the assessment of rolling bearing condition, i.e. kurtosis expressed by the formula

$$K = \int_{-\infty}^{\infty} x^4 p(x) / (RMS)^4 \quad (15.1)$$

determined within a band of 5-15 kHz;

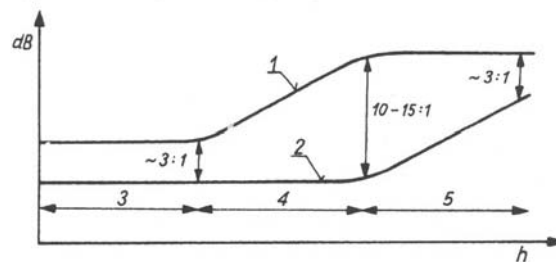


Fig. 15.1. Trend in signal level variation depending on adopted rolling bearing condition symptom: 1 – peak value, 2 – RMS value, 3 – undamaged bearing, 4 – partially damaged bearing, 5 – damaged bearing.

Bearing defect excite high-frequency vibrations (see fig. 16.6) corresponding to the free vibration of the bearing's components. The measurement of RMS vibration in a range of 3.5-10 kHz is described in paper [15.1]. This signal was further processed to

increase the reliability of the diagnosis. The signal envelope was sought in accordance with the principles given in chap. 10.

The cepstrum function (chap. 10) is used to detect the vibration components originating from the vibration of the rolling bearings. Examples of the application of vibration analysis to the assessment of the condition of large rolling bearings similar to the bearings used in the belt conveyor drums are given in [15.2]. A constant-percentage vibration spectrum in which the frequencies corresponding to the frequency with which the damaged ball passes around the damaged outer race (BPFO) have been identified and the latter frequency's 2nd, 3rd and 4th harmonics are shown in fig. 15.2.

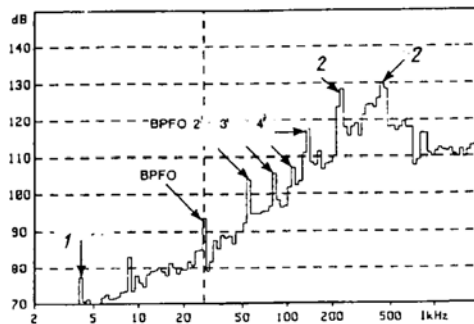


Fig. 15.2. Modified third octave vibration spectrum reflecting rolling bearing condition [15.2]; BPFO – frequency with which ball passes over damaged place; 2', 3', 4' – harmonics, 1 – shaft revolutions frequency, 2 – 1st and 2nd harmonic of gearing

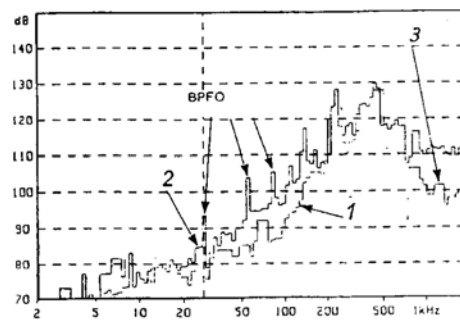


Fig. 15.3. Defective rolling bearing condition spectrum against spectrum for new bearing [15.2]; BPFO – frequency with which ball passes over damaged place and harmonics; 1 – reference spectrum, 2 – actual spectrum, 3 – increase in vibration level for high frequencies.

A constant-percentage spectrum means that for 6% of bandwidth at filter midband frequencies of 100 and 1000 Hz the filter bandwidth is respectively 6 and 60 Hz. The vibration component originating from the rotational speed, and the meshing frequency and its second component are also shown in the figure. The spectrum represents the RMS vibration acceleration in dB. Fig. 15.3 shows a spectrum for a new bearing against a spectrum for the same but defective bearing. Substantial increases in the level of vibrations and harmonics within the BPFO (Ball Passing Frequency Outer Race) range and increases in vibration at higher frequencies are visible. The next example is shown in fig. 15.4 which features a reference spectrum (new bearing) and the actual spectrum, with marked harmonics of the frequency of passage over the damaged outer race. The difference between the levels in the spectra is shown in the bottom part of the figure. The signal cepstrum, the rahrmonics corresponding to the basic BPFO rahmonic and the other rahmonics are shown in fig. 15.5. The notion of rahrmonic was introduced to represent spectral components (being the inverse of frequency) as a function of time.

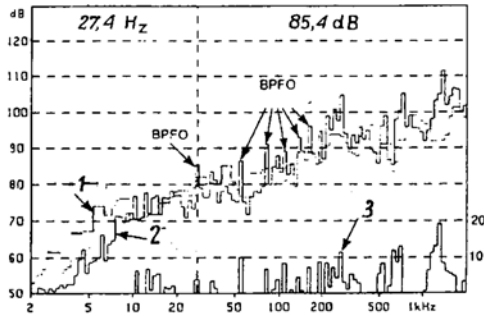


Fig. 15.4. Actual (defective) rolling bearing condition against new bearing condition and spectrum of signal differences [15.2]; BPFO – frequency of ball passage over damaged place, and harmonics; 1 – reference spectrum, 2 – actual spectrum, 3 – differential spectrum.

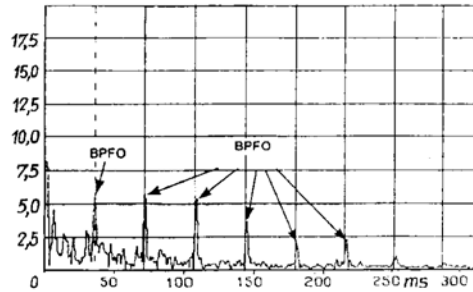


Fig. 15.5. Cepstrum for condition of rolling bearing with damaged outer race [15.2]; BPFO – frequency of ball passage over damaged place.

The increments in the spectrum in the period 25.01-8.02. 1988 are shown in fig. 15.6. As one can see, an increase in the intensity occurred in the 4th harmonic. The trend of the 4th harmonic is shown in fig. 15.7.

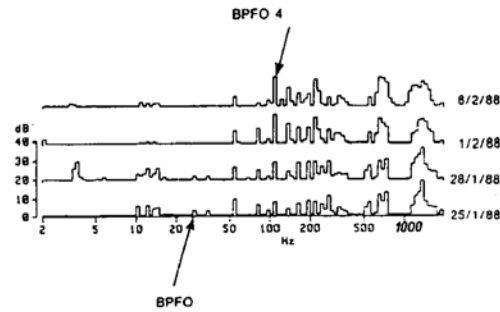


Fig. 15.6. Comparison of difference spectra for rolling bearing [15.2]; BPFO – frequency of ball passage over damaged place, 4 – 4th harmonics.

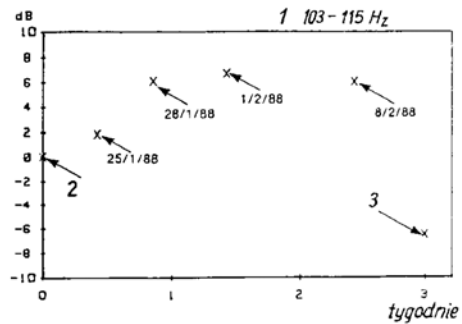


Fig. 15.7. 4th harmonic of frequency of ball passage over damaged place on outer race; 1 – frequency range, 2 – reference level, 3 – level after rolling bearing replacement.

Also a method known as SPM (Shock Pulse Method), developed by the firm SKF (a rolling bearings manufacturer), is used in the diagnosis of rolling bearings.

As it has been established, bearings generate high-frequency vibrations whose range may extend up to 100 kHz. SKF used the measurement of vibrations in a frequency band of 32 kHz. The signal in the 32 kHz band was amplified by the sensor's resonance and electronically. As shown in [15.3], the signal can be used to check if the lubrication of the rolling bearing is proper. The quality of the lubrication can be assessed by measuring the electric current passing through the rolling bearing. If there is no contact between metallic surfaces (they are separated by a lubricating film), hydrodynamic lubrication occurs and no electric current flows through the bearing. The relationship (in percent) between the fraction of time in which there is no contact between metallic surfaces in the rolling bearing and the value of Λ which is ratio h_{min}/σ , where h_{min} is the minimum thickness of the lubricating film at which the latter remains unbroken and σ is a the root of the sum square of the surface irregularities of the contacting parts that are lubricated, is shown in fig. 15.8. The values of Λ can be determined by applying the theory of hydrodynamic lubrication. The relationship between a drop in the level of the diagnostic signal in the 32 kHz band and the percentage of bearing contact-free operation (no current flows through the bearing's elements) for determining the correctness of lubrication is given in fig. 15.9. The SKF meter for measuring the correctness of lubrication gives lubricating film thickness h_{min} in code numbers (fig. 15.10). The code number value is proportional to the thickness of the lubricating film. It has been proved that the code numbers are functions of the type of rolling bearing. As it is shown in fig. 15.11, the higher the code number, the greater the value of Λ , i.e. the greater the thickness of the lubricating film. According to fig. 15.11, better lubricating conditions can be obtained for roller bearings than ball bearings. The components reflecting the damage on the outer race against the other components (BPFI – Ball Passing Frequency Inner Race) are shown in fig. 15.12.

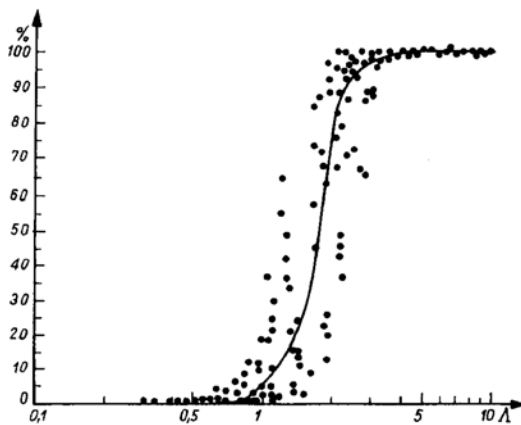


Fig. 15.8. Relationship between coefficient Λ and percentage of bearing contact-free operation (rolling bearing elements separated by lubricating

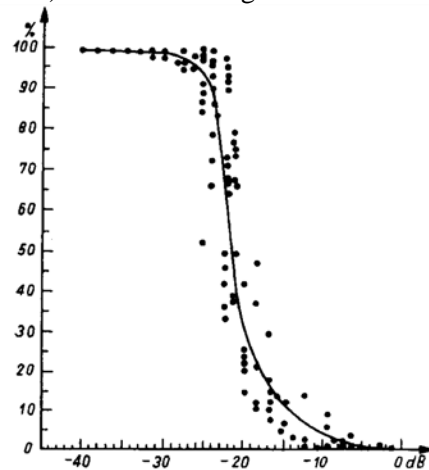


Fig. 15.9. Relationship between drop in signal level (dB) and percentage of bearing operation free of metallic contact.

film).

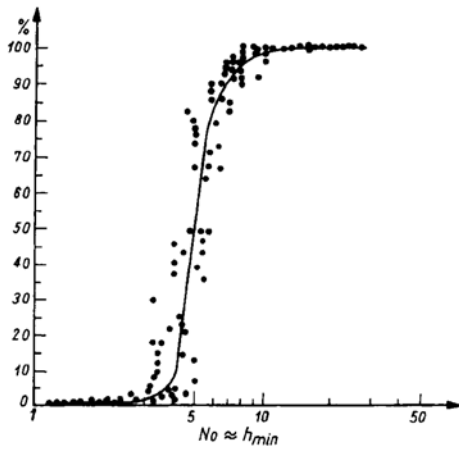


Fig. 15.10. Relationship between code number (proportional to lubricating film thickness) and percentage of contactless operation.

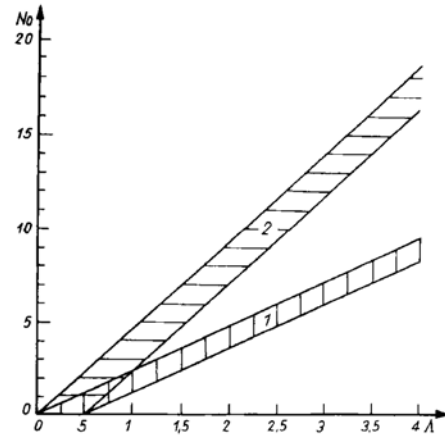


Fig. 15.11. Simplified diagram of relationship between value Λ and code number depending on rolling bearing type: 1 – ball bearing, 2 – roller bearing.

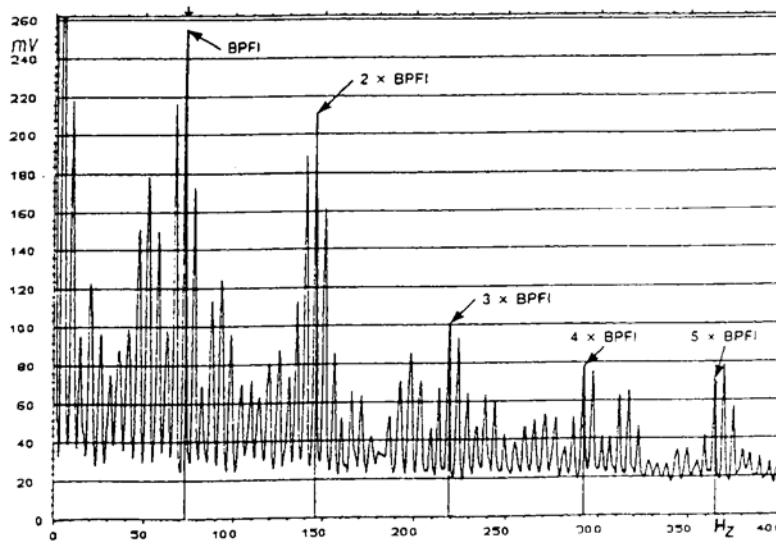


Fig. 15.12. Envelope spectrum of signal generated by rolling bearings: BPF1 – frequency of ball passage over damaged place (I – inner race).

Different vibration components may be generated in the case of a simultaneous occurrence of damage to the inner and outer races and to a ball. In practice, it may be difficult to identify the components when two faults occur simultaneously. Therefore research aimed at improving the envelope signal method is under way [15.4].

As mentioned earlier, the signal envelope method consists in the filtration of the signal to cut off low-frequency components arising from shaft runout and gear wheel meshing. After filtration the signal is subjected to the Hilbert transformation (10.56) and the envelope is found (chap. 10.1). Filtration can be performed for different frequency ranges. The impulses arising from damage may excite the natural frequency of the mechanical system or the signal receiver in a range up to 100 kHz. If several elements fail simultaneously, e.g. the inner race, the outer race and the rolling element, the faults may excite different resonance frequencies or one resonance frequency and thus increase the component density of the envelope spectrum.

| 1 | 2 | 3 | 4 | f_o, f_i, f_b, f_c |
|------|------------------------------|------------------------|--------|---|
| 50Hz | B&K 8307(#1) B&K 4393(#2) | 240N (#1) 260N (#2) | 100kHz | 152.47, 247.53, 198.52, 19.06Hz (5) |

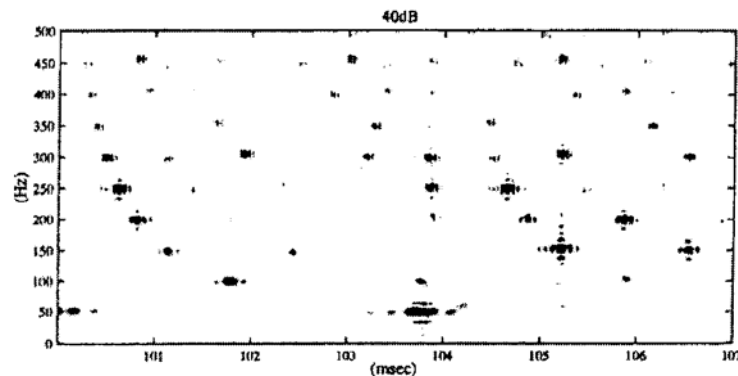


Fig. 15.13. Signal of rolling bearing condition, frequency versus period (filtered signal, signal above 10 kHz was assumed): 1 – shaft revolutions frequency, 2 – kind of piezoelectric transducer, 3 – value of applied radial force, 4 – signal sampling rate, 5 – frequency of ball passage over damage.

The method of assessing the condition of rolling bearings proposed for the case when several faults occur simultaneously consists in the analysis of the envelope signal obtained through synchronous summation, with a proper signal band filtered off. The spectrum is represented on a plane whose axes are functions of the synchronous period and frequency. The intensity of the signal is represented by the proper intensity of the colour filling the points, as shown in figs 15.13 and 15.14. The fault frequencies calculated from the formulas given in table 11.1 are listed in the table in fig. 15.13. The vibration periods corresponding to these frequencies are marked on the horizontal axis in the figures. Signal synchronous summation was performed for the 100-107 ms

range (fig. 15.13) and the 99-107 m. s range, passing the signal for frequencies higher than 10kHz (fig. 15.13). The result of the analysis for the signal passed through the filter within a range of 40-43 kHz is shown in fig. 15.14. After the filtering, signal envelopes were obtained which were subjected to synchronous summation with synchronous periods within the ranges given in figs 15.13 and 15.14. As a result, the signal generated by a defective bearing was cleaned of broad-band noise.

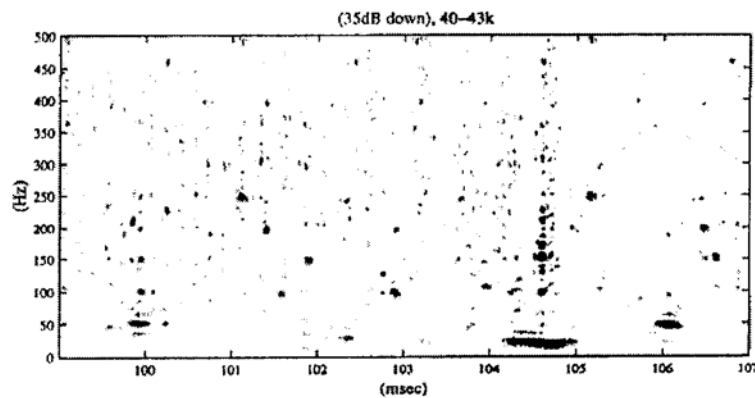


Fig. 15.14. Signal of rolling bearing condition, frequency versus period (filtered signal, signal from 40-43 kHz band was assumed).

15.1. References

- [15.1] Bartelmus W.: Vibration Condition Monitoring of Gearboxes, *Machine Vibration*, No. 1, pp. 178-189, 1992.
- [15.2] Brown D., Tensen T.: The Use of Spectrum Comparison Bearing Fault Detection, Briel & Kjaer Application Note BO 0253-11.
- [15.3] Sohoel E.: Shock Pulses as a Measure of the Lubricant film thickness in Rolling Element Bearings, *Proceedings of an International Conference on Condition Monitoring*, University College of Swansea, Pineridge Press U.K., 1984.
- [15.4] Wen-Yi Wang, Harrap M.: Sync-Period Frequency Analysis and its Application to the Diagnostic of Multiple Element Defects of Rolling Bearings, *Tribotest*, 1997.

16. Diagnostics of belt conveyors

16.1. Introduction

A schematic representation of the technical means used to monitor the condition of belt conveyors is shown in fig. 1.7. The diagnostic tool is a belt condition assessment gauge.

A belt conveyor (one of many designs) is shown schematically in fig. 16.1. The following can be distinguished there:

- a) driving drums,
- b) a return drum,
- c) a tightening drum,
- d) a guiding drum.

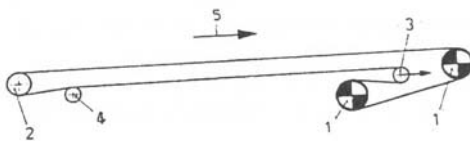


Fig. 16.1. Schematic of belt conveyor:
1 – driving drum, 2 – return drum,
3 – tightening drum, 4 – guiding drum,
5 – direction of belt movement.

The design of the driving drum and the guiding drum of a LEGMET belt conveyor is shown in fig. 16.2a and fig. 16.2b, respectively. The kinematic pairs which are subject to diagnosis are: the rolling elements and the races (outer and inner) of the rolling bearing. Also the balance of the drums (the balancing problem is presented in chap. 4.6) and their perpendicularity to the movement of the belt are diagnosed. The conveyor belt is supported by runners [16.1] in different arrangements (see fig. 16.3: the active section – arrangements A and the passive section – arrangements B). An exemplary runner design is shown in fig. 16.4 [16.1]. The diagnostics of the runner covers its rolling bearings, runout and unbalance.

The driving drum is driven by a power transmission system (fig. 16.5) consisting of an electric motor whose flexible or hydrodynamic coupling drives a gear transmission. The gear transmission's function is to reduce the rotational speed and increase the torque transmitted to the driving drum. The diagnosis covers the condition of the rolling bearings in the electric motor and the gear transmission, the condition of the gear transmission gearing, the balance of the coupling and the position of the gear trans-

mission relative to the driving drum. The methods of diagnosing the above subassemblies are the subject of the subsections that follow.

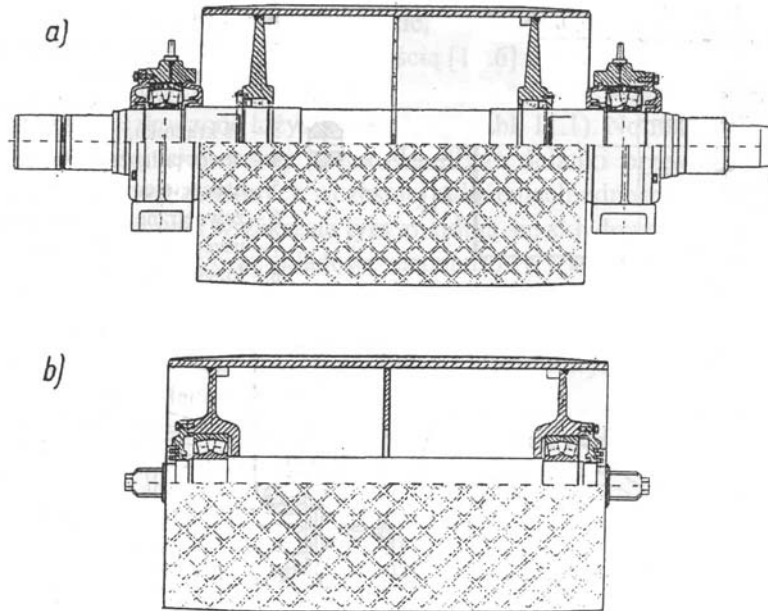


Fig. 16.2. Driving drum design, (a) guiding drum, (b)- LEGMET belt conveyor.

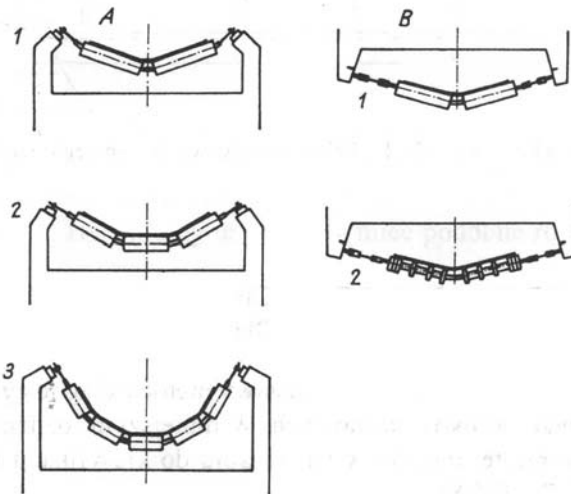


Fig. 16.3. Runner sets: A – runner sets supporting driving strand, 1 – two-runner set, 2 – three-runner set, 3 – five-runner set, B – runner set supporting driven strand, 1 – plain runners in V arrangement, 2 – runners with cleaning rubber rings in V arrangement.

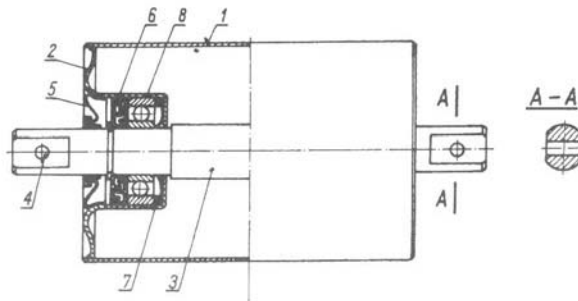


Fig. 16.4. Belt conveyor runner design:

- 1 – runner shell,
- 2 – rolling bearing casing,
- 3 – runner axis,
- 4 – connecting hole,
- 5 – outer seal,
- 6 – outer labyrinth seal,
- 7 – inner seal,
- 8 – runner bearing.

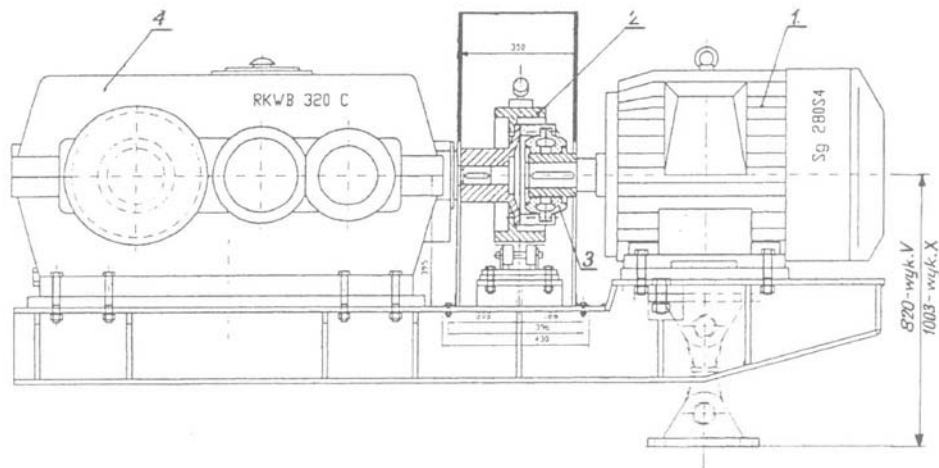


Fig. 16.5. Belt conveyor power transmission system: 1 – motor, 2 – brake drum, 3 – flexible coupling, 4 – gear transmission.

16.2. Diagnostics of belt conveyor gear transmissions

The fundamentals of the diagnostics of gear transmissions which drive belt conveyors are presented in [16.2] ÷ [16.6]. In this chapter an outline of the method, as it relates to the parameter classifications recommended in standards [16.7] and [16.8], is given.

Standard [16.7] (fig. 13.1) has the character of a general recommendation and it can be applied to the classification of gear transmission condition parameter values. The condition parameter is the wall vibration RMS value determined in the 10÷1000 Hz band. For gears (reducers) driven by motors with a rated speed of 750÷1500 rev./min the high-speed shaft runout components and harmonics and the gearing components and harmonics are in the 10÷1000 Hz band. Some illustrative spectra are shown in figs 11.3 and 11.8. By measuring the vibration RMS value in the 10÷1000

Hz band one cannot establish unequivocally the cause of a change in gear transmission condition. Measurements show that gearing components (the first two gear transmission stages) dominate in their intensity over the components originating from the high-speed shaft operating condition, i.e. the components generated by a defective bearing (components in table 11.1) [16.6]. Canadian standard [16.8] recommends measuring the RMS value of the gear transmission wall vibration velocity in a range of 10÷10000 Hz. For the assumptions about the rotational speed of electric motors made above, the components linked to the causes and the resonance vibration components excited by the impulses generated by defective rolling bearings are in this range. The above components are different than the kinematic components associated with the frequency of passage of a rolling element over a damaged place on a race (tab. 11.1). A classification of gearing condition parameters corresponding to narrowband components can be found in [16.9]. A condition classification method for signal parameters in the three ranges: 10÷1000 Hz, 100÷3500 Hz, 3500÷10000 Hz (tab. 16.1) is described in [16.2]-[16.6].

Tab. 16.1. Conventional set of preferred physical quantities. 1 – frequency range, 2 – vibration velocity, 3 – vibration acceleration

| 1 | 2 | 3 |
|------------|---|---|
| 1-100Hz | + | |
| 100-3500Hz | + | + |
| 3.5-10kHz | | + |

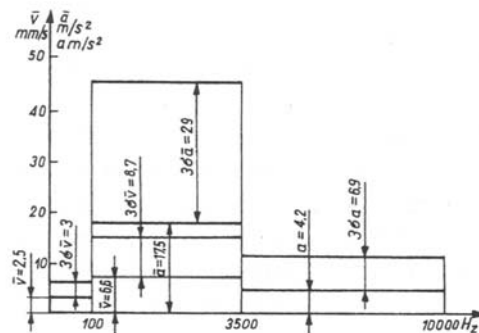


Fig. 16.1. Range of gear transmission condition symptoms values \bar{V} (10-100 Hz) mm/s, \bar{V} (100-3500 Hz) mm/s, \bar{a} (100-3500) m/s², a (3.5-10 kHz), mean value of set plus three standard deviations σ .

Fig. 16.6 shows why it is necessary to divide the signal into the bands. The signal in the 100÷3500 Hz dominates. Proper parameters are selected in the way described in [16.10]. The method of determining whether a proper place for the reception of the signal has been selected consists in comparing measurement histograms. The histograms should show similar distributions. The similarity can be established by finding a

match between the actual distributions and the theoretical ones (g – gamma, g_p – shifted gamma, l_n – logarithmic-normal, l_{np} – shifted logarithmic-normal). The degree of fit (expressed by a confidence level) to the above distributions is given in fig. 16.7. If the confidence levels for the gamma distribution are compared between the four signal reception points in fig. 16.8, one can notice a marked difference in point 3.

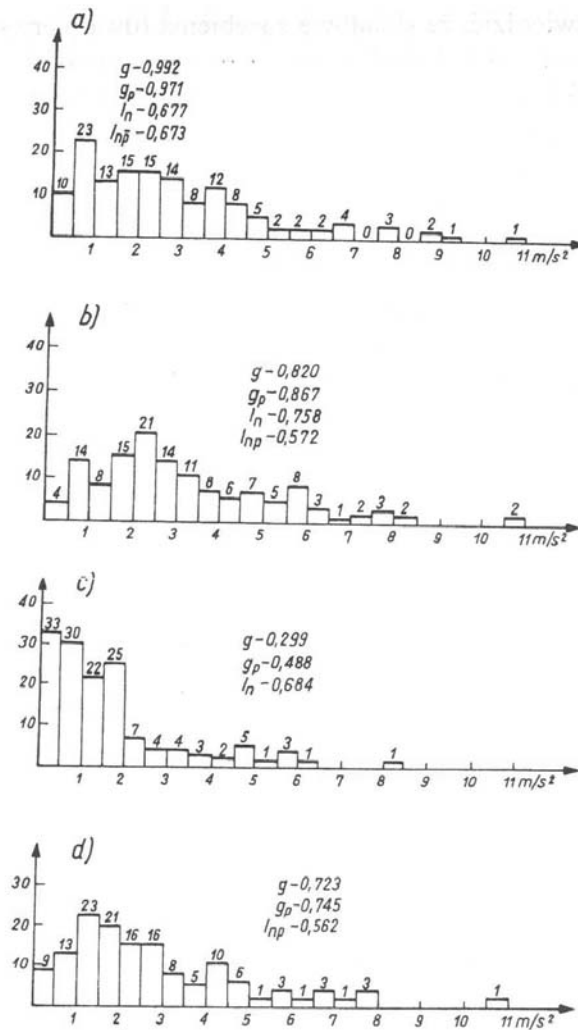


Fig. 16.2. Histograms of acceleration measurements for 3.5-10 kHz:
 a – measuring point 1, b – measuring point 2, c – measuring point 3, d – measuring point 4
 Confidence levels for: g – gamma distribution, g_p – shifted gamma distribution, l_n – logarithmic-normal distribution, l_{np} – shifted logarithmic-normal distribution. On axis of ordinates number of gear transmissions

16. Diagnostics of belt conveyors



Fig. 16.4. Diagnostic inference algorithm of gear transmission condition diagnostics system.

The classification of gearing condition according to [16.3] for parameter (symptom) a [m/s^2] (100÷3500 Hz) and a histogram of the measured values are presented in fig. 16.10. It follows from the classification that the parameter values are a function of the load. To plot the parameter in time, its values should be reduced to one load (fig. 16.11 – measurements x, y were reduced to values a, b).

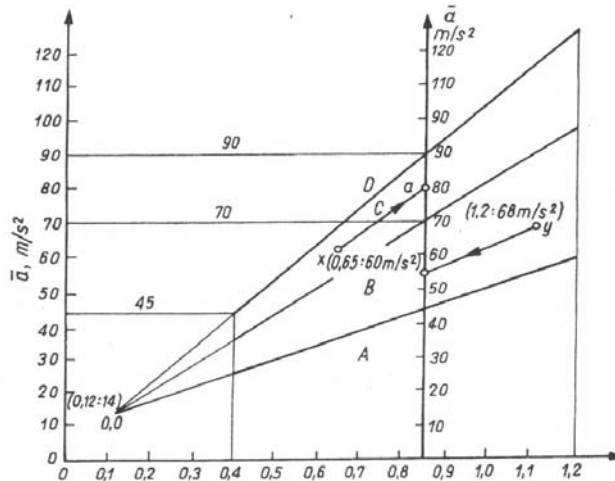


Fig. 16.6. Nomogram for converting measurement data for average acceleration values in range 100-3500 Hz: A+D – classes of gear transmissions, illustrative conversion of data: x to a and y to b .

When taking an operational decision one should check if relation $a = f(I/I_n)$ holds, where I/I_n is a relative value of driving motor current intensity (I_n – the rated current value). The check consists in determining the slope of a straight line in the linear relation by calculating the coefficient

$$\psi = (\bar{a}_2 - \bar{a}_1)/(I_1 - I_2) \quad \text{m}/(\text{s}^2\text{A}) \quad (16.1)$$

where \bar{a}_1, \bar{a}_2 – mean values calculated according to the above description for the 100÷3500 Hz for respectively: a load of about $0.85I_n$ and $0.5I_n$; I_1, I_2 – values corresponding to the smaller and greater load, respectively. The calculated values of ψ were taken into account in the inference algorithm in fig. 16.9. The operating condition of the high-speed shaft was divided into two classes A and B. The upper limit of class A was determined from the formula

$$\bar{v}_{lim} = \bar{v}_m + 3S_v \quad (16.2)$$

where S_v – the standard deviation (see fig. 16.6 where $v_{lim} = 5.5$ m/s which is within the ISO standard (fig. 13.1) and the condition is described as satisfactory (group T)). Therefore it was assumed that all the gear transmissions for which parameter \bar{v} differs

much from the rest should be checked and the cause of the deviation should be determined (improper motor setup, coupling runout, etc.).

The classification of rolling bearings is shown in fig. 16.12. The values of parameters (symptoms) a [m/s^2] (3.5 - 10 kHz) are a function of nD , where n – rotational speed [rev./min], D – the mean bearing diameter [m]. The upper limits of the classes were determined from the formulas:

- a) for class A $a_m + S_a$,
- b) for class B $a_m + 2S_a$,
- c) for class C $a_m + 3S_a$.

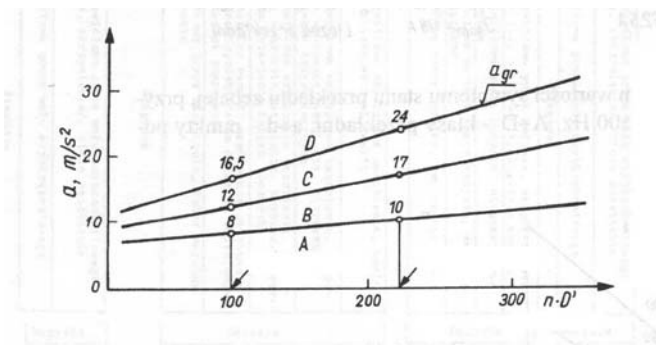


Fig. 16.7. Classification of rolling bearing condition for band 3.5-10 kHz: A→D – classes of gear transmissions, n – rotational speed, D' – the bearing diameter.

$n \cdot D'$ for points 3 and 4
 $n \cdot D'$ for points 1 and 2
 rev./min·m

If a histogram is drawn, most of the measurements should be within the limits of class A. When calculating parameters a_m and S_a of a set, all the recorded measured values should be taken into account.

A method of dividing the parameters (symptoms) into two classes, which according to the above interpretation corresponds to the economical replacement level, is given in [16.12]. In interpretation of gear transmission condition the interactions between the gear transmission's parts as shown in fig. 16.22 should be considered. Diagnostic signal parameters are represented against machine operation time as trends in gear transmission condition parameters (symptoms), as shown in figs 16.13 and 16.14. In the plots one can distinguish a gear transmission running-in period, a normal operation period and the beginning of a change in the condition. Figs 16.13a and b show plots for cases when the gearing condition parameters exceeded the boundary values and the gear transmissions were sent for repairs.

The condition of the gear transmissions was classified on the basis of experimental [16.13] and literature data [16.14]-[16.19], using the ferrographic method. The wear products were assigned the symbols of the existing classes and described as regards

their largest dimensions: l – particle size and g – particle thickness. Planar and volumetric particles of the scuffing and pitting type were distinguished. Scuffing particles were the result of intensive friction while pitting particles were the outcome of the fatigue of the working surfaces of the gearing and the rolling bearings. In addition, elements in the form of wires, spirals and balls of very small diameters (1–5 μm) were distinguished.

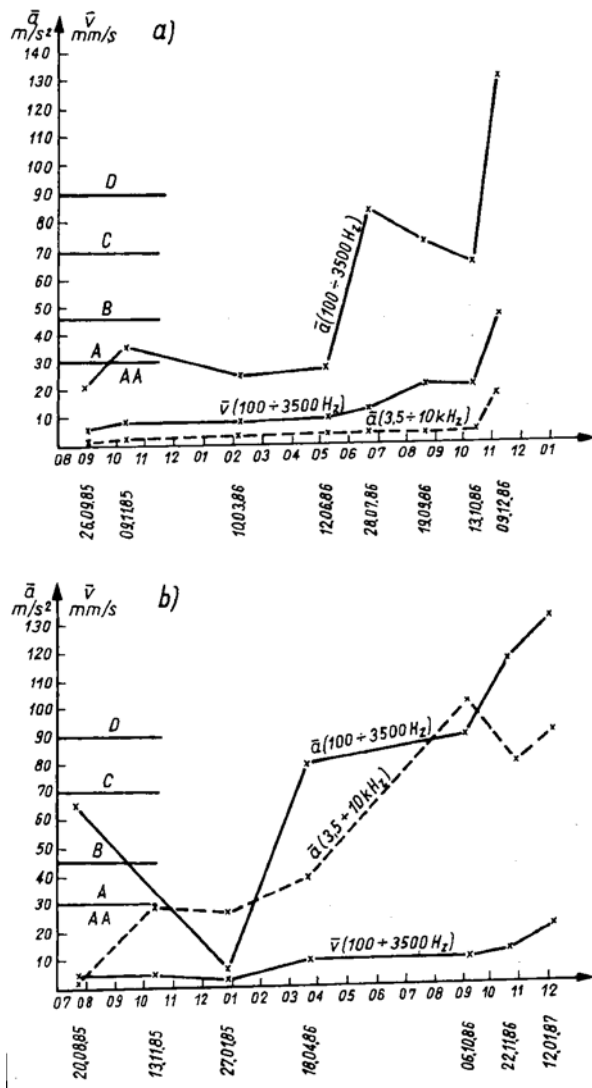


Fig. 16.8. Illustrative actual trend in belt conveyor gear transmission condition: examples (a) and (b), AA÷D – gear transmission classes.

The conditions described in standard [16.20] and reflected in ferrographic images should correspond to the particular classes of gear transmission condition:

Class AA – fine wear particles defined as wear products or micropitting, whose size is not larger than $15\ \mu\text{m}$ and thickness in the order of $0.25\div 0.5\ \mu\text{m}$ – according to [16.18], whereas according to [16.20], this corresponds to nonabrasive wear (super-finish wear) (compare fig. 9.1 and fig. 9.2). According to [16.20], characteristic micropitting flakes form (this is referred to as flaking).

Class A – temporary occurrence (at the beginning of service) of products resulting from abrasion or insufficient lubrication and possible occurrence of intensive micropitting (particles as large as $50\ \mu\text{m}$). According to [16.18], particles in the form of wires and spirals occur. Scratches propagating in the direction of slip (according to [16.20]), the problem of slip in gearing are considered in chap. 6.2.

Class B – wear products appear as a result of intensive friction (scuffing according to [16.18]) and pitting flakes with torn edges, much thicker than micropitting flakes occur.

Class C – the intensity of the products described in class B increases (size over $50\ \mu\text{m}$) and volumetric products of wear occur.

Class D – condition as in C, also large pitting damage occurs which is too large to be observed by ferrography (one should look for it on magnetic collectors or filters), this condition corresponds to destructive pitting. Also particles in the form of wires and spirals ($25\text{-}100\ \mu\text{m}$) occur.

A concise description of the relationship between the form of a particle and the class is provided below:

for gearing:

class AA – planar particles $l < 15\ \mu\text{m}$, $g = 0.25\div 0.5\ \mu\text{m}$;

class A – planar particles $l < 50\ \mu\text{m}$, $g = 0.25\div 0.5\ \mu\text{m}$;

class B – volumetric particles, scuffing $l = 20\div 50\ \mu\text{m}$, wires and spirals $25\div 100\ \mu\text{m}$;

class C – volumetric particles, scuffing $l > 50\ \mu\text{m}$, wires and spirals;

class D – volumetric particles, scuffing $l > 50\ \mu\text{m}$, pitting $l \gg 50\ \mu\text{m}$, wires and spirals $25\div 100\ \mu\text{m}$;

for rolling bearings:

class A – planar particles $l < 5\ \mu\text{m}$;

class BC – planar particles $l \leq 50\ \mu\text{m}$, wires and spirals $25\div 100\ \mu\text{m}$, balls $1\text{-}5\ \mu\text{m}$;

class D – volumetric particles pitting $l = 20\div 50\ \mu\text{m}$, pitting $l \gg 50\ \mu\text{m}$, wires and spirals $25\div 100\ \mu\text{m}$, balls $1\text{-}5\ \mu\text{m}$;

More information on the interpretation of particles (Z_a ; K ; Z_a) is given in chap. 10.2. Summing up, a vibration diagnostics method which consists in the analysis of the signal in wide bands $10\div 100\ \text{Hz}$; $100\div 3500\ \text{Hz}$ and $3.5\div 10\ \text{kHz}$ has been presented here (chap. 16.2). Good results and a significant economic effect were achieved by applying this method (chap. 16.5). The method's drawback is that fundamental gearing components occur in the $100\text{-}3500\ \text{Hz}$ band for the first and second stage. As a result it was impossible to determine whether a change in condition was taking place

in the gear transmission's first or second stage. On the whole, however, changes in condition occurred mostly in the first stage (approximately at a ratio of 100/1).

To separate the causes one should use the narrowband analysis (10.22) described in chap. 11. Also synchronous summation can be used to determine the time plots (figs 10.17 and 14.5) and the synchronous spectrum (10.45). Many ways of interpreting the plots of signals obtained by synchronous summation are presented in chap. 6.6-6.9 and in chap. 14. The signals were obtained by computer simulation.

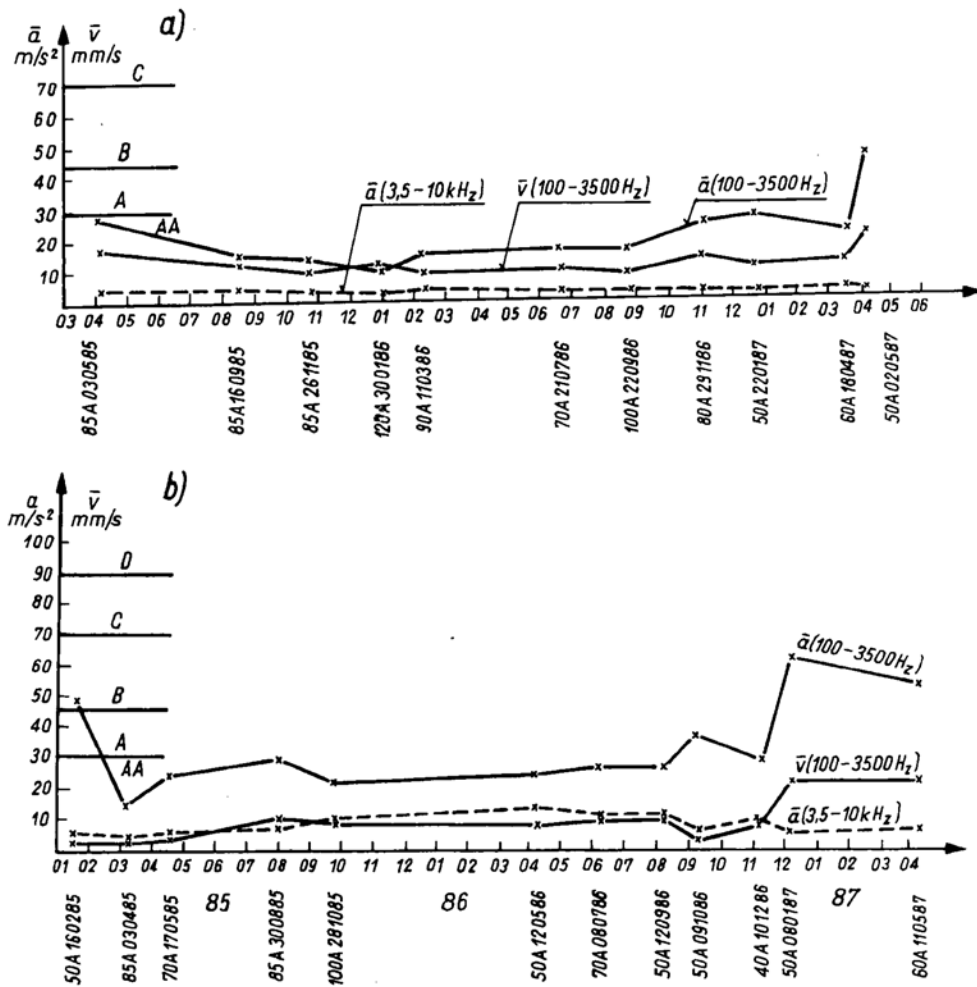


Fig. 16.9. Trend in condition of gear transmission from its installation in belt conveyor driving station to beginning of increase in condition parameters (a) and (b), AA+D – classes of gear transmissions.

16.3. Diagnostics of runners

16.3.1. Application of thermovision to runner diagnostics

The thermal phenomena that occur in the machine are described in general in chap. 10.3. The application of thermography to the assessment of the condition of belt conveyor runners is described in [16.23] where the results of tests carried out on 10000 runners are discussed. The condition of the runners was assessed on the basis of their temperature distributions near the rolling bearings. The increase in temperature above the ambient temperature and the temperature trend were determined (fig. 16.15). The following principle was adopted for condition assessment and repair policy formulation: if the runner rise 5°C over the ambient temperature, the runner shows a tendency towards a change in its condition and it should be replaced after three weeks (see fig. 16.15), the repair costs in this case amount to about 50% of the cost of a new runner; when the temperature rises more than 15°C above the ambient temperature, the runner is unreparable.

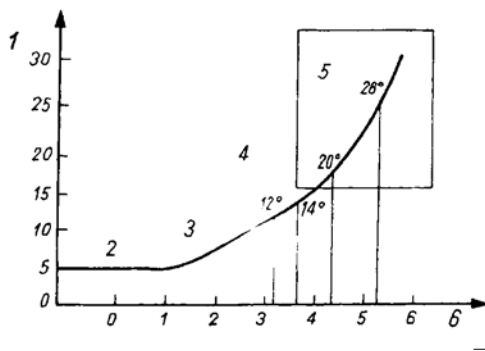


Fig. 16.1. Runner operating temperature trend reflecting changes in runner condition.

- 1 – rise in temperature above ambient temperature,
- 2 – rise in temperature for runner in suitable condition,
- 3 – rise in runner temperature caused by change in condition – runner can be repaired,
- 4 – rise in runner temperature caused by change in condition – runner cannot be restored to its original condition,
- 5 – failure condition temperature range,
- 6 – number of weeks.

16.3.2. Use of vibration and noise for assessment of runner condition

Also vibration and acoustic signals can be used in the diagnostics of runners. The way in which vibration and acoustic signal data are processed is described in [16.24] where measurements obtained from Dr G. Meltzer from the German Academy of Sciences Institute of Mechanics were subjected to a statistical analysis. The data related to 55 rolling bearings and had the form of measured quantities referred to as runner bearing condition symptoms. The symptoms were denoted by s_1-s_{12} . Symptoms s_1-s_4 were associated with noise, i.e.

s_1 – the level of noise in a frequency range of 500÷2000 Hz, dB;

s_2 – the level of noise in a frequency range of 4÷16 kHz, dB;

s_3 – the acoustic pressure determined on the basis of s_1 , mP;

s_4 – the acoustic pressure determined on the basis of s_2 , mP.

Symptoms s_5 - s_{12} were associated with vibration accelerations m/s^2 , i.e.

s_5 – vibration accelerations measured in the axial direction, frequency range 0.1÷1 kHz, m/s^2 ;

s_6 – vibration accelerations measured in the axial direction, frequency range 1÷11 kHz, m/s^2 ;

s_7 – (vertical) vibration accelerations measured in the radial direction, frequency range 0.1÷1 kHz, m/s^2 ;

s_8 – (vertical) vibration accelerations measured in the radial direction, frequency range 1÷11 kHz, m/s^2 ;

s_9 – (horizontal) vibration accelerations measured in the radial direction, frequency range 0.1÷1 kHz, m/s^2 ;

s_{10} – (horizontal) vibration accelerations measured in the radial direction, frequency range 1÷11 kHz, m/s^2 ;

s_{11} – resultant vibration accelerations as vector sum $s_5 + s_7 + s_9$,

s_{12} – resultant vibration accelerations as vector sum $s_6 + s_8 + s_{10}$.

It follows from the above vibration and noise frequency ranges that the only source of vibration and noise over 100 Hz are the bearings in the runners. Runner runout and unbalance may occur below 100 Hz.

The third octave spectrum of belt conveyor noise is shown in fig. 16.16. One of the symptoms (s_1) is the noise level in the 500÷2000 Hz range which includes the third octave components of highest intensity noise.

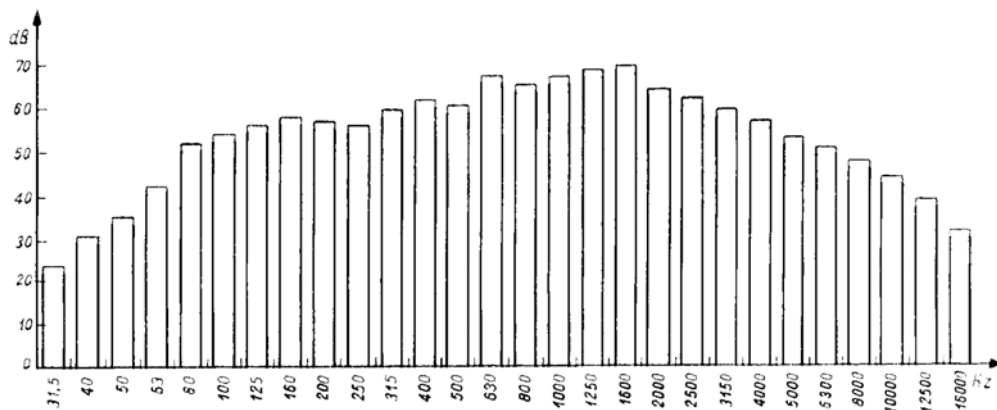


Fig. 16.1. Third octave spectrum of belt conveyor noise at distance of 3 m and height of 1.2 m.

A dynamic model of a section of a belt conveyor route is presented in chap. 9 where also the effect of runner runout and unbalance on the generation of vibrations by belt conveyor runners is analyzed. According to [16.25] and [16.26], the possible cause of the high intensity of noise in the 500÷2000 Hz band is excitation due to a change in the belt's stiffness or the unevenness of the belt's surface – causes unrelated to the condition of the rolling bearing. The noise components in the above band are also modulated by the low-frequency components. This results in the spectrum shown in fig. 8.11. Therefore one say that the noise in the 500÷2000 Hz band has no relation to the condition of rolling bearings. The vibration or noise components arising from local damage to *rolling element–race* kinematic pairs do not occur in the 500÷2000 Hz band. The frequencies of the components can be calculated from formulas (7.10), (7.16) and (7.36) and in the considered case they are below 500 Hz. This raises doubts about the results reported in [16.24] and the recommendations about the selection of rolling bearing condition symptoms made there. The recommendations comprise many different combinations of symptoms which include symptoms s_1 and s_3 that do not carry information about rolling bearing condition. Since the diagnostics of the condition of runner rolling bearings arouses controversies, further research in this area is under way, e.g. [16.25], [16.26] and [16.27].

16.4. Diagnostics of condition of conveyor belts with steel cables

The structure of the conveyor belt which incorporates steel cables is shown in fig. 16.17. The belt consists of an upper and lower cover and a core with cord made of steel cables sealed in it. Structural details of different conveyor belts can be found in [16.28].

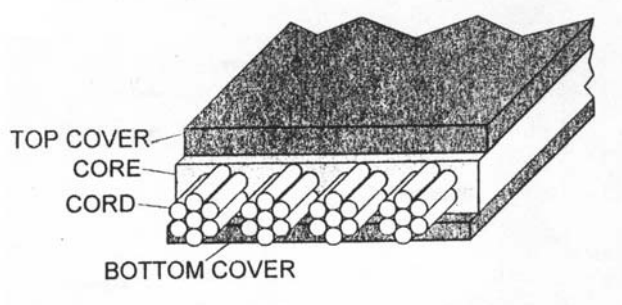


Fig. 16.1. Structure of conveyor belt with steel cables

The diagnostics covers external and internal corrosion of the steel wires and splices in the steel cables (fig. 16.18). As a result of corrosion the wires may be broken with their ends still being in contact (16.19a) or separated by a gap (fig. 16.19b). The diag-

nostics also covers belt splices (the layout of steel cables in a belt splice is shown in fig. 16.20).

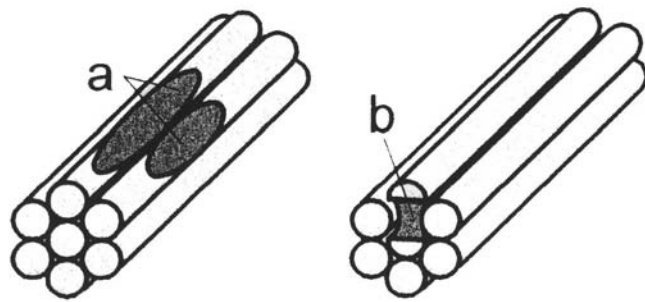


Fig. 16.2. External (1) and internal (2) corrosion of steel cables.

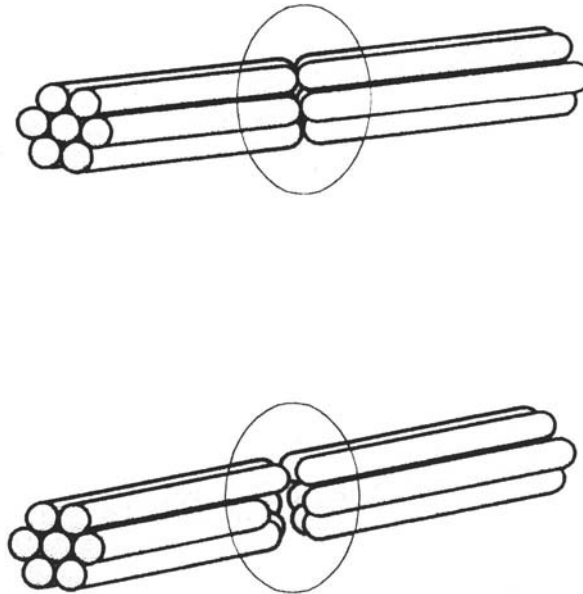


Fig. 16.3. Ends of broken steel cables: (a) being in contact and (b) separated by gap.

The latest method of assessing the condition of a belt with steel cables, called BELT C.A.T. (Cable Anomaly Tomography), is described in [16.29]. The method is based on a recently patented measuring technique consisting in the measurement of differential magnetic reluctance. In this way data on the condition of the steel cables in the belt are generated. The data are unaffected by fluctuations in belt velocity, belt flutter (vertical vibrations), the structure of the residual magnetism in the belt, strong external electromagnetic fields, the size of the wires in the cord or the pitch (the distance between the steel cables).



Fig. 16.4. Structure of belt splice.

Assessments can be made for a fully loaded conveyor running at full belt speed. Only one set of measuring heads mounted on one side of the belt is used. The BELT C.A.T. method enables the accurate measurement of the condition of the splice and all types of damage to the steel cables with the precise location of damage along the belt's length and width.

The conveyor belt monitoring method (C.B.N) developed by Harrison [16.30] has been widely used in the world. However, as pointed out in [16.29], it has several limitations:

- a) it is sensitive to belt flutter – two sets of measuring heads on both sides of the belt are needed to reduce this effect,
- b) low sensitivity – small faults are undetectable,
- c) low accuracy in locating damage along the belt's width,
- d) the measured signal is recorded by an analog plotter and so low resolution between faults along the belt's length is obtained,
- e) errors caused by the residual magnetism in the steel cables can occur.

The BELT C.A.T. method is free of the above limitations owing to the application of modern digital methods of data processing. For example, 750000 measurement data per second are recorded at a belt width of 2640 mm and a belt velocity of 7 m/s. The same data are recorded on two independent disks: the data from one of the disks are processed electronically to diagnose the condition of the belt while the other disk is stored in an archive in case the data are lost prior to their processing. The data are

processed to produce a report as shown in fig. 16.21 (the actual image is not black and white but a multicolour one). Green indicates a mass decrement in belt damage, red – a mass increment in the steel cord skeleton.

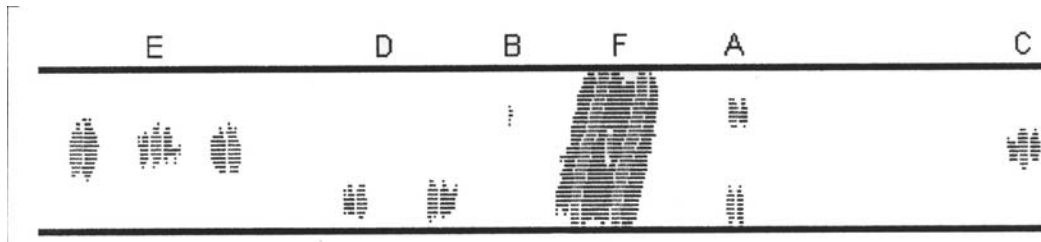


Fig. 16.5. Image obtained from diagnosis of belt with steel cables [16.29].

If corrosion occurs (fig. 16.21A), the image shows a series of green dots along the belt. In the case of severe corrosion, the image shows a series of red dots situated lengthwise. If the wires are damaged so that their ends become separated (fig. 16.21b), the image will show red or green dots situated transversely to the direction in which the belt runs. The colour depends on the degree of damage to single wires: the wider the image in the transverse direction, the larger the number of damaged wires. Since the black and white image does not allow full interpretation, fig. 16.21 will not be interpreted. But it should be noted that fig. 16.21f shows an image of a belt splice, which is used for the assessment of the quality of belt splice execution and the in-service condition of the belt splice.

16.5. Benefits stemming from use of technological diagnostics

The benefits resulting from the use of technological diagnostics are shown by applying the diagnostic method presented in chap. 16.2 and the gear transmission diagnostics subsystems described in chap. 19.2. to the diagnosis of 1000 kW gear transmissions in belt conveyors. The belt conveyors transport overburden with a high sand content. Fine sand particles are easily carried by wind and get into the gear transmissions, causing abrasive wear of the rolling bearings. This leads to a change in the condition of intermeshing, particularly that of the bevel gears. The interaction of the particular gear transmission elements is shown in fig. 16.22. Before the introduction of the objective assessment of the condition of the gear transmissions, the condition had been evaluated subjectively on the basis of auditory impressions and routine surveys consisting in the indirect measurement of the gear transmission high-speed shaft clearance (by shifting the shaft axially and lifting it within the clearance limits). In practice, gear transmissions degraded beyond repair would often be sent for repairs.

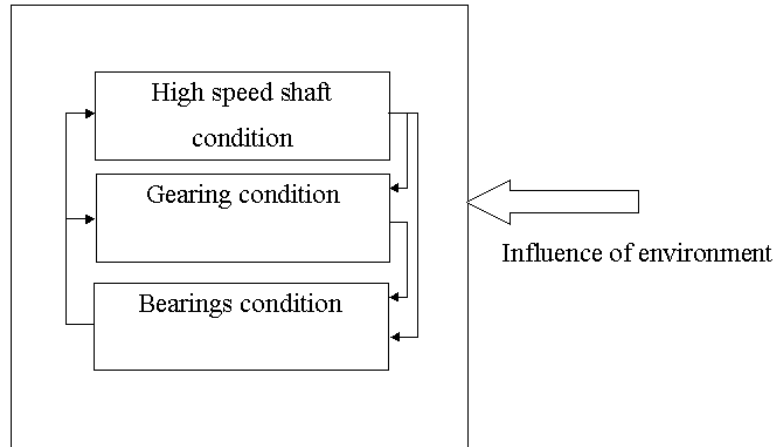


Fig. 16.1. Interaction between gear transmission elements.

The gear transmissions are monitored mainly to avoid failures which may lead to production losses or losses associated with the restoration of a gear transmission to its original condition (corresponding to a new gear transmission). Besides the avoidance of failures, the use of the objective diagnostic method contributes towards the optimization of durability and a reduction in the costs of repairs. Owing to the early detection of a change in the condition of a gear transmission one can set a date for its repair taking into account the production tasks (the decision taking problem is discussed in chap. 19.2). The benefits which resulted from the introduction of technological diagnostics are listed in tables 16.3 and 16.4. The main objective was to avoid a gear transmission failure which could lead to the stoppage of the technological process. In table 16.3, $\Sigma[h]$ stands for the total number of stoppage hours due to a gear transmission failure. The data are for the period of one year: 1984/85, 1985/86 and 1986/87, respectively. As table 16.3 shows, the main objective was achieved: stoppages due to gear transmission failures were eliminated. Also the life of the gear transmissions was extended. Previously, the life of the gear transmissions had been estimated at 3.5 years. The mean life of the gear transmissions was calculated as the ratio of number of installed gear transmissions N_z to number of gear transmissions sent for repairs N_r . According to table 16.3, this ratio in the period 1984/85 was 2.8, i.e. the mean life of the gear transmissions was 2.8 years. In the period 1985/86 it was only two years. $N_z = 160$ was assumed in each of the periods and the installed new gear transmissions were not taken into account. Before the diagnostic method was introduced the mean gear transmission life had been 2.8 and showed downward tendency in comparison with the original life of 3.5. It had been impossible to restore the gear transmissions to their original condition because the decisions about sending them for repairs had been taken on the basis of subjective evaluations (the gear transmissions had been highly degraded). According to table 16.3, in the second year after the introduction of techno-

logical diagnostics the life increased to 5 years and was sustained in the following years. Table 16.1 gives also the number of manhours spent on the repairs of the gear transmissions. The table shows a marked decrease in manhours, which means a cost reduction. The decrease in the costs of repairs is also reflected in table 16.4 in which the elements which were replaced during the repairs are listed and their number is given.

Tab. 16.1. Effect from use of technological diagnostics for 1000 kW gear transmissions.

| Specification | Before introduction of diagnostic method (1984/85) | First year (1985/86) of use of diagnostic method | Second year (1986/87) of use of diagnostic method |
|---|--|--|---|
| Number of installed gear transmissions | 160 | 200 | 200 |
| Number of gear transmissions sent for repairs | 57 | 81 | 40 |
| $\Sigma(h)$ | 42.3 | 19 | 0 |
| Total manhours spent on repairs, h | 27139 | 21579 | 7509 |
| Total economic effect, zł | | 20017176PLN | 31685416PLN |

Tab. 16.2. Replaced gear transmission parts before and after introduction of diagnostic method.

| Part name | Number of replaced parts before introduction of diagnostic method | Number of replaced parts in second year of use of diagnostic method | Difference (pieces) |
|---------------------|---|---|---------------------|
| Bearing 293332 | 85 | 61 | 24 |
| Bearing22232 | 67 | 49 | 18 |
| Bearing22252 W35 | 8 | 13 | -5 |
| Bearing23152 | 37 | 32 | 5 |
| Bearing23152 W33 | 6 | 8 | -2 |
| Bearing23096 | 30 | 26 | 4 |
| Bearing23096 W33 | 8 | 6 | 2 |
| Bearing22332 | 124 | 80 | 44 |
| Bronze sleeve | 12 | 8 | 4 |
| Bevel toothed shaft | 11 | 7 | 4 |
| Bevel gear | 3 | 1 | 2 |
| Transverse shaft | 3 | 1 | 2 |

The effects obtained by introducing technological diagnostics stem from optimization, which covers expenditures on diagnostics, and the substantial costs of repairs of gear transmissions (labour and materials costs, tables 16.3 and 16.4) and production losses (table 16.3, $\Sigma[h]$). The total costs involved in the maintenance of gear transmissions have a certain optimum value illustrated in fig. 16.23. A reduction in the costs of repairs and in production losses is obtained by increasing expenditures on diagnostics.

Optimum expenditures on diagnostics should be determined in order to obtain optimum expenditures on maintenance and diagnostics.

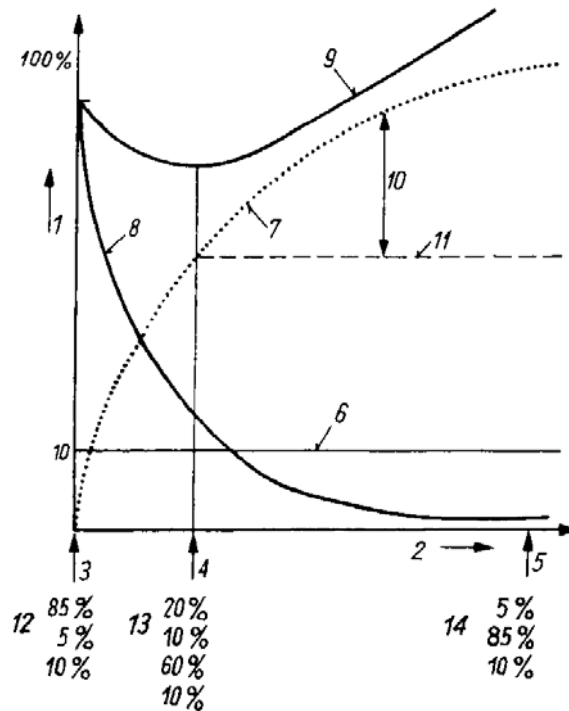


Fig. 16.2. Machine diagnostics and maintenance expenditures optimization curve.

1 – total costs of maintenance of machines; 2 – degree of commitment to maintenance of machines; 3 – no program of machines maintenance; 4 – economic commitment to machine maintenance; 5 – excessive commitment to machine maintenance; 7 – costs in case of no machine maintenance strategy, operation until failure; 9 – total costs of machine maintenance; 10 – cost of excessive commitment to machine maintenance; 11 – optimum level of machine maintenance costs; 12 – cost components: 85% – repairing damage caused by unforeseen failure, 5% – repairing damage caused by anticipated failures, 10% – other costs; 13 – cost components: 20% – cost reduction under planned machine maintenance strategy, 10% – repairing damage caused by unforeseen failures, 60% – repairing damage caused by anticipated failures, 10% – other costs; 14 – cost components: 5% – repairing damage caused by unforeseen failures, 85% – repairing damage caused by anticipated failures, 10% – other costs.

16.6. Statistical analysis of diagnostic database

Such data as the mean value or the standard deviation which belong to the set of diagnostic data are helpful in determining condition classes (16.2) on which diagnostic decisions are based. In this chapter results of statistical analyses which may be useful in the case of simple diagnostic methods are reported. The analyses of the results vali-

date the method of gear transmission diagnosis presented in chap. 16.2. The gear transmission measurement data were for two periods: 1) the first year of use of the diagnostics described in chap. 16.2, which led to the elimination of the gear transmissions being in improper condition and 2) the following year – in which the data were analyzed and compared with the actual condition of the gear transmissions and on this basis boundary values represented by condition classes (gearing condition classes regarded as most important for the assessment of gear transmission condition) were adopted (fig. 16.11). The ranges of the data for gear transmissions being in good condition are shown in fig. 16.6. Also the class limits shown in fig. 16.12, the mean values of the sets and the standard deviations were determined. Types of theoretical distributions were assigned to the obtained statistical data. Illustrative histograms of the statistical data are shown in fig. 16.7. The gamma distribution, the shifted gamma distribution and the logarithmic-normal distribution showed the highest confidence levels for statistical data assignment to theoretical distribution. It should be noted that the economic factor, i.e. the costs of repair of the gear transmission, was taken into account when selecting the boundary values. The classes are separated by standard deviation values or their multiples (16.2). This means that condition boundary values are determined in a somewhat subjective way since an expert or a team of experts ultimately decides what gear transmission condition limits are adopted. To investigate the parameters and the shape of the distribution more closely, the statistical analysis described in [16.31] was carried out. Diagnostic measurements were made at every two months as shown in fig. 6.14a and b. The next measurements for a given set of measurements are referred to as: first, second, third, etc. For the respective sets of parameters (first, fourth, fifth, sixth and seventh) the values of the distribution parameters, i.e. the mean value (tab. 16.5) and the standard deviation (tab. 16.6) were calculated.

The table shows some variation in the values of the parameters, but on the whole they remain pretty constant. Also the type of theoretical distribution which they can be described by was determined. The distribution is the logarithmic-normal distribution. In [16.32] a way in which machine condition critical value could be determined on the basis of the statistical distribution of data was sought. The data distribution is regarded as a machine reliable operation probability density distribution. Since the data are symptoms of machine condition, as their values increase, the probability of fulfilling the tasks by the machine and hence its reliability decrease. Nevertheless, a small probability that it will fulfil its tasks still remains. Therefore a decision must be taken whether the machine is in failure condition at a given value of symptom S_b . Two errors are possible:

1. the machine is in good condition but is judged to be defective (probability – P^{b1}),
2. the machine is defective, but it is judged to be “good” (probability – P^{b2}).

S_b should be selected as optimum from the point of view of a certain criterion. The Neyman-Pearson criterion $P^{b1} = const$; $P^{b2} - min$ was adopted in [16.32].

Tab. 16.1. Mean values of distribution parameters.

| | | | | | |
|--------------------------|------|------|-------|------|-------|
| \bar{v} (10 -100Hz) | 1.65 | 1.02 | 1.44 | 0.87 | 1.09 |
| \bar{v} (100 - 3500Hz) | 2.89 | 2.75 | 3.0 | 3.32 | 2.88 |
| \bar{a} (100 - 3500Hz) | 9.26 | 9.23 | 11.77 | 8.81 | 10.10 |
| 1p. a(3.5 - 10kHz) | 2.95 | 2.55 | 2.57 | 2.63 | 3.28 |
| 2p. a(3.5 - 10kHz) | 2.50 | 2.38 | 2.67 | 2.70 | 2.75 |
| 3p. a(3.5 - 10kHz) | 1.51 | 1.18 | 1.19 | 1.29 | 1.45 |
| 4p. a(3.5 - 10kHz) | 2.04 | 1.57 | 2.30 | 2.17 | 2.29 |

(1p.-4p. refers to points 1-4)

Tab. 16.2. Standard deviation values.

| | | | | | |
|--------------------------|-------|-------|-------|-------|-------|
| \bar{v} (10 -100Hz) | 2.56 | 2.37 | 2.70 | 2.38 | 2.65 |
| \bar{v} (100 - 3500Hz) | 6.57 | 6.67 | 6.59 | 6.82 | 6.51 |
| \bar{a} (100 - 3500Hz) | 16.89 | 17.52 | 17.38 | 17.65 | 18.33 |
| 1p. a(3.5 - 10kHz) | 3.67 | 3.70 | 3.73 | 3.99 | 3.99 |
| 2p. a(3.5 - 10kHz) | 3.97 | 3.81 | 4.20 | 4.46 | 4.56 |
| 3p. a(3.5 - 10kHz) | 1.77 | 1.82 | 1.79 | 1.95 | 2.24 |
| 4p. a(3.5 - 10kHz) | 2.99 | 2.82 | 3.11 | 3.15 | 3.52 |

(1p.-4p. refers to points 1-4)

In [16.32] one can find the following equation for the critical value:

$$\int_{s_b}^{\infty} p(s) ds = A / P_g \quad (16.3)$$

where: $p(s)$ – a diagnostic symptom probability density distribution,

A – probability of doing unnecessary repairs,

P_g – a coefficient of machine utilization.

Ratio A/P_g includes a permissible risk of making error 1 (proposed values 0.02÷0.05). The results of a statistical analysis of the data contained in a gear transmission database are reported in [16.33]. The diagnostic method which was used there is described in chap. 16.2. It was found that most of the statistical data could be described by the logarithmic-normal distribution. For this purpose, tests were carried out to determine to what distributions they belonged. The Erlang distribution, the gamma distribution, the logarithmic-normal distribution and the Weibull distribution were considered. The results of the analysis conforming to [16.32] for the logarithmic-normal distribution are presented in table 16.7 where values of the distribution parameters are given for the assumed error risk of 5% and 2%.

Tab. 16.3. Analytical results for logarithmic-normal distribution.

| Diagnostic parameter | Distribution parameter | Value 5% | Value 2% | Used critical values |
|---|------------------------|----------|----------|----------------------|
| Velocity v [mm/s] 10-100Hz | 2.67 1.57 | 5.609 | 7.02 | 7 |
| Velocity v [mm/s] 100-3500Hz | 7.56 3.923 | 14.98 | 18.29 | 13, 20, 25,30 |
| Acceleration a [m/s ²] 100-3500Hz | 35.19 13.88 | 61.19 | 71.48 | 30, 45, 70, 90 |
| Acceleration a [m/s ²] 3.5-10kHz, pints 1, 2 | 3.16 2.93 | 8.47 | 11.69 | 9.85, 16, 23 |
| Acceleration a [m/s ²] 3.5-10kHz, Points 3, 4 | 2.67 2.09 | 6.55 | 8.69 | 7.51, 10.83, 14.95 |

The obtained results showed some agreement with the used boundary values. According to table 16.7, the boundary value for vibration velocity should be 7.02 mm/s for 2% error 1. A boundary value of 7 mm/s is assumed according to (16.2) and the parameters given in table 16.7. A gearing condition classification based on the vibration acceleration parameter is presented in fig. 16.11. According to this classification, the upper vibration acceleration value is 70 m/s² for class B and the boundary value (table 16.7) for a 2% error is 71.48 m/s². The interpretation of gear transmission condition classes in fig. 16.9 indicates that a class C gear transmission has a limited life – the gearing and the rolling bearings are defective. According to figs. 16.9 and 19.7, the gear transmission will be included in a group of gear transmissions which should be replaced and sent for repairs.

The results of the statistical analysis presented in [16.33] as statistical distribution parameters, i.e. the mean value and the standard deviation, show an increment in comparison with the previous results presented in fig. 16.6 and tables 16.5 and 16.6. The obtained increase in the parameter values indicates that most of the gear transmissions were sent for repairs when their condition had deteriorated much. This puts in doubt the economic benefits gained in the first period of use of the diagnostics (see chap. 16.5).

16.7. References

- [16.1] Durst W., Vogt W.: Bucket Wheel Excavator, Tans Tech Publications, 1988.
- [16.2] Bartelmus W.: Reliability and Diagnostics of Toothed Gears for Belt Conveyor Drives, 1st International Conference on Reliability and Durability of Machines and Machinery Systems in Mining, Szczyrk Poland, 1986, Gliwice, Silesian Polytechnic, 1986.
- [16.3] Bartelmus W.: Classification of Bevel Gear Conditions, Proceedings of International Conference on Condition Monitoring, University College of Swansea, Pineridge Press U.K., 31st March–3rd April 1987.

- [16.4] Bartelmus W.: Diagnostic of Bevel and Cylindrical Gears in Surface Mines, Proceedings of the Second International Symposium on Continuous Surface Mining, Austin Texas, 1988, pp. 131-144, Rotterdam A. A. Balliema, 1988.
- [16.5] Bartelmus W.: Vibration Diagnostics of Bevel Gear Transmissions (in Polish), *Zagadnienia Eksploatacji*, No. 4, pp. 561-571, 1989.
- [16.6] Bartelmus W.: Vibration Condition Monitoring of Gearboxes, *Machine Vibration*, No. 1, pp. 178-189, 1992.
- [16.7] ISO 3945–1997: Mechanical Vibration of Large Rotating Machines With Speed Range from 10-200 rev/s, Measurement and Evaluation of Vibration Severity in Site.
- [16.8] Vibration Limits for Maintenance, Canadian Government Specification CDA/MS/NVSH 107, Criteria for Bearing Vibration Measurements (10-10000 Hz).
- [16.9] Vibration and Acoustic Measurement Handbook, Spartan Books, New York–Washington, 1972.
- [16.10] Bartelmus W.: Selection of Diagnostic Parameters and Diagnostic Signal Receiving Points, Proceedings of International Conference on Noise Control Engineering, Cracow Poland, September, 1988, Vol. II, pp. 533-536, Cracow, AGH 1988.
- [16.11] Bartelmus W.: Diagnostics of Gear Transmissions (in Polish), *Górnictwo Odkrywkowe*, No. 2, pp. 1-44, 1991.
- [16.12] Cempel C.: Passive Diagnostic and Reliability Experiment and its Application in Machine Condition Monitoring, *Condition Monitoring 84*, University College of Swansea, Pineridge Press U.K., 1987.
- [16.13] Bartelmus W., Fleszyńska B.: Ferrographic Investigations Carried Out on Hydraulic Systems and Gear Transmissions of Bucket Wheel Drives of Excavators (in Polish), Wrocław, Poltegor 1989, Arch. No. 1823/ONB (unpublished).
- [16.14] Scott D., Seifert W., Westcott V. C.: Ferrography – an Advanced Design Aid for the 80s, *Wear*, Vol. 34, pp. 251-260, 1975.
- [16.15] Levis D.S.: Machinery Health Monitoring Evaluation at Mining Research and Development Establishment, *Condition Monitoring 84*, University College of Swansea, pp. 470-484, April 1984.
- [16.16] Mason A. R.: The Development, Proving and Application of an In-Line Metal Particle Detector (MPD), *Condition Monitoring 84*, University College of Swansea, pp. 637-659, April 1984.
- [16.17] Reda A.A., Bowen R., Westcott V. C.: Characteristics of Particles Generated at the Interface Between Sliding Steel Surfaces, *Wear*, Vol. 34, pp. 261-273, 1975.
- [16.18] Yarrow A. S. Gadd P.: The Role of Ferrography in the Monitoring of Helicopter Assemblies, *Condition Monitoring 84*, University College of Swansea, pp. 503-524, April 1984.
- [16.19] Bowen E.R., Westcott V. C.: *Wear Particle Atlas*, Prepared for the Naval Air Engineering Centre, Lakehurst, July 1976.
- [16.20] PN–67/M–88506 Gear Transmissions, *Wear and Failures*, Terms and Definitions (in Polish).
- [16.21] Bartelmus W.: Application of Some Vibration Signal Statistical Estimators as Gearing Condition Assessment Criteria (in Polish), *Scientific Papers of Silesian Polytechnic, Mining*, No. 616, 1979.
- [16.22] Bartelmus W.: Application of Some Statistical Estimators of Vibration Signal as Criteria of Assessment of Mesh State, Proceedings of an International Conference on Condition Monitoring, University College of Swansea, April 1984.
- [16.23] Riley LR.: Infra-red Condition Monitoring Application, Proceeding of an International Conference on Condition Monitoring, University College of Swansea, U. K., pp. 635-643, March 1994.
- [16.24] Nowicki R. et al.: Evaluation of Vibroacoustic Diagnostic Symptoms by Means of the Rough Sets Theory, *Knowledge Engineering, Computer in Industry*, Vol. 20, pp. 141-152, 1992.

- [16.25] Bartelmus W., Gładysiewicz L., Sawicki W.: Causes of Belt Conveyor Noise (in Polish), Scientific Papers of Institute of Mining, Wrocław University of Technology, No. 79, Conferences No. 19.
- [16.26] Bartelmus W., Gładysiewicz L., Sawicki W.: Structure of Belt Conveyor Route Noise Spectrum (in Polish), No. 80, Conferences, No. 20.
- [16.27] Bartelmus W.: Mathematical Modelling and Computer Simulation of Conveyor Belt Mechanical parts Cooperation for Supporting Diagnostic Inference, Proceedings of the Sixth International Symposium on Mine Planning and Equipment Selection, Ostrava, the Czech Republic, 1997, Rotterdam. A. A. Balliema, 1997.
- [16.28] Żur T., Hardygóra M.: Belt Conveyors in Mining (in Polish), Katowice, Wyd. „Śląsk”, 1996.
- [16.29] Kuzik L., Blum W.: Scanning Steel Cord Conveyor Belts with the „BELT C.A.T.TM” MDR System, Bulk Solids Handling, Vol. 16, No. 3, 1996.
- [16.30] Harrison A.: Use of Reference Signatures to Monitor Belt Splices, SME Bulk Material Handling by Conveyor Belt, Technical Symposium Compendium, pp. 49-53.
- [16.31] Bartelmus W., Rekuć L.: Computer Analysis of Acquired Diagnostic Data (in Polish), Wrocław, Poltegor, Arch. No. 1840/ONB (unpublished), 1989.
- [16.32] Cempel C.: Passive Diagnostic Experiment, Symptom Reliability and its Applications in Vibration Condition Monitoring, Zagadnienia Eksploatacji Maszyn, Vol. 25, No. 2-3, 1990.
- [16.33] Rekuć L.: Analysis of Statistical Data Stored in Belchatów Brown Coal Mine Databases (in Polish), Wrocław, Poltegor, No. 2793/IGO (unpublished), 1991.

17. Diagnostics of bucket wheel excavators and stackers

17.1. Introduction

The bucket wheel excavator with the elements to be monitored to ensure its safety is shown in fig.1.6. As already mentioned, mainly the operating and safety parameters are monitored. To devise condition monitoring for the kinematic pairs of BWE subassemblies one must know the structure of the excavator, including that of the kinematic pairs which determine the reliability of its operation. The main parts of BWE are shown (after [17.1]) in fig. 17.1. These are: crawler travel gear (1), undercarriage (2), turntable (3), slew load-bearing structure (4), boom (5), bucket wheel (6), hoisting mechanism (7), discharge boom (8).

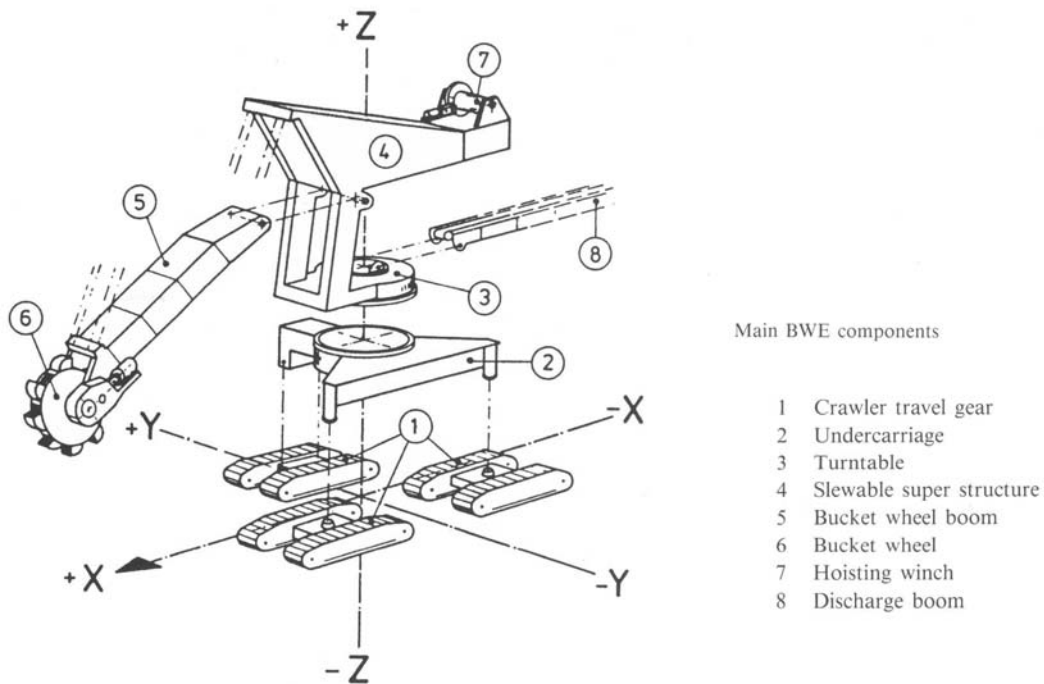


Fig. 17.1. Main subassemblies of BWE:

1 – crawler travel gear, 2 – undercarriage, 3 – turntable, 4 – slewable superstructure, 5 – boom, 6 – bucket wheel, 7 – hoisting winch, 8 – discharge boom.

The main subassemblies which should be under diagnostic assessment are:

1. the gear transmission of the excavator BW drive;
2. the gear transmissions of the crawler travel gear drive;
3. the main bearing of the slewing unit;
4. the hydraulic system equalizing the load on the slewing unit;
5. the hydraulic system hoisting the excavator's boom;
6. other hydraulic and lubrication systems;
7. the electric motors of the BW drive, the crawler travel gear drive and the slewing unit drive;
8. fixed and movable ropes.

The principal kinematic pairs in the above subassemblies are: bearings with rolling elements divided into ring-rolling element pairs, the gearing of the gear transmissions and so on. The subassemblies are not present all at the same in every excavator. Their presence is determined by the design of a particular excavator. The gear transmissions in the bucket wheel's drive have different designs depending on the excavator's capacity. The kinematic scheme of the drive of an SchRs 1200 excavator's bucket wheel is shown in fig. 17.2.

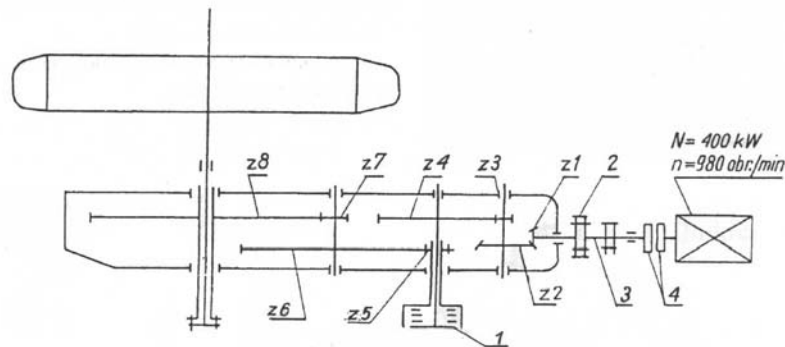


Fig. 17.2. Power transmission system of SchRs 1200 excavator's excavating mechanism: 1 – overload clutch, 2 – brake, 3 – jointed shaft, 4 – hydrodynamic coupling with elastic support.

$N = 400 \text{ kW}$, $n = 980 \text{ rev./min}$

The gear transmission during assembly is shown in fig. 1.3 [17.1] and a diagram of a two-path drive is shown in fig. 17.4 [17.1]. In the diagram one can see: gearbox (1), fixing element (2) preventing the gearbox from revolving around bucket wheel axle (3), electric driving motors (4), Cardan shafts (5) and hydrodynamic couplings (6). A gear transmission driven by four motors is shown in fig. 17.5 [17.1]. In the figure one can see: bucket wheel (1), BW drive gearbox (2), BW shaft (3) and driving motors (4).

Structural details of the boom are shown in fig. 17.6 [17.1]. In the figure one can see: right-handed truss (1), left-handed truss (2), lower bracing (3), upper bracing (4), transverse brace behind BW (5), fixed BW shaft bearing (6), floating BW shaft bearing (7) and structure for mounting BW drive motors (8). The crawler travel gear drive is shown in fig. 17.7a and b. It is driven by motor (1) via Cardan shaft (2) and worm-planetary gear (3); the other elements are: caterpillar chain (4), arm (5) preventing the gear transmission from revolving, and tilting (max. tilt 1:10) crawler tread (6).

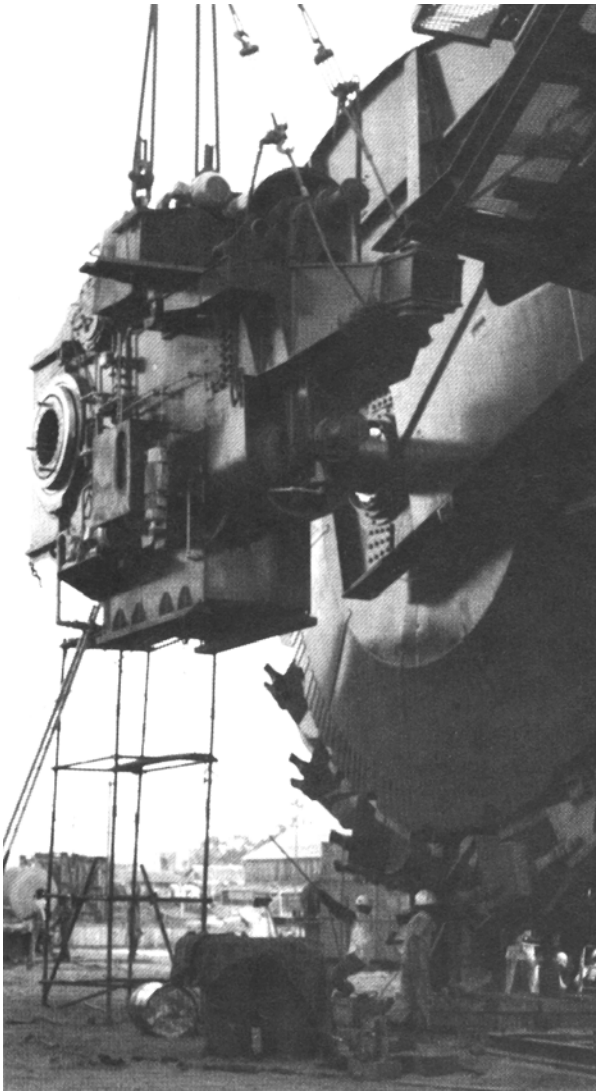


Fig. 17.3. Assembly of bucket wheel excavator's bucket wheel gearbox.

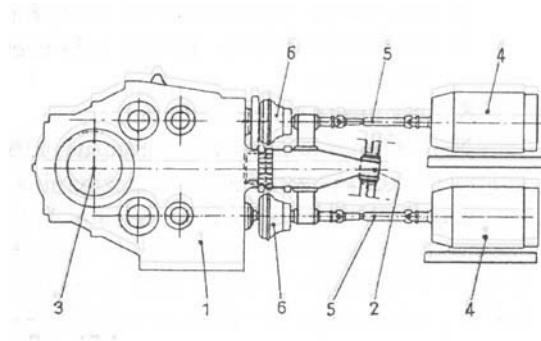


Fig. 17.4. Power transmission system of BWE:

1 – BW drive's gearbox; 2 – single-point support; 3 – BW shaft, two-point support; 4 – driving motors; 5 – Cardan shafts; 6 – hydrodynamic clutch

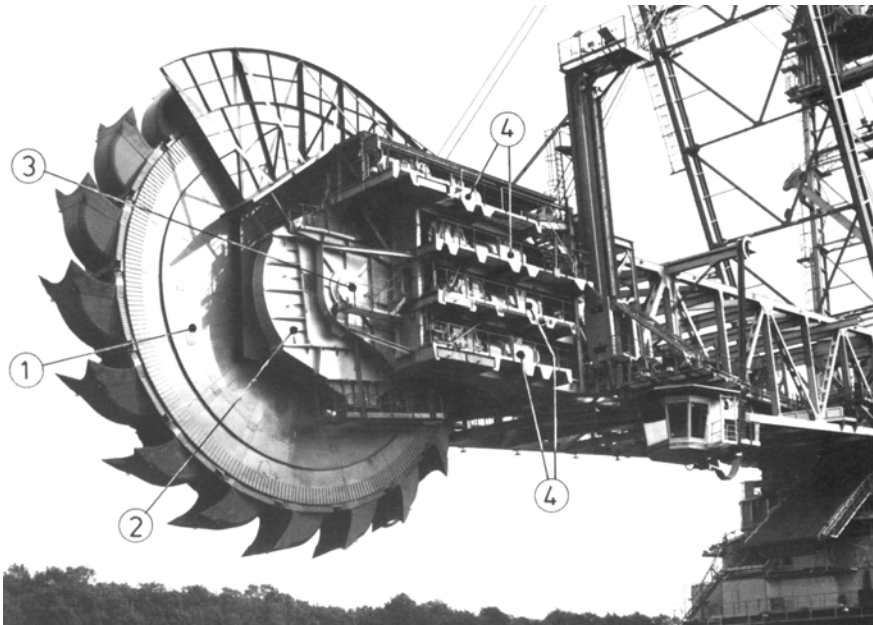


Fig. 17.5. BW drive: 1 – bucket wheel, 2 – BW drive gear transmission, 3 – BW shaft, 4 – motors driving bucket wheel.

Lubrication determines the proper operation of the gear transmission. A diagram of the BW drive's pressure lubrication system is shown in fig. 17.8 [17.1]. The system consists of: pressure vessel (1), preliminary filter (2), oil pumps (3), excess pressure gauge (monitor) (4), flowmeter (5), double filter (6), pressure gauge (7), wheel-side oil injection nozzles (8), motor-side oil injection nozzles (9) and cutoff valve (10). Further structural details of the subassemblies subject to diagnostic assessment are described in the subsections that follow.

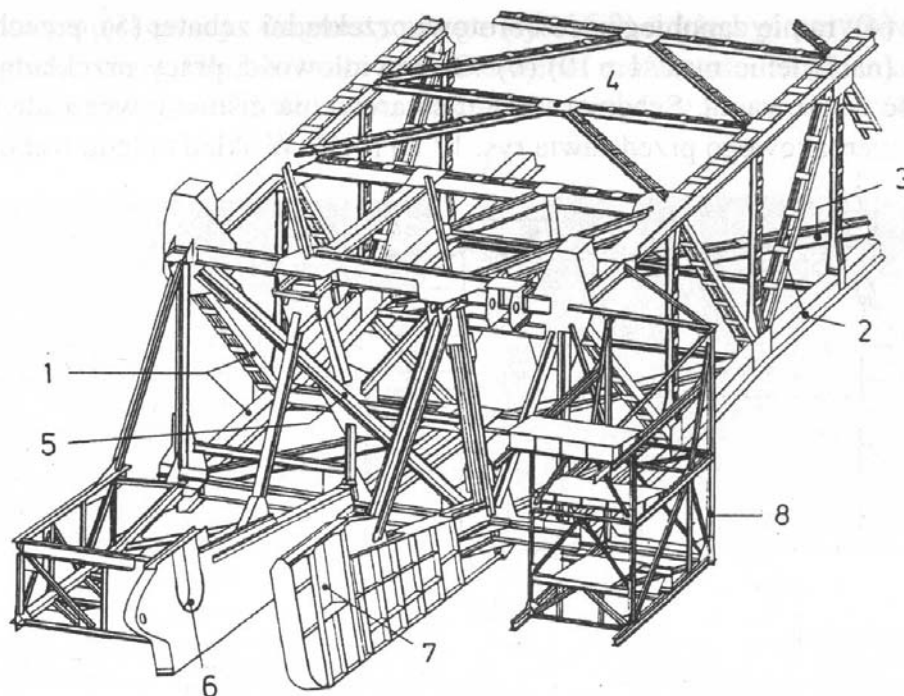


Fig. 17.6. Boom structure of large BWE: 1 – right-hand truss, 2 – left-hand truss, 3 – lower bracing, 4 – upper bracing, 5 – transverse brace behind BW, 6 – fixed BW shaft bearing, 7 – floating BW shaft bearing, 8 – support truss for mounting BW drive motors.

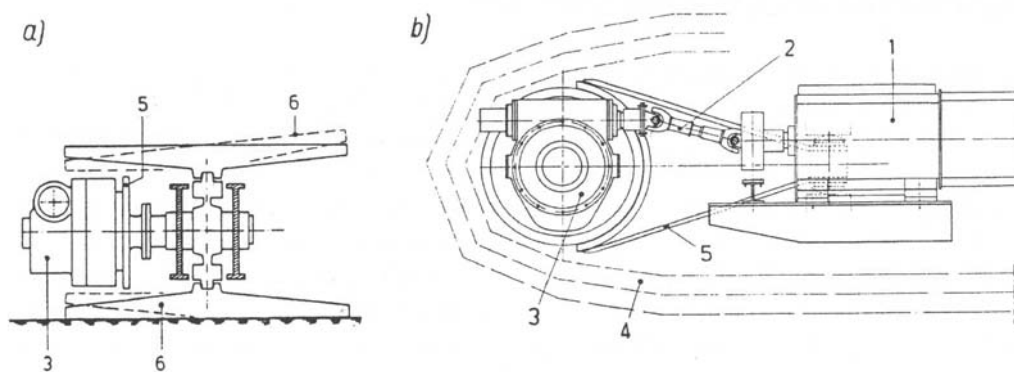


Fig. 17.7. Crawler travel gear drive's worm-planet gear: 1 – driving motor, 2 – Cardan shaft, 3 – worm gear, 4 – caterpillar chain, 5 – arm preventing gear transmission from revolving, 6 – tilting crawler tread (1:10); in projections a and b.

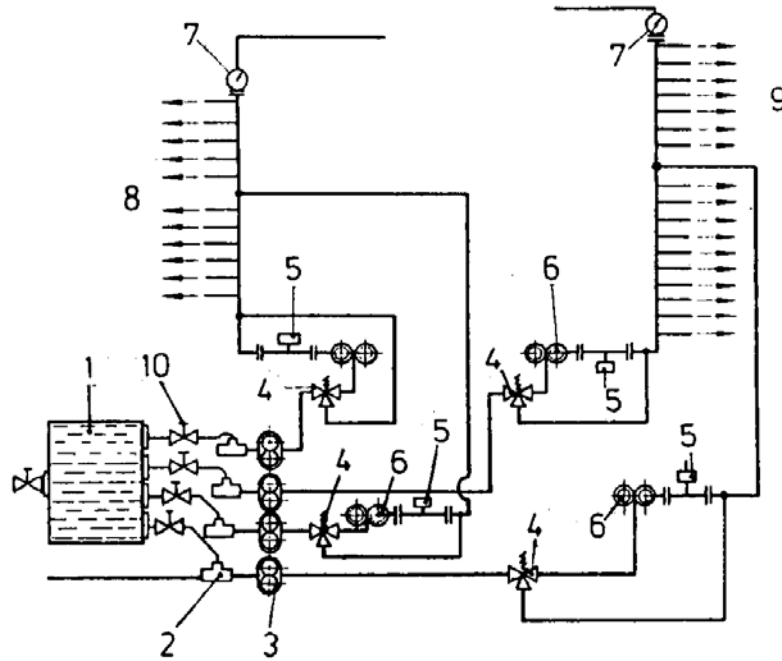


Fig. 17.8. Diagram of forced lubrication system used in BWE: 1 – oil tank, 2 – coarse filter, 3 – oil pump, 4 – excess pressure monitor, 5 – flowmeter, 6 – double filter, 7 – pressure monitor, 8 – oil injection nozzles on BW side, 9 – oil injection nozzles on motor side, 10 – cutoff valve

17.2. Diagnostics of gear transmissions

To drive the various subassemblies of bucket wheel excavators and stackers, highly complex gear transmissions are used (figs 17.2÷17.5, 17.7). The bucket wheel's gear transmissions are particularly complex. They consist of a complicated gearing system and a lubrication system (sometimes also complicated) (fig. 17.8). To determine the condition of the systems, diagnosis based on the analysis of the wear products (chap. 10.2) and the vibration signal can be used. Results of ferrographic analyses of wear products are reported in [17.2]. The gear transmissions of the bucket wheels of SchRs4000, SchRs4600 and Srs2000 excavators were investigated. The aim was to demonstrate the applicability of analytical ferrography to the assessment of the condition of gear transmissions and thus to enlarge the set of interpretation tools for the condition classes presented in fig. 16.9. A concise interpretation of gearing and bearing condition classes which facilitates the acquisition of data (information) about the condition of gear transmissions can be found in chap. 16.2. A condition assessment

based on the diagnostic inference scheme (fig. 16.9) can be validated by ferrographic examinations. To illustrate this point, some ferrograms are presented.

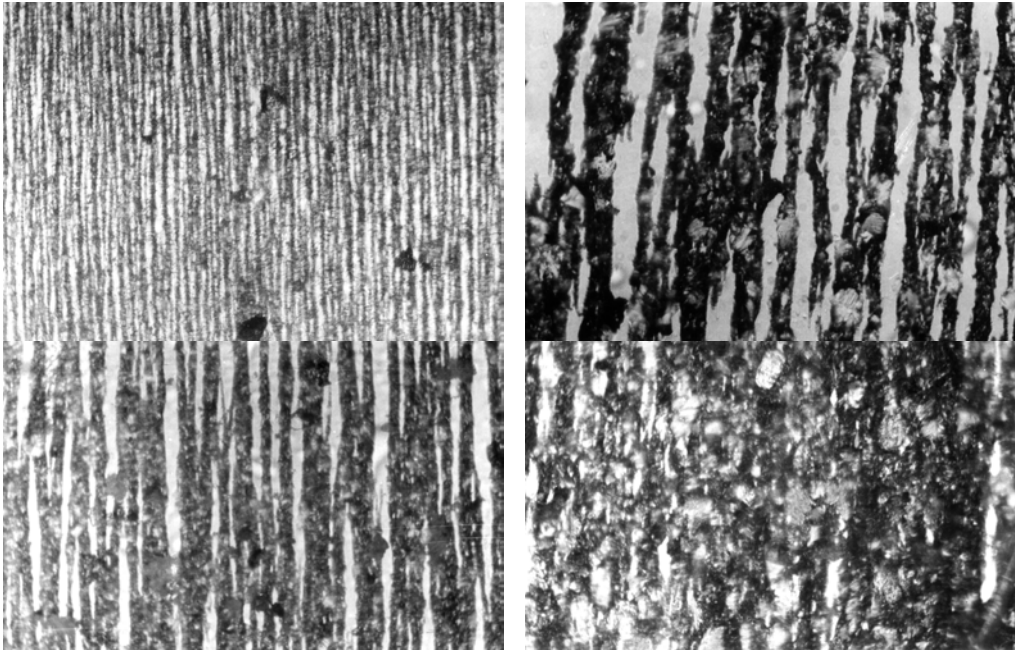


Fig. 17.1. Examples of different ferrographic images of particles from BW drive gear transmission (a+d).

Fig. 17.9a shows a ferrographic image with visible numerous ferromagnetic particles up to $15\ \mu\text{m}$ in size. Single nonferromagnetic particles about $40\ \mu\text{m}$ in size appear at a distance of 1.2 cm from the beginning of the ferrogram. The latter comes from an analysis of the particles on the BW drive of SRs2000 excavators. On the basis of this and other ferrograms the condition of the four excavators was determined as belonging to class A. Scuffing and seizing particles (figs 10.23 and 10.33) were detected in one of the excavators. The gear transmission was placed in class B. Fig. 17.9b shows a ferrogram with a large number of particles up to $50\ \mu\text{m}$ in size, which is evidence of considerable teeth interference (scuffing) during meshing. A single nonferromagnetic particle of about $100\ \mu\text{m}$ in size is visible at a distance of 2 cm from the beginning of the ferrogram at its bottom edge. The numerous ferromagnetic particles of about $40\ \mu\text{m}$ in size visible at a distance of 0.5 cm from the beginning of the ferrogram indicate scuffing.

The ferrograms were made using oil samples taken from the main drive gear transmission of the SchRs4600 excavator. The gear transmission was placed in class B. The oils samples were taken at about one month intervals. Large amounts of impurities consisting of metal, coal and sand particles were observed to precipitate in the samples. In a sample coming from one machine the impurities constituted 1/3 of the

total volume. This is a sign of the improper operation of the gear transmission. The fouling (especially with sand) of the oil and the excessive number of metallic particles contribute to the intensive abrasive wear, particularly of rolling bearings.

Material losses due to abrasion in the bearings result in improper intermeshing (scuffing). Scuffing manifested itself in the presence of particles on the ferrograms.

A computer system for the diagnostics of the BW drive of a bucket wheel excavator of 100000 tons per 24 h is presented in [17.3]. Vibration signals about the condition of the gear transmission were received from 16 transducers located at different places on it. In addition, 16 reference transducers were installed to check if the working transducer functioned properly. The correctness of the functioning of the former transducers was checked periodically.

Transducers of this type (detect-method MicroTecGmbH) are used in the motor vehicle industry. Signals from 16 or 32 transducers are sent to a multiplexer and then via one line to an on-board computer situated in the operator's cab. The signals received from the multiplexer were pre-processed to obtain envelopes of the 16 signals representing gear transmission vibrations. The way in which the envelope is formed is described in chap. 10.1. Envelope signals are processed by an analog-to-digital converter. Besides the signals coming from the vibrational transducers also the gear transmission loads and rotational speeds are monitored. Signals from the on-board computer are sent to a computer where analyses of gear transmission condition are performed. The signals transmitted to the on-board computer are always received under similar conditions determined by the operational factors (chap. 6.4), i.e. under a similar gear transmission loading and rotational speed. The recording of signals is actuated by the on-board computer. The traces of the numerical signals are subjected to fast Fourier transformation (FFT) and a signal power spectrum is obtained (chap. 10.1). Some frequencies which are directly linked with gear transmission condition, e.g. the frequencies originating from faults in the races of the rolling bearings (7.10), (7.16) or the balls (7.36) (see also table 11.1), are selected from the spectrum. An illustrative vibrational signal envelope spectrum for a damaged rolling bearing is shown in fig. 15.12.

The authors of [17.3] plan to use an on-board computer for the full analysis of the diagnostic signal and to use a diagnostic system similar to the one described above to analyze the condition of belt conveyor drive gear transmissions. Only the diagnostics of rolling bearings are presented in [17.3]. Rolling bearings represent an important element of gear transmission operation condition, but the diagnostics of the gear transmission should not be limited to only the diagnostics of the rolling bearings. In the case of the intensive abrasive wear of the latter, a change in their condition will not be indicated (as opposed to what is described in [17.3]) by a vibrational signal (a signal envelope) reflecting the rolling bearing condition. This kind of wear of the rolling bearings in the gear transmissions of the BW drive may often occur in strip mine conditions. Therefore the analysis of the diagnostic vibrational signal should be extended

to cover the state of intermeshing. The most suitable would be signal analysis using synchronous summation which makes it possible to represent the signal as in figs 6.36 and 6.40. The figures show a change in the signal, which can be anticipated in the case of the uneven wear of the rolling bearings (see the commentary on changes in the form of the diagnostic signal generated by the gearing when its condition changes, chapters 6 and 14).

17.3. Diagnostics of hoisting ropes

Fixed and movable ropes can be distinguished in bucket wheel excavators. Fixed ropes make up the elastic suspension of the load-carrying system. They carry the static loads and loads stemming from the vibrations of the system's suspended masses, generated in reaction to excavation resistance. The ropes are subject to corrosion and fatigue (caused by changing loads), particularly near the suspensions. Movable ropes are installed in the hoisting and holding up mechanism of the excavator's boom.

The hoisting ropes form two independent systems driven by two electric motors in large excavators or by one motor in smaller excavators – figs 17.10 and 17.11. In fig. 17.10 one can see: A – rope system A, B – rope system B, G_A – drive unit A, G_B – drive unit B, C – a holding brake, D – operating brake, S_A – winch drum system A, S_B – winch drum system B. The load capacities of the ropes are such that they ensure the needed suspension capacity with only one of the rope systems functioning. The safety factor of one of the rope systems should be larger than 3. From one end the movable ropes are attached to the hoisting mechanism's drum (fig. 17.10). From the drum the ropes pass through several rope pulleys/sheaves. The ropes are protected against overloading.

During hoisting and lowering, different sections of the rope move at different rates (relative to a fixed point). The rate changes from the tangential velocity of the drum to zero. Also the particular rope sections have different length. The longest rope section starting from the hoisting mechanism drum moves at the tangential velocity of the drum. Finally, the velocity of the ropes must be reduced to the boom's hoisting velocity.

One of the main causes of the fatigue processes that occur in movable ropes is the bending of the rope on the rollers. The rate at which the rope loses its fatigue strength increases with increasing ratio d/D (d – the rope's diameter, D – the rope pulley's diameter). Another factor adversely affecting the rope is contact stresses between the rope and the groove of the pulley (made of steel or cast iron). Still another factor contributing to the degradation of the rope is corrosion caused by the action of the open pit environment.

To sum up, the above factors are responsible for the following degradation of the hoisting ropes:

- the wires of the rope lose their fatigue strength and break,
- the wires both on the surface and inside the rope are abraded,
- corrosion.

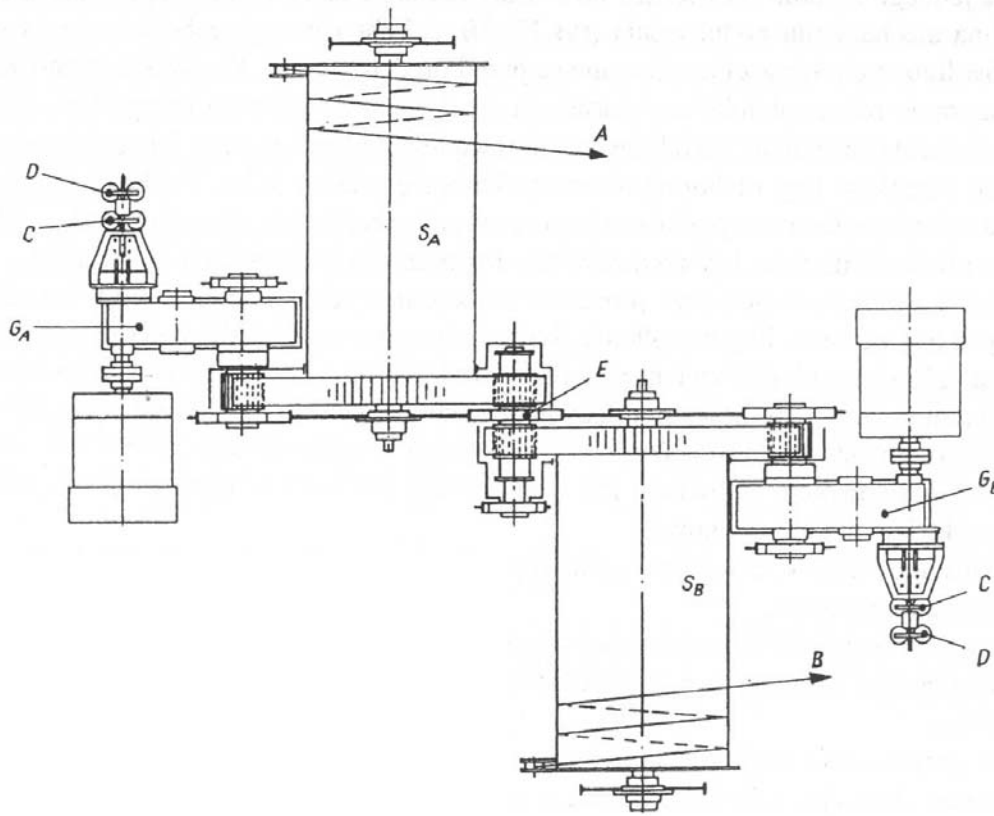


Fig. 17.1. Structure of double power transmission system of BWE boom hoist:

A – rope system – drive A;

B – rope system – drive B;

G_A – drive unit A;

G_B – drive unit B;

E – clutch, C – holding brake;

D – operating brake; S_A – winch drum of drive A; S_B – winch drum of drive B.

In the case of ropes being in partial linear contact, wire abrasion and corrosion are the predominant forms of wear, whereas wire breakage due to fatigue is the main form of wear for ropes in point contact.

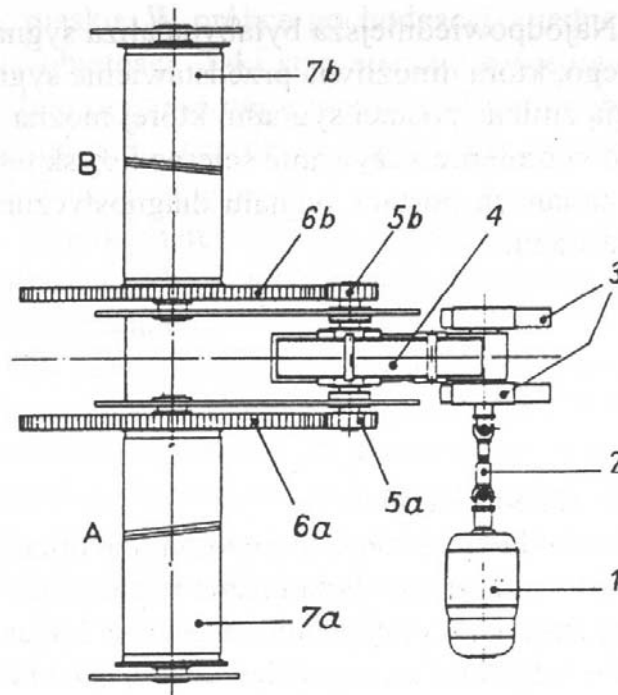


Fig. 17.2. Structure of one power transmission system of BWE boom hoist:
 1 – driving motor, 2 – Cardan shaft, 3 – brake, 4 – gear transmission, 5a – pinion of drum A gear transmission, 5b – pinion of drum B gear transmission, 6a – gear of drum A gear transmission, 6b – gear of drum B gear transmission, 7a – rope drum A, 7b – rope drum B.

The wear of the ropes over their length is not uniform. An analysis [17.4] of damage to the ropes of SchRs800, Srs800 and Schrs1200 excavators showed that the section which runs from the drum through a set of pulleys is most susceptible to damage. To assess the condition of a movable rope, the measuring head is installed in the section with the highest risk of damage. The places at which the measuring head is installed are shown for the SchRs6300 excavator in fig. 17.12. An analysis of the rope systems of bucket wheel excavators has shown that to monitor the condition of the hoisting ropes the equipment used should enable:

- the assessment of ropes of up to 65 mm in diameter;
- the assessment of local damage such as: single broken wires, point corrosion, cuts, pits, damage distributed uniformly over longer lengths;
- measurements when the rope moves at rates higher than 0.1 m/s;
- the movement of the measuring head (equipped with an individual drive) relative to the rope.

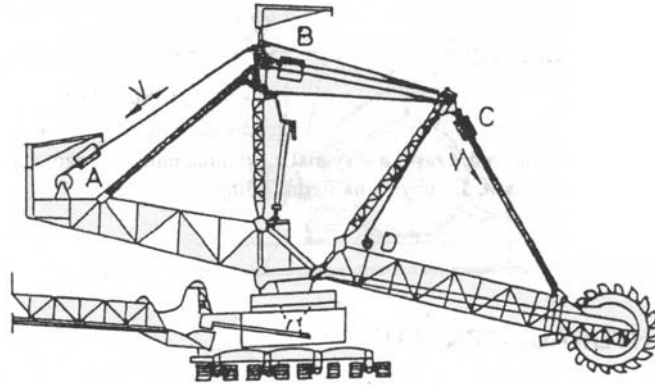


Fig. 17.3. Arrangement of measuring heads for monitoring condition of wire ropes:
 A – measuring point at drum, B – measuring point at multirunner system, C – point of head mounting on stationary rope, D – location of movable head

17.3.1. Equipment for magnetic inspection of ropes – assessment of rope condition

The measuring head can magnetize the rope with a static magnetic field. The source of the magnetic field are permanent magnets. The head also has sensors which generate electric signals indicating rope faults. If changes in the rope's cross-section are anticipated, then an induction gauge exploiting the Hall effect is used to detect them. Rope inspection equipment is made (in Poland) by the Academy of Mining and Metallurgy in Cracow.

Illustrative traces of rope condition parameters are shown in fig. 17.13. Trace A represents a time marker, trace B – the induction gauge signal (numeral 2 marks broken wires) and trace C – the signal from the Hall generator (1 – missing wire, 3 – 1% rope mass decrement).

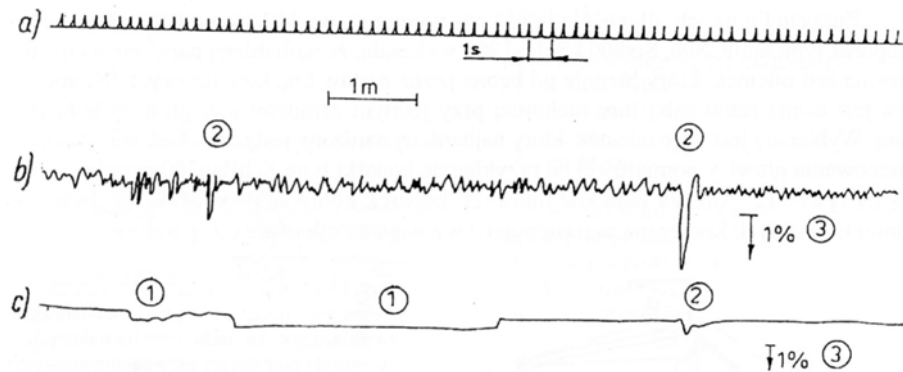


Fig. 17.1. Picture representing wire rope condition: a – time marker, b – induction gauge signal, c – Hall generator signal, 1 – missing wire, 3 – decrement in rope diameter.

17.4. Diagnostics of hydraulic systems

Exemplary subassemblies of hydraulic systems are shown in figs 17.14-17.17. The BWE slewing unit supported by sets of double rollers on hydraulic props is shown in fig. 17.14. Structural details of the slewing unit are shown in fig. 17.15 [17.1] and the hydraulic steering system of the crawler travel gear is shown in figs 17.16 and 17.17 [17.1].

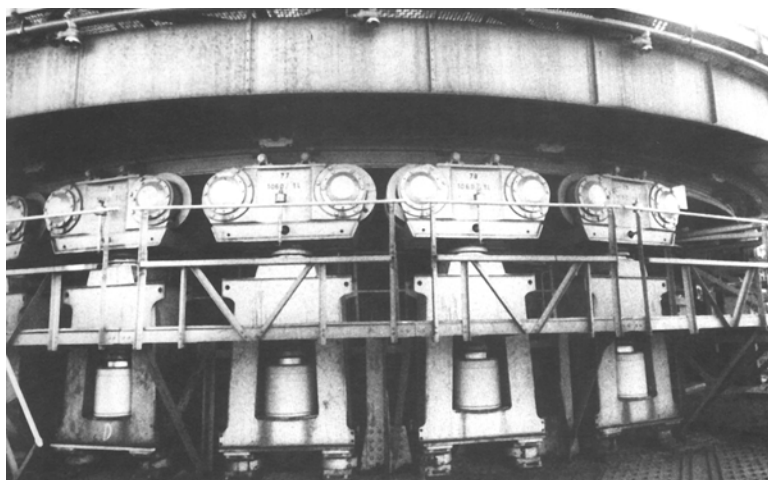


Fig. 17.1. BWE slewing unit with hydraulically supported rollers.

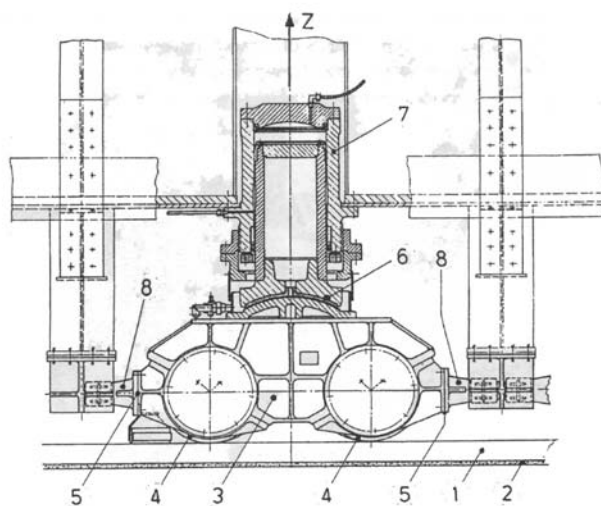


Fig. 17.2. Hydraulically supported rollers: 1 – rail on substructure, 2 – packing layer, 3 – two-wheeled bogie, 4 – rollers, 5 – slide rails, 6 – spherical support, 7 – hydraulic cylinder, 8 – horizontal force stops.

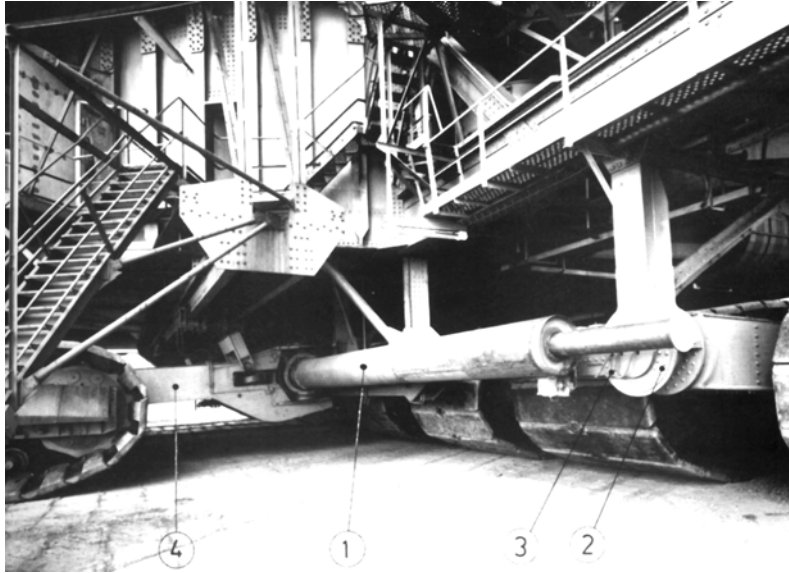


Fig. 17.3. Hydraulic system steering crawler travel gear turn: 1 – hydraulic turn cylinder, 2 – cylinder mounting on undercarriage, 3 – oil feed tubes, 4 – steering tiller.

Sample ferrographic investigations of the power transmission system of the LZKS loader-stacker for three machines denoted as 1, 2 and 3 are presented in [17.2]. The loader-stacker is shown in fig. 17.17. The investigations were undertaken because of the short life of the system's subassemblies, in particular that of the hydraulic engines.



Fig. 17.4. View of LZKS loader-stacker.

Wear particles up to $60\ \mu\text{m}$ in size were observed in the ferrographic images of the hydraulic system of machine no. 1. This indicates that the particle size substantially exceeds the boundary values for hydraulic systems. The particles should not be larger than $5\ \mu\text{m}$. The relationship between life and particle size is illustrated in fig. 13.2.

In the case of machine no. 2, ferrograms showed the presence of particles in the form of chips up to $600\ \mu\text{m}$ in size and volumetric particles as large as $350 \times 400\ \mu\text{m}$. This particle size indicated a danger that the hydraulic engine would seize up. The ferrographic pictures are shown in fig. 17.18a where one can see a particle in the form of a single chip (up to $600\ \mu\text{m}$ long). A $350 \times 400\ \mu\text{m}$ volumetric particle is shown in fig. 17.18b. This state was attributed to the running in of the hydraulic engine (the latter had just undergone repairs) since at later stages of its operation the particle size decreased. Nevertheless the durability of the systems remained unsatisfactory and so ferrographic investigations were undertaken.

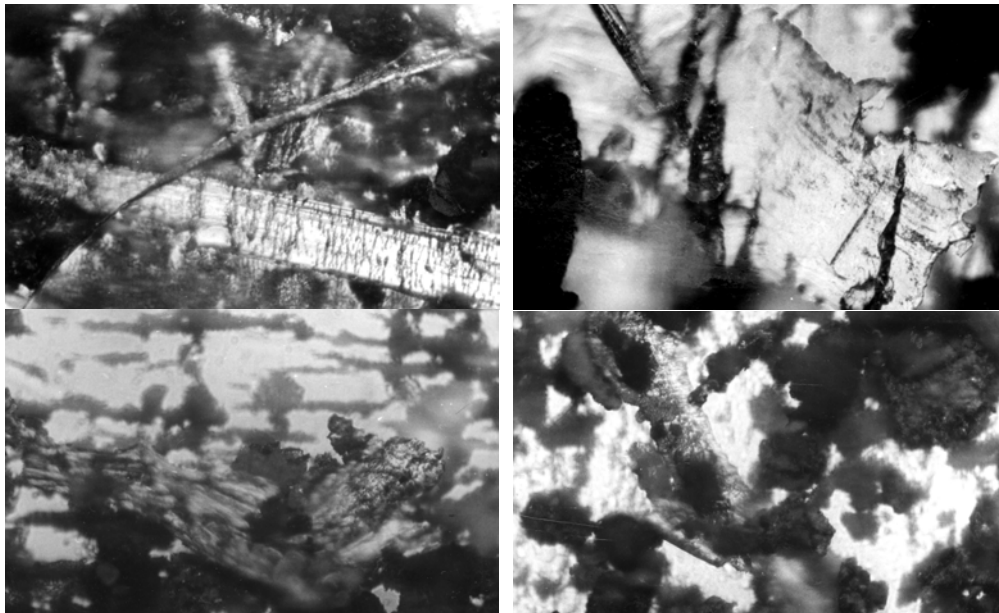


Fig. 17.5. Examples of ferrographic images of particles (Z_u , K , Z_a) from hydraulic system of loader-stacker BW drive.

The ferrograms for machine no. 3, shown in figs 17.18c and d, revealed single chips up to $300\ \mu\text{m}$ long. Since the system was not in the running-in stage the hydraulic engine might seize up.

The probable causes of the short life of the hydraulic engines are impurities (particles up to $60\ \mu\text{m}$ in size) in the oil in the hydraulic systems and parts not manufactured by the original producer put in during repairs. The parts do not interact properly with

the other elements in the hydraulic engine whereby particles of size as for machine no. 2 are produced.

Taking into account the above, it becomes necessary to employ technological diagnostics, systematically monitor particle size and change oil regularly in the hydraulic system to clean the latter. 60 μm particles shortened the life of the engine considerably and made it difficult to repair it. The improperly done repair shortened the engine's life even more and the costs of maintaining the machines increased enormously.

Wear products as the signal of the condition of a machine are described in detail in chap. 10.2. Also methods of monitoring the condition of hydraulic systems (fig. 10.36) are presented there. However, no experience with the use of these methods in surface mining machines is available. It is expected that in the nearest future the methods will be used to monitor the condition of new machines. The signals about the condition of the machines (bucket wheel excavators, stackers, loader-stackers) will be sent to the operator's cabin). As the mining process becomes fully automated, systems monitoring the condition of the particular kinematic pairs will become a necessary element ensuring reliable, continuous operation of the technological systems. Signals about their condition will be transmitted by radio to a dispatcher computer. In reference to chap. 10.2, one should also take into account the places of taking samples of particles (Z_u , K , Z_a) in the oil cycle or in the tank to make sure that the samples are representative of the condition of the system's elements. It is recommended to take samples at places where turbulence occurs, i.e. where the hydraulic medium undergoes mixing. Samples should not be taken at "dead" places where the hydraulic medium stagnates. In pipes, release valves should be situated in their sides, not their bottom where particles settle. If hydraulic medium samples are to be taken from the tank, they should be taken 30 minutes after starting the machine. The medium should have an average temperature.

17.5. Diagnostics of slewing unit's principal bearing

An example of a design of the slewing unit's principal bearing, including the lubrication system, is shown in fig. 17.19 [17.1]. The durability of the slewing unit's principal bearing is determined by the continuity of lubrication and the purity of the lubricant during the operation of the bearing. In strip mine conditions, particles (Z_u , K , Z_a) (described in chap. 10.2) get into the lubricant, lowering the durability of the rolling bearing.

The relationship between durability and particle (Z_u , K , Z_a) size is illustrated in fig. 13.2 in chap. 13.3. If the lubricant is kept suitably pure, the life of the principal bearing can be extended as shown in fig. 17.20 where the relationship between the durability of the bearing and the total wear is illustrated [17.5]. By monitoring the impurities one could extend the life of the bearing. The diagnostic methods described in

chap. 10.2 can be used to analyze the particles occurring in the lubricant. Besides the mentioned above excavator assemblies and kinematic pairs, also the ball bearing, shown in fig. 17.21 [17.1], which transmits the load between the truck-gear assemblies and the lower part of the load-bearing structure supporting the balls of the slewing unit's bearing should be subjected to diagnostic monitoring

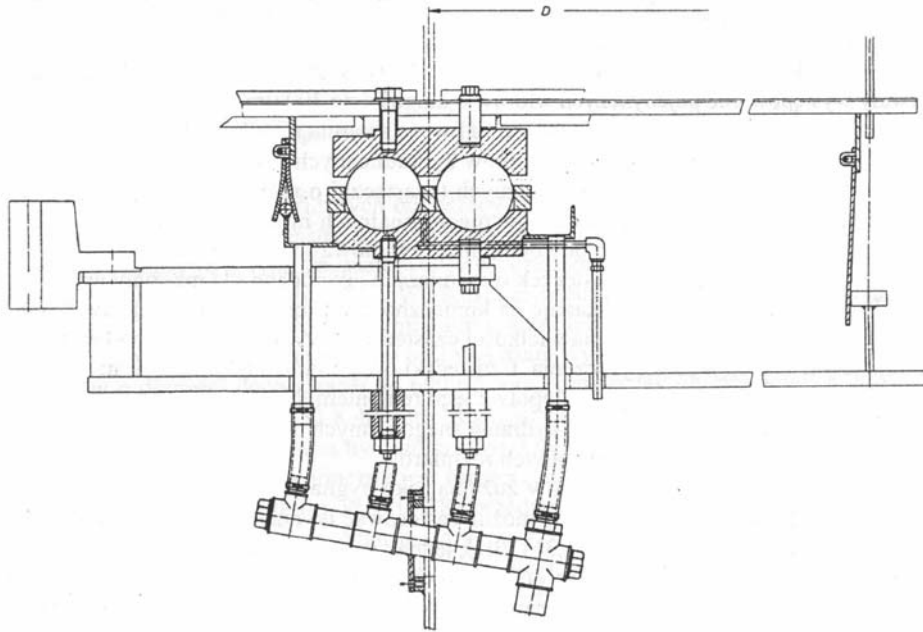


Fig. 17.1. Structure of lubrication system of excavator slewing unit principal bearing.

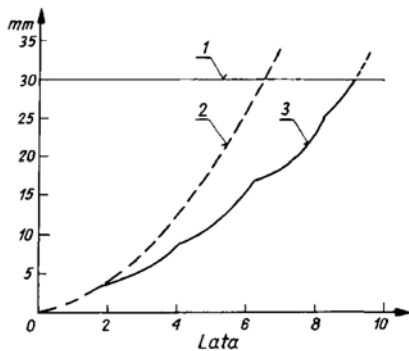


Fig. 17.2. Life of principal bearing versus cleaning for stacker: 1 – permissible wear limit, 2 – wear curve for bearing which is not cleaned, 3 – wear curve for bearing cleaned every two years [17.5].

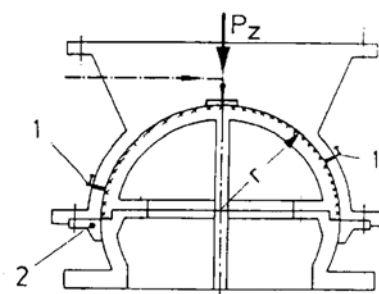


Fig. 17.3. Schematic of ball bearing between crawler travel gear and slewing unit: 1 – oil filters, 2 – seal and retaining ring [17.1].

17.6. References

- [17.1] Durst W., Vogt W.: *Bucket Wheel Excavator*, Trans Tech Publications, 1988.
- [17.2] Bartelmus W., Fleszyńska B.: *Conducting Ferrographic Investigations of Hydraulic Systems of Excavator BW Drives and Gear Boxes (in Polish)*, Poltegor, Archive No. 1823/ONB (unpublished), 1989.
- [17.3] Kessler W., Heuvel B., Bauer B., Geropp B.: *Online Fault Diagnosis of a Bucket Wheel Gear Box in a German Open Cast Coal Mine*, *Proceedings of Mine Planning and Equipment Selection*, A.A. Balkema, pp. 431-435, Rotterdam, 1995.
- [17.4] Hansel J., Lankosz L., Tytko A.: *Non-Destructive Testing of Wire Ropes on Surface Mining Equipment*, *Proceedings of International Symposium on Continuous Surface Mining*, A.A. Balkema, Rotterdam.

18. Expert systems in technological diagnostics

18.1. Expert system

The fundamentals of diagnostic inference are interspersed throughout this book. The diagnostician must have wide knowledge in many fields. To facilitate the process of diagnostic inference, computer expert systems are introduced. An expert system uses a heuristic approach in contrast to ordinary programs with their algorithmic approach. In an algorithm there is a specified number of steps leading to the solution of a problem. An expert solves a problem on the basis of data from many sources, assesses the weight of different possible solutions and suggests a final conclusion to be drawn. The way which best describes, in the expert's opinion, the solution to the problem is adopted, while the other ways are rejected. This is a heuristic approach which computer expert systems use.

The solution of a problem in technological diagnostics has the form of a diagnosis of the condition of a technical object – a machine. The accuracy of the diagnosis depends on the range of knowledge which the expert has at his/her disposal. Thus the knowledge stored in the database determines the correctness of the solution of a problem. Expert systems consists of the following components:

- a database (knowledge base) for a certain limited range of technical objects, e.g. rolling bearings, toothed gears, shafts, steel cables, hydraulic systems, load-bearing systems and conveyor belts, necessary to assess the condition of machinery in strip mines;
- a diagnostic reference engine;
- input and output devices for entering: data enriching the database, data on the machine to be diagnosed and diagnosis results to form a basis for drawing conclusions about the technical condition;

Expert systems solve problems according to diagnostic inference rules IF THEN, e.g. rule 1: if the first vibration harmonic for rotary motion, then unbalance of the rotating element.

Recently, besides conventional expert systems inferring according to rules, systems of machine condition recognition employing systems patterned on the behaviour of human neurons are being developed. Such machine condition recognition systems are called neural networks.

18.2. Expert systems based on neural networks

Expert systems based on neural networks are one of the latest ways of solving the machine condition assessment problem. This way is closest to the inference by an expert diagnostician. Exact knowledge contained in rules of diagnostic inference is required in a traditional expert system, whereas an expert system based on a neural network needs knowledge in the form of specific facts or features which are classified and generalized. A neural network imitates the biological neural network of the human brain. The latter contains about 50÷100 billion nerve cells (neurons) which form groups called networks. Each network includes several thousand of interconnected neurons, each of which performs specialized functions. The brain exploits the multiple parallelism between neurons and their networks. It can recognize pictures (e.g. character recognition), classify (differentiate between animals, plants, minerals) and generalize (e.g. I know that I know nothing).

One should not jump to conclusions about the capabilities of the artificial neural network just because there is an affinity between it and the biological neural network. According to [18.1], in one extreme interpretation the artificial neural network is regarded as a class of mathematical algorithms yielding solutions for many specific problems and in another extreme interpretation, as a network emulating the biological neural network. The first interpretation is closer to reality. An artificial neural network consists of repeated elements arranged in layers. The input layer distributes signal features throughout the network. The output layer generates a suitable response. The intermediate (hidden) layers function as a detector of recognition features. Each detector seeks a characteristic feature in the output signal and it gets strongly excited when it identifies a feature it has found. The occurrence or non-occurrence of characteristic features is recognized through weights. Weights make up the relative value of input signals. Weights are created on the basis of the features of a set of input signals and they constitute the memory of the neural network. They form during the learning of the neural network. Owing to this approach a neural-network based expert system is continuously modified on the basis of a set of current facts. This enhances its ability to recognize features without programming the alterations and restructuring the inference rules.

18.3. Reference

- [18.1] Zurada J.: Introduction to Artificial Neural Systems, New York West Publishing Company, 1992.

19. System of technological diagnostics for strip mine

19.1. Introduction

The system of technological diagnostics must be incorporated into the strip mine's general information system which should reflect the current trends towards complete automation of deposit mining. Such possibilities appeared when it became possible to determine precisely the position of a machine in the strip mine. The machine's position is determined using the Global Positioning System (GPS). It should be noted, however, that autonomous GPS alone is not enough since its positioning accuracy is far too low for this purpose. The accuracy of positioning was improved by employing Differential GPS (DGPS) and it is now 5 cm. The positioning is relative to a reference point located on the strip mine site. An even higher positioning accuracy was achieved by introducing the Real Time Kinematic (RTK) system which allows one to determine the position of objects (machines) in motion with an accuracy of 2 cm. The mining of the deposit can be fully automated if an appropriately high degree of reliability of the machinery is ensured. As made evident in chap.1, one of the ways of maintaining a high degree of reliability of machines is to operate them depending on their condition (chap. 3). Therefore the mine's information system must include a system of technological diagnostics. A computer-aided system of technological diagnostics consists of subsystems. The division into subsystems may be based on the use, e.g. the subsystem of gear transmission diagnostics described in chap. 19.2. The system of technological diagnostics may constitute a subsystem of a computer system, machinery maintenance management system. An example of a belt conveyor maintenance subsystem is provided in chap. 19.3. It does not include, however, condition based maintenance or the problems connected with the technological diagnostics of belt conveyors described in chap. 16.4. In chap. 3 three methods of maintaining machines were distinguished. The subsystem described in chap. 19.3 is for the planned-preventive maintenance of conveyor belts. A machine management subsystem which includes technological diagnostics elements is described below.

The computer management of machine maintenance comprises:

- the management of orders for servicing and (routine or damage) repairs,
- the management of spare parts,

- a database of suppliers,
- a database of machines,
- a database of the history of servicing and repairs,
- the management of reports on machinery condition and on the performance of servicing and repair tasks,
- graphic analysis.
-

Reports on the condition of the machinery are supplied by the diagnostic subsystems. Task execution orders, describing the type of machine, the measuring points, the state of load and the measurement conditions, are made out to monitor the condition of the machines. As mentioned in chap. 16.2, diagnostic measurements consisting in the measurement of vibration parameters should be made at the gear transmission load corresponding to at least 40% of the power consumed by the gear transmission during normal running. If ferrographic diagnostics is used, certain conditions connected with the taking of oil samples for the assessment of the condition of a machine must be fulfilled (chap. 10.2 and 17.4). In the case of greater computer support, machine condition signals can be transmitted to the operator and the load conditions during diagnostic measurements are stored automatically by a computer system of direct data acquisition. Such a subsystem for the diagnosis of the drive of the wheel excavator's bucket wheel is described in chap. 17.2. Then there is no need to make out orders for diagnostic measurements. After they are recorded, measurements are entered into a system of diagnostic data analysis and the diagnostician determines the condition of the machine. The signals can also be analyzed by an expert system (chap. 18) and in critical cases the diagnostician accepts or rejects the computer diagnosis. The diagnostician can also use mathematical models enabling computer simulation whose result may have a bearing on the diagnosis.

The fundamentals of the development of mathematical models are given in chap. 4, those of gear transmission modelling – in chap. 6, those of rolling bearing modelling – in chap. 7 and those of belt conveyor route section modelling – in chap. 8. Results of computer simulations for gear transmissions are presented in chap. 6 and 14. The subsystem monitoring the condition of the gear transmission of the BW drive, described in chap. 17.2, can send both a diagnostic analysis and information to the operation supervision dispatcher. Thus it can be used in the fully automated mining of the deposit in a strip mine. The machine maintenance management system's computer graphic analysis component can represent the operating costs, the costs of spare parts and the production losses due to stoppages of the excavator-conveyor-stacker systems.

19.2. Gear transmission diagnostics subsystem

An algorithm of diagnostic inference for gear transmissions [after 19.1, 19.2] is shown in fig. 16.9. A computer system aiding the inference and diagnostic data acquisition was developed on the basis of this algorithm. The system is also presented in [19.3, 19.4]. An application for an IBM PC or XT compatible microcomputer (minimum requirements: CPU with primary memory of 640 KB RAM, a Hercules graphics adapter, a 20 MB hard disk, a matrix printer with 80 characters per row, a monochrome monitor, operating system DOS 3) was developed. The computer system enables data acquisition for 500 gear transmissions in a period of three years. Besides data selection according to the classifications given in fig. 16.9, it enables the representation of the condition parameters as a function of time for 12 measuring points. The system generates reports about the condition of gear transmissions for a particular production process or a specific group of gear transmissions. The menu of the diagnostic software is shown in figs 19.1-19.6.

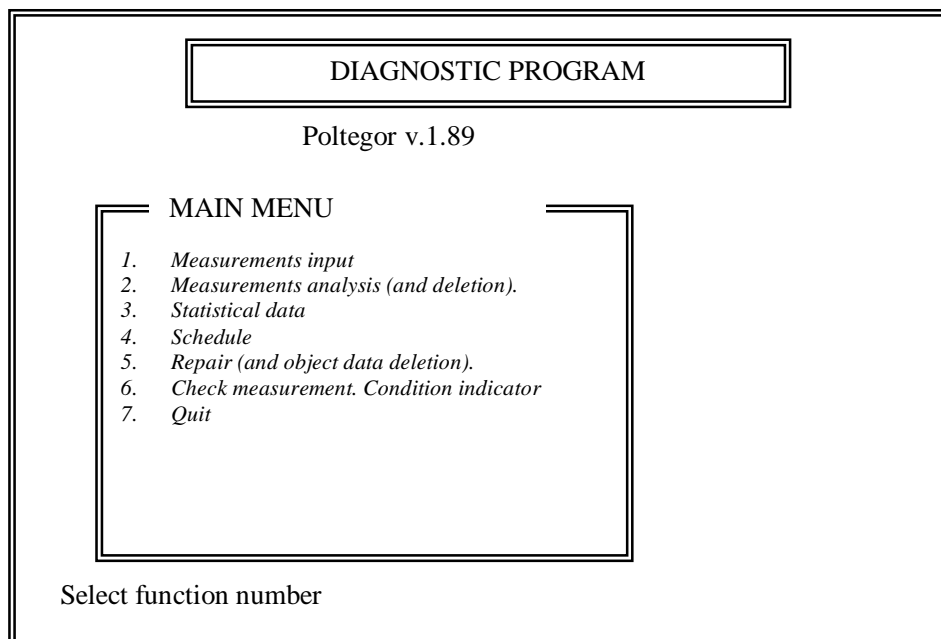


Fig. 19.1. Main folder menu of gear transmission diagnostics system.

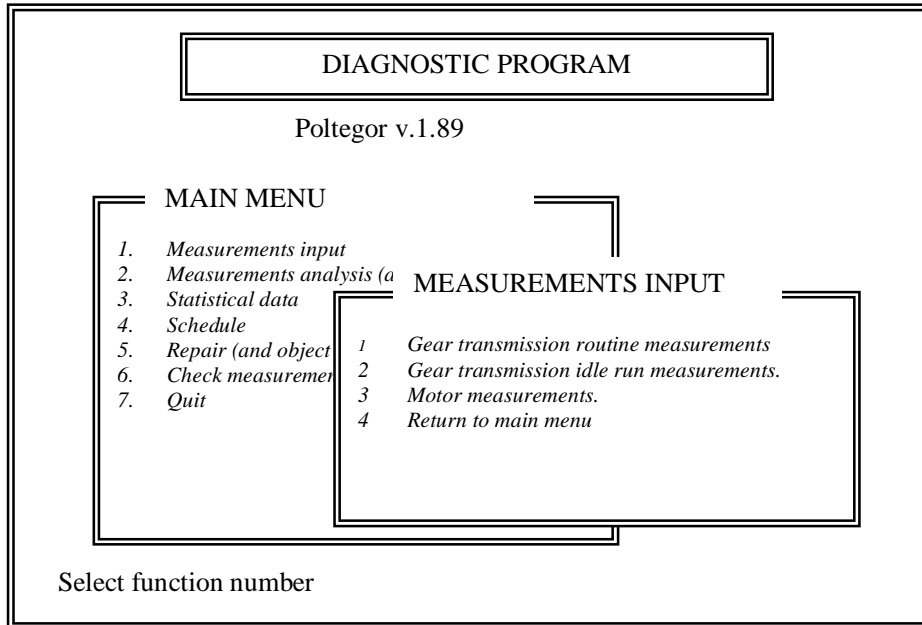


Fig. 19.2. "Measurements input" folder menu against main folder of gear transmission diagnostics system.

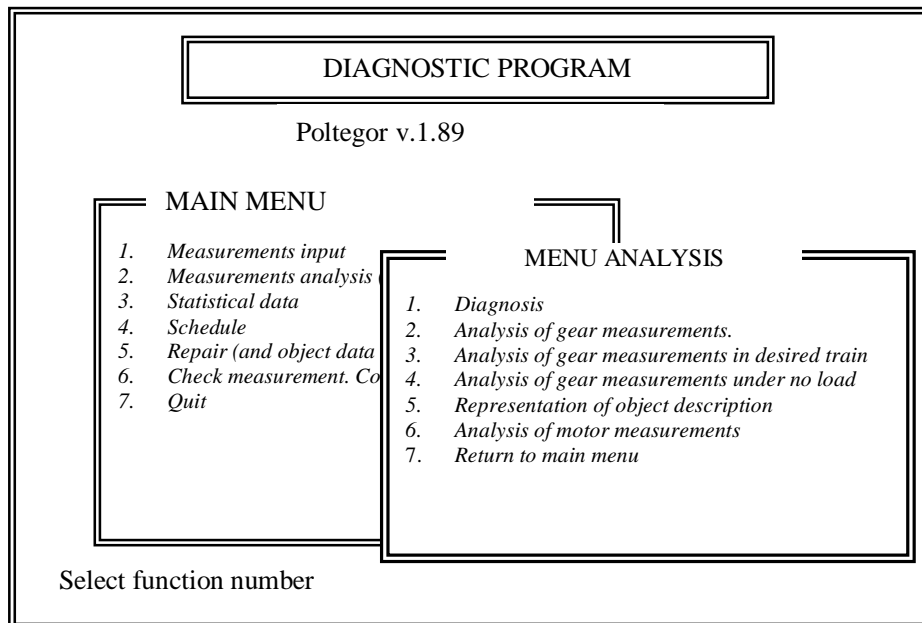


Fig. 19.3. "Analysis" folder menu against main folder of gear transmission diagnostics system.

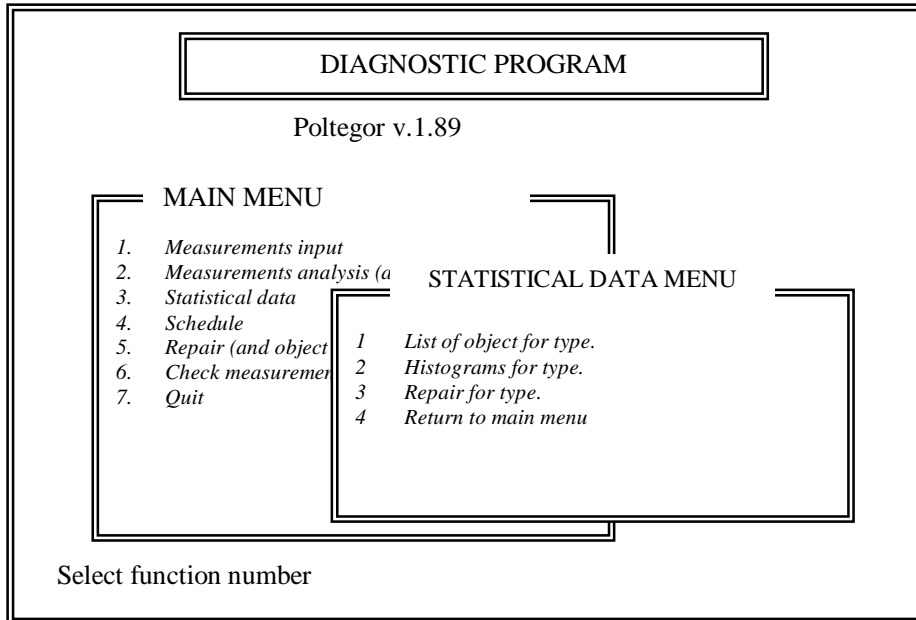


Fig. 19.4. "Statistical data" file menu against main folder of gear transmission diagnostics system.

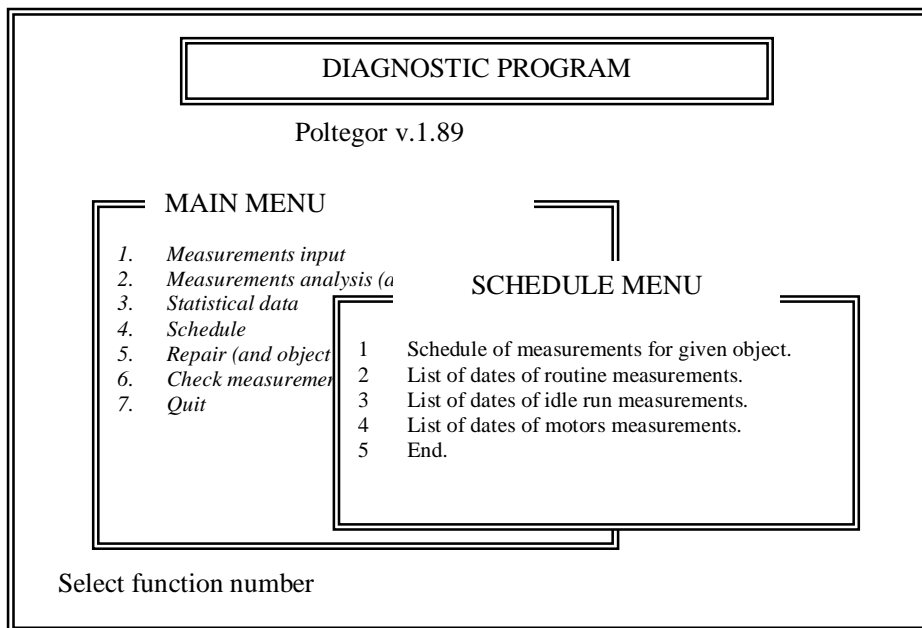


Fig. 19.5. "Schedule" file menu against main folder of gear transmission diagnostics system.

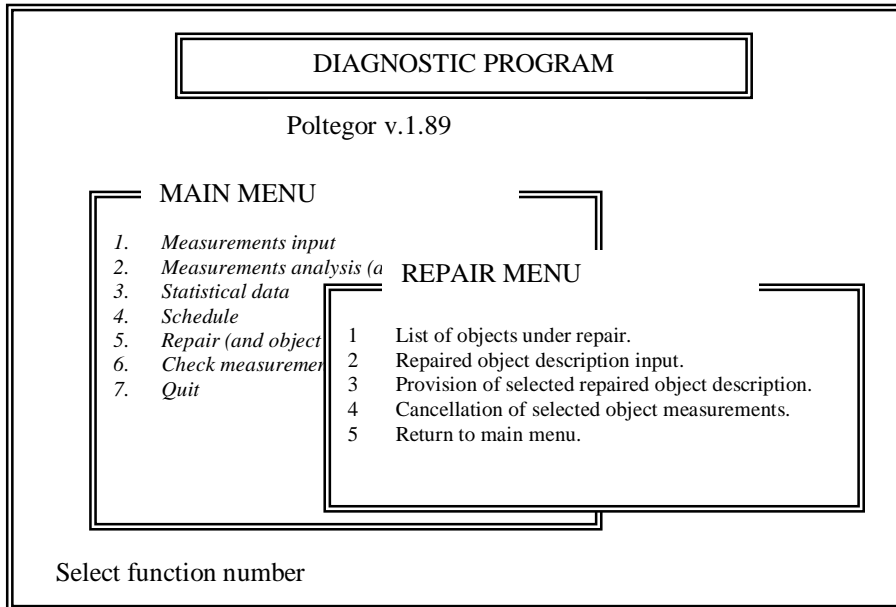


Fig. 19.6. "Repair" file menu against main folder of gear transmission diagnostics system.

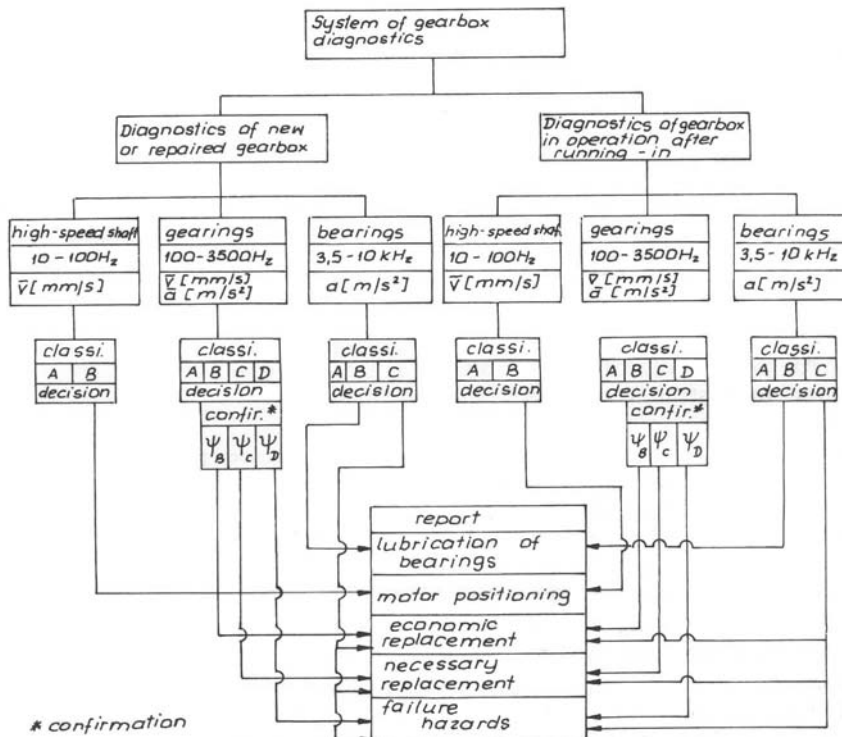


Fig. 19.7. Schematic diagram of diagnostic inference.

The principle of diagnostic inference is presented in the form of a block diagram in fig. 19.7. The block diagram according to which the diagnostic system operates is shown in fig. 19.8 [19.5]. Diagnostic inference algorithm, routine measurements (6 signal reception points were assumed)

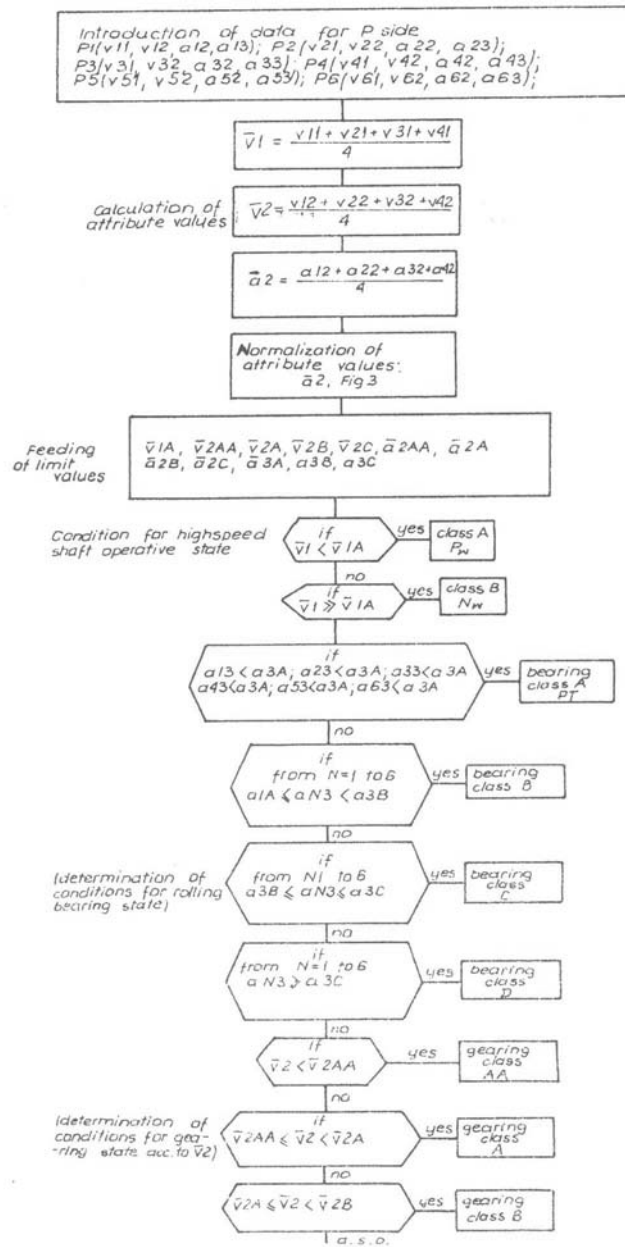


Fig. 19.8 Diagnostic inference algorithm.

To understand better the principle on which the inference system is based a simplified version of the Geardiag program [after 19.3] is shown in fig. 19.9. The simplified program was written in Pascal. It incorporates the basic principles of gear transmission condition classification. To simplify our considerations it is assumed that gear transmission condition signals are received from four points (denoted as $npoint = 4$ in the program). Boundary values {1} (fig. 19.9) are denoted: for the shaft as s , for gearing as g , for vibration velocity as v and for vibration acceleration as a . Physical quantities form an ARRAY table of values. A table of readouts (measurements) was fixed for a given gear transmission for appropriate measuring points. Boundary values {2} for rolling bearing condition are given as a function of rolling bearing pitch circle tangential velocity. They are shown in fig. 16.2. Readouts and parameters {3} are described by numbers of teeth: z_1, z_2, z_3, z_4 for a two-stage gear transmissions. The outside and inside bearing diameter is entered as Dz and Dw . The actual program {4} begins with an insert procedure. Bearing mean diameter tangential velocity {5} is calculated for rolling bearings 1 and 2. The condition of bearings 1 and 2 and bearings 3 and 4 is determined on the basis of $vo1$, measure [1] [4], measure [2] [4] and FUNCTION data boundary values {2}, using PROCEDURE class (1, 2). Then the values of attributes {6} for the high-speed shaft – $atr1$ and gearing attributes $atr2$ and $atra2$ are calculated and attributes {7} are normalized. The normalization consists in the referring of the measured values to one load value. The principle of normalization is illustrated in fig. 16.11. Attributes are classified according to {8}.

The diagnostic system whose menu is shown in figs 19.1-19.6 operates as follows. As the first item (Measurements input) in the main file is selected, the table shown in fig. 19.10 appears. Also illustrative values measured when the signal was received from four measuring points (there are zero values for point 5 since originally 5 points had been declared) are given in this figure.

According to the table in fig. 19.10 one can declare up to 12 points. If main file item 2 is selected, a screen as shown in fig. 19.3 will appear on the monitor. If item 2 in the analysis file is selected, the system will prompt us to mark the object either by its current location or by its inventory number. Once object data are entered, a diagnosis as shown in fig. 19.11 will appear. The diagnosis is for the gear transmission denoted by number 1RP and it reveals that the high-speed shaft functions properly (class A), the gearing functions improperly (class D) and the condition of the bearings assessed at 1÷4 is proper (class A).

To make a diagnosis about the condition of an object, one must enter the basic object data as shown in fig. 19.12. The data given in the table inform us, for example, that the gear transmission is installed in production process line Z3. The gear transmission of type KA16 operates on belt conveyor 62.06B, where B stands for the location in a drive consisting of four gear transmissions A, B, C and D. To characterize the gearing contact trace on the gear transmission's bevel stage, the degree of contact can be expressed as a percentage in the height and width of the teeth.

```

PROGRAM geardiag;
  USES
    Crt,Printer;
  CONST
    Nvalue=4;
    Npoint=4
    As1=7;Ag1v=20;Bg1v=25;Cg1v=30;Ag1a=45;Bg1a=70;Cg1a=90; {1}
TYPE
  value=1..nvalue;
  points=1..npoint;
  phisquant=ARRAY[value]OF real;
  object=ARRAY[points]OF phisquant;
VAR
  measure:object;
  nov:value;
  nop:points;
n1,n2,n3,z1,z2,z3,z4,Dz1,Dw1,Dz2,Dw2,Dz3,Dw3,Dz4,Dw4,:real;
vo1,vo2,vo3,A1,B1,v,sum,load,atr1,atr2,atra2:real
be,en:integer;
  FUNCTION limitbA(v:real):real;
  BEGIN
    limitbA:=2*(v-225)/125+10;
  END;
  FUNCTION limitbB(v:real):real; {2}
  BEGIN
    LimitbB:=7.5*(v-225)/125+24;
  END;
PROCEDURE insert;
  VAR
    nov:value;
    nop:points;
  BEGIN
    writeln('insert readings');
    FOR nop:=1 TO npoint DO
      FOR nov:=1 TO nvalue DO
        read(measure[npo][nov]);
      writeln('insert n1');
      read(n1);
    writeln('insert diameters');
    writeln('Dz1,Dw1');
    read('Dz1,Dw1');
    writeln('Dz2,Dw2');
  END;

```

```

        read('Dz2,Dw2');
        writeln('Dz3,Dw3');           {3}
        read('Dz3,Dw3');
        writeln('Dz4,Dw4');
        read('Dz4,Dw4');
        writeln('insert load');
        read('load');
    END;
PROCEDURE class(be,en):integer;
    VAR
        nov:value;
        nop:points;
    BEGIN
        nov:=4
        A1:=limitbA(v);
    BEGIN
        FOR nop:=be TO en DO
            IF(measure[nop][nov]<A1) THEN
                writeln('classA');
            END;
            B1:=limitbB(v);
        BEGIN
            FOR nop:=be TO en DO
                IF(measure[nop][nov]>A1) AND (measure[nop][nov]<=B1) THEN
                    writeln('classB');
                END;
            FOR nop:=be TO en DO
                IF(measure[nop][nov]>B1) THEN
                    writeln('classC');
                END;
            END;
        END;
    END;
    { actual program }                 {4}
BEGIN
    insert;
    writeln('bearing1 and 2');
    vo1:=n1*(Dz1+Dw1)/2;              {5}
    v:=vo1;
    class(1,2);
    writeln('bearing3 and 4');
    vo1:=n1*(Dz2+Dw2)/2;
    v:=vo2;
    class(3,4);

```

```

{condition of gearing and shaft}
{attribute of shaft}
    nov:=1;
    sum:=0.0;
BEGIN
    FOR nop:1 TO 4 DO
        sum:=sum+measure[nop][nov];
        atrv1:=sum/4;
    END;
    nov:=2;
    sum:=0.0;
BEGIN
    FOR nop:1 TO 4 DO
        sum:=sum+measure[nop][nov];
        atrv2:=sum/4;
    END;
    nov:=3;
    sum:=0.0;
BEGIN
    FOR nop:1 TO 4 DO
        sum:=sum+measure[nop][nov];
        atra1:=sum/4;
    END;
    IF atra2>14 THEN
        {normalisation}
        atra2:=(atra2-14)+88/(load-12)+14;
{inferring}
    writeln('shaft classification');
    IF atrv1<=As1 THEN
        writeln('classA')
    ELSE
        writeln('classB');
        writeln('gear-classification');
        IF (atrv2<=Aglv) THEN
            writeln('classAv');
        IF (atrv2>Aglv) AND (atrv2<=Bglv) THEN
            writeln('classBv');
        IF (atrv2>Bglv) AND (atrv2<=Cglv) THEN
            writeln('classCv');
        IF atrv2>Cglv THEN
            writeln('classDv');

```

{6}

{7}

```

IF atra2<Ag1a THEN
writeln('classAa');
IF (atra2>Ag1a) AND (atra2<=Bg1a) THEN
writeln('classBa');
IF (atra2>Bg1a) AND (atra2<=Cg1a) THEN
writeln('classCa');
ELSE
writeln('classDa');
END.
    
```

Fig. 19.9. Simplified program "gearing".

| ROUTINE MEASUR. 559/F2 | | | | TYPEK16 | Conv. 6.06AN Date90.12.11 Load 85.0 | | | |
|------------------------|---------------------|--|------------------------------------|---------|-------------------------------------|--|------------------------------------|--|
| M | 10-100Hz v[mm/s] | 100-3500Hz v[mm/s] a[m/s ²] | 3500-10000 a[m/s ²] | M | 10-100Hz v[mm/s] | 100-3500Hz v[mm/s] a[m/s ²] | 3500-10000 a[m/s ²] | |
| 1 | 1.9 | 11.0 55.0 | 11.0 | 7 | | | | |
| 2 | 2.1 | 6.6 31.0 | 12.0 | 8 | | | | |
| 3 | 1.2 | 13.0 22.0 | 2.0 | 9 | | | | |
| 4 | 1.8 | 7.0 30.0 | 6.5 | 10 | | | | |
| 5 | 0.0 | 0.0 0.0 | 0.0 | 11 | | | | |
| 6 | | | | 12 | | | | |

Annotation

Fig. 19.10. Table for entering measurement data.

```

Gear 599/F2 Date of last measurement88.03.10
Within 10-100Hz v-av.in cl.A.
Range II pnt3-cl.A;
Within 100-3500Hz a-av..v-av.in cl.A.
Range III:
Pnt.1 in cl.A
Pnt.2 w cl.A
Pnt.3 - cl.A
Pnt.4 - cl.B
Pnt.5 - cl.A

Check lubrication of bearing.a4-cl.B;

Is it to be printed out?(Y/N)
    
```

Fig. 19.11. Exemplary diagnosis of gear transmission condition.

| | | | | | | | | | | | | |
|--|----------|---------|-------|--------|------|----------|------|----|-------|-----|-----|-----|
| DESCRIPTION GEAR NO. 559/F2 | | | | | | | | | | | | |
| TR. Z3 | TYPE K16 | CONV.NO | 6.06A | T.CONV | N | RAT.1000 | LOAD | RT | 118.0 | | | |
| CHARACTERISTIC OF ADHESION TRACE height % width % | | | | | | | | | | | | |
| NUMBER OF MEASURING POINTS 5 | | | | | | | | | | | | |
| NUMBER OF PNT. TO BE AVERAGED 4 | | | | | | | | | | | | |
| n1[r/m] 985 | | | | | | | | | | | | |
| DIAMETERS Dz,Dw BEARINGS and no.of cor. ROT.SPEED for msng.points: | | | | | | | | | | | | |
| | p1 | p2 | p3 | p4 | p5 | p6 | p7 | p8 | p9 | p10 | p11 | p12 |
| Dz | 0.29 | 0.29 | 0.44 | 0.44 | 0.70 | | | | | | | |
| Dw | 0.16 | 0.16 | 0.26 | 0.26 | 0.47 | | | | | | | |
| n(1-6) | 1 | 2 | 2 | 3 | | | | | | | | |
| NUM.of TEETH: | Z1 | Z2 | Z3 | Z4 | Z5 | Z6 | Z7 | Z8 | Z9 | Z10 | | |
| | 22 | 99 | 44 | 155 | | | | | | | | |
| <P>-printout <U>-updating <C>-change of inven.no. <E>-end U | | | | | | | | | | | | |

Fig. 19.12. Table for entering gear transmission data.

Five measuring points were declared but data were averaged only for points 1-4 to obtain \bar{a} and \bar{v} . Dz and Dw were specified for respectively the inside and outside diameter of the rolling bearings. The values are used to calculate mean bearing diameter D and product nD , where n is the rotational speed of the shaft on which the rolling bearing operates. To calculate values $n1-n6$, high-speed shaft rotational speed $n1$ and number of gear wheel teeth $z1$ to $z10$ was given. The particular measuring points must be located in the vicinity of the rolling bearings. This is denoted by 1, 2, 3, etc., where 1 corresponds to rotational speed $n1$, 2 to rotational speed $n2 = n1z2/z1$ and so on. If item 3 from the main folder is selected, then a histogram of the measured values can be displayed to compare them visually in order to determine (see chap. 16.2 (fig. 16.7)) if the place for the reception of the diagnostic signal and the diagnostic parameters is proper. If item 4 (schedule) in the main folder is selected, a list of objects for a given production line process can be obtained to determine the dates of, for example, the last measurements, etc. If item 5 in the main folder is selected, the "repair" folder, which contains a list of objects under repair, the condition of the objects prior to repair and the cancellation of a given object's measurements, is displayed. Item 6 in the main folder is used to support diagnostic decisions about objects. If it is selected, screen 19.13 appears in which states are distinguished according to fig.19.7. The first two items are related to prevention and indicate the beginnings of improper operation of the bearings and the necessity of correcting the position of the motor relative to the gear transmission. The next operational decisions relate to the replacement of objects to be repaired. The other three items inform us that a particular object should be sent for repairs at the economical replacement level (fig. 19.7) to keep the costs at a minimum. If the object must be left in operation, then it can be operated up to the parame-

ter level indicating a danger of failure. A list of objects at any of the five gear transmission condition parameter level can be printed (fig. 19.14). The printout can be for a particular production process or for all the gear transmissions.

```

1 Lubrication of bearings...
2 Positioning motor-gear, coupling run-out...
3 Economic replacement...
4 Necessary replacement...
5 Failure hazard...

Select type of hazard:      0

```

Fig. 19.13. Gear transmission states.

```

"FAILURE HAZARD..."
62.06B 1.RP      88.03.08 - occurred 2 time(s)
Range II pnt3-cl.D; Range II- a, v cl.D;

88.03.08 - previous msr.
Range II pnt3-cl.D; Range II- a, v cl.D;

-----
6206B 1.RP      88.03.08 - occurred 1 time(s)
II zakr.- a, v kl.D;
-----

```

Fig. 19.14. List of gear transmissions with risk f improper lubrication.

19.3. Steps to be taken into account when introducing technological diagnostics method

The steps to be taken when introducing technological diagnostics are illustrated in the block diagram in fig. 19.15 [19.6]. These steps are to be considered when introducing the diagnostic method for a given object – a machine.

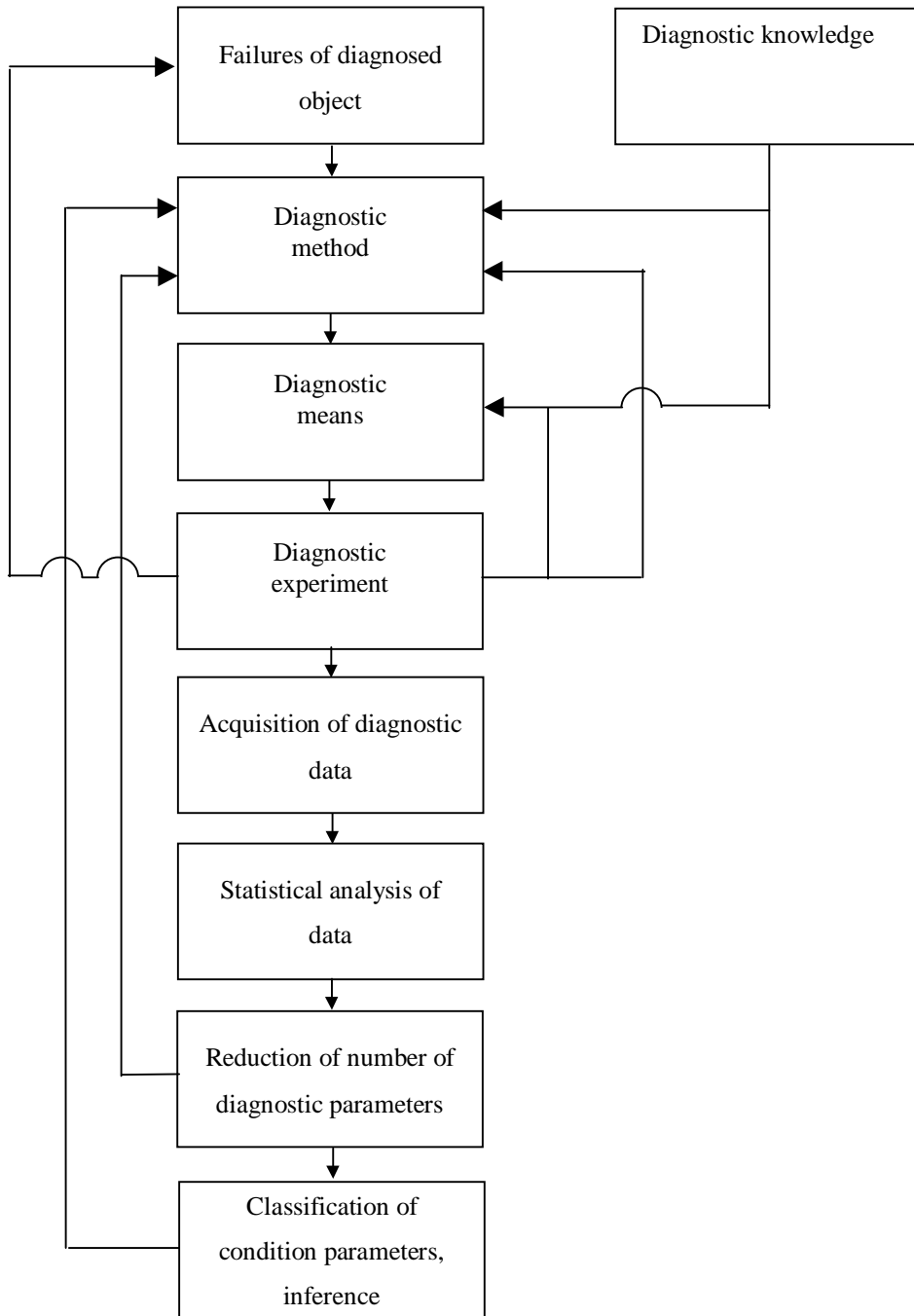


Fig. 19.1. Steps to be taken when introducing (in collaboration with a research unit) technological diagnostics.

The choice of a suitable diagnostic method is of key importance. The method is chosen considering: the features of the diagnosed object and the existing diagnostic knowledge. At the same time diagnostic means are selected. The chosen diagnostic method and the diagnostic means are validated and diagnostic experiments are performed. The results of the diagnostic experiments are taken into account in the validation of the diagnostic method and the diagnostic means. This process is represented by feedback arrows in fig.19.15. As the diagnostic method is being put into practice, diagnostic data are stored in databases. The data are subjected to statistical analysis (chap. 16.6) as a result of which the number of parameters is reduced and the most essential parameters (symptoms) are chosen. The statistical analysis is also a basis for the classification of diagnostic parameters and diagnostic inference methods. The reduction in the number of diagnostic parameters and the verification of the classification of the parameters result in the improvement of the diagnostic method.

Now a slightly modified approach is possible. As shown in fig. 19.15, a diagnostic method is selected on the basis of the features of the machine to be diagnosed. These are the features of the individual kinematic pairs of which the machine is made up. The behaviour of the features should be considered in the context of the whole dynamic system of the machine. For this purpose physical and mathematical models (see chap. 4.5, 5, 6.2-6.4, 7 and 8) are constructed. Having a proper mathematical model of the machine one can simulate the latter's behaviour on a computer and investigate the factors which affect this behaviour (represented as diagnostic signals). A computer simulation of the behaviour of a machine may have a significant influence on the choice of a diagnostic method and the interpretation of the results (signals) of the diagnosis. Modelling and computer simulation are used to generate diagnostic signals which are processed similarly as the signal received from the actual object (machine). Computer simulation considerably reduces the number of diagnostic experiments performed on the actual object. Results of computer simulations are presented in many chapters (chap. 4, 5, 6, 8 and 14) of this book and processed signals obtained by computer simulation are shown in chap. 11.

19.4. Example of machines operation subsystem

Information system SZEPT aiding the belt conveyor transport operation management system [19.7, 19.8] is an example of a machine's operation subsystem. The operation management system consists of a decision system and an information system which supports it. The latter includes a system of acquiring, storing, processing, retrieving and making available information on the processes proceeding in the in the operation realization system (using, maintaining and delivering the fixed assets which make up the belt conveyor transport system (BCTS). The information system's func-

tion is to reduce the uncertainty in decision taking by furnishing the user with accurate, timely and useful information [19.9]. The belt conveyor transport operation information system covers:

- the inventory of transport system objects (belt conveyors, winning receiving points, feeders and storage reservoirs);
- the documenting and viewing of objects' and subassemblies' technical data (the belt can be a subassembly);
- the recording, viewing and analysis of worktime and the quantity of conveyed winning for objects and subassemblies as well as the causes and durations of standstills of objects;
- the documenting, viewing and analysis of replacements, unserviceabilities, failures, periodic maintenance and repairs of subassemblies;
- the planning of preventive maintenance,
- the documenting, analysis and planning of supply management for essential materials and parts of subassemblies;
- the recording of the personal details of employees and the control of the expiration dates of professional authorizations.

Information system SZEPT aiding the belt conveyor transport operation management system includes:

1. A system of coding operation objects.
A uniform classification of technological objects being part of BCTS (conveyors, winning receiving points, feeders and storage reservoirs) has been developed and implemented. Each object is uniquely located in the structure of the transport system [19.10]. For all the kinds of objects a structural expansion comprising all alternative object designs was defined. A subassembly is a basic element of the object. A subassembly is subject to service, repairs and replacement. The principles of identifying objects and subassemblies were defined. The identification of spare parts and materials is identical as the one used in the materials management system.
2. Classification of states and operational events.
For inventory control and machine use analysis, operational states of objects (investment, operation, permanent uselessness, superfluousness, disposal) and subassemblies were defined. The systematics of stoppages of transport objects and principles of evaluating the use of their available time were introduced.
3. Formalization of operational tasks.
Three main groups of operational tasks (activities): replacements, routine maintenance and repairs of subassemblies were distinguished. A uniform system of reports documenting the subject, range and labour consumption of the performed tasks was created.
4. Organization of local materials management.

Starting from the adopted materials management documentation principles, elements of planning, inventory taking and stock control for spare parts and materials essential for the operation of the belt conveyor transport system were developed.

5. System of preventive maintenance.

The preventive maintenance system includes:

- the documentation of the worktime of belt conveyor transport objects and the quantity of winning conveyed by them;
- the specification of routine maintenance for transport object subassemblies (the range of maintenance and the overhaul life are specified);
- the current documentation of performed services and repairs;
- the recording of scheduled stoppages of transport objects;

The above data enable the planning of preventive maintenance for belt conveyor transport objects. It should be noted that the user has current information on the materials stock level in the mine section store.

The following objects can be stored in the information system's database:

- stocks of conveyor belts, materials for belt repairs and splices;
- conveyor distribution complex;
- belts installed on belt conveyors;
- splices made;
- removed belts and splices.

The information system should perform the following functions:

- document the stock management of belts and materials for belt repairs and splices;
- generate and update data on belt conveyors and belts operated in the mine;
- supply information selected by the user and carry out statistical analyses of belt conveyors, belts and splices taking into account the risks involved;
- acquire data for statistical studies, including analyses of the mean life of belts and splices working in different conditions.

The system is easy to operate and does not require any information science training. The messages displayed by the system facilitate work and ensure operational use comfort. Multilevel protection when creating and updating a database (e.g. keyboard redefinition, checking the range of entered data, forced acknowledgment of the correctness of entered data) makes the system resistant to unintended errors made by the user and to accidents. For better and faster orientation, the monitor's screen is divided into fixed areas in which information supplied by the system is displayed, data are entered and printouts are produced. At each program level the user has a choice of several paths described in the menu.

The SUFLER system consists of five programs: STORE, STRUCTURE, UPDATING, BROWSING AND HISTORY. Each of them is an autonomous unit and performs functions implied by its name. UPDATING is used for updating the current condition of conveyors, belts and splices. This can be done through the description of belt or splice replacements or the modification of the previously entered data.

BROWSING makes it possible to view the acquired information about the belt conveyors and the belts and the splices according to:

- any browsing key,
- a selected standard.

The user can select the kind of description (brief, extended and other) and the output device (the screen or a printer).

HISTORY performs the same functions as BROWSING but for removed belts and splices. Browsing here is augmented by the statistical analysis of the mean worktime of belts and splices.

The SUFLER system is based on time-preventive operation of machines, which is its drawback. It is necessary to modify the system so that the whole belt conveyor is operated depending on its technical condition. The basic principles of operation depending on condition are given in chap. 3. The whole book gives the background to condition based maintenance

19.5. References

- [19.1] Bartelmus W.: Algorithmic Computer-Aided Diagnostic Inferring System, The 6th International Symposium of IMEK0 TC 10, Technical Diagnostics 89.
- [19.2] Bartelmus W., Rekuć L., Szwarc H.: Microscopic System for Diagnostic Inference, Technical Documentation, Instructions for Use of Diagnostic Data Acquisition System, Performance Tests (in Polish), Poltegor, Wrocław, 1988 (unpublished).
- [19.3] Bartelmus W.: Vibration Condition Monitoring of Gearboxes, Machine Vibration, No. 1, pp.178-189, 1992.
- [19.4] Bartelmus W.: Gear Transmission Diagnostics (in Polish), Górnictwo Odkrywkowe, No. 2, 1991.
- [19.5] Bartelmus W.: Inference about Condition of Gear-Boxes on the Basis of Reduced Attributes of Vibration Signals. Proceedings of an International Conference on Condition Monitoring, Stadthalle, Erding, Germany, Pineridge Press UK, 1991.
- [19.6] Bartelmus W.: Computerised Monitoring System for Technical Diagnostics of Machinery and Equipment for Opencast Mines, Proceedings of Conference on Management of Economic and Environmental Aspects in Coalmining Industry, Prague, Czechoslovakia, 1991, Rotterdam, A.A. Balkema, 1991.
- [19.7] Dałkowski B.T., Jurzdziaik L., Kawalec W.: Computer-Aided Management of Belt Conveyor Transport Operation (in Polish), Scientific Papers of Wrocław University of Technology, No. 63, Series: Conferences, No. 12, Fundamental Problems of Mine Transport, Wrocław, 1990.
- [19.8] Dałkowski B.T.: Introduction to Technological Objects Operation (in Polish), the 8th Scientific School: Fundamental Problems of Mine Transport, Szklarska Poręba, 1990, Wrocław University of Technology, Wrocław, 1990.

- [19.9] Dałkowski B.T., Jurdziak L., Kawalec W.: Personal Computer System for Maintenance Management of Belt Conveyor Systems, Proceedings of the 22nd International Symposium on the Application of Computers and Operations Research in the Mineral Industry (APCOM'90), 17-21 September 1990.
- [19.10] Hac D., Skarżyński R., Kawalec W.: Information System for Belt Conveyor Transport Operation Management in Rudna Mine (in Polish), Scientific Papers of Wrocław University of Technology, No. 63, Series: Conferences, No. 12, Fundamental Problems of Mine Transport, Wrocław 1990.